National Technical University of Athens

Civil Engineering Department

Numerical Analysis of Single Pile Response Due to Seismic Liquefaction and Lateral Spreading

Ashkan Afnani

Vida Niki

Supervisor: *George Bouckovalas*

Professor, School of Civil Engineering, NTUA

October 2011

To our friends in BIHE, who are now imprisoned for the guilt of education…

Acknowledgement

We would like to express our gratitude to our supervisor, Prof. George Bouckovalas, whose guidance and encouragement made this project possible. We are also grateful to Mr. Yannis Chaloulos for his kind guidance from the initial to the final level.

It is a pleasure to thank Prof. Manolis Papadrakakis, who has made available his support in a number of ways throughout our master's studies. We would like to acknowledge the financial and academic support of the Civil Engineering Department of the National Technical University of Athens.

Lastly, we would like to thank our families for their everlasting help and patience and our friends, especially Ms. Mehrvash Maanian, who helped us feel like home with her limitless assistance.

Abstract

Liquefaction-induced lateral spreading has been responsible for extensive damages to pile supported structures in several recent earthquakes. In this phenomenon, permanent lateral displacement of soil occurs in slightly sloping ground or near small topographic irregularities due to liquefaction, imposing large kinematic loads to piles.

In practice, this problem is normally dealt with the “Beam on Nonlinear Winkler spring Foundation” or simply the p-y method, in which soil is modeled by a series of springs at particular depths. The pile is modeled as a beam element. Soil springs are attached to the pile on one end and fixed at the other. Kinematic loads are applied at the fixed-end of the springs. Soil displacements are usually estimated through empirical relationship, which do not account for the existence of the pile and possible pinning effects. Accurately determining the force-displacement law of these springs (or the p-y curves) is the main factor in obtaining accurate results for the response of the pile. Different methodologies exist in literature for determining the p-y curves in nonliquefied soil (e.g. Reese et al., 1974; Murchison and O'Neill (1984) – API (2002); and etc.), and liquefaction is modeled by applying a degradation multiplier to the nonliquefied curves. Several researches have tried to correlate this factor to different soil, pile and excitation properties (e.g. Dobry et al., 1995; Brandenberg, 2005; Cubrinovski, 2005). However, new research data reveal the need of further investigation since several detrimental parameters are not included in the correlations such as soil permeability, the stiffness of the pile, etc. Additionally some researchers concluded that the concept of the degradation multiplier may be over simplifying due to the complexity of the problem (Haigh, 2002; Gonzalez et al., 2009).

In order to study the effect of each parameter in the response of the pile, a series of numerical analyses has been performed in FLAC3D finite difference code. NTUA-Sand is used as the constitutive model of the liquefied soil and a sinusoidal excitation is applied at the base of the model. Tied nodes technique is utilized as the lateral boundary of the 3D mesh and in order to determine the pinning effect of the pile of boundary lateral

displacements, each time a separate analysis is performed in which the pile is deleted from the mesh.

The results are presented in terms of pile, boundary and free-field lateral displacements. The pore pressure ratio time-histories are plotted throughout the soil layer, near the pile and in free-field and the p-y curves are found along the length of the pile in points with a distance of 1 meter. By dividing the p-y curves with their static counterparts (i.e. the nonliquefied soil), the normalized p-y curves are obtained in order to have a view of the degradation multiplier. The following conclusions can be made after analyzing the results of the parametric analyses:

- **Soil Relative Density, D_r;** affects both the lateral displacements and the lateral pressure considerably. The lateral displacements decrease with increase in soil density. The p-y curves, however, change strangely when soil with smaller relative density yields larger lateral resistance.
- **Soil Permeability, k;** have considerable effects on the lateral displacements and the p-y curves: more permeable sample yields smaller lateral displacement and lateral load and vice versa. In addition, more detailed simulation of variable permeability with r_u does not seem to significantly affect the response.
- **Excitation Period, T;** Increase in T results in larger free-field lateral displacements. Additionally, its effect on the lateral resistance of the soil cannot be overlooked. It was concluded that a threshold should exist for excitation period to be determinant on the response of the pile, which is a function of soil permeability.
- **Pile Diameter;** Analyses indicate that the effect is minor, with piles of smaller diameter yielding smaller degradation of soil resistance. However, numerical results reveal that questions still remain with regard to the way the effect of pile diameter should be investigated numerically.

- **Pile Stiffness;** is quite a detrimental parameter. Stiffer pile undergoes smaller lateral displacements, which keeps the whole mesh to displace less. Apart from that, the p-y curves are significantly affected and a considerable increase in the lateral resistance of soil is observed in the model with stiff pile.
- **Pile Installation Method;** the model which simulated the driven pile condition had smaller lateral displacements due to stiffer soil around the pile. On the other hand, the effect on the liquefied p-y curve was negligible.
- **Pile Head Constraint;** a fall in the lateral resistance of the soil boundary is observed in the model with fixed-head pile which is quite normal. Moreover, significantly larger lateral loads are exerted on the pile in shallow depths, while no specific change is observed in the lower half of the pile.

Table of Contents

Chapter 1

Introduction

1.1. Problem Statement

In cases where the bearing capacity of soil is not sufficient for the loads exerted by the superstructure, deep foundations are extensively used in order to transfer the loads to deeper and stronger layers. Piles are the most common types of deep foundations and are used in a variety of structures.

Although piles are primarily used to transfer vertical loads, they may be subjected to lateral loading especially during earthquake excitation. This loading is applied either as concentrated horizontal load from the superstructure or kinematic loading from soil.

Numerous methodologies for design of pile foundations embedded in dry soil and subjected to lateral loading are proposed by many researchers. However, large variations exist between the results obtained by different methodologies which have different assumptions about the soil behavior. For example some of them take into account the soil continuity and elasto-palstic behavior whereas the others model the soil as a discontinuous and elastic medium and there are methodologies which take into account one of these two factors. Among the methodologies, the p-y method is the most widely used one which treats the pile as a beam on a foundation and soil is modeled by a series of discrete nonlinear springs with specific distance along the pile.

On the other hand, in the case of piles embedded in loose saturated sand, the situation can sometimes be more complicated and a phenomenon may occur which is called “liquefaction”. Since loose sand has a tendency to contract as a response to an applied load, if soil is saturated, the pore pressure tends to increase. If enough time exists, water finds its way to travel to lower pressure areas and dissipate. However, when the loading rate is high enough such that water cannot dissipate in each cycle, the water pressure tends to increase and as a result of constant total stress, the effective stress will decrease. The effective stress in some cases can reach zero which means that soil particles lose their contact and all the pressure in carried out by water and soil behaves as a liquid.

In places where ground with small inclination (about 2 to 4 percent) or small topographical irregularities exist – a situation mostly observed near river and lake banks – the liquefied soil starts to flow and undertakes permanent lateral displacement. The phenomenon is called “lateral spreading”.

In the case of earthquake-induced liquefaction and lateral spreading, the response of the pile changes dramatically and extensive damage to structures due to the failure of pile as a result of lateral spreading is reported during the past earthquakes. Lateral spreading imposes large kinematic loads on the pile which results in large residual horizontal displacement, shear forces and bending moments in the pile. This can lead to the rupture and cracking of the pile along with permanent lateral and vertical displacements which can have profound effects on the superstructure. (e.g. Japanese Geotechnical Society (JGS) 1996, 1998; Hamada & O’Rourke, 1992; Youd, 1993).

In current practice, the decrease in the strength of liquefied soil is taken into account by the use of degradation multiplier applied to the non-liquefied p-y curves. Different researchers have correlated the multiplier to different soil characteristics, excitation properties and pile parameters (e.g. Dobry et al., 1995; Brandenberg, 2005; Cubrinovski 2005). However large differences exist between the results obtained by different methodologies, which is an indicative of huge uncertainties in the subject. It should be mentioned that some researchers declare that due to the complexity of the problem, the

degradation multiplier concept is a simplistic approach (e.g. Haigh, 2002; Gonzalez et al., 2009). Overall, the problem is not considered as solved in the literature and extensive research is carried out by numerous researchers around the world on the subject.

1.2. Research Objective

As mentioned before, the response of the pile in laterally spreading ground is influenced by various parameters. In this thesis, based on a wide literature survey, a number of parameters are chosen and a parametric analysis is carried out. These parameters could be categorized in two main groups:

- Soil and excitation characteristics: Soil Relative Density, D_r; Soil Permeability, k and Excitation Period, T.
- Pile characteristics: Diameter, Stiffness, Pile Installation Method and Head Constraint

In order to investigate these factors, a series of numerical analyses have been performed in FLAC3D which is an explicit finite difference code mostly used in geotechnical engineering. In these analyses, a single pile is embedded in liquefiable ground which has an infinite slope of 2 degrees and NTUA-Sand – a bounding surface, critical state, plasticity model with a vanished elastic region – is used as the constitutive model for soil.

A sinusoidal excitation is applied at the base of mesh which causes liquefaction and due to the slope of the ground, lateral spreading occur imposing lateral displacement to the pile.

In order to have a thorough view of the mechanisms for each parameter, time histories of excess pore pressure ratio, r_u, soil resistance and relative displacement are kept throughout the soil sample and relevant figures are plotted in selected depths.

1.3. Scope of the Study

Following this introduction,

Chapter 2 presents a comprehensive literature survey of the laterally loaded piles in dry soil and the design methodologies that deal with this problem. The focus is on the p-y method and the proposed p-y curves in literature.

Chapter 3 discusses the methods of estimating lateral ground displacement in liquefaction induced lateral spreading along with modifications that are applied on the nonliquefied p-y curves in order to deal with the case of lateral spreading. Recent investigations on the effect of important parameters on the response of the pile are presented.

Chapter 4 provides an introduction to FLAC3D code and NTUA-Sand constitutive model and details of the numerical modeling. Additionally, the characteristics of the basic analysis along with the typical results are illustrated in this chapter.

Chapter 5 and ***6*** are dedicated to the results of the analyses dealing with soil and excitation properties and pile characteristics respectively. In these two chapters, the main observations and conclusions about the effects of each parameter are discussed.

Chapter 7 includes the final research findings and conclusions.

Chapter 2

The Static p-y Method

2.1. General

In cases where soil of low bearing capacity extends to a significant depth, deep foundations are used. Deep foundations extended far below the ground surface (usually more than 3m below ground level), therefore the applied loads are transferred to deeper and stronger layers. Piles, pile walls, diaphragm walls are some type of deep foundations.

Piles are long and slender elements that transfer vertical loads to a layer strong enough in any depth. They are used in offshore structures, wind turbines, high rise buildings, high retaining walls and tall chimneys.

In addition to vertical loads piles are also subjected to horizontal loads. The horizontal loads are applied either as concentrated loads acting on the center of mass of the superstructure and pile cap or as imposed displacements along the pile (force or moment).The magnitude of lateral load depends on the type of structure for example foundation of a moderate building is not subjected to a high magnitude of lateral load whereas in the designing of a jetty the horizontal load plays an important role.

The present chapter thoroughly describes design methods for laterally loaded piles in sand. Emphasis is given on the pseudo static p-y method, which is widely used in practice. This presentation although not clearly related to the topic of the thesis is

necessary, since static p-y curves are also used in dynamic analyses, of course properly modified.

2.2. Pile types

There are two types of piles: long piles and short piles. Long pile is the one which is embedded enough in soil in order to its base doesn't experience any moment, shear, deflection or rotation and therefore is motionless. The required length and stiffness of the pile to fulfill this situation depends on the pile and soil properties. Long piles typically fail when one (for free head piles) or two (for fixed head piles) plastic hinges form along the length of the pile due to the bending moment which become greater than the plastic moment at cross section. The different modes of failure for long piles are illustrated in **Figure 2.1.**

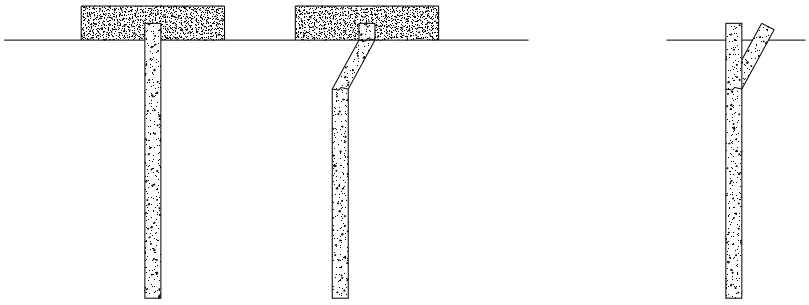

Figure 2.1: Long pile modes of failure: a) Fixed head b) Free head

Short pile's embedment and its stiffness is not enough to prevent base motion so these kinds of piles normally fail due to rigid body motion or rotation. The former will happen for fixed head and the latter for free head piles as shown in **Figure 2.2**.

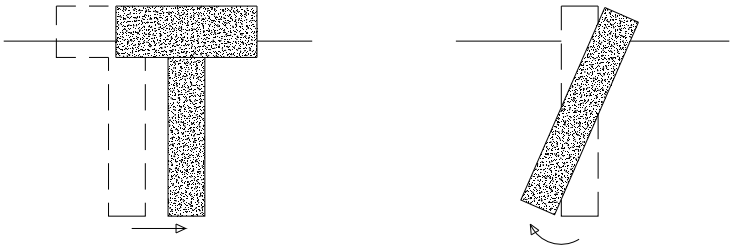

(a) (b)

Figure 2.2: Short pile modes of failure: a) Fixed head b)Free head

2.3. Methods for the analysis of laterally loaded piles

In analyzing the laterally loaded piles, there is two kind of approach, one of them deals with ultimate load and the other one with lateral displacement. In most of the cases where serviceability is more critical, it is more useful to calculate the lateral displacement rather than ultimate load. Based on this classification, we can categorize the existing methods for analysis of laterally loaded piles into five groups (Fan and Long (2005)):

- The limit state method
- The elasticity method
- The advanced numerical method
- The subgrade reaction method
- The *p–y* method

2.3.1. The limit state method

One of the simple limit state methods is the Broms (1964a) method. He made a simplified assumption for ultimate soil resistance along the pile length. He divides piles into two groups: short rigid and long flexible. His criterion for this classification is:

$$Short\ pile: \quad \frac{L}{T} \leq 2 \qquad (2.1)$$

$$Long\ pile: \quad \frac{L}{T} \geq 2 \tag{2.2}$$

Where L is pile length and T is defined as:

$$T = \left[\frac{E_p I_p}{k_g}\right]^{1/5} \tag{2.3}$$

Where: $E_p I_p$ pile stiffness

k_g Coefficient of subgrade modulus

Broms based on this classification proposed a relation in order to determine the ultimate lateral resistance.

$$p_{ult} = 3.k_p.\sigma_{v0}'.D \tag{2.4}$$

Where: K_p Passive earth pressure coefficient

D Pile diameter

σ_{v0}' Vertical effective stress

Although this method is applicable for short and long piles with any kind of fixity and takes into account purely cohesive and cohesion less soils, it has some deficiencies. For example it is not applicable for layered profiles and *c*-ϕ soils. In addition, it does not take into account the effect of vertical load on lateral capacity of piles.

2.3.2. The elasticity method

This method takes into account the soil continuity and the soil response is assumed to be elastic whereas its behavior is elasto-plastic. Therefore, this method can be applied only for small strains and is not appropriate for determining the ultimate lateral resistance.

2.3.3. The advanced numerical method (FEM, FDM)

This method which is recently used is able to take into account the soil continuity, nonlinear behavior and pile-soil interaction. In this method the deformation and

ultimate lateral resistance can be determined and the results are more accurate than the other methods provided that the constitutive model is well defined.

Although the complexity of the three dimensional model makes the analyses a little bit time consuming and computationally demanding, this method is the best alternative for advanced complicated projects.

2.3.4. The subgrade reaction method and P-y method

The subgrade reaction method is the simplest method for determining the soil resistance due to a given horizontal deflection. This method evaluates the beam response on elastic foundation and since this concept was firstly developed by Winkler in 1867, it is sometimes known as Winkler method.

In Winkler method, the soil constitutes of a series of discrete springs and the foundation slab lies on it. The springs are linear and expressed as:

$$P = k.\delta \tag{2.5}$$

Where: P force at the node that spring connected to the slab

k constant in units of force per unit displacement

δ displacement

Consequently, in subgrade reaction method (Reese and Matlock, 1956), the laterally loaded pile is assumed to be a beam on elastic foundation and the soil is modeled by a series of independent and elastic springs. In this method, the reaction of beam, P, at each point will linearly related to the deflection, y, at that point by a constant coefficient, k.

$$P = k.y \tag{2.6}$$

In order to apply the assumption, the pile is modeled as a beam element and the soil will be substituted with a series of discrete linearly elastic springs with stiffness equal to k (coefficient of subgrade reaction). The model is demonstrated in **Figure 2.3**.

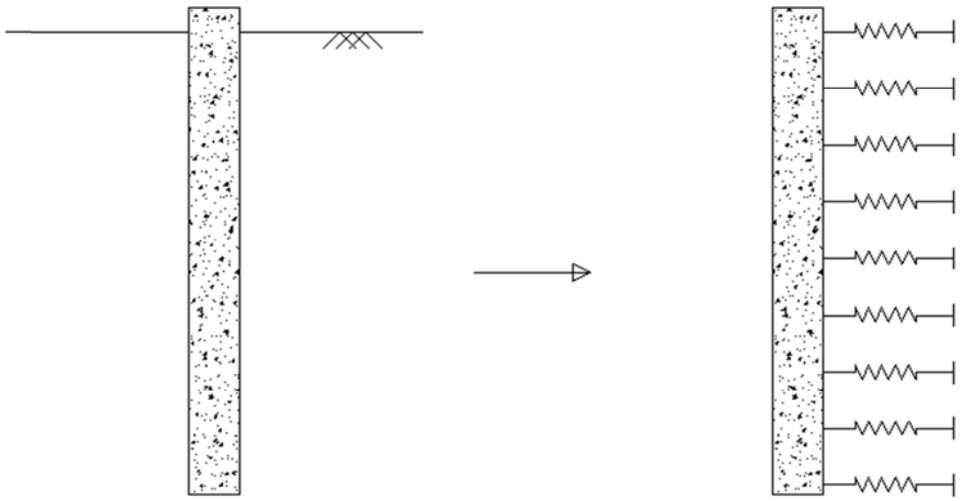

Figure 2.3: Winkler Model: soil is substituted by discrete springs

Although, this method is widely used due to its simplicity, it has some disadvantages such as:

1. Unlike the subgrade reaction method, full-scale tests represent a nonlinear relationship between soil resistance and pile deflection.

2. As the method applies the Winkler approach, discontinuous springs does not represent soil continuity

3. The subgrade reaction method cannot predict the ultimate lateral resistance.

These problems made researchers to make modifications to the Winkler approach which led to the introduction of *p-y method.* In this method like the subgrade reaction method, the pile is treated like a beam and the soil is modeled by discrete uncoupled nonlinear springs and by applying Winkler approach the lateral deflection of pile is determined. However, in this method the deficiencies of Winkler method (subgrade reaction method) are solved. It means that, the soil resistance is assumed to be nonlinearly dependent on the deflection. In addition, in P-y method the ultimate lateral resistance can be determined. The p-y method is the most widely used method and will be described thoroughly in the following.

2.4. The p-y method

As mentioned before, in this method three main assumptions are considered (**Figure 2.4Error! Reference source not found.**):

1. Pile, pile cap and superstructure are modeled as beam.

2. Soil-pile interaction is modeled by lateral springs.

3. External loads are applied either as imposed displacements on the fixed end of the springs or as concentrated loads applying on the center of mass of the superstructure and pile cap.

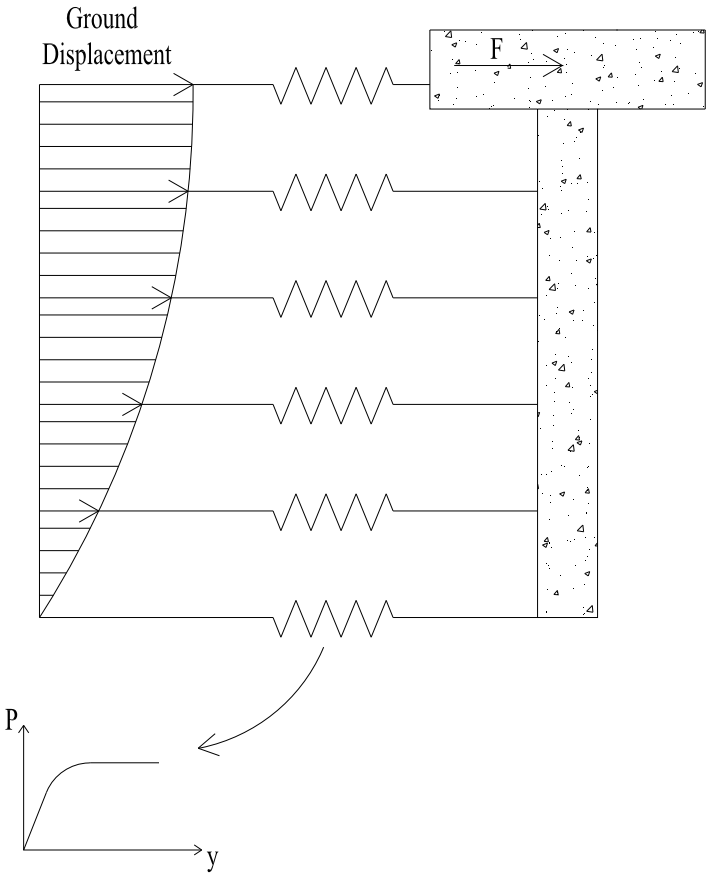

Figure 2.4: Main assumptions in p-y method

2.4.1.Analytical Background (Hetenyi 1946)

The governing differential equation of the deflection of laterally loaded pile is as below:

$$E_p I_p \frac{d^4y}{dz^4} + P_z \frac{d^2y}{dz^2} + P = 0 \qquad (2.7)$$

Where $E_p I_p$ is the flexural rigidity of pile, z is the depth, y is the lateral deflection, P_z is axial load of pile and P is the soil reaction per unit length and is expressed as follows:

$$P = E_s y \qquad (2.8)$$

Where E_s the soil modulus

Hetenyi (1946) solved this differential equation and provided solutions for a series of beams on elastic foundation that can be used for free and fixed head piles. Equation (2.7) shows his proposed analytical solution.

$$u = \left(\frac{2H\beta}{k_h D}\right)\left(\frac{\sinh \beta L \cos \beta z \cosh \beta(L-z) - \sin \beta L \cosh \beta(L-z)}{\sinh^2 \beta L - \sin^2 \beta L}\right) \qquad (2.9)$$

Where: $\beta = \left(\frac{k_h D}{4E_p I_p}\right)^{\frac{1}{4}}$ (2.10)

D	Pile Diameter
$E_p I_p$	Pile Stiffness
k_h	Coefficient of Subgrade Reaction
Z	Depth

The differential equation will be solved if the soil modulus can be obtained. Therefore, many researchers such as Reese et al. (1974), Reese and Welch (1975) and Bhushan et al. (1979) by the aid of the differential equation and using Winkler concept due to pile's deflection nonlinearity, worked on a new method called p-y

method. The advantage of this method is its capability in modeling the nonlinear behavior of soil.

2.4.2. Assemblage of a p-y model

In p-y method, due to pile's deflection nonlinearity, the pile is divided into small segments and the Winkler concept is adopted. Therefore, a family of curves is produced that represents the soil reaction, p, as a function of deflection, y, in order to define a numerical solution of soil modulus. The concept of p-y curve is illustrated in **Figure 2.5**.

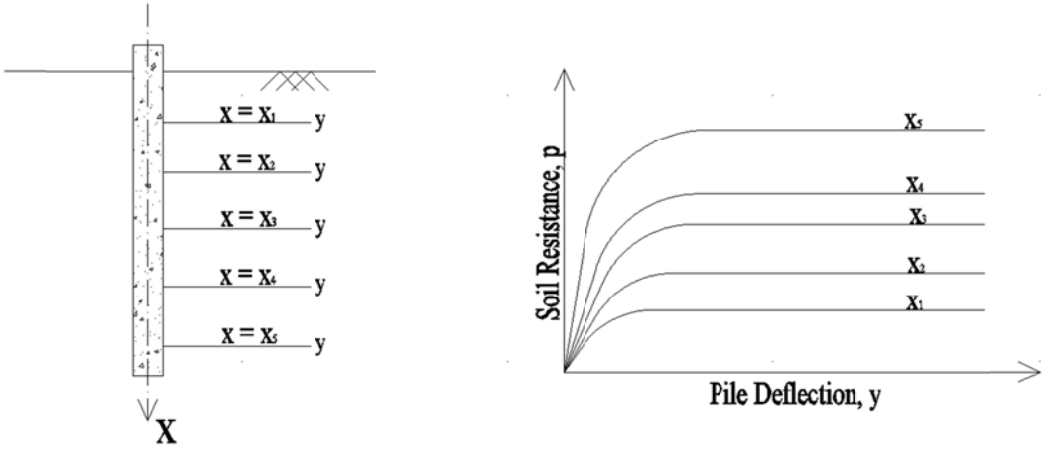

Figure 2.5: The concept of P-y curve

As mentioned before, the shape of proposed curves are nonlinear and influenced by many factors such as depth, soil shear strength, number of load cycles (Reese 1977) and pile types. In the following paragraph, the shape of the curves for sand is discussed in details.

2.5. P-y curves for sand

2.5.1. Elements of a P-y curve

As mentioned before, a p-y curve is indicative of the nonlinear relationship between the soil resistance and the lateral pile deflection. In order to form the p-y curve three quantities are required to be evaluated: Initial subgrade modulus (K_{ini}) which

determines the initial behavior of soil, mathematical formula expressing the non-linear shape of the curve and Ultimate Soil Resistance (p_{ult}) that represents the soil ideal plastic behavior.

A typical shape of p-y curve and these three quantities are shown in the **Figure 2.6**.

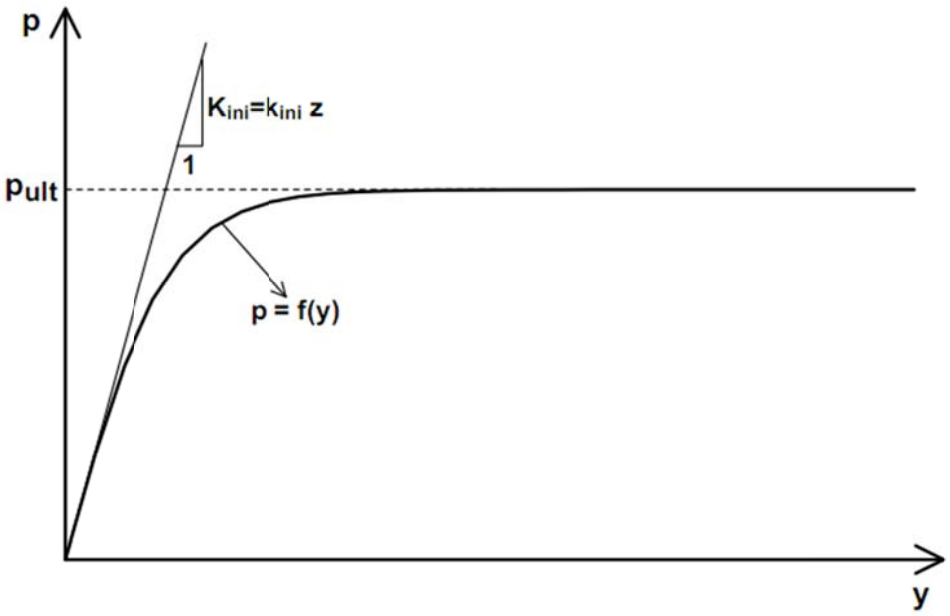

Figure 2.6: Typical shape of p-y curve

In the literature different suggestions by various researchers for developing P-y curve can be found. These methodologies are mainly based on tests and some of them will be described in the following.

2.5.2. Reese et al. (1974)

Reese et al. (1974) proposed a unified framework to estimate ultimate soil resistance, nonlinear shape and initial stiffness. His suggestions were based on the experiments that were performed in Mustang Island, Texas as described by Cox et al. (1974).

The test layout and basic soil and pile properties are demonstrated in **Figure 2.7**. Two open ended steel piles with 0.61m diameter and 9.5mm wall thickness ($E_pI_p = 168000kNm^2$) were used. The distance between two piles was 7.5m and the

embedded length of the piles was 21m (slenderness ratio of L/D=34.4). 34 strain gauges were bonded to the inside of the piles and the load cell was installed between the piles. The relative density and friction angle which had been evaluated from the boreholes were 90% and 39^{o} respectively. The piles were subjected to two static and five cyclic tests by applying a horizontal displacement at the head of the pile and the observations resulted in the expressions which will be described in the following.

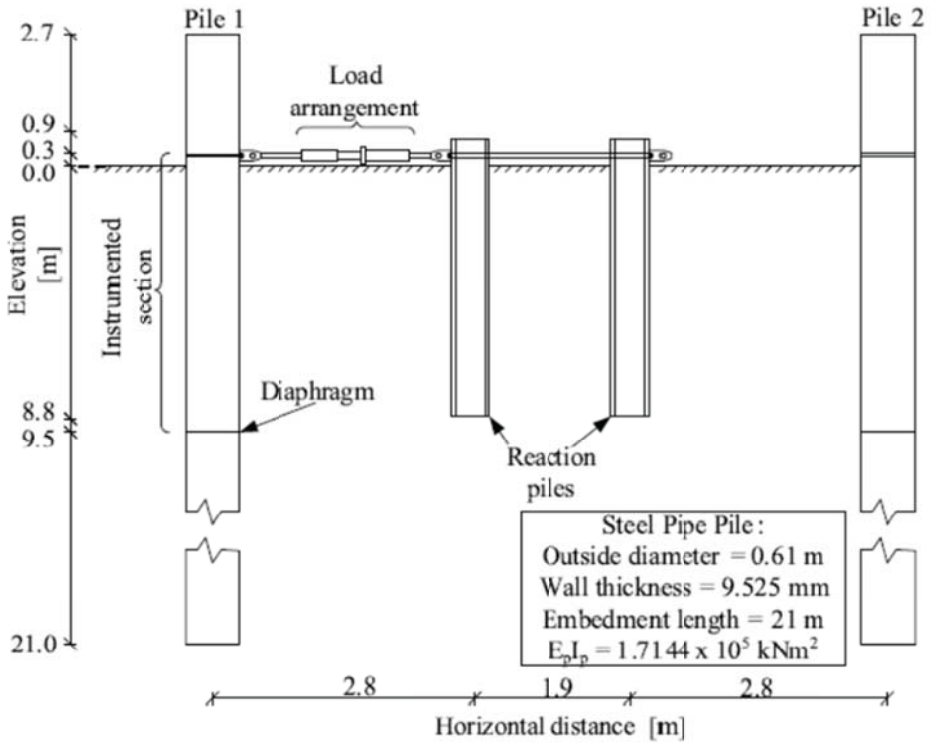

Figure 2.7: Full scale test in Mustang Island, Texas (Cox et al. 1974)

Researchers identified two modes of failure depending on the depth. For shallow depths, a wedge was assumed to form in front of the pile and extend to ground surface while a horizontal plane stress mode of failure was assumed for large depths as shown in **Figure 2.8.**

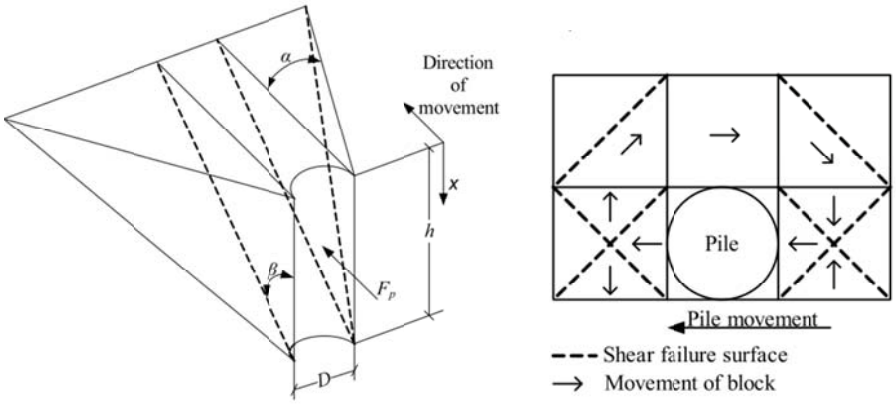

Figure 2.8: a)Plain Stress mode of failure b)Wedge-shaped mode of failure (after Reese et al. 1974)

The following formulas were proposed for the passive ultimate resistance per unit length at shallow and large depths, P_{cs} and P_{cd} :

$$P_{cs} = \gamma' z \left[\frac{K_o z tan\varphi_{tr} sin\beta}{\tan(\beta - \varphi_{tr})cos\delta} + \frac{tan\beta}{\tan(\beta - \varphi_{tr})}(D + z tan\beta tan\alpha)\right] + \gamma' z[K_o z tan\beta(tan\varphi_{tr} sin\beta - tan\alpha) - K_a D] \quad (2.11)$$

$$P_{cd} = K_a D\gamma' z(tan^8\beta - 1) + K_o D\gamma' z tan\varphi_{tr}.tan^4\beta \quad (2.12)$$

Where: γ' Buyonant unit weight of the soil

Z Depth below the ground surface

D Pile diameter

K_o Coefficient of horizontal earth pressure at rest

K_a Coefficient of minimum active earth pressure

φ_{tr} Internal angle of friction based on triaxial tests

The following assumptions were made by the authors regarding the above parameters:

$$\alpha = \frac{\varphi_{tr}}{2} \tag{2.13}$$

$$K_a = \tan^2(45 - \frac{\varphi_{tr}}{2}) \tag{2.14}$$

$$\beta = 45 + \frac{\varphi_{tr}}{2} \tag{2.15}$$

$$K_o = 0.40 \tag{2.16}$$

However, it was observed that the values obtained from equations (2.11) and (2.12) were much smaller than the experimental data especially for the small depths. Therefore, the authors introduced an empirical coefficient factor A which can be evaluated form **Figure 2.9** as a function of depth and the type of loading (i.e. static or cyclic). Hence, the ultimate resistance, P_{ult}, is expressed as follows:

$$P_{ult} = AP_c \tag{2.17}$$

Where P_c is the minimum of P_{cs} and P_{cd} .

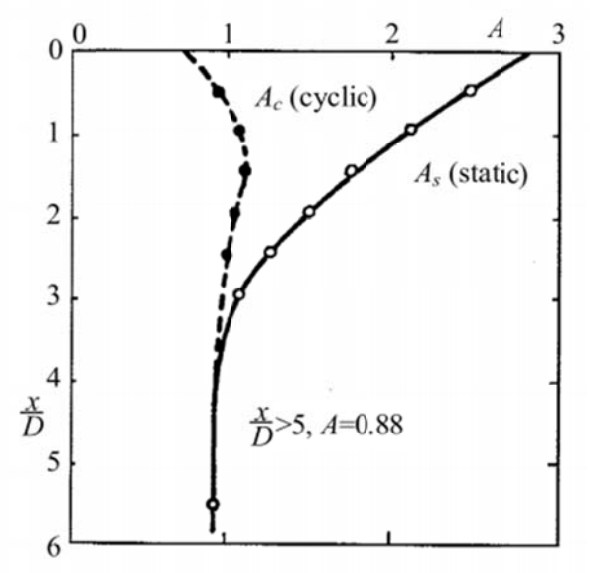

Figure 2.9: Non-dimensional coefficient A for determining the ultimate soil response

As mentioned before, apart from the ultimate load, the initial subgrade modulus and the nonlinear shape is required to build up the p-y curve. For the subgrade modulus, it was assumed that it varies linearly with depth:

$$K_{ini} = k_{ini}.z \quad (2.18)$$

Where: K_{ini} initial subgrade modulus

k_{ini} subgrade modulus coefficient

Z depth

The authors stated that the relative density and the water table level are two effective factors on determining k_{ini}. Their recommended values are shown in **Table 2.1**.

Table 2.1: Representative values of k_{ini} for sands (after Reese et al. 1974)

Relative Density	Loose	Medium	Dense
k_{ini} (below the water level) in kN/m^3	5400	16300	34000
k_{ini} (above the water level) in kN/m^3	6800	24400	61000

As for the nonlinear shape of the curve, the authors suggest that it consists of three parts: a linear part which stars from zero displacement with a slope of K_{ini}, a second line which ends at the ultimate load and a parabola connecting the two as shown in **Figure 2.10**. It is illustrated in the following step-by-step procedure. (Reese and Van Impe, 2001)

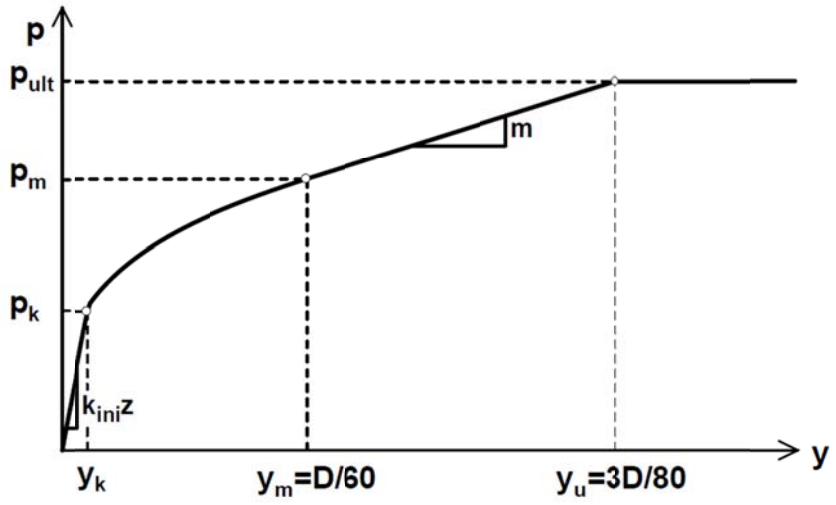

Figure 2.10: Characteristic p-y curves for sands (after Reese et al. 1974)

- Obtain values for the friction angle φ, the soil unit weight γ and pile diameter D.
- Select a depth at which the p-y curve is desired
- Calculate p_{ult} based on equations (2.11), (2.12) and (2.17)
- Establish y_u as 3D/80
- Establish y_m as D/60
- Calculate p_m based on the following equation

$$p_m = Bp_c \tag{2.19}$$

where B as shown in **Figure 2.11**, is an empirical non-dimensional coefficient depending on the depth and type of loading.

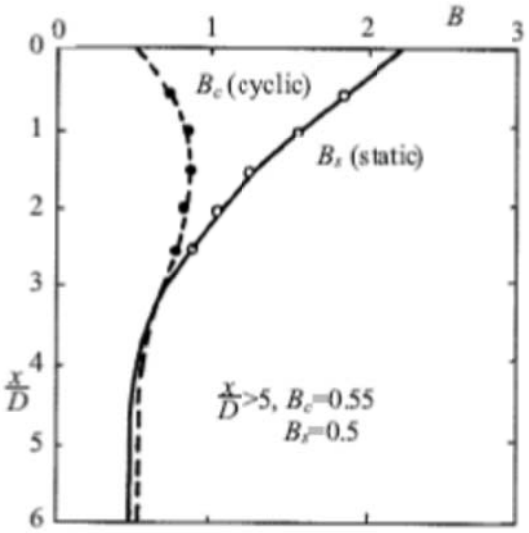

Figure 2.11: Values of non-dimensional coefficient B for soil resistance versus depth

- Establish the first straight-line section of the curve, choosing the appropriate value of k_{ini} from **Table 2.1**:

$$p = (k_{ini}z)y \tag{2.20}$$

- Establish the parabolic section of the p-y curve:

$$p = \bar{C}.y^{\frac{1}{m}} \tag{2.21}$$

- Fit the parabola between points k and m as follows:
  - Calculate the slope of the line between m and u

$$m = \frac{p_{ult} - p_m}{y_u - y_m} \tag{2.22}$$

  - Obtain the power of the parabolic section

$$n = \frac{p_m}{m y_m} \tag{2.23}$$

  - Calculate coefficient $\bar{C}$

$$\bar{C} = \frac{p_m}{y_m{}^{\frac{1}{m}}} \tag{2.24}$$

- Determine point k as follows:

$$y_k = \left(\frac{\bar{C}}{k_{ini}z}\right)^{\frac{n}{m-1}} \quad (2.25)$$

2.5.3. Murchison and O'Neill (1984) – API (2002)

Based on the work of Reese et al. (1974) and with the aid of additional experiments, Murchison and O'Neill (1984) proposed slightly modified and more simplified expressions for the formulation of the p-y curve. In this method, a hyperbolic tangent function was used to describe the nonlinear shape of the curves. Furthermore, three factors C_1, C_2 and C_3 were introduced and graphical representations were presented to replace lengthy equations for determining the ultimate soil pressure. The chart of adjustment factor A was also replaced by a linear equation. These modified p-y curves were accepted by *American Petroleum Institute (API, 1993; API, 2002)* committee as design guidelines for laterally loaded piles.

The procedure is presented in the following:

1. The ultimate soil resistance due to the wedge failure P_{cs} and due to the plain stress failure P_{cd} is calculated from relations (2.26) and (2.27) respectively. The minimum of the two is picked as the ultimate soil resistance.

$$P_{cs} = (C_1 z + C_2 D)\gamma' z \quad (2.26)$$

$$P_{cd} = C_3 D \gamma' z \quad (2.27)$$

Where $C_1, C_2\ and\ C_3$ can be obtained from **Figure 2.12**:

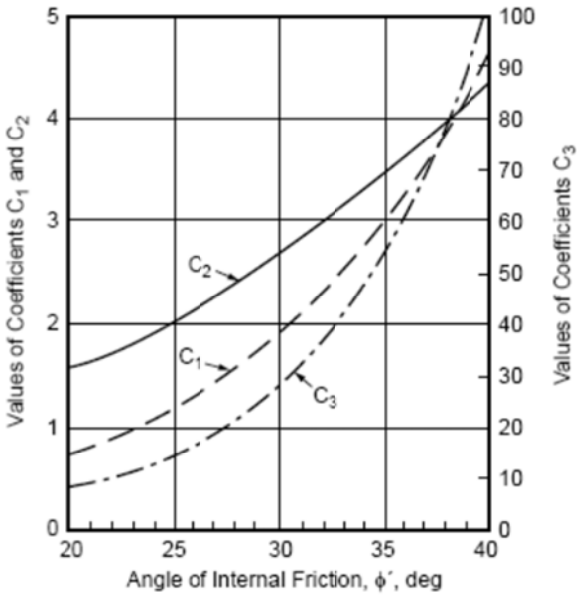

Figure 2.12: C1, C2 and C3 Coefficients as a functions of φ (API 2002)

2. The coefficient factor A is calculated from:

$$A = (3.0 - 0.8\frac{Z}{D}) \geq 0.9 \qquad \text{for static loading} \qquad (2.28)$$

$$A = 0.9 \qquad \text{for cyclic loading} \qquad (2.29)$$

3. The initial subgrade modulus – which is again assumed to vary linearly with depth – can be obtained from **Figure 2.13** as a function of relative density or the friction angle of the soil.

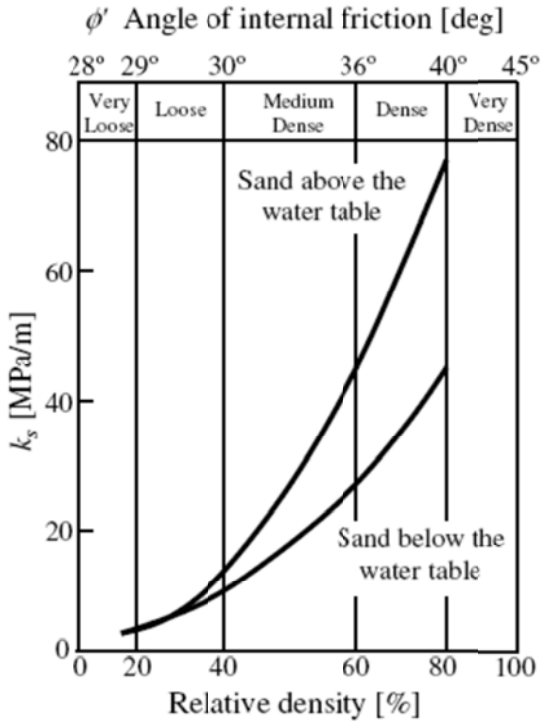

Figure 2.13: Initial modulus of subgrade reaction as a function of relative density of the friction angle of the soil (API 2002)

4. As mentioned before, a hyperbolic tangent function is used to describe the nonlinear shape of the curve which is estimated by the following expression:

$$P = P_{ult} \tanh\left(\frac{k_{ini} z y}{P_{ult}}\right) \qquad (2.30)$$

2.5.4. Georgiadis et al. (1992)

Based on centrifuge experiments on three open-ended steel pipes in dry sand, Georgiadis et al. (1992) proposed a methodology for determining the p-y curves for sands. The relative density of the sand was equal to 60%, corresponding to a unit weight of 16.3 kN/m^3 and the friction angle equal to 36˚. All three piles had the same length (L=9.05m) and the same material (E=1.928*10^8) but different diameter and wall thickness resulting in different flexural stiffness. The properties of the piles are summarized in **Table 1.1**.

Table 1.1: Properties of the piles used in centrifuge experiment (Georgiadis et al. 1992)

Piles	P_1	P_2	P_3
Outside Diameter (m)	1.092	1.224	1.229
Wall Thickness (mm)	44.45	17.25	15.25
Flexural Stiffness EI ($MN.m^2$)	3878.5	2495.0	2066.0

The lateral load was applied through a steel cable and was measured by a 2.5 kN load cell. The pile displacements were measured at two separate points above the soil surface and numerous strain gauges were installed along piles to evaluate the bending moment diagram along the depth.

The interpolation of the results led to the following suggestions for the construction of p-y curves for sands:

1. The ultimate soil resistance

The analytical model proposed by Reese et al. (1974) was used for the estimation of P_{ult} with a slightly different form for the empirical coefficient A as following:

$$A = 2 - \frac{z/D}{3} \geq 1 \qquad (2.31)$$

The values obtained by equation (2.31) are slightly smaller than the ones predicted by Reese et al. (1974) and API. However, the authors noted that the results are not sensitive to parameter A.

2. The initial subgrade modulus

The initial subgrade modulus was assumed to vary linearly with depth. However the use of values proposed by Terzaghi (1955) was recommended in order to estimate the gradient. These values are presented in **Table 1.2** which result in significantly smaller values compared to Reese et al. (1974) and Murchison and O'Neill (1984).

Table 1.2: Gradient of initial subgrade modulus (Terzaghi, 1955, recommended by Georgiadis et al. 1992)

Relative Density	Loose	Medium	Dense
K_{ini} (kN/m^3)	1100-3300	3300-11000	11000-23400

3. Nonlinear shape

For the nonlinear shape, the use of the following hyperbolic function, originally proposed by Kodner (1963) was recommended:

$$p = \frac{y}{\frac{1}{z.k_{ini}} + \frac{y}{p_{ult}}} \quad (2.32)$$

2.5.5. Det Norske Veritas (1980)

The Norwegian classification society Det Norske Veritas (1980) proposed a methodology based on empirical methods and a few full-scale tests. The various elements of the curve are defined as follows:

1. Ultimate Resistance

Based on the type of loading (i.e. static or cyclic), the ultimate load can be calculated:

Static loading:

$$p_{ult} = 4K_p\sigma_v D \quad (2.33)$$

Cyclic loading:

$$p_{ult} = 3K_p\sigma_v D \quad \text{for depths } z > 2D \quad (2.34)$$

$$p_{ult} = 3\frac{z}{2D}K_p\sigma_v D \quad \text{for depths } z \leq 2D \quad (2.35)$$

Where: K_p passive pressure which can be found from: $K_p = \frac{1+sin\varphi}{1-sin\varphi}$

σ_v effective overburden presssure

φ angle of shearing resistance

z depth

D pile diameter

2. Initial Subgrade Modulus

As for all the aforementioned methodologies, the linear variation of initial subgrade modulus is assumed. However, the values are modified according to **Table 1.3**.

Table 1.3: Initial subgrade modulus (Det Norske Veritas, 1980)

Relative Density	Loose	Medium	Dense
K_{ini} (kN/m^3)	5000	12000	18000

3. Nonlinear Shape

For the nonlinear shape of the curve, the same assumption of Georgiadis et al. (1992) is adopted, which is the use of hyperbolic function proposed by Kodner (1963). However, a factor $\alpha > 1$ is multiplied by p_{ult} in the function, resulting in a stiffer response of soil. It means that instead of p_{ult}, the asymptote of the hyperbola is $p = \alpha . p_{ult}$ which is shown in **Figure 2.14.**

$$p = \frac{y}{\frac{1}{z.k_{ini}} + \frac{y}{\alpha . p_{ult}}} \tag{2.36}$$

The multiplier α can be found from:

$$\alpha = \frac{1}{1 - \frac{p_{ult}}{0.04 k_{ini} z D}} \tag{2.37}$$

The latter is only valid when $\beta D > \frac{p_{ult}}{z.k_{ini}}$. Otherwise, the hyperbola is replaced by a straight line.

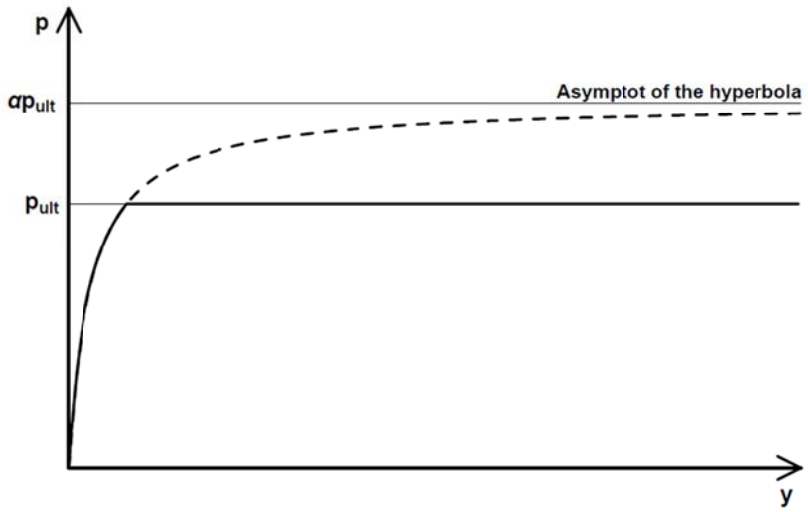

Figure 2.14: Characteristic shape of p-y curves (Det Norske Veritas, 1980)

It should be mentioned that the above formulas are mostly designed for offshore structures under lateral loads due to waves. In this case, the piles diameters are in the order of 1-1.5 meters and therefore, relatively stiffer than pile foundations normally used in geotechnical engineering projects.

2.5.6. Estimation of ultimate soil resistance based on passive earth pressure theory

A number of researchers tried to estimate the ultimate soil resistance of the soil based on passive earth pressure theory mostly for the case of short piles (for definitions refer to section 2.2.) which is a common case for piles subjected to lateral kinematic loads.

It should be noted that in the estimation of the ultimate resistance, it is assumed that the active earth pressure at the back of the pile is negligible. Besides, it is assumed that the passive earth pressure in front of the pile is significantly larger than the values obtained by passive earth pressure theory due to the shearing resistance on the vertical sides of the failure wedge of the soil. In order to include these effects, a multiplier α_u is utilized to increase the values given by Rankine theory to the desired ones. Consequently the ultimate pressure will have the following form:

$$p = \alpha_u K_p \gamma z D \quad (2.38)$$

Where: P soil resistance per unit length

α_u aforementioned multiplier

K_p passive earth pressure coefficient

γ unit weight of the soil

D diameter of the pile

Bransby (1996) states that he value of the α_u multiplier depends on the type of lateral loading, namely, active and passive pile loading shown in **Figure 2.15a** and **Figure 2.15b.** In active pile a horizontal force is applied at the head of the pile and passive pressures develop at the front of the pile. In passive pile loading, there is lateral ground displacement which causes the development of passive pressure at the back of the pile. Therefore, earth pressures act as resisting forces for active piles, and as stimulating force in passive piles.

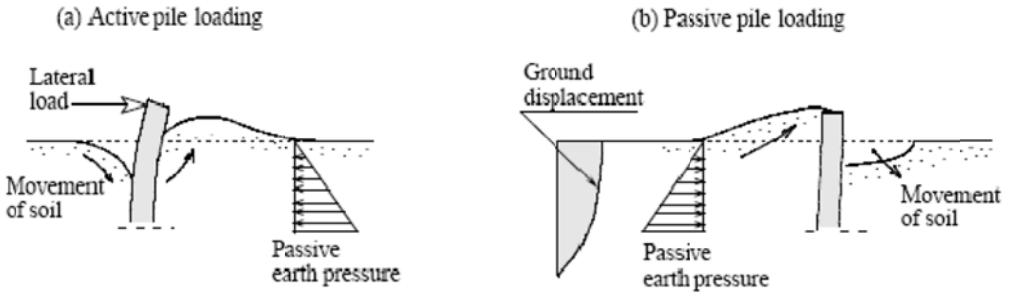

Figure 2.15: a) active and b) passive lateral loading of piles (Cubrinovski et al., 2005)

Based on experimental data, different formulas have been developed to estimate α_u which has a range between 3 and 7. It should be noted that the smaller values correspond to the active lateral loading of the piles whereas the larger ones refer to the case of passive loading. The selected formulas are presented:

Broms (1964) $\alpha_u = 3$

Fleming et al. (1992) $\alpha_u = K_p$

Prasad & Chari (1999) $\alpha_u = \frac{10^{1.3 \tan \varphi + 0.3}}{K_p}$

Cubrinovski et al. (2005) $\alpha_u = 4.5$

2.5.7. Japanese Regulations

According to Japanese Design Specifications (JRA, 2002), soil reaction can be found as a function of the pile deflection from the following expression:

$$p = k_h D y \tag{2.39}$$

Where k_h is the coefficient of subgrade reaction and D is the diameter of the pile. It should be mentioned that k_h is normalized with respect to the pile diameter. Therefore in order to make in comparable with the aforementioned value of initial subgrade reaction – which is normalized with respect to depth – we have to use the following formula:

$$k_{ini} = k_h \frac{D}{z} \tag{2.40}$$

In AIJ (Recommendations for Design of Building Foundations) k_h is evaluated as:

$$k_h = \alpha \xi E_0 B^{-3/4} \quad \text{kN/m}^3 \tag{2.41}$$

$$E_0 = 700N \quad \text{kN/m}^2$$

Where: y the lateral displacement of pile (in cm)

α constant (=80 for E_0 evaluation from N in sands)

ξ coefficient for the effect of group piles (=1.0 for a single pile)

E_0 Young's modulus (kN/m^2)

B width of the pile (cm)

According to JRA (Recommendations for Highway Bridges), the following formulas can be used to determine k_h:

$$k_h = k_{h0}\left(\frac{B_H}{0.3}\right)^{-\frac{3}{4}} \quad (2.42)$$

$$B_H = \sqrt{D/\beta} \quad (2.43)$$

$$\beta = \sqrt[4]{\frac{k_h D}{3EI}} \quad (2.44)$$

$$k_{h0} = \frac{\alpha E_0}{0.3} \quad (2.45)$$

$$E_0 = 2800N$$

Where: B_H normalized width of the pile (m)

D pile diameter (m)

B characteristic value

EI flexural stiffness of the pile ($kN.m^2$)

α constant value (=2 for E_0 evaluated from N-value)

E_0 Young's modulus (kN/m^2)

N SPT blow count

Finally in RTRI (Design Standards for Railway Facilities) k_h is estimated as:

$$k_h = f_{rk}(0.6\alpha E_0 D^{-\frac{3}{4}}) \quad (2.46)$$

$$E_0 = 2500N \quad (kN/m^2)$$

Where: F_{rk} resisting factor of soil (=1.0)

α constant value (=2 for E_0 evaluated from N-value)

D pile diameter (m)

E_0 Young's modulus (kN/m^2)

2.6. New numerical analysis

Given the uncertainties with regard to existing static P-y methodologies, the problem was investigated numerically by Vasilis Papaopoulo (2010). Namely, he performed a set of parametric analyses in which he investigated the effect of D_r , D, installation, head constraint, in which P-y curves were established numerically. Typical curves are shown in **Figure 2.16**.

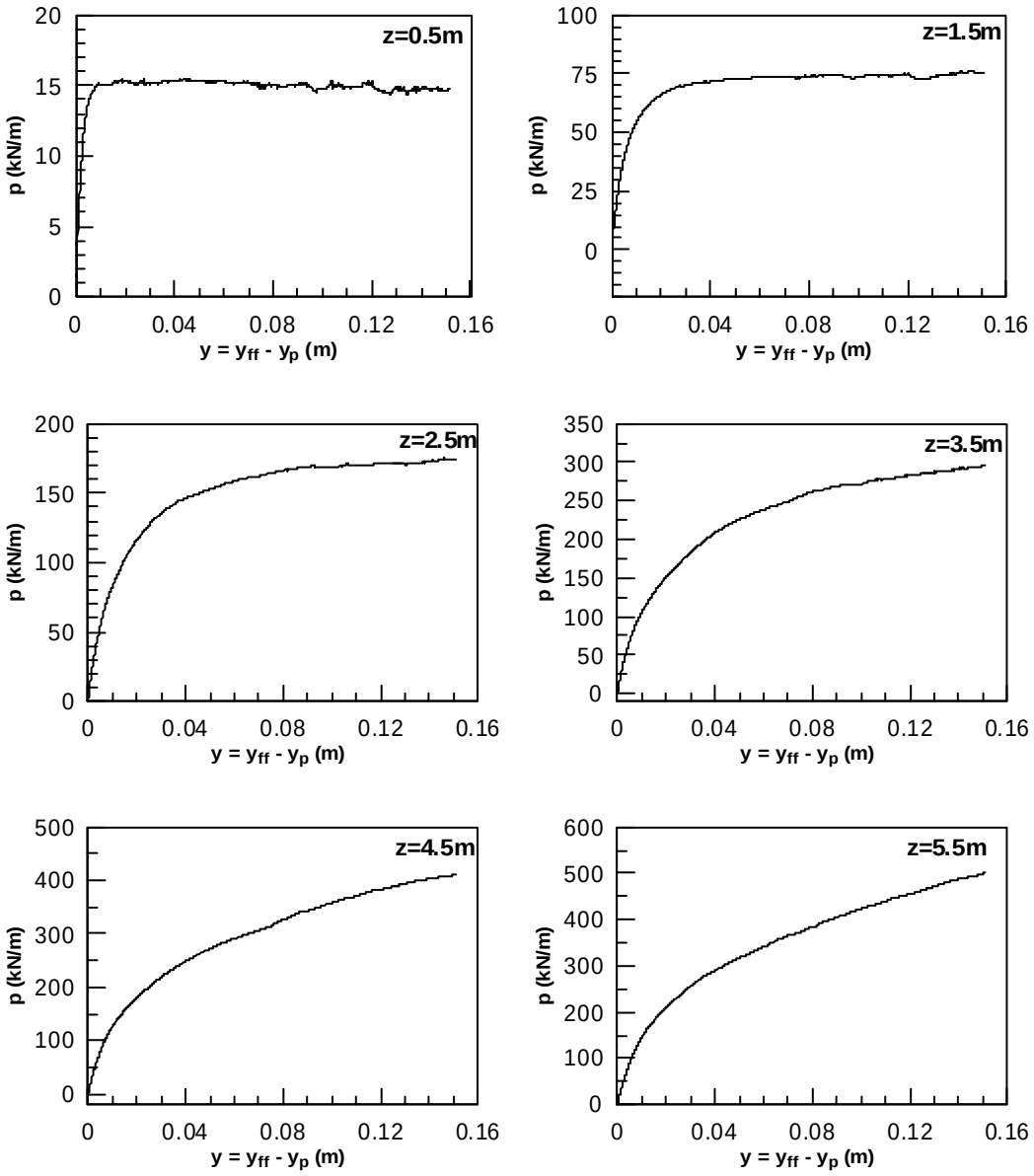

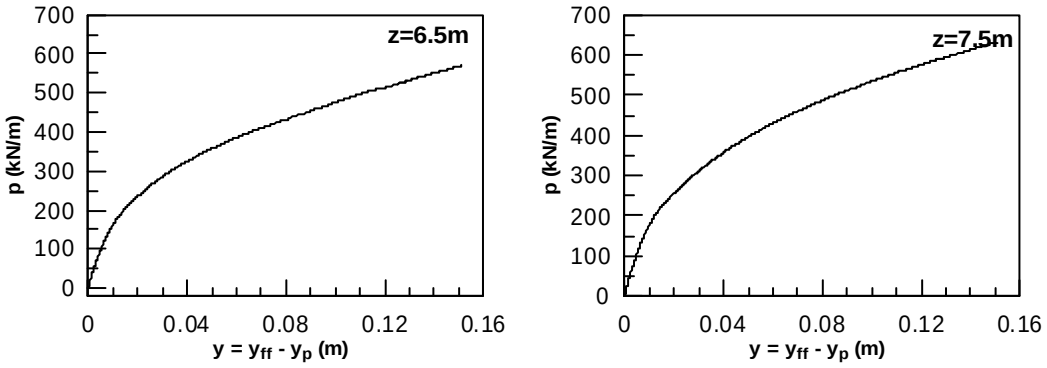

Figure 2.16: Typical static p-y curves (after Vasilis Papaopoulo (2010))

In this present thesis, those curves will be used as reference to evaluate degraded soil response due to liquefaction.

2.7. Conclusions

- **Differences between methods:** Numerous methodologies in order to estimate the lateral resistance of soil in terms of p-y curves are presented in the preceding paragraphs. It should be noted that these different methodologies do not result in similar predictions for any of the three important parameters in building a p-y curve (k_{ini}, P_{ult} and the shape). Therefore, still uncertainties exist in the adoption of any of them.
- **Limited range of parameters:** All the aforementioned methodologies are based on experimental tests and hence on a very narrow range of values for the various parameters involved. Consequently, the application of these methods for new conditions may not be wise.
- **Absence of other critical parameters:** A number of other parameters that may be crucial in the response of a laterally loaded pile are absent from the methodologies and their effect is ignored.

  For instance, all the experiments are done for the drilled piles and it is a question whether they can be applied for the cast-in-place piles as well noting that pile installation can alter the soil conditions around the pile significantly. Kim et al. (2004) performed a series of tests on driven and pre-installed piles

who concluded from the results (**Figure 2.17**) that pile installation method *does* affect the response.

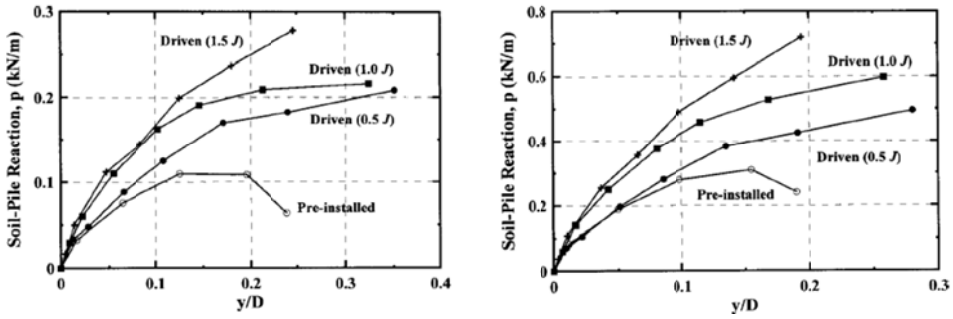

Figure 2.17: Effect of pile installation method on the lateral response of the soil (after Kim et al. 2004)

Taking into account all the uncertainties, in the large scale project, the use of full-scale field tests in order to define the p-y curves is recommended.

Chapter 3

The Cyclic p-y Method

3.1. General

Liquefaction and lateral spreading can alter the response of pile foundations to the lateral loads dramatically, and numerous case histories of damages due to this phenomenon have been observed in the past earthquakes (Hamada and O'Rourke 1992, Tokimatsu et al. 1996, etc.) due to the large lateral displacements which is detrimental to civil engineering structures. During lateral spreading, the buried pipelines are destructed to a great extent, the transportation routes are disrupted due to the destruction of the pavements, the subgrades and the destruction of bridge piers and piles. The buildings may also suffer significantly due to the failure of the pile foundations. Therefore, the importance of this phenomenon is undeniable and proper methods should be utilized to mitigate the risk or lower it to acceptable levels.

In current practice, design of piles is mostly performed with the p-y method, as described in the previous chapter. However, in the case of lateral spreading, the response of the pile is governed by the kinematic loading (i.e. load applied by the laterally spreading ground). Therefore, the setup of the method is changed as the following: Firstly, the ground displacements are calculated using existing methodologies available in the literature, and secondly, the calculated ground displacements are applied to the ends of the Winkler springs in order to calculate moments and deflections of the pile (Tokimatsu 1999, Boulanger et al 2003). In addition, soil liquefaction affects both the stiffness and the ultimate resistance of the soil. Hence, p-y curves, used to describe the response of the

degraded soil, should be properly modified. In this context, the present chapter focuses on the following:

a) Briefly introduce the lateral spreading phenomenon and present methodologies to evaluate the lateral soil displacement;
b) To present the current methodologies used in order to degrade the p-y curves;
c) Current experimental and numerical findings which introduce us previously ignored parameters in pile foundations response in laterally spreading soil.

3.2. Lateral Spreading and evaluation of horizontal displacements

"Liquefaction-induced lateral spreading" is defined as the lateral displacement of soil in a slightly sloped ground as a result of liquefaction which is in turn a consequence of pore pressure build up during the earthquake motion. It is apparent that the prerequisite of lateral spreading is a kind of topographical irregularities which allows the liquefied soil to *flow* during liquefaction. However, it should be noted that if liquefaction occurs in moderate to steep slopes, tremendous flow of the material in very large distances will occur. Therefore, here by lateral spreading we mean relatively moderate movement of mild slopes of 0.3 to 5% as described by Bartlett & Youd (1992), who state that the presence of a shallow water table and loose sands are also prerequisite of liquefaction-induced lateral spreading; a case mostly found near river banks or shore.

It should be noted that during the lateral spreading, settlement (vertical displacement) also occurs at a result of travelling of small particles to the ground surface. However the lateral displacement is of more practical importance to the civil engineering structures in general and pile foundations in particular. Consequently, the rest of the paragraph is devoted to methodologies that are used to estimate the horizontal displacements due to lateral spreading.

Evaluating this parameter is a highly difficult and nonlinear problem and includes a large number of factors. According to Bartlett & Youd (1992) the magnitude of lateral ground displacement in lateral spreading is controlled by four factors:

1. The degree of shear strength loss due to liquefaction;
2. Boundary conditions;
3. Static and dynamic shear forces acting on the mass of moving soil; and
4. The length of time when the exerted forces is larger than the resisting forces

The methodologies which exist in the literature for evaluation of lateral spreading displacement can be divided into 3 major groups:

1. Numerical Analyses (e.g. Finite difference methods)
2. Analytical Methods (based on simplified analytical relations); and
3. Empirical Relations based on statistical accumulation of case histories and experimental data.

Each of these categories is discussed separately in the following pages.

3.2.1. Numerical Methodologies

Numerical methodologies have the advantage that can take into account interaction of different factors such as time-history of the motion, the seepage related characteristics of the ground, exact geometry and local characteristics of the soil, etc. However, they are quite time consuming which make them inappropriate for practical purposes. Furthermore, their accuracy is highly dependent on the constitutive model that they use for the behavior of the soil, which, if not provided accurately, can give wrong results.

One of the earliest attempts has been done by Finn et al. (1990, 1991, 1994) who used a simple elasto-plastic constitutive model in a finite element mesh. He used codes with adaptive mesh procedure that permitted modification of the finite element grid to account for large deformations during the simulation. It was assumed that during liquefaction, the stress-strain curved kept its shape and just the residual shear strength reduced. This loss of strength caused an imbalance in the model which activated deformations up to a level where the redistribution of stresses led to a new equilibrium.

Similar attempt but rather simpler model was used by Kuwano et al.(1991) and Argano, (2002) Gu et al. (1993). In the latter, for simplification, undrained conditions were used along with a simple constitutive model for the liquefied soil.

More recently, several researchers have used more sophisticated constitutive models to account for the phenomenon. Examples are models that simulate the liquefied soil as a non-Newtonian liquid (Uzuoka et al. (1998); Hadush et al. (2000)) and simulation of soil response through multiple yield surface plasticity models (Elgamal & Yang (2000)) or bounding surface models (Valsamis et al. 2010; Dakoulas et al. (2006)).

3.2.2. Analytical methods

Analytical methods can be divided into two main categories: the one that are based on the Sliding Block Theory (Newmark, 1965) and those that are based on the Minimum Potential Energy Theory (Toehata et al. 1991, 1992).

Newmark's Sliding Block Theory

Newmark's theory is used to determine the residual displacements of a block on a frictional plane subjected to horizontal motions. The block moves relative to the plane when the inertial forces exceed the resisting force and the displacements in each cycle are calculated by double integration of the acceleration time-histories in time durations when the inertia forces exceed the resisting force. Adding these values during the whole time-history will give the accumulated displacement. Therefore, if the exact acceleration history of the excitation is available, the residual displacements can be found by using numerical integration methods. However, it is not possible to predict accurately the future earthquake excitation in a site. Hence, a number of simplified approaches exist which replace the real acceleration time-history with a simpler function. **Jibson (1993)** proposed that the acceleration history be replaced by a single measure of the total shaking intensity (i.e. Arias intensity ($I_a = \frac{\pi}{2g}\int a^2 dt$). After analyzing numerous records from real excitations, he proposed the following relationship:

$$\log D = 1.460 \log I_a - 6.642 a_y + 1.546 \quad (3.1)$$

Where: D predicted ground displacement (in cm)

I_a Arias intensity (in m/s); and

a_y yield acceleration (in g)

Another approach in order to bypass the uncertainty with regard to the real acceleration history is the use of *equivalent* base acceleration history (Yegian et al. (1991)). In this way, a mathematical function is used to express the excitation, for which, the integration can be performed in the closed-form. Thus, the predicted displacements can be calculated as:

$$D = N_{eq}\, T^2\, a_p\, f(\frac{a_y}{a_p}) \tag{3.2}$$

Where: D predicted displacements,

a_y yield acceleration

N_{eq} number of cycles

T period

a_p peak acceleration

f dimensionless function which depends on the assumed shape of the base acceleration record.

Authors proposed the following polynomial for the function f after analyzing 86 actual ground motion records:

$$\log f\left(\frac{a_y}{a_p}\right) = 0.22 - 10.12\left(\frac{a_y}{a_p}\right) + 16.38\left(\frac{a_y}{a_p}\right)^2 - 11.48\left(\frac{a_y}{a_p}\right)^3 \tag{3.3}$$

With a similar approach **Baziar et al. (1992)** assumed a sinusoidal function as the equivalent base acceleration and proposed that the displacement can be calculated from equation 3.4:

$$D = N_{eq}(\frac{{v_p}^2}{a_p})\ f(\frac{a_y}{a_p}) \tag{3.4}$$

Where a_p and v_p are the peak horizontal acceleration and velocity of an earthquake record.

Baziar et al. (1992) also followed a different approach in order to estimate the lateral displacement. The authors expressed the yield acceleration in terms of the normalized undrained strength of the liquefied soil (S_u/σ'_v) (It should be noted that S_u is the maximum shear stress measured during failure in an undrained test and not the shear stress on the actual plane and is assumed to remain relatively constant at large strains). In this kind of analysis, no upslope movement is computed due to the assumption that the liquefied soil will fill the tension cracks that form in the lateral spread. The proposed relation is:

$$D = N_{eq}\left(\frac{V_p}{a_p}\right)\frac{1}{f\left(\frac{a_y}{a_p}\right)} \tag{3.5}$$

Another approach based on Newmark's sliding block theory has been proposed by Byrne et al. (1992) which replaced the equilibrium of forces with the conservation of energy (i.e. the change in kinetic energy of the sliding block is equal to the difference in the input energy and the work done to overcome resistance of the soil). This model can express changes in shearing resistance as a function of displacement.

Haigh et al. (2001, 2002) proposed the use of a model based on effective stress and therefore, leading to a time-dependent simulation of lateral spreading. This modification changed the classic Newmark's *sliding accelerations* from relations (3.6) and (3.7) to (3.8) and (3.9).

$$\alpha_{upslope} = -\frac{g(\tan\beta+\tan\varphi)}{1-\tan\beta.\tan\varphi} \tag{3.6}$$

and

$$\alpha_{downSlope} = \frac{g(\tan\beta-\tan\varphi)}{1+\tan\beta.\tan\varphi} \tag{3.7}$$

to:

$$\alpha_{upslope} = -\frac{g(\tan\beta+\tan\varphi-\frac{(u\tan\varphi)(1-r)}{\sigma_v\cos\beta})}{1-\tan\beta.\tan\varphi} \quad (3.8)$$

and

$$\alpha_{downSlope} = \frac{g(\tan\beta-\tan\varphi-\frac{(u\tan\varphi)(1-r)}{\sigma_v\cos\beta})}{1+\tan\beta.\tan\varphi} \quad (3.9)$$

Where β slope angle

φ soil friction angle

σ_v total normal stress on the slip surface

u pore pressure; and

r ratio of the residual shear strength of the fully liquefied soil to the maximum strength with zero excess pore pressure

More recently, Arulmoli et al. (2004) proposed an iterative methodology in order to take into consideration the *Pinning Effect* of the piles. To accomplish this, they added shear forces developed in the pile to the residual shear strength of the soil. Hence, the required number of piles in order to reduce the lateral displacement to tolerable limits could be determined.

To sum up, it should be mentioned that although the methods based in Newmark's sliding block theory are theoretically strong and give rational values, they have several shortcomings which can adversely affect the accuracy of the results. The most important difficulties are:

1. Accurate evaluation of residual shear strength of the liquefied soil is not an easy task;
2. The lack of a well-defined slip surface in lateral spreading case makes it unrealistic to use a simple yield acceleration; and
3. Lateral spreading can continue after the end of excitation which is not possible to be captured by this type of model.

Minimum Potential Energy Model

The concept is based on the work by Towhata et al. (1991, 1992) who followed a completely different approach in order to estimate the lateral displacement. They assumed that the flow continues until the mass of the soil reaches the minimum level of potential energy. Consequently, it underlies the assumption that the excitation is long enough to mobilize the full capacity of the flow in the liquefied soil. As a result, this model can give an estimate of the maximum possible lateral displacement of a specific site.

Since then, a number of researches have proposed derivations from Towhata's model namely Tokida et al. (1993), Towhata & Toyota (1994). However, they main drawback which is the estimation of the maximum possible displacement still exist. Furthermore, since the methodology consist of integration over the volume of the soil in order to define the potential energy, its application is limited to simple geometries.

3.2.3. Empirical Relations

Unlike analytical methods, empirical relations do not depend on a mechanical idealization of the lateral spreading phenomenon. Instead, they just try to correlate the displacement with various parameters which can be *seismological parameters* (i.e. properties of the earthquake motion), *engineering parameters* (i.e. geotechnical properties of the site), or a combination of the both. Various attempts have been done to find such empirical relations from which the most widely used are presented here.

Youd & Perkins (1987) developed a correlation between ground displacement and earthquake parameters suitable for developing regional maps of liquefaction hazard. Based on case histories of earthquakes in Western United States and Alaska and came up to relation 3.10:

$$\log LSI = -3.49 - 1.86 \log R + 0.98\, M_w \qquad (3.10)$$

Where: LSI *Liquefaction Severity Index* defined as the general maximum magnitude of ground displacement, measured in millimeters divided by 25;

R horizontal distance to the earthquake source (in km)

M_w moment magnitude of the earthquake excitation

Since then, the authors have enriched the database and revised the formula to include more parameters. The newest version according to Youd et al. (2002) is:

$$\log D = -16.213 + 1.532\,M - 1.406\log R^* - 0.012R + 0.338\log S + 0.540\log T_{15} + 3.413\log(100 - F_{15}) - 0.795\log(D_{5015} + 0.1\ mm) \quad (3.11)$$

$$\log D = -16.713 + 1.532\,M - 1.406\log R^* - 0.012R + 0.592\log \mathrm{W} + 0.510\log T_{15} + 3.413\log(100 - F_{15}) - 0.795\log(D_{5015} + 0.1\ mm) \quad (3.12)$$

Where: D predicted ground displacement at the ground surface (in m)

M moment magnitude of the earthquake excitation

R horizontal distance to the earthquake source (in km)

R* $R^*=R_o+R$ where $R_o=10^{(0.89M-5.64)}$

T_{15} average cumulative thickness of the saturated granular layers with corrected blow count $(N_1)_{60}$ less than 15 (in m)

F_{15} average fines content of the granular soil included in T_{15} (in percent)

D_{5015} average mean grain size of granular soil included in T_{15} (in mm)

S ground slope (in percent)

W free-face ratio (defined as the height of the free face divided by the distance from the base of the free face of the desired point (in percent)

It should be noted that the aforementioned relations give an upper-bound of the displacements and not the realistic values.

Hamada et al. (1986, 1987) studied the data from case histories of lateral spreading in Niigata and Noshiro, Japan and the San Fernando Valley, California to obtain the correlation 3.13 which used engineering parameters:

$$D = 0.75\sqrt[2]{H}\sqrt[3]{\theta} \quad (3.13)$$

Where: D horizontal displacement (in m)
H thickness of the liquefied layer (in m)
θ slope (in percent)

Hamada (1999) upgraded the previous relation by including the soil density and the earthquake density to:

$$D = \frac{0.0125H^{0.5}\theta}{\bar{N}^{0.88}}\sum {a_i}^{0.48}t_i \quad (3.14)$$

Where: $\bar{N}$ average corrected SPT blow count of the liquefied layer
α_i mean horizontal acceleration in the i-th parth of the acceleration time-history
t_i time length of the i-th part of the acceleration time-history

Rauch & Martins (2000) developed a methodology based on case histories from 15 earthquake excitations. It should be noted that their correlation is meant to give the average ground displacement and not the absolute maximum. Depending on the available sort of data, the authors proposed three relations. Relation (3.15) solely includes seismological data, relation (3.16) seismological and geometrical data of the site and finally equation (3.17) includes geotechnical data apart from the aforementioned parameters. According to Rauch & Martin (2000), relations that include more data, give more accurate results:

$$Avg_{Horz} = (0.613M - 0.0139R - 2.42A_{max} - 0.0114T_d - 2.21)^2 + 0.149 \quad (3.15)$$

$$Avg_{Horz} = \big(0.613M - 0.0139R - 2.42A_{max} - 0.0114T_d + 0.000523L_{slide} + 0.0423S_{top} + 0.0313H - 2.44\big)^2 + 0.111 \quad (3.16)$$

$$Avg_{Horz} = \left(0.613M - 0.0139R - 2.42A_{max} - 0.0114T_d + 0.000523L_{slide} + 0.0423S_{top} + 0.0313H + 0.0506Z_{FS\,min} - 0.0861Z_{liq} - 2.49\right)^2 + 0.124 \quad (3.17)$$

Where: Avg_{Horz} average value of the predicted lateral displacement (in m)

- A_{max} peak horizontal ground acceleration (g) in absence of liquefaction
- T_d duration of the strong motion, defined as the time between the first and the last occurrence of surface acceleration larger than 0.05g (in sec)
- L_{slide} maximum horizontal head to toe length of lateral spread along the prevailing direction of movement (in m)
- S_{top} average slope along the direction of lateral spreding (in percent)
- H_{face} height of the free-face (in m)
- $Z_{FS\,min}$ average depth to the minimum factor of safety in the potentially liquefiable soils (in m)
- Z_{liq} average depth of the top of the liquefied soil (in m)

The most recent seismological correlated relation is proposed by Zhang et al (2005) based on the database of Youd et al. (2002). Although their relations give more accurate result compared to the correlation proposed by Youd et al. (2002), it is significantly more difficult to apply since it requires much more parameters to be defined in advance. The relations are not presented here and the reader is referred to Zhang et al. (2005) for more information.

Aydan et al. (2005) found the following correlation:

$$D = \frac{\gamma_s H^2}{G_1} \sin(\theta . v_{max}) \quad (3.18)$$

Where: γ_s unit weight of the liquefied soil (in kN/m^3);

- v_{max} maximum ground surface velocity (in m/sec);
- θ ground inclination (in percent); and
- G_1 residual shear modulus during liquefaction (in kPa).

Valsamis et al. (2010) proposed equation (3.19), based on extensive numerical parametric study of the problem:

$$D_h = 38.6\left(\frac{\alpha_{max}\tan i}{(N_1)_{60}}\right) H_{liq}^{tot} T_d (1-FC)^{3.5}\left(\frac{\alpha_{mean}}{\alpha_{max}}\right)^{0.5} \quad (3.19)$$

Where: D_h horizontal ground displacement
α_{max} maximum acceleration
i inclination of the ground surface
H^{tot}_{liq} cumulative thickness of the liquefied layer
T_d duration of strong excitation
FC fines content
A_{mean} mean value of the acceleration

The authors also studied the accuracy of 11 empirical relationships against the numerical data and case histories and concluded that the best estimations were obtained by Hamada (1999) and Youd et al. (2002).

Finally, it should be mentioned that regarding the inaccuracies of all of the aforementioned methodologies, along with the inaccuracies in determination of the input data to be used in each method, the application of more than one method in prediction of lateral displacements is recommended.

3.2.4. Variation of lateral displacement with depth

It should be mentioned that apart from the maximum displacement (which occurs at the ground surface) the variation of the ground lateral displacement with depth is also of great importance in the evaluation of the response of the pile foundations. It is unanimously accepted that the maximum ground displacement occurs at the surface and that the displacement at the maximum depth of the liquefied layer is equal to zero. However, two different relations are suggested for the shape of the displacement profile. Sento et al., 1999, for instance, have suggested linear relation whereas Ishihara &

Kubrinovski, 1998; Tokimatsu, 1999; Towhata, 2005 and Valsamis et al. 2010 have suggested sinusoidal relation that can be expressed as:

$$D(z) = D_H \sin\frac{\pi(H-z)}{2H} \quad (3.20)$$

Where: z depth where the displacement is desired (in m)
H thickness of the liquefiable soil layer (in m)

3.3. Effect of Liquefaction on p-y Curves

Liquefaction and lateral spreading has caused extensive damages to the pile foundations in major earthquakes around the globe. The degradation of the stiffness and strength of the liquefied soil can cause severe overloading to the pile foundation during the earthquake motion. An extensive database of observations and case histories of damages have been documented (e.g. Hamada and O'Rourke 1992, Tokimatsu et al. 1996 and Japanese Geotechnical Society JGS 1996, 1998). The problem is exacerbated in the case of lateral spreading where soil exerts lateral loading on the pile rather than providing support for the lateral load applied by the super structure.

Liquefaction can significantly modify the response of a laterally loaded pile due to the pore pressure build up in the liquefied soil which can alter the interaction mechanism between the pile and the soil, therefore, modified p-y curves should be used to model liquefied soil.

In practice, degradation is simulated by applying reduction multipliers on the original p-y curve (i.e. nonliquefied soil). This degradation factor has been correlated to a number of parameters (excess pore pressure, soil pile relative displacement, relative density of the soil, etc.) by different researchers (Dobry et al., 1995; Brandenberg, 2005; Cubrinovski 2005). However, some methods are difficult to apply because the correlated parameter may not be easy to measure in site. Additionally the results of different methodologies

are significantly different for a particular soil condition which shows the uncertainty of the results. It should also be noted that recent studies (Haigh, 2002; Gonzalez et al., 2009; Boulanger et al., 2007) have shown that the reduction multiplier approach may be over simplifying since the phenomenon is highly complicated and dependent on a variety of parameters. Consequently, the problem is not considered as *solved* in the literature and extensive research is being carried out by different research groups using numerical methodologies along with experiments in order to define the effect of different parameters on the response of the pile foundations in laterally spreading ground. After performing a vast literature survey, the following paragraphs present current methodologies and approaches are presented along with recent attempts to identify the remaining crucial parameters in the response of a pile foundation in laterally spreading ground.

One of the earliest attempts to estimate the degradation factor was done by **Dobry et al. (1995)** who performed centrifuge test including post-liquefaction cyclic loading – which continued while the excess pore pressure dissipated – for a pile foundation in soil specimen with relative density D_r = 40%. By analyzing the bending moment response of the pile, the researchers found a linear relation between the degradation factor m_P and the excess pore pressure ratio. As it is shown in **Figure 3.1** m_P reaches a value of 0.1 for complete liquefaction.

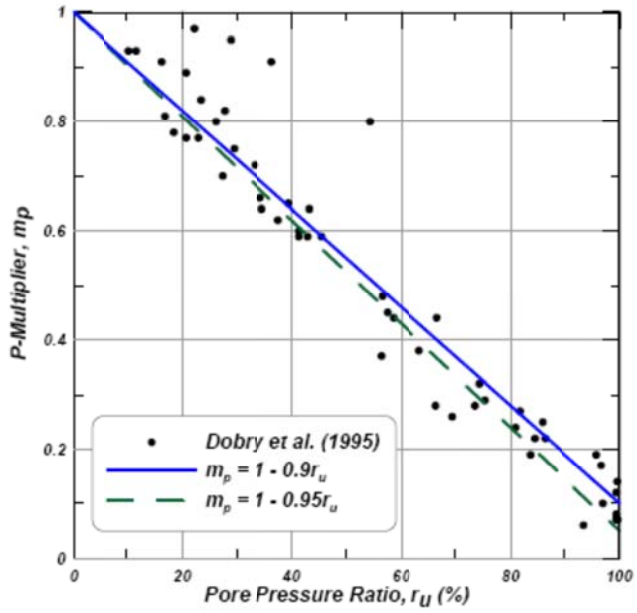

Figure 3.1: m_p multiplier as a function of excess pore pressure ratio (After Dobry et al., 1995)

Similarly, Senoto et al. (1999) found a linear correlation between the excess pore pressure build up and the degradation factor (which was called β in this study) based on analyzing pile failure during Kobe earthquake:

$$\beta = 1 - r_u \tag{3.21}$$

This becomes equal to zero for the case of complete liquefaction.

In a more recent study, based on result from shaking table test and numerical analyses, Han et al. (2007) found an exponential relationship:

$$m_P = e^{-3.2431(r_u)} \tag{3.22}$$

The most important disadvantage of the three above relations is that they are difficult to apply since the excess pore pressure with depth is hard to predict. In addition, response is mostly controlled by pore pressure build-up near the pile and not the free-filed.

Wilson et al. (1999, 2000) used centrifuge tests on piles installed in level ground profile (i.e. no lateral spreading). They found that the resistance was dependent on the relative density of the soil. Furthermore, they found that apart from the relative density, rate effects and drainage conditions affects the response.

Brandenberg (2000) suggests the use of API (1995) curves with a degradation factor that depends on the SPT blow-count$(N_1)_{60-CS}$. The researchers also state that there is not enough data available to determine the effect of other parameters and therefore a safety factor of 2 should be used.

Abdoun et al. (2003) performed centrifuge tests on different models including 2 and 3 soil layers, single and group piles and in some cases, local densification of the liquefied soil around the pile to simulate pile driving. They observed that in all cases, the maximum bending moment occurred at the boundaries between the liquefied and non-liquefied soil. Additionally, they observed that the presence of local densification caused an increase in the maximum bending moment due to an increased effective area of the pile foundation exposed to the lateral soil pressured, indicating the importance of pile installation method on the response to the lateral spreading.

Brandenberg et al. (2005) conducted centrifuge tests on single and group piles of different stiffness in laterally spreading ground under different earthquake motions. They also observed that for relatively stiff piles, the liquefiable soil pushed the piles downslope along the crust. While for more flexible piles, liquefiable soil produced large upslope forces against the downslope pressure of the crust.

Large transient increase in the subgrade reaction (called “dilation spikes”) was observed due to the transient drop of excess pore water pressure around the pile as a result of soil

dilation. These dilation spikes were different for motions with different frequency content indicating that the loading rate effects should also be taken into account.

Brandenberg et al. (2007) used Static beam on nonlinear Winkler foundation analyses to evaluate design guidelines against a suite of centrifuge test data for pile in laterally spreading ground. Lateral displacement of the ground was simulated by two methods: imposing free-field soil displacements to the free ends of the p-y elements (BNWF_SD) or imposing limit pressures directly to the pile nodes (BNWF_LP). The results showed that BNWF_SD analyses provided reasonable predictions with pile bending over-predicted and pile cap displacements under-predicted on average and was more accurate for stiffer piles. The alternative BNWF_LP analyses only provided reasonable predictions for large motions, but over-predicted the bending moment for small and medium motions because the ground displacements were not large enough to mobilize the limit pressures. It was also observed that permeability affects the rate of excess pore water pressure dissipation around the pile and affects the subgrade reaction behaviour. The same observation had been seen during centrifuge experiments by Gonzales (2005) and numerical analyses performed by Uzuoka et al. (2005)

Brandenberg (2005) and Brandenberg et al (2007) proposed the chart shown in **Figure 3.2** for estimating m_P. The figure compares the aforementioned recommendations with AIJ (2001) (Japanese Recommendations for design of building foundations) which shows agreement for soils with low density only. It should be noted that the proposed degradation factor is only a function of relative density of the soil while the experiments showed dependence of subgrade reaction to the stiffness of the pile, frequency content of the motion and the permeability of the soil.

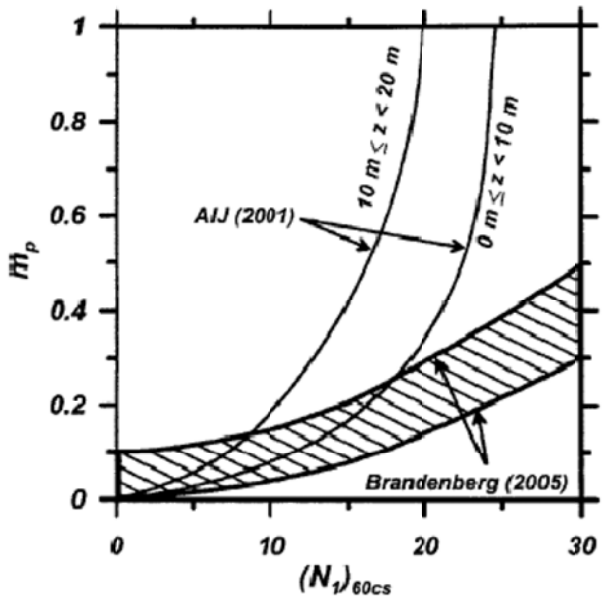

Figure 3.2: Degradation multiplier m_p correlated to relative density (After Brandenberg et al. 2007)

A group of researchers tried correlating the degradation multiplier with the relative displacement between the pile and the ground. One of the earliest studies has been done by Ishihara & Cubrinovski (1998) who based on large scaling tests proposed the use of the chart shown in **Figure 3.3** which gives the degradation factor β as a function of the thickness of the liquefied layer and the relative displacement.

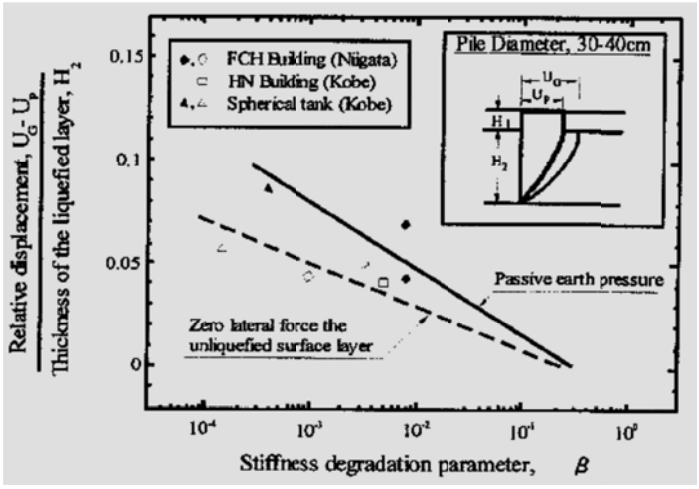

Figure 3.3: Degradation multiplier β correlated to the thickness of the liquefied soil and the relative displacement (After Ishihara & Cubrinovski 1998)

Orense et al. (2000) performed large scale shaking table test in order to correlate degradation factor to the relative displacement. The layout of the test and the results are shown in **Figure 3.4** and **3.5.**

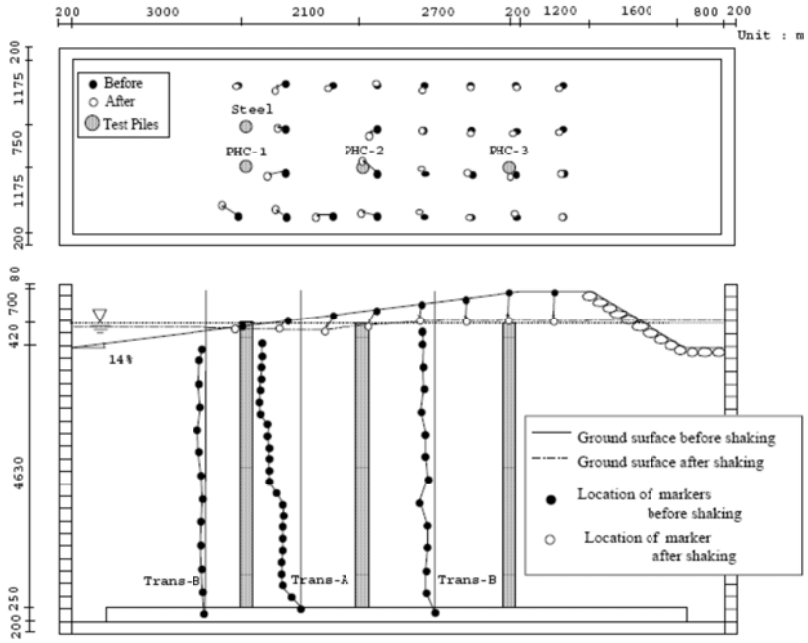

Figure 3.4: Layout of the test to determine the degradation factor as a function of relative displacement (after Orense et al., 2000 and Yasuda et al., 2000)

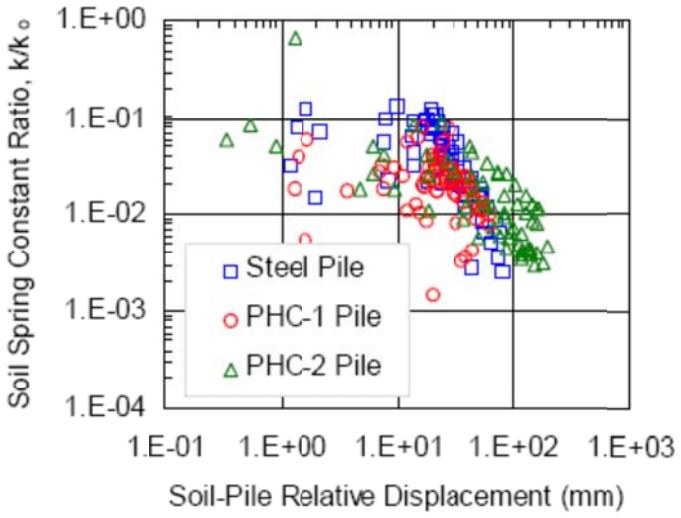

Figure 3.5: Degradation factor as a function of relative displacement (Orense et al., 2000)

Overall, the authors concluded that the degradation factor β is reduced when the relative displacement is increased, form 0.1 to 0.002 for relative displacement from 1 to 200mm respectively.

Cubrinovski et al. (2006) performed shaking table tests on stiff and flexible piles in order to evaluate the degradation factor which led to the chart shown in **Figure 3.6** as a function of the relative displacement with an average value of 1/55. It should be noted that the scatter of the data is significant for small values of relative displacement which shows the importance of other parameters particularly pile stiffness because the scatter in large lateral displacements (i.e. flexible piles) is considerably lower.

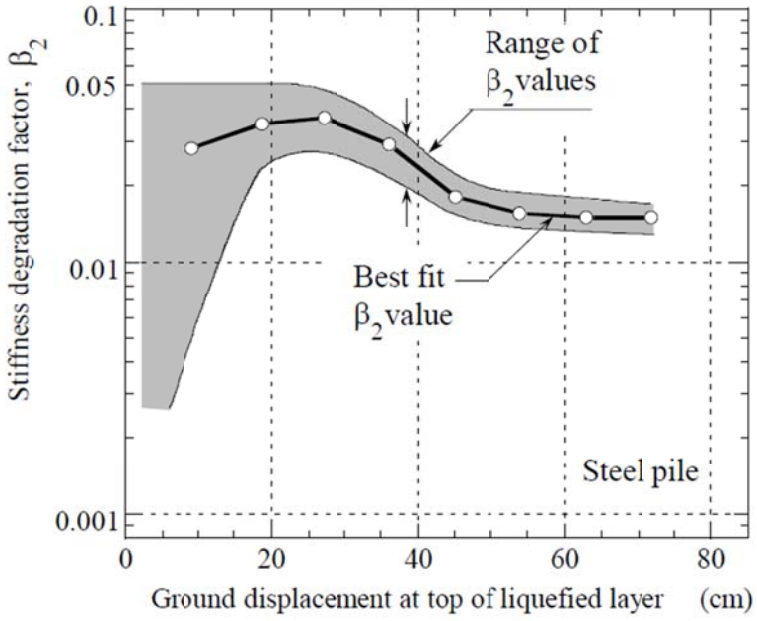

Figure 3.6: Degradation multiplier β correlated to the relative displacement (After Cubrinovski et al. 2006)

Tokimatsu & Suzuki (2004, 2009) performed shaking table test to investigate the mechanisms that govern the reaction of the liquefied soil. They concluded that unlike the dry soil where the subgrade reaction is induced by the compression of the soil due to pile

oscillation, the response in the liquefied soil is dependent on excess pore pressure changes and soil dilation around the pile. Back calculation of the p-y curves showed transient hardening response (i.e. in each individual cycle) due to large dilation but an overall softening behaviour. It was seen that the transient variations were more significant for denser soils and stiffer piles which confirms the dependence of the response to the relative density of the soil and the stiffness of the pile.

Bowles (2005) focused on the shape of the liquefied p-y curve of the liquefied soil. Using the results of the large scale tests performed by Ashford and Rollins (2000) he concluded that the shape of the p-y curve changes completely due to liquefaction and changes from a softening curve to hardening. The same results were found by Dash et al. (2008). The authors analyzed the results of the experiments carried on earlier by Yasuda et al. (1999), Takahashi et al. (2002) and Rollins et al. (2005) and found a S shaped p-y curve for the liquefied sand as showed in **Figure 3.7** However, the seems to simulate the behaviour of the liquefied soil in a single load cycle and the overall response of the soil seems to be softening (Tokimatsu & Suzuki 2004, 2009).

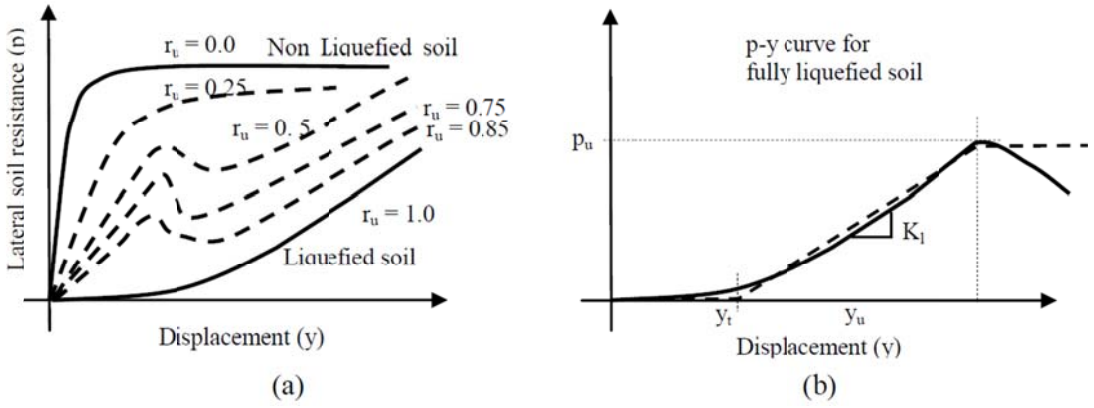

Figure 3.7: (a) p-y curve for saturated sandy soil during the process of liquefaction. (b) Simplified p-y curve model for liquefied soil. (After Dash et al. 2008)

Dungca et al. (2005) studied the effect of soil permeability and loading rate on the lateral resistance of the liquefied soil and observed that the resistance increased as the ratio of lateral loading rate over permeability increased. The results are shown in **Figure 3.8.**

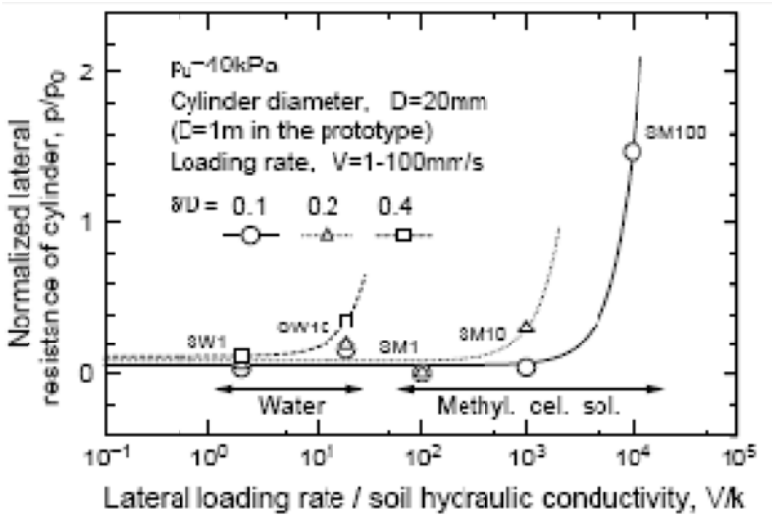

Figure 3.8: Lateral resistance versus the ratio of loading rate over soil permeability (After Dungca et al. 2005)

Uzuoka et al. (2005) performed numerical analyses using finite element model for spatial discretization of the equilibrium while finite difference model was used to simulate pore water pressure. The researchers studied the effects of soil permeability, pile diameter, degree of liquefaction and loading rate and correlated the lateral resistance with the dimensionless time factor T* defined as:

$$T^* = \frac{kK}{\gamma_w D v} \tag{3.23}$$

Where: k soil permeability
K the bulk modulus
D diameter of the pile
V velocity of the pile

The correlation is shown in **Figure 3.9** for two values of pile displacements: 0.125 and 0.25 m. It shows that the pile displacement is also an important factor not captures by the concept of the dimensionless time factor.

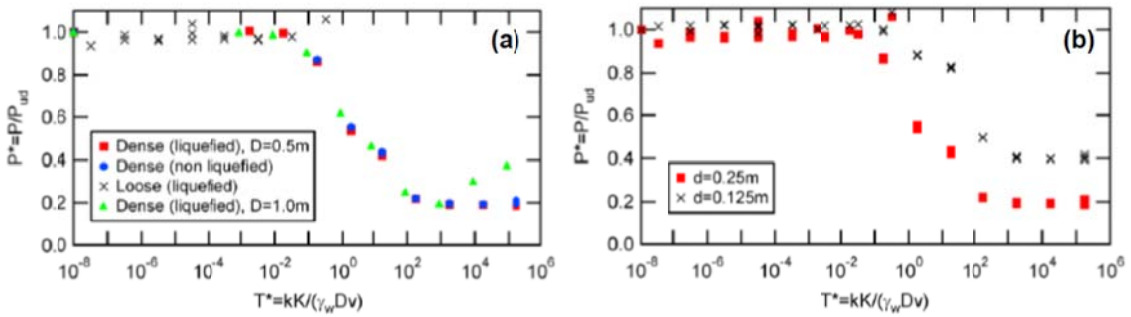

Figure 3.9: Lateral resistance versus the time factor for displacement of the pile equal to: a) d=0.25m and b) d=0.125m (After Uzuoka et al. 2005)

Gonzalez et al. (2009) also examined the effect of soil permeability on the response of end-bearing single and group pile subjected to lateral spreading. They conducted centrifuge tests once using water and another time using a viscous liquid as the pore liquid hence simulating two sands of different permeability in the field. They observed that although the soil acceleration in free field was not significantly affected by the soil permeability, drastic differences occurred in the near field especially at shallow depths. It was observed that the reduction in excess pore water pressure in low permeable specimen caused the development of a non-liquefied zone around the pile with the shape of an *inverted cone* (**Figure 3.10**). Consequently, larger area is affected while in highly permeable sample, water came from the free field to dissipate the negative pore pressure.

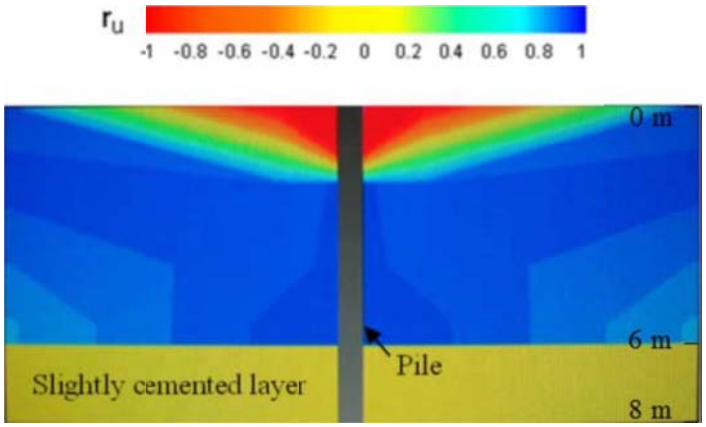

Figure 3.10: Pore pressure ratios r_u during shaking (After Gonzalez et al. 2009)

As a result, in the more permeable sample (i.e. water as pore liquid), displacement reached a maximum and bounced back since soil started to flow around the pile after a few second. In the other sample, however, displacement continued to increase an ended up with much larger final displacement. The back calculated p-y curves for the two models are shown in **Figure 3.11** which shows the undeniable effect of soil permeability in piles in laterally spreading ground.

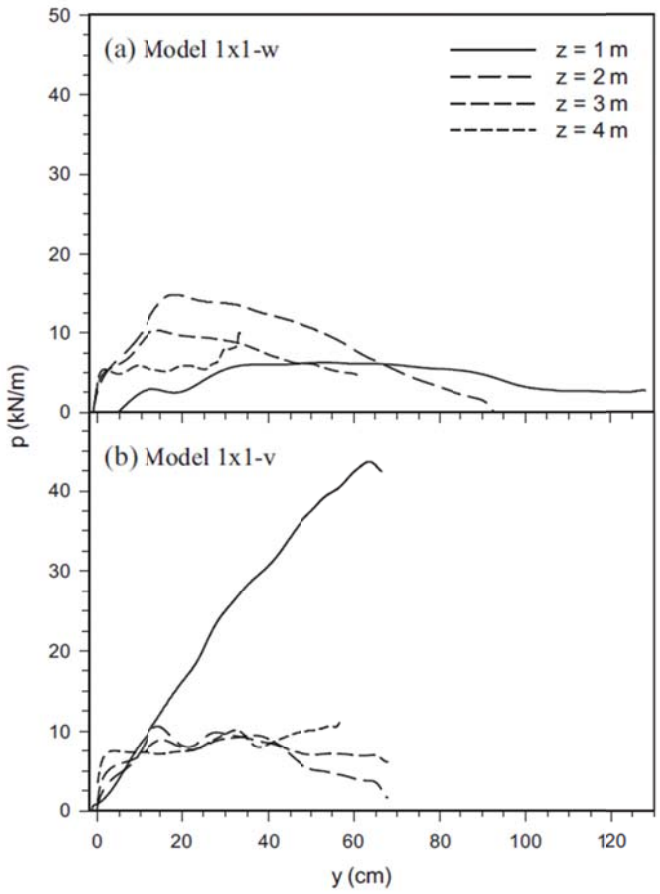

Figure 3.11: p-y curves calculated for a) high and b) low permeability material (After Gonzalez et al. 2009)

Tokimatsu and Suzuki (2009) conducted large shaking table test on soil-pile structure models with dry and saturated sand to examine the effects of inertial and kinematic forces on the lateral response of the soil. They concluded that in non-liquefied soil the inertial forced exerted by the superstructure are dominant while in the liquefied soil, both the

inertial forces of the superstructure and the kinematic loads (i.e. cyclic displacements) are to be considered. Finally, in the case of lateral spreading, only kinematic forces (i.e. permanent displacements) are of great importance. It was also uttered that factors like foundation embedment and the natural period of the superstructure compared to the soil play important role in the response of the soil.

3.4. Conclusion

Based on the materials presented in previous paragraphs, there is not a full agreement on the effective parameters in the response of a pile foundation in laterally spreading ground. Apart from that, there is a large variation in the effect of each parameter presented by different researchers due to the lack of e experimental and numerical data. Therefore, there is not enough information to provide a firm background for a unified methodology which can be used in different soil conditions and a wide range of earthquake excitation with different pile properties. Each method uses a limited number of parameters and the others are widely overlooked – factors that may have profound effects under specific conditions. Consequently, the need for further investigations in this filed in justified.

Based on the literature survey, a number of parameters are selected that have the potential to be determinant in the response of the pile foundation in the case of lateral spreading. These parameters can be categorized in three groups: soil conditions, pile properties and excitation properties.

Soil Conditions

Different properties of soil have been examined to be important in lateral spreading. Among them, one of the most important parameters is the *relative density* D_r, which is the main parameter that a number of researchers have found a correlation of the response to this one only (Brandenberg et al., 2007, etc.).

The other key parameter that was discussed in the previous paragraphs is the *permeability* of the liquefiable soil layer which have found to have significant impacts on the response of the pile (Uzuoka et al., 2005; Gonzalez et al., 2009, etc.). The incorporation of this

factor in the numerical simulation is a demanding task which is discussed in more detail in chapter 4.

Pile Properties

The key properties of the pile foundation are examined in the numerical analysis. These include the *diameter* and the *stiffness* of the pile. The effect of *installation method* – which have stated by some researchers to have considerable effects – is studied by defining specific stress field around the pile as an effect of pile driving. The *head fixity* of the pile which may be as a result of large, stable superstructures is also examined by imposing a constraint at the uppermost point of the pile.

Excitation Properties

A sinusoidal excitation is applied at the base of the liquefiable layer as discussed in chapter 4. As mentioned before, the change in the loading rate can have dramatic effects on the response of the liquefied soil. Therefore, it is examined by applying excitations with larger and smaller period compared to the basic analysis and the results are compared separately.

Chapter 4

Methodology of Numerical Analysis

4.1. General

In the present chapter the numerical model built to investigate pile response to lateral spreading loads is thoroughly described. The model makes use of the widely used commercial code FLAC3D (Itasca 2006).

In addition, sand behaviour is modeled using an advanced constitutive model developed in NTUA(Papadimitriou and Bouckovalas, 2002; Andriauopoulos et al. 2010; Kavamitros, 2009). Hence, prior to the description of the numerical model, a brief description of the numerical code, as well as the constitutive model is given.

Finally, typical results, by means of a basic analysis, are presented to verify the model's capacity to capture basic response characteristics of the problem.

4.2. FLAC3D finite difference code

FLAC3D (Fast Lagrangian Analysis of Continua) is a three-dimensional explicit finite-difference program to study the mechanical properties of a continuous medium as it reaches equilibrium or steady plastic flow and is mostly used for geotechnical engineering computations. The material is modelled by polyhedral elements (or so-called "zones" in the program terminology) which are surrounded by a grid that can be adjusted to model the geometrical shape of the problem. Each zone behaves according to the defined constitutive model in response to the applied forces and boundary conditions. Some advantages that make this program suitable for the study of liquefaction related problems include:

- It allows the yielding of the material and the grid can deform in large scale and therefore, large displacements and the plastic collapse of the material observed in liquefaction problems can be modelled accurately.
- Unlike finite element model, no matrices are formed. Therefore, large three-dimensional calculations can be made without excessive memory requirements.
- It allows the modeling the fully coupled groundwater flow with dynamic effective stress analysis which is a prerequisite for the close studying of liquefaction related problems.
- FLAC contains a programming language FISH, which allows the user to define his own functions. It can be utilized to introduce the desired input parameters along with the capability of controlling the desired output such as time-histories of the user-defined parameters, etc.
- FLAC3D allows the introduction of the constitutive model written in C++ and compiled as Dynamic Link Libraries (DLL) which is three times faster than using the built-in programming language FISH.

4.2.1. Explicit finite difference method

The finite difference method is primarily a numerical technique to find the solution of sets of differential equations having the initial and boundary values. In this method, each derivative in the set of governing equations is replaced by an algebraic expression in terms of field variables (i.e. stress, displacements, etc.) at discrete points in the space. It should be noted that unlike the finite element method, these parameters are not defined within the elements (or zones) in the finite difference method.

Although it can be shown that the resulting differential equations of the two methods are identical, the way of their usage throughout the years has been different. In other words, in finite element programs, element matrices are often combined into large global stiffness matrix, while this is not carried out in finite difference method because it is more efficient to regenerate the differential equations at each step. Additionally, all the problems –even the static ones – are treated by the use of dynamic equations of motion basically in order to ensure that the numerical scheme is stable in case that the material being modelled undergoes physical instability in which the strain energy is converted into kinetic energy and is dissipated through radiation from the source. This phenomenon can be modelled directly since inertial terms are included in the equations of motion. The computations sequence of this method is shown in **Figure 4.1**. First, the equations of motion are used to derive the new velocities and displacements from stresses and forces. Then, from the velocities, strain rates are obtained and by the use of constitutive model, the stress rates are calculated based on strain rates. Finally, by having the stress rates, new stresses and forces are derived and a cycle is completed. Each complete cycle is called a *timestep.*

It should be realized that each box in **Figure 4.1** updates the grid values from previously known values that remain fixed while control is within the box. For example, the upper box (equations of motion) takes the stresses and forces already calculated, and computes the new velocities and displacements while the stresses are assumed to be frozen for the operation of the box. That is to say, the newly calculated velocities do not have any effect

on the stresses. It may seem unreasonable since the change in the velocities and displacements will have impact on neighbouring elements configuration and will change

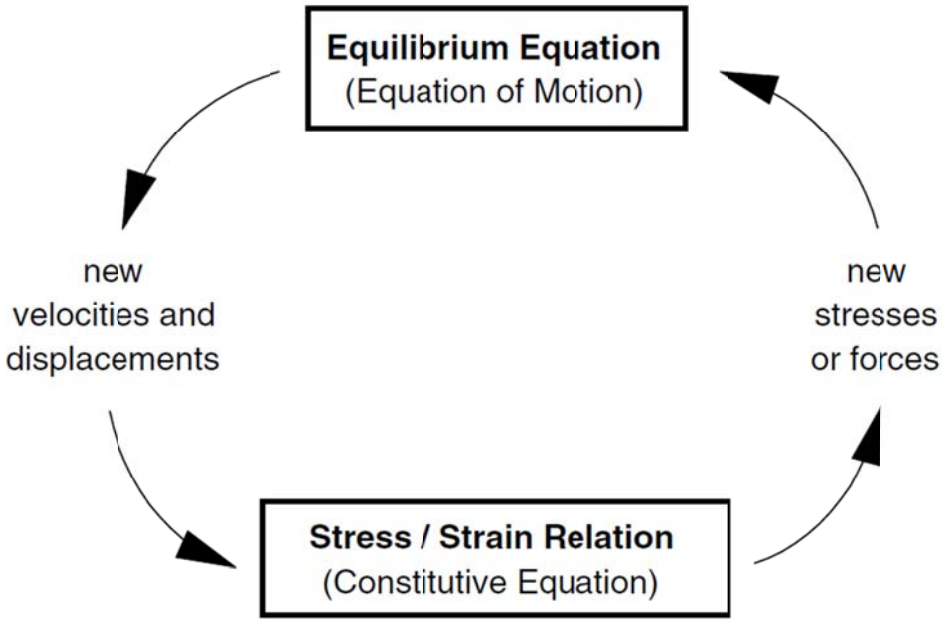

Figure 4.1: Basic calculation cycle in explicit finite difference method

their stresses and forces. This problem is overcome by assigning adequately small timestep through which the information cannot find time to propagate to other zone. In other word, the computational propagation of information should keep ahead of the physical propagation. Therefore, the timestep simultaneously depends on the p-wave velocity of the material and the size of the finite difference zones.

The most important advantage of this method is that unlike implicit method which is mostly used in finite element method, no iteration is needed in finding stresses from strains even when highly nonlinear constitutive models are used. The disadvantage of this model is the necessity of choosing a small time step that increases the computational cost to a great extent. To sum up, the explicit finite difference method is effective when

working with systems that undergo high nonlinearities, large strain or physical instability, while the implicit method is efficient in modeling linear systems. Therefore, in modeling geotechnical problems and most specifically, liquefaction related problems where large nonlinearity exists and the system is prone to physical instability, the explicit finite difference method is the more effective one.

4.3. NTUA-SAND constitutive model

The NTUA-SAND model is a bounding surface, critical state, plasticity model with a vanished elastic region which is proposed by Papadimitriou et al. (1999, 2001, 2002) and modified by Andtianopoulos (2006). The key parameters of this model include:

- The incorporation of the critical state theory of soil mechanics (Schofield & Wroth, 1968) and the use of state parameter $\psi = e - e_{cs}$ to determine the shear behaviour (where e is the void ratio, and e_{cs} the void ratio at the critical state with the same mean effective stress p (Been & Jefferies, 1985) which allows the simulation of the initial state with a single set of model parameters.
- The formulation based on Ramberg-Osgood adapted for elastic strain increments. It can simulate the hysteretic behaviour of sands (i.e. decrease in the shear modulus and increase in the hysteretic damping with increase in cyclic shear strain (Vucetic & Dobry, 1991, Ishibashi & Zhang, 1993)) at low strain levels.
- A vanished elastic region which increases the efficiency of the computational effort since it overcomes the need of iterative procedures to estimate the crossing point of the yield surface and ensure the consistency condition. It should be noted that this does not mean that the strain increments do not have any elastic component. Reversely, the elastic and plastic components continue to apply and therefore, the plastic component always exists even for small strain values.

- Introduction of an empirical index in order to simulate the effect of fabric evolution during shearing accurately, which allows the accurate estimation of the excess pore pressure build-up during liquefaction.

The model requires the calibration of 13 dimensionless and positive constants for cyclic loading, among which 10 can be directly estimated from monotonic and cyclic tests, while the remaining 3constants need the trial and error scheme. Details regarding the constants calibration procedures can be found in Andrianopoulos et al. (2006). The calibrated aforementioned values for Nevada sand are presented in **Table 4.1**.

Table 4.1: NTUA-SAND constants calibrated for Nevada sand

Parameter	Physical meaning	Value
M_c^c	Deviatoric stress ratio at critical state in triaxial compression	1.25
c	Ratio of deviatoric stress ratios at critical state in triaxial extension	0.72
Γ_{cs}	Void ratio at critical state for p=1 kPa	0.910
λ	Slope of critical state in the [e-lnp] space	0.022
B	Elastic shear modulus constant	600
υ	Elastic Poisson's ratio	0.33
k_c^b	Effect of ψ on peak deviatoric stress ratio in TC	1.45
k_c^d	Effect of ψ on dilatancy deviatoric stress ratio is TC	0.30
γ_1	Reference cyclic shear strain for non-linearity of elastic shear modulus	0.025%
α_+	Non-linearity of elastic shear modulus	0.6
A_o	Dilatancy constant	0.8
h_o	Plastic modulus constant	15,000
N_o	Fabric evolution constant	40,000

4.4. Numerical Simulation of Pile in Laterally Spreading Ground

In this paragraph, the numerical model which is implemented in FLAC3D is described in details. In order to study the effect of each of the parameters, two analyses were performed: one with the pile foundation and one without it in order to account for the free-field conditions (i.e. at the absence of the pile). This is done because in p-y method, in its conventional form, the displacement applied at the fixed-end of the p-y spring is, in most cases, estimated based on empirical relationships, like the ones presented in chapter 3 in which the presence of a pile foundation embedded in the soil is not considered. The latter, however, has been found to affect the resulting displacement, a phenomenon termed in literature as "Pinning Effect", extensively investigated by many researchers (e.g. Boulanger, 2005; Gonzalez & Abdoun, 2005). As it is shown in section 4.3, the p-y curves are constructed using both the boundary displacements of the model containing pile, and the displacements obtained by the second analysis (which we call it free-field analysis).

The analysis is performed in two stages:

- Generation of proper stress field for static equilibrium of the infinite slope.
- Application of dynamic loading at the base of the model.

4.4.1. Finite Difference Mesh

The schematic of the mesh used in the numerical analysis is shown in **Figure 4.2**.The size as well as the discretization of the mesh is chosen based on the work previously done in the diploma thesis of Vasilis Papadopoulos (2010). In the basic analysis, the thickness of the liquefied layer is equal to 8 meters (z direction) while the width of the soil is chosen to be 22m in the direction parallel to the inclination (x-axis) and 5m in the direction perpendicular to it (y-axis). The diameter of pile is 0.6 meters. It should be

noted that since all the properties are symmetric with respect to the y-axis, half of real problem is modelled in order to diminish the numerical cost.

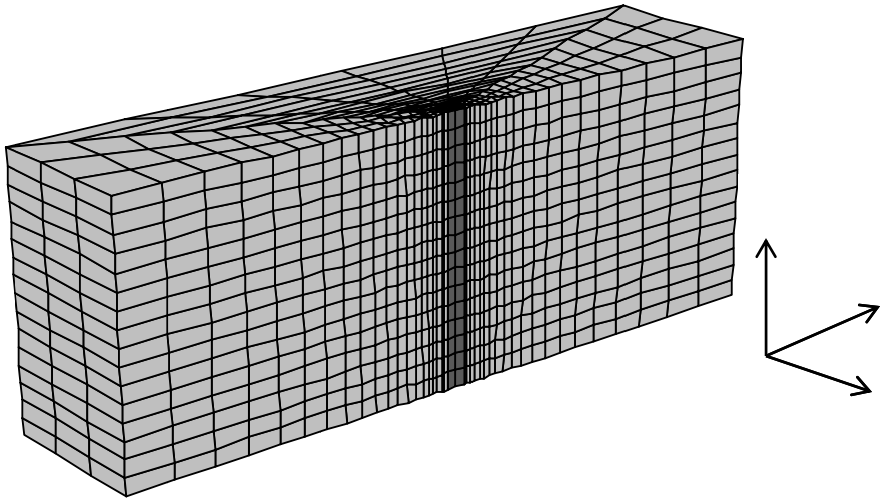

Figure 4.2: Finite difference mesh used for the parametric numerical analyses

Since the pile is cylindrical and the soil mesh is rectangular, the best predefined mesh zone of FLAC3D is "Radially graded mesh around cylindrical-shaped tunnel" or *radcylinder,* which is shown in **Figure 4.3**. It should be noted that half of the model is produced by the use of radcylinder and then, it is mirrored with respect to the P0-P2-P3-P5 plane in order to obtain the whole mesh.

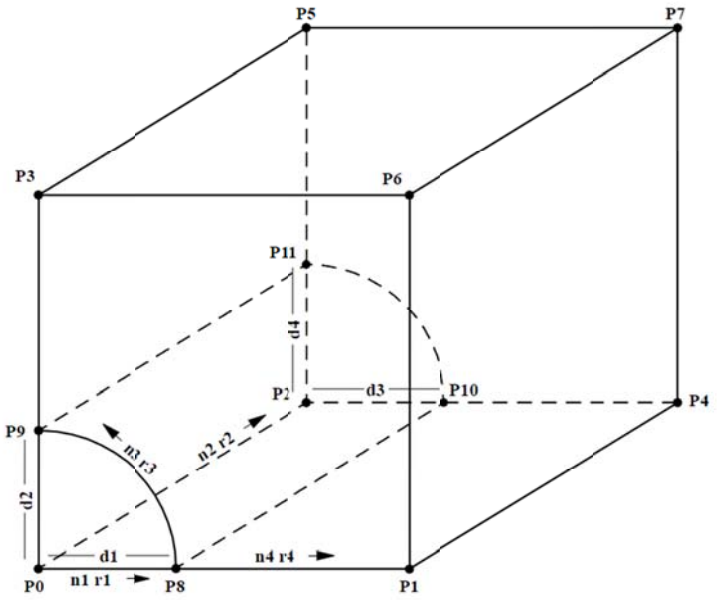

Figure 4.3: Radially graded mesh around cylindrical-shaped tunnel- FLAC3D

Since the radial deformation of the pile is negligible, only one zone is assigned in the radial direction (n1 in **Figure 4.3**) and the cylinder is discretized in the two remaining directions only: 16 zones (every 0.5 m) in the longitudinal direction (n2) and 6 zones in the angular direction (n3) as shown in **Figure 4.4**.

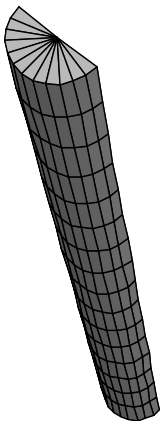

Figure 4.4: Discretization of pile

In soil, 20 zones are defined in the angular direction (n4) with a ratio of 1.15 between the subsequent zones. Consequently, the farther from the pile foundation, the less dense the discretization.

Although the soil is assumed to have an inclination of 2 degrees, for numerical convenience the mesh is chosen to be horizontal and the inclination is modelled by a horizontal component of the gravitational force equivalent to the aforementioned inclination which is discussed in detail in 4.4.2. Initial Stresses.

Interface Elements

As the connection of pile and soil cannot be assumed to be rigid due to the possibility of slippage and separation of the two surfaces, interface elements are utilized to model the real situation.

Prior to the excitation, large values of stiffness are assigned to the interface element in order to reach equilibrium easily. Additionally, the permeability is switched off for the interface in order to prevent the complete drainage of the water in the system through the interface between pile and soil.

During shaking, large stiffness values are preserved so that resulting soil pressures are a result of soil and net interface deformation. Furthermore, since the soil modeled is cohesionless, no cohesion is specified ($c_{int} = 0$), while the friction angel is set equal to the half of the friction angel of the soil. This value is widely used for piles in sandy soils.

Soil and Pile Properties

The 8 meter soil layer corresponds to a uniform Navada Sand deposit with Relative Density, D_r=50%. For this Relative Density, the permeability is equal to k=6.1e-5 m/s, as obtained from constant-head permeability tests (Arumoli et al.; 1992). Basic Navada Sand characteristics are summarized in **Table 4.1**. Navada Sand response was simulated using the NTUA- Sand model described earlier.

The pile was assumed to have a diameter D=0.6 m and a yielding a flexural stiffness EI=8000 kN.m^2. An elastic model was assumed for the pile, as pile failure is not considered as an acceptable design case in the current investigation.

4.4.2. Initial Stresses

As mentioned before, the 2 degree inclination is modeled by a horizontal mesh and a 2 degree inclined gravitational vector as shown in **Figure 4.5**.

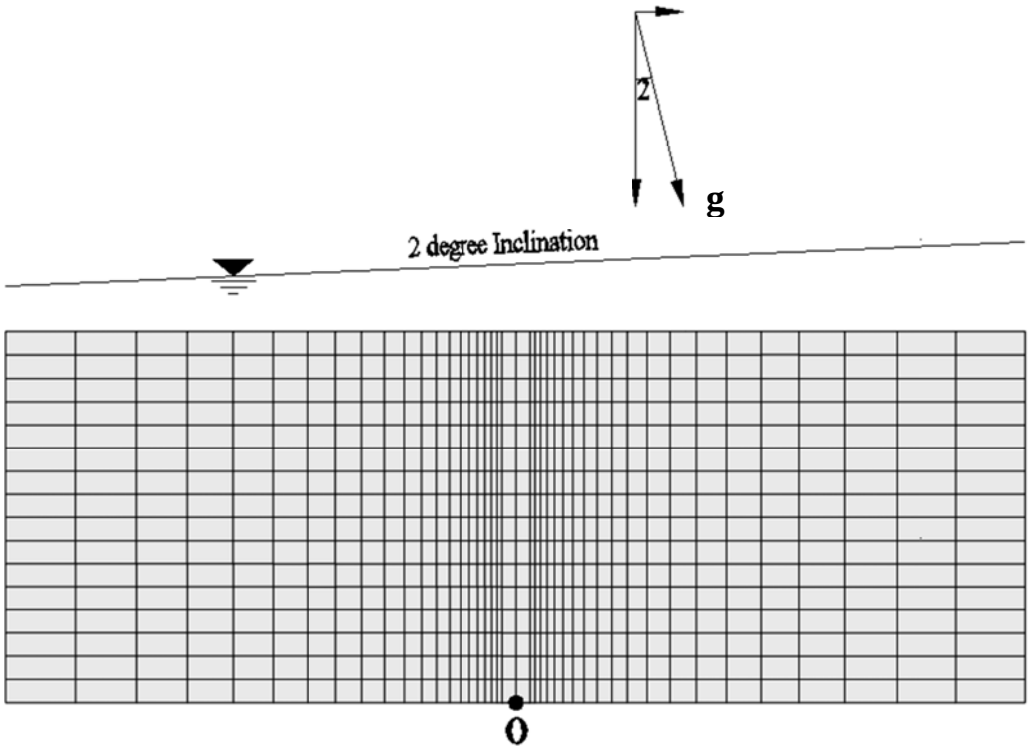

Figure 4.5: Schematic of the initial stresses

The horizontal and vertical components of the gravitational acceleration are calculated as:

$$g_z = g.\cos 2^o = 9.81 \times \cos 2^o = 9.804\ m/s^2 \quad (4.1)$$

$$g_x = g.\sin 2^o = 0.342\ m/s^2 \quad (4.2)$$

Where: g Gravitational Acceleration

g_x Equivalent Horizontal Gravitational Acceleration

g_z Equivalent Vertical Gravitational Acceleration

The level of water ground is assumed to be 1 meter above the surface in order to maintain full saturation during the shaking. Apart from that, in order to keep equilibrium of water in static condition and prevent flow of water, the water surface is assumed to have an inclination of 2 degrees as shown in **Figure 4.5**.

It should be mentioned that in FLAC3D, total stresses (rather than effective stresses) are specified as initial stresses. In order to assign the initial stresses of the whole model, the normal and shear stresses at a specific point should be given to the software and the values at other parts of the model are assigned by applying the rate of change of stresses with respect to each of the Cartesian coordinates. Point "O" in **Figure 4.5** is assumed as the basis and the values are calculated as the following:

$$\gamma_{sat} = (\rho + n).g_y = (1.543 + 0.411) \times 9.804 = 19.157 \ KN/m^3 \quad (4.3)$$

$$\gamma_{dry} = 19.157 - 9.804 = 9.353 \text{ kN/m}^3 \quad (4.4)$$

Where: γ_{sat} Saturated Unit Weight

ρ Density

n porosity

γ_{dry} Dry Unit Weight

Therefore, the vertical total stress at point O can be found by adding the effective stress and pore pressure, noting that the column of water on this point has a depth equal to the depth of the soil (8m) plus one extra meter added by the contribution of the inclination as:

$$depth = 8 + 1 + 11 \tan 2 = 9.384 \ m$$

$$\sigma_{zz} = -(\sigma'_{zz} + u) = -8 \times 9.353 - 9.384 \times 9.804 = -166.82 \text{ kPa} \quad (4.5)$$

Note that, according to FLAC's sign convention, negative stresses correspond to compression.

The gradient is equal to - 0.342, 0 and 19.157 in x, y and z directions respectively. In order to calculate the horizontal normal stresses, Rankine at-rest lateral coefficient is utilized:

$$K_0 = 1 - \sin\varphi = 1 - \sin 35 = 0.426 \quad (4.6)$$

$$\sigma_{xx} = \sigma_{yy} = -(K_0.\sigma'_{zz} + u) = -121.93 \text{ kPa} \quad (4.7)$$

Where: K_0 Rankine at-rest lateral coefficient

φ Soil Friction Angel

Which have a gradient of - 0.342, 0 and 13.55 in x, y and z directions respectively. Due to the inclination of the soil, the shear stress σ_{xy} also exists which is necessary to equilibrate the horizontal gravity component. It can be calculated as:

$$\sigma_{xy} = \rho_{dry}.g_x.H = (0.954 \times 0.3424 \times 8) = 2.612 \text{ kPa} \quad (4.8)$$

It is obvious that the shear stress has a variation only in z direction which is equal to

$$\rho_{dry}.g_x = 0.3265 \quad (4.9)$$

4.4.3. Boundary Conditions

Two different kinds of boundary conditions are used in the static equilibrium phase and the subsequent excitation. In the former, the simple fixities of the boundary in the desired directions are used. This includes the fixity of the horizontal plane at the bottom of model (z=0 plane) in x, y and z direction. The vertical planes at x=-11 and x=11 meters are restrained in x and z directions. It should be noted that the fixity in z direction is because of the inclination of the model which is applied by the component of gravity in x direction and finally the two vertical planes at y=0 and y=5 are fixed in y direction.

During the excitation, on the other hand, while the horizontal displacements in the lowermost plane of the model are restrained in order to simulate the rigid bedrock conditions, *Tied-node condition* is used for the lateral boundaries of the model. In order to achieve this, a FISH function is used which imposes the same velocities at nodes of the same elevation. This method is considered as a numerical simulation of laminar box which is mostly used in dynamic tests and has been used extensively in the analysis of liquefaction related problems (eg. e.g. Ghosh & Madabhushi, 2003, Elgamal et al, 2005, Liu & Song, 2005 and ohers).

4.4.4. Excitation

For the basic analysis, the input acceleration applied at the base of the model consists of a sinusoidal time history with a period of 0.3 seconds and an amplitude of a_{max}=0.2g as shown in **Figure 4.6**. It can be seen that shaking has 10 cycles with the maximum acceleration and 2 cycles in the increasing and the diminishing part which overall forms 14 cycles which lasts for 4.2 seconds. The implementation of the excitation is performed by FISH, which is a built-in programming language of the FLAC and FLAC3D as mentioned before.

The initial cycles of increasing amplitude are essential to ensure that applied motion is baseline corrected (leaves no residual displacement at the base of the model after shaking). Response of the system is recorded by means of acceleration, pore pressure ration (r_u), displacement (y) and soil reaction (p) timehistories. The latter are calculated through a FISH function, for various depths, based on the stresses at the nodes of the interface elements.

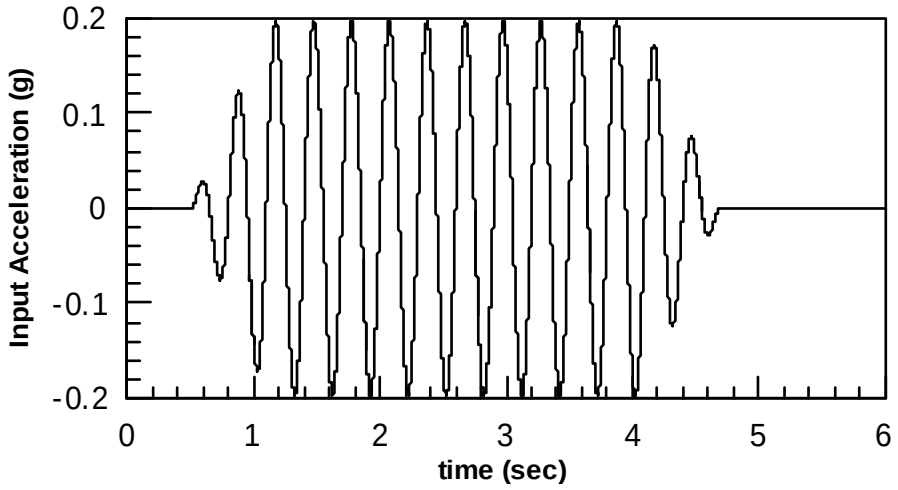

Figure 4.6: Time history of the applied excitation at the base of the model

4.2.5. Free-field Analysis

As mentioned earlier, an additional dynamic analysis that does not involve a pile foundation is also performed. Numerically, this is achieved using the exact same model described previously, but leaving out the installation of the pile and the interface elements.

4.3. Typical Results

In order to obtain a thorough understanding of the behaviour of pile and the liquefied soil, time-histories of different parameters are kept at different depths and in different distances from the pile both in upstream and downstream of the pile. These include the excess pore pressure build-up which presented by means of the "excess pore pressure ratio, r_u" concept. It is defined as the ratio of the excess pore pressure at any instance divided by the initial effective stress. It is apparent from the definition that if r_u equals unity, full liquefaction has occurred and the effective stress is equal to zero.

$$r_u = \frac{\Delta u}{\sigma'_{vo}} \qquad (4.10)$$

Typical results are presented here for the basic analysis, the soil, excitation and pile properties of which are presented in **Table 4.2**. It should be noted that the soil properties used in all analyses are that of Nevada sand and just the permeability and the relative density are changed in parametric analysis.

Table 4.2: Soil, excitation and pile properties in the basic analysis

Soil Properties	Relative Density (D_r)	50%
	Permeability (k)	6.1e-5 m/s
excitation properties	Amplitude	0.2g
	Period (T)	0.3 sec
Pile Properties	Diameter (D)	0.6 m
	Stiffness (EI)	8000 KNm^2

The results are presented hereafter:

1. Contours of horizontal displacement and the excess pore pressure at the end of shaking are shown in **Figure 4.7** a and b respectively. From the first one, for instance, the deformation of the pile and the boundaries can be seen which shows that the pile acts as a cantilever while the displacements in the boundaries don't follow that of the pile. The second graph shows the contours of excess pore pressure build up at the end of the shaking which shows that apart from some areas close to the pile, complete liquefaction has occurred. Close to the pile, large dilation is observed as a result of lateral stress reduction and large shear straining.

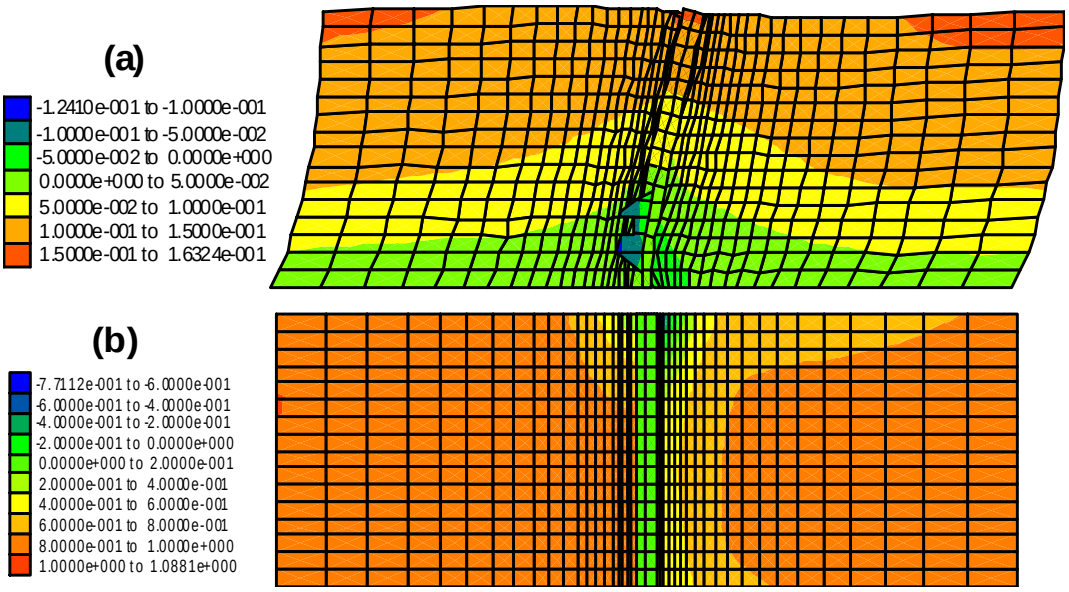

Figure 4.7: Contours of a) Horizontal Displacement, y and b) excess pore pressure ratio, r_u at the end of shaking

2. Profiles of lateral horizontal displacement at end of shaking are shown in **Figure 4.8**. The graph consists of 3 plots: the profile of the pile displacement, displacements at

the boundary of the model containing pile and the displacements obtained by the free-field analysis. It is clear from the figure that the "pinning effect" which is discussed earlier, is profound: it has decreased the maximum free-field displacements from approximately 0.2 m to about 0.15 m. It should be noted that it is more profound near the ground surface where pile displacements are larger.

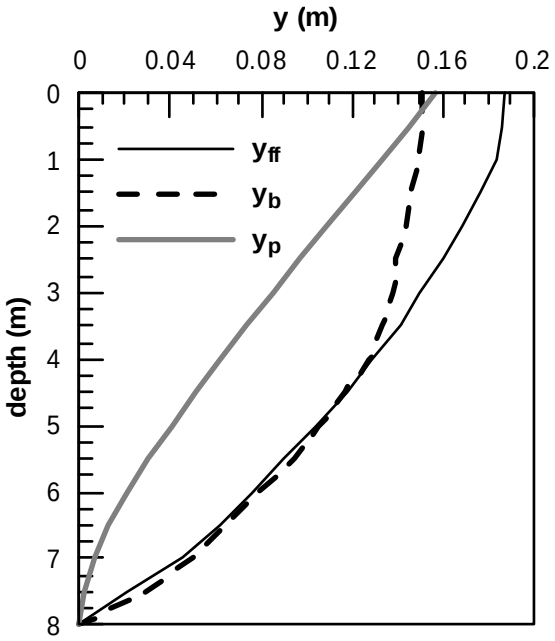

Figure 4.8: Profile of lateral displacements at the end of shaking

3. Time-histories of the excess pore pressure ratio: the time histories are plotted in 3 depths: 0.75m, 3.25m and 6.25m from the ground surface at the following locations:
   3.1. ***Near field-Upstream***: Very close to the pile (in the finite difference zone next to the pile) in the upstream of the lateral displacement (i.e. x<0) and very small y component (0.1m).
   3.2. ***Near field-Downstream***: As previous one but one the other side (x>0)
   3.3. ***Far field-With pile***: is in a point away from the pile in order to simulate free-filed excess pore pressure build up (x=8.86, y=0.1m)
   3.4. ***Far field-Without pile***: is the excess pore pressure build-up in the free-field analysis (i.e. analysis without pile)

The aforementioned figures corresponding to the basic analysis are shown in **Figure 4.9**. It can be observed that in complete liquefaction has occurred in the free-field after about 0.5 seconds of the excitation, with transient drops in the excess pore pressure ratio (r_u) as a result of dilation. The results are quite similar for the two cases of analysis with and without the pile. However, large dilation has occurred near the pile especially in shallow depths for both upstream and downstream of the pile.

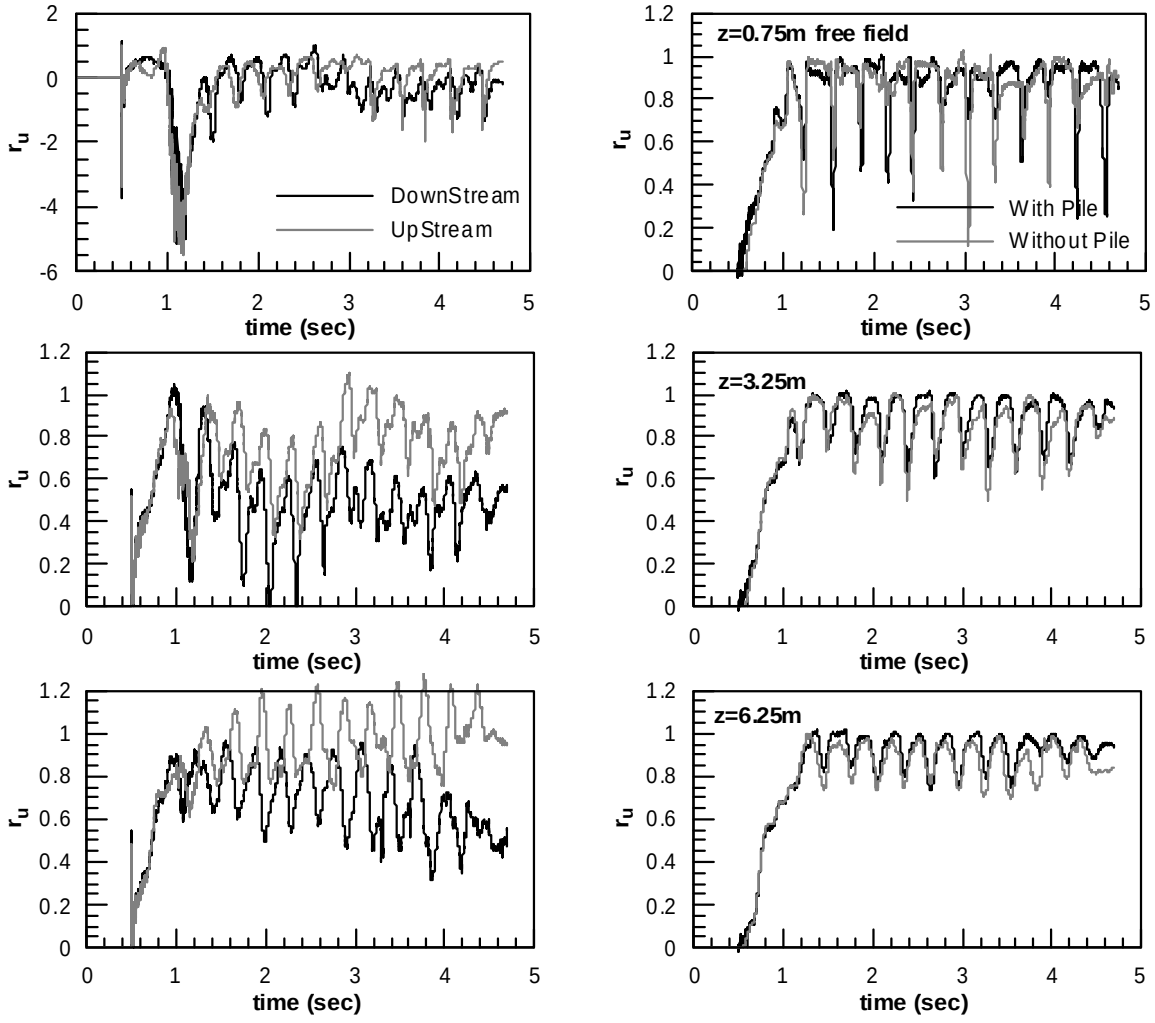

Figure 4.9: Time-histories of excess pore pressure ratio throughout the soil layer

4. P-y curves: P-y curves are plotted with the use of time-histories recorded at different depths. Therefore, the curves are provided for depths equal to 0.5, 1.5, 2.5, … ,7.5 meters.

As mentioned before, two sets of p-y curves are provided: one with respect to the relative lateral displacement taking into account the boundary displacements of the analysis with the pile, and one using the displacements obtained by the analysis without the pile as the reference to find the relative displacements. The results are plotted together with the static p-y curves. The latter have been obtained numerically, using the same mesh configuration and soil and pile properties, as part of the diploma thesis of Vasilis Papadopoulos (2010).

These results are plotted in

Figure 4.10 and **Figure 4.11** for the basic analysis. The following observations are made from these figures:

- Large degradation of the ultimate soil capacity has occurred as a result of liquefaction which is more significant at larger depths.
- Despite the transient ups and downs within each cycle, an overall softening response is observed in the liquefied p-y curves.
- Normally, the dynamic p-y curves reach their ultimate values at relatively small displacements compared to the static curves.

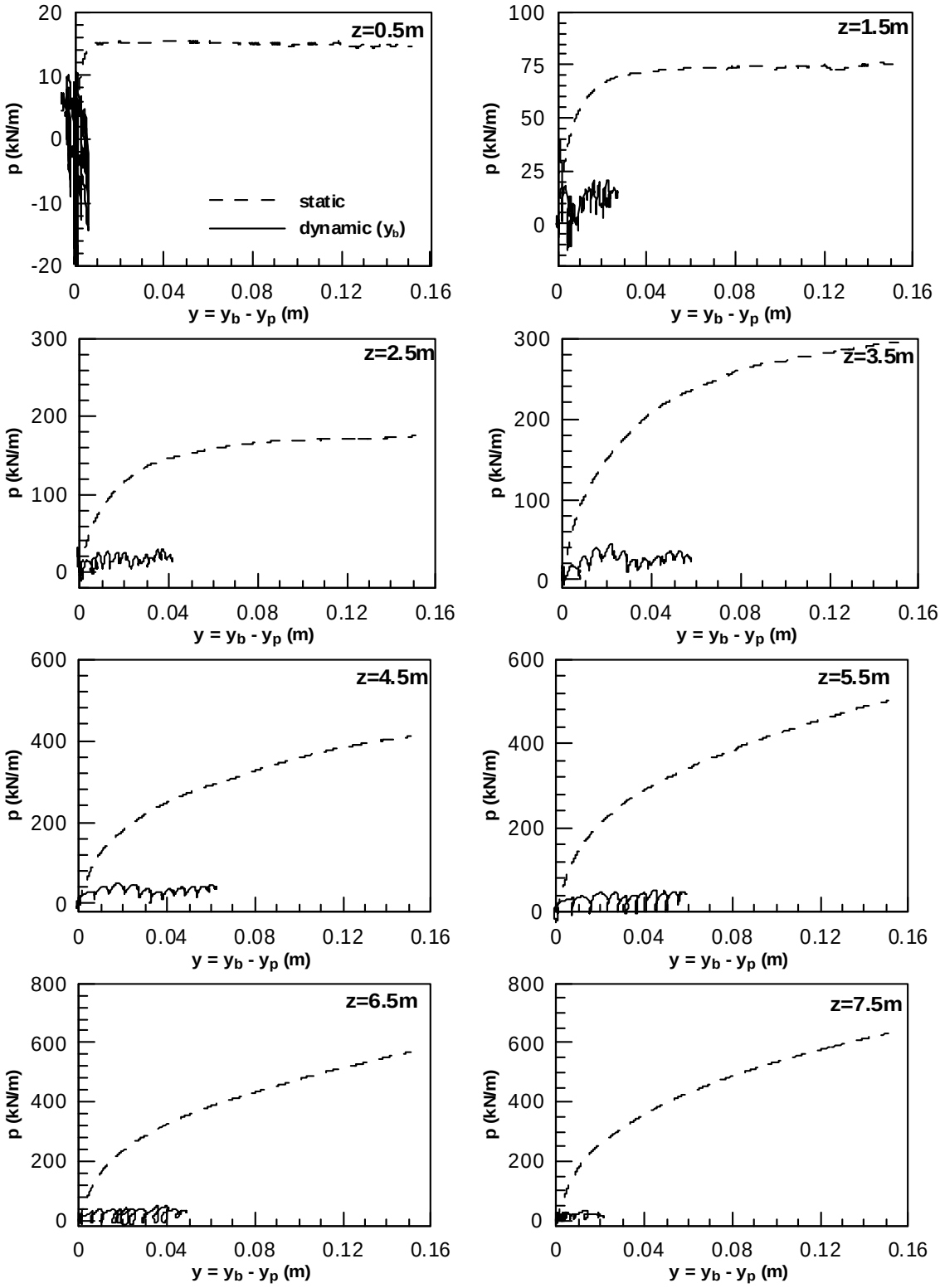

Figure 4.10: Static and Dynamic p-y curves using boundary displacements

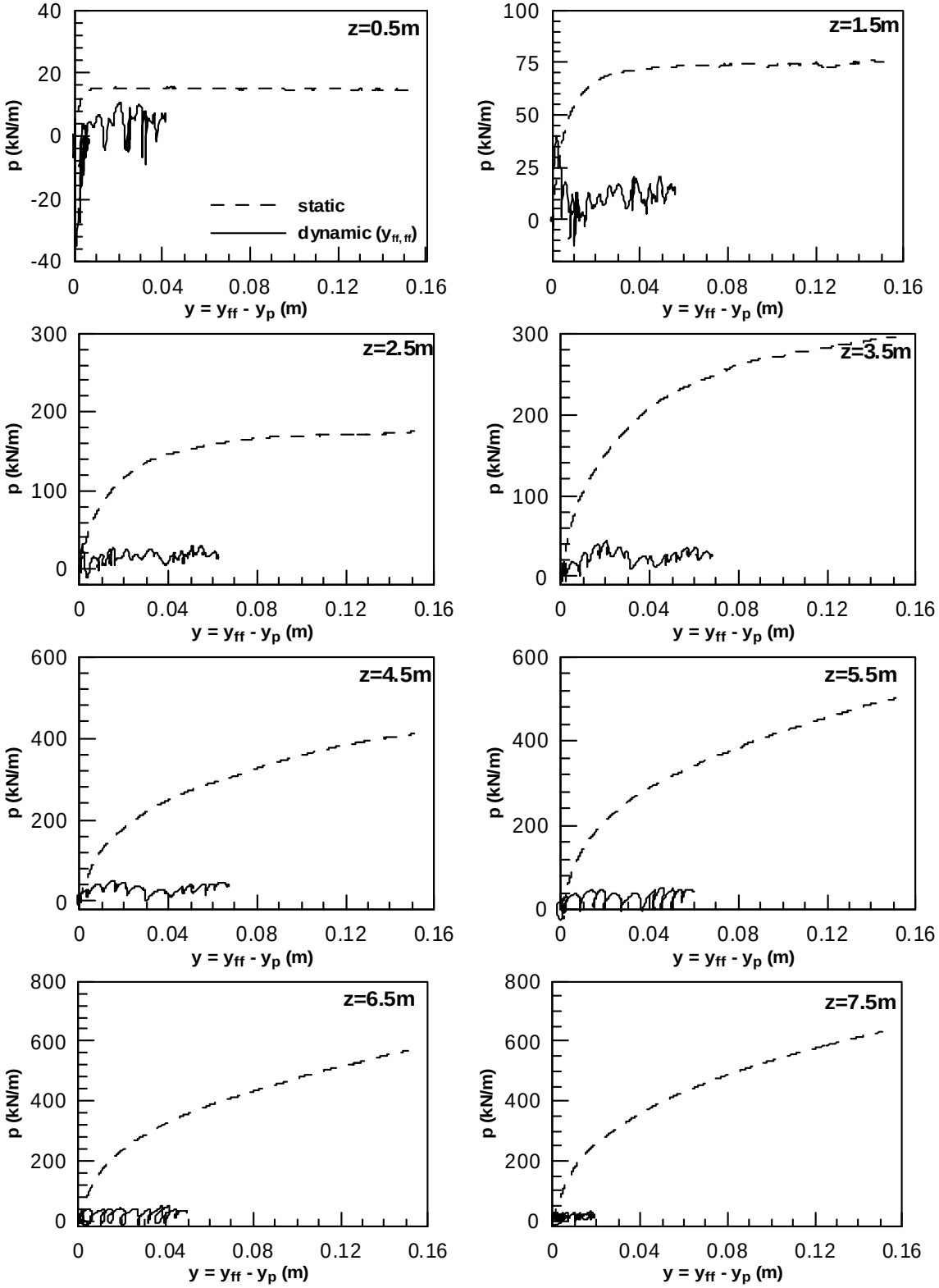

Figure 4.11: Static and Dynamic p-y curves using free-filed displacements

5. Normalized p-y curves: In order to have a magnitude of degradation of the p-y curves as a result of lateral spreading, normalized p-y curves over the static curves are presented. To reach this end, the dynamic p-y curves are divided by the value of the static ones in the corresponding displacement – not the ultimate load. Like the previous graphs, they are plotted both against the boundary displacements and the free-field displacements. This type of comparison emanates from the fact that, as discussed in chapter 3, liquefaction effect on p-y curves are treated in design method by means of a coefficient factor called m_p multiplier.

   Since the ratios got large values at small displacements, the logarithmic scale is used for the vertical axis which leads to a clearer view over both the initial values and also the values at large displacements. The results for the basic analysis are shown in **Figure 4.12** and **Figure 4.13**

   .

   Two basic trends can be observed in the values of m_p multiplier:

   - Firstly, the values of m_p multiplier are larger for small depths and decrease with the increase in the depth of soil. It can be explained by the fact that dilation is larger in shallow depths which can be concluded from negative values of r_u in those areas. This causes soil to be stiffer in these areas and provide larger lateral resistance. In larger depths, however, liquefaction is more complete and smaller p values are observed.

   Secondly, the m_p multiplier gets smaller values with increase in the relative displacements. The reason can be explained as the following: These graphs are the result of dividing the dynamic curves by the static ones (

   - **Figure 4.10** and **Figure 4.11**) and as discussed earlier, the liquefied curves reach their ultimate values in smaller relative displacements while the static curves continue to rise until large relative displacements. Consequently, dividing these two graphs at equal depths means dividing relatively constant values (liquefied / dynamic) by an increasing curve (static). Therefore, as the relative displacements increase, the values of the values of m_p multiplier decrease.

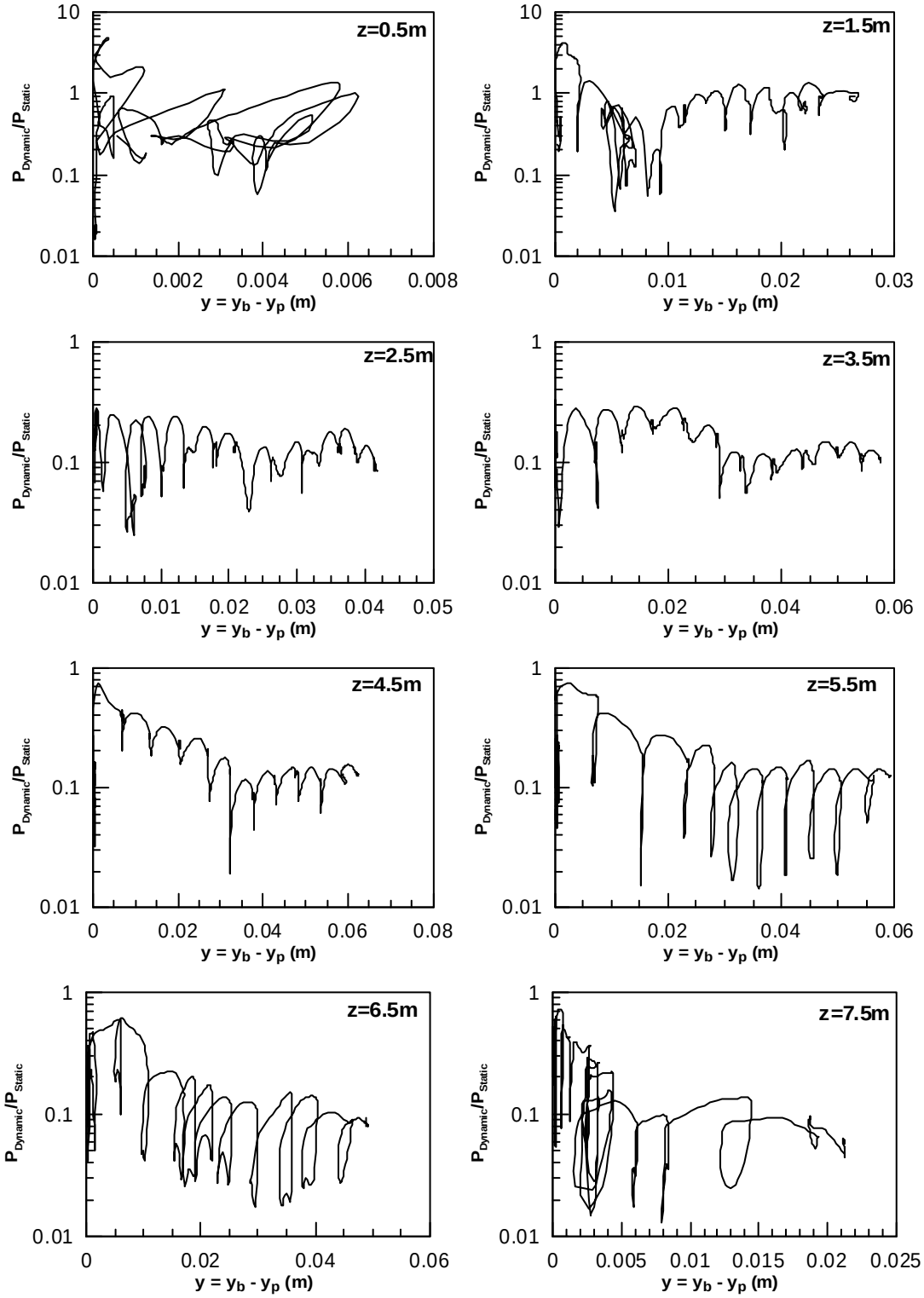

Figure 4.12: Normalized p-y curves using boundary displacements

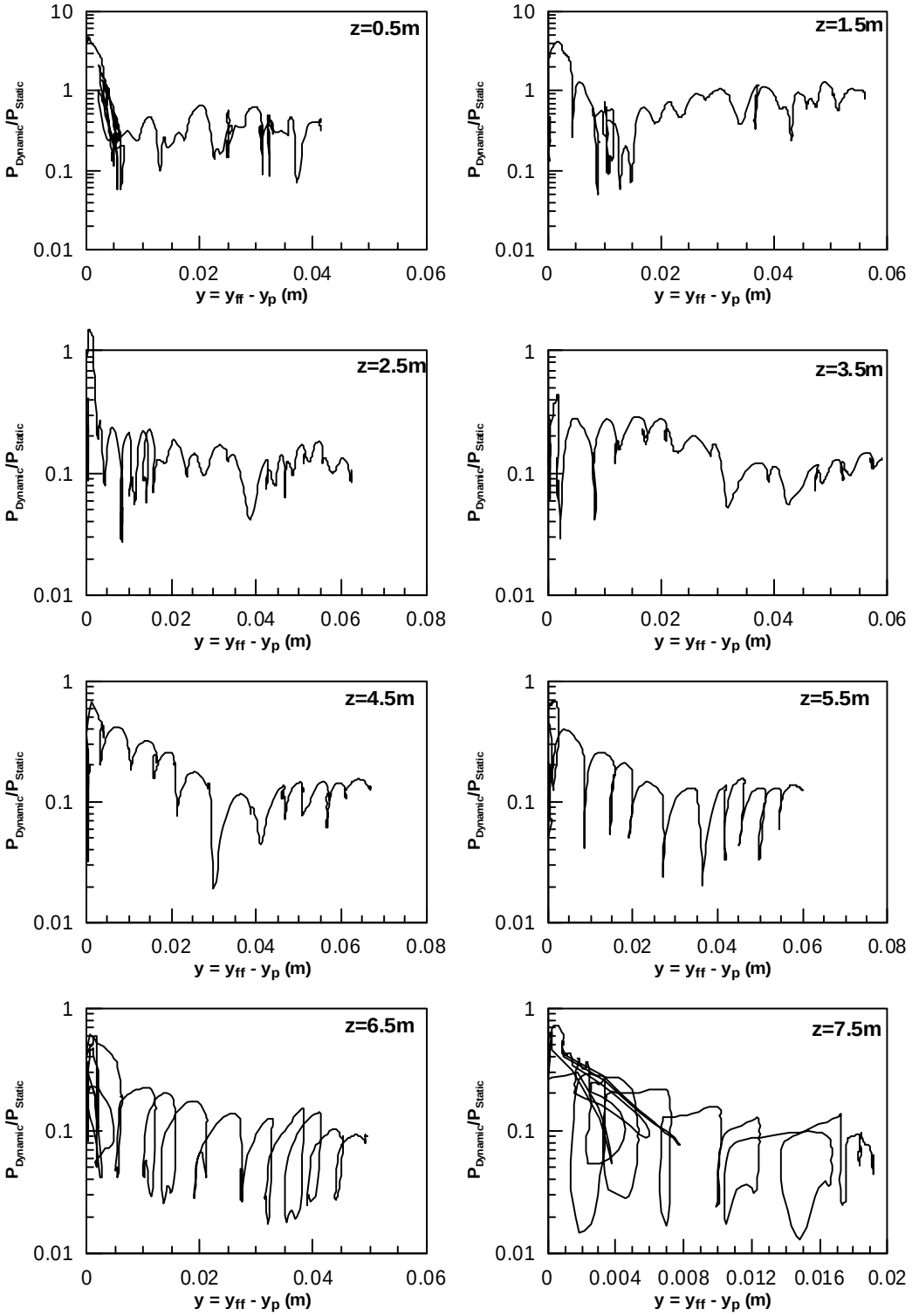

Figure 4.13: Normalized p-y curves using free-field displacements

4.4. Parameters to be examined

Based on the literature review, a number of parameters are chosen for the parametric analysis since FLAC3D allows the modification of a variety of parameters.

As mentioned before, the soil sample is modelled to represent the properties of Nevada sand. The relative density and the permeability are the parameters that are included in the parametric analysis. The Relative Density of 30% and 90% are examined while different approaches are examined to include the effect of soil permeability which is discussed in details in chapter 5.

For the excitation, the effect of period is examined using excitations with periods of 0.1 and 0.5 seconds. More details are presented in chapter 5.

And finally, the effects of some properties of the pile foundation are examined. To achieve this end, a pile with a large value of stiffness replaced the basic one. Apart from that, the effect of pile installation method is examined by changing the stress properties of an area close to pile in order to simulate driven piles. The effect of head constraint is also examined by imposing fixity at the uppermost point of the pile. Piles with different diameters are also examined, one larger and one smaller that the basic. The overall overview of the parametric analysis is summarized in **Table 4.3**. The shaded areas in table depict the specific parameter that is examined in each analysis.

Table 4.3: Parametric analysis layout

D_r (%)	D (m)	EI (kNm^2)	T (sec)	Installation	k (m/sec)	head fixity
50	0.6	8000	0.3	NO	6.10E-05	NO
30	0.6	8000	0.3	NO	6.10E-05	NO
90	0.6	8000	0.3	NO	6.10E-05	NO
50	0.4	8000	0.3	NO	6.10E-05	NO
50	1	8000	0.3	NO	6.10E-05	NO
50	0.6	1000000	0.3	NO	6.10E-05	NO
50	0.6	8000	0.1	NO	6.10E-05	NO
50	0.6	8000	0.5	NO	6.10E-05	NO
50	0.6	8000	0.3	YES	6.10E-05	NO
50	0.6	8000	0.3	NO	6.10E-04	NO
50	0.6	8000	0.3	NO	2.10E-05	NO
50	0.6	8000	0.3	NO	0	NO
50	0.6	8000	0.3	NO	$k(r_u)$	NO
50	0.6	8000	0.3	NO	6.10E-05	YES

Chapter 5

Effect of Soil and Excitation Characteristics on Liquefied p-y Response

5.1. General

In this chapter the effect of parameters that correspond to soil or excitation is investigated. These parameters include:

- Soil Relative Density, D_r
- Soil Permeability, k
- Excitation period, T

In the following sections, the results of each parameter analysis will be discussed separately. In addition, in each part, the modifications that should be done in the input file in order to take into account the effect of each parameter will be described clearly.

5.2. Effect of Relative Density, D_r

The relative density of soil in the basic analysis is equal to 50%. In order to observe the effects of relative density on the liquefied p-y response, two different models with relative density of 30% and 90% are considered.

Since there is a relation between relative density and void ratio, in order to change the value of soil relative density in the constitutive model, the value of void ratio is changed. Relation between relative density and void ratio is as follows:

$$D_r = \frac{e_{max} - e}{e_{max} - e_{min}} \quad (5.1)$$

Where: D_r Soil relative density

e Soil current void ratio

e_{max} Soil void ratio at its loosest condition

e_{min} Soil void ratio at its densest condition

In the constitutive model the maximum and minimum void ratio, e_{max} and e_{min}, are equal to 0.887 and 0.511 respectively, values that correspond to Nevada sand.

The current void ratio which is defined as ***m_void*** in the input file, corresponds to relative density equal to 50%. This value is equal to 0.699:

$$0.5 = \frac{0.887 - e}{0.887 - 0.511} \quad \rightarrow \quad e = 0.699$$

Therefore, by the aid of this formula we can calculate the corresponding value of void ratio to the desired relative density:

$$D_r = 30\% \quad \rightarrow \quad 0.3 = \frac{0.887 - e}{0.887 - 0.511} \quad \rightarrow \quad e = 0.774$$

$$D_r = 90\% \quad \rightarrow \quad 0.9 = \frac{0.887 - e}{0.887 - 0.511} \quad \rightarrow \quad e = 0.549$$

Figure 5.1 compares the profile of lateral displacement in each analysis which reasonably indicates that when the soil is denser, smaller lateral displacement occurs. As a result, the displacement of the pile is also smaller in this case. Also large differences are observed between the free-field displacements, as they are calculated from the analyses with and without the pile. Namely the analysis with the pile yields displacements which are in some cases 1.8 times larger.

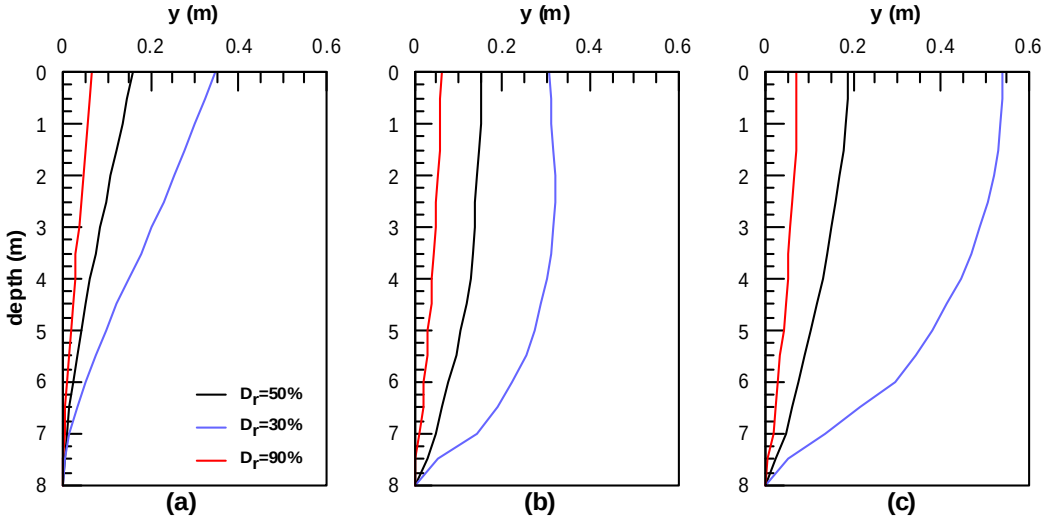

Figure 5.1: Effect of soil relative density on the profile of lateral displacement of a) pile, b) boundary and c) free-field at the end of shaking

The large lateral displacements in the soil with D_r=30% causes dilation in soil and therefore large negative excess pore pressure is developed in the vicinity of pile, both in upstream and downstream, as shown in **Figure 5.2** and it is more significant in shallow depths.

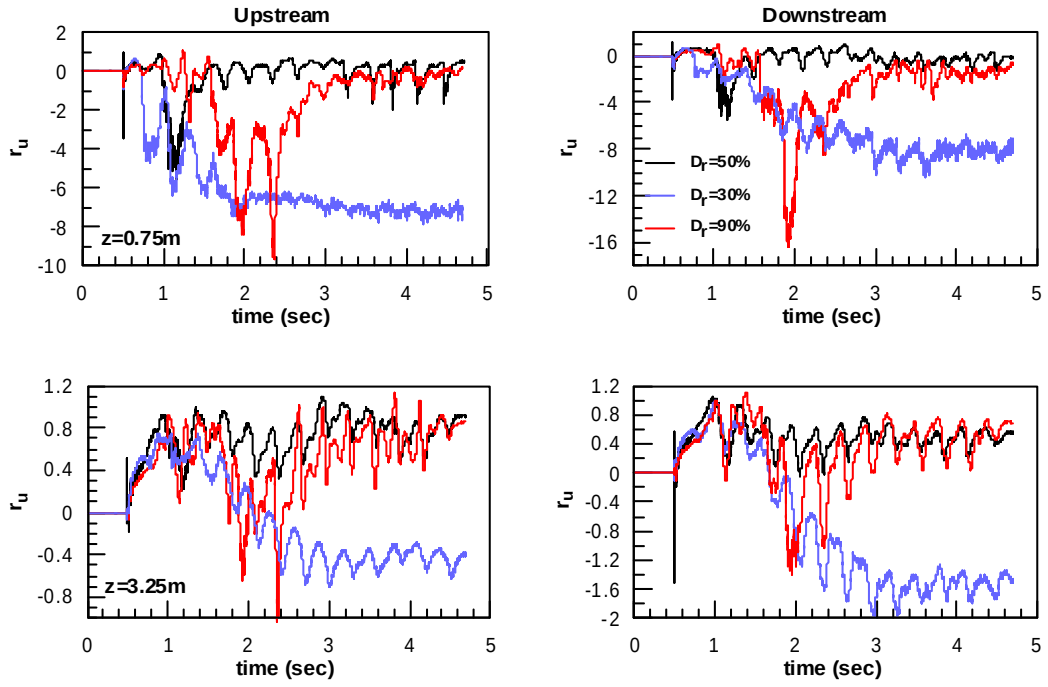

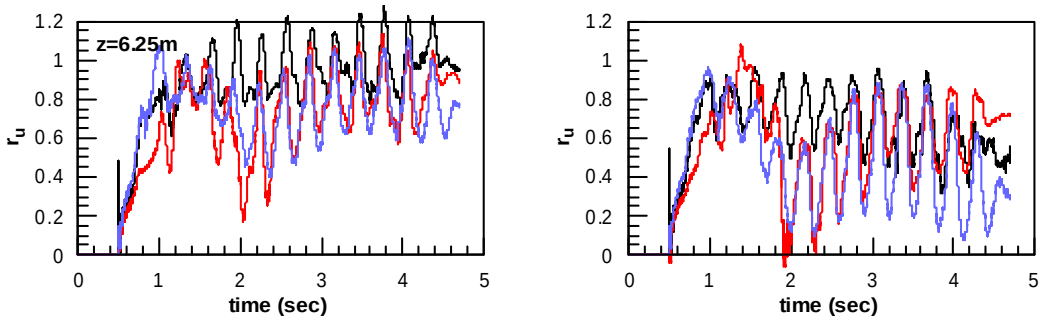

Figure 5.2: Effect of soil relative density on pore pressure build-up near the pile at a) upstream and b) downstream.

The r_u build-up in the free-field is depicted in **Figure 5.3**. It shows that the overall response is quite similar and complete liquefaction has occurred in all the analyses within 0.5 seconds after the start of excitation. The only significant point is the large dilation spikes developed in the sample with relative density equal to 90%. The reason can be explained by taking into account the critical state theory: when void ratio is smaller, soil is more likely to transform from contractive behavior to dilative. Therefore, this sample tends to undergo drops in the excess pore pressure ratio. The same thing – but less sever – occurs in the basic analysis while in the loose sand (D_r=30%) the figure is the most smooth one.

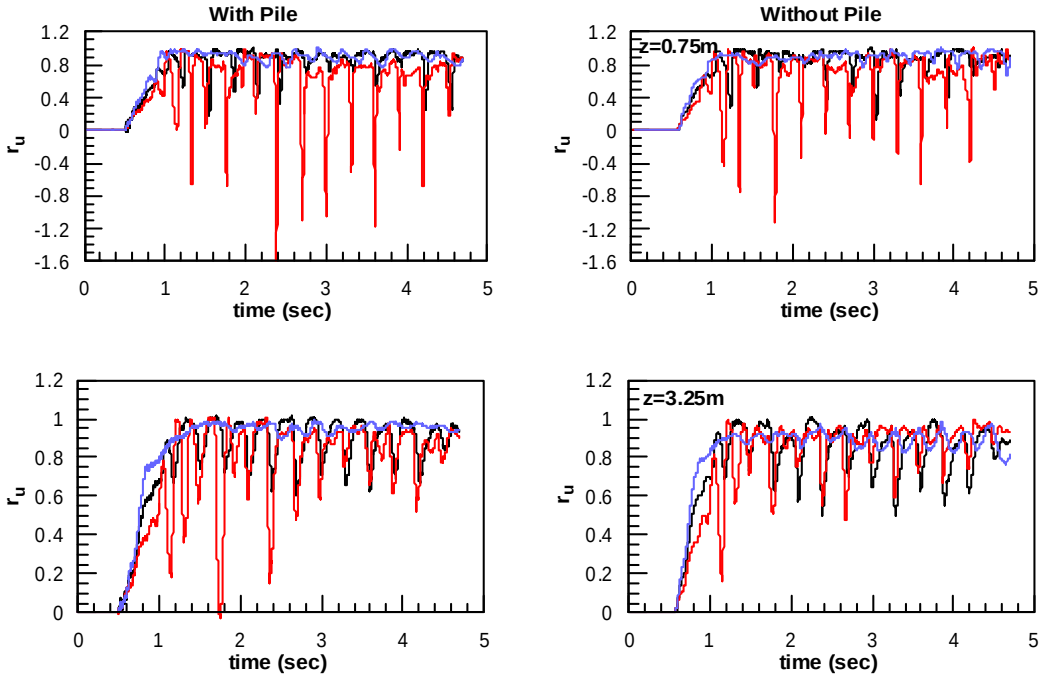

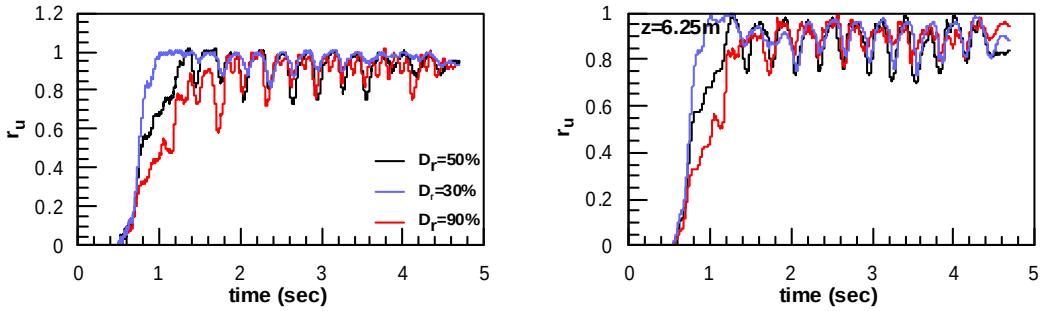

Figure 5.3: Effect of soil relative density on pore pressure build-up at free-field a) with pile and b) without pile.

Figure 5.4 and **Figure 5.5** compare the dynamic p-y curves for the three analyses. Namely in **Figure 5.4** soil subgrade reaction is plotted for various depths as a function of the relative displacement between the free-filed displacement (as obtained from the analysis with the pile) and the pile displacement. On the other hand, in **Figure 5.5** relative displacement is defined in terms of the free-filed displacement as obtained from the analysis without the pile.

These figures indicate that the relative displacement of the pile has a reverse dependency on the relative density. In the loose sand (D_r=30%), as a result of the negative pore pressure build-up in the loose sand which is an indicative of large dilation, larger lateral loads are applied specially in large relative displacement. The basic sample (D_r=50%) stands in between and the dense sand with relative density equal to 90% yields the smaller resistance for all relative displacements.

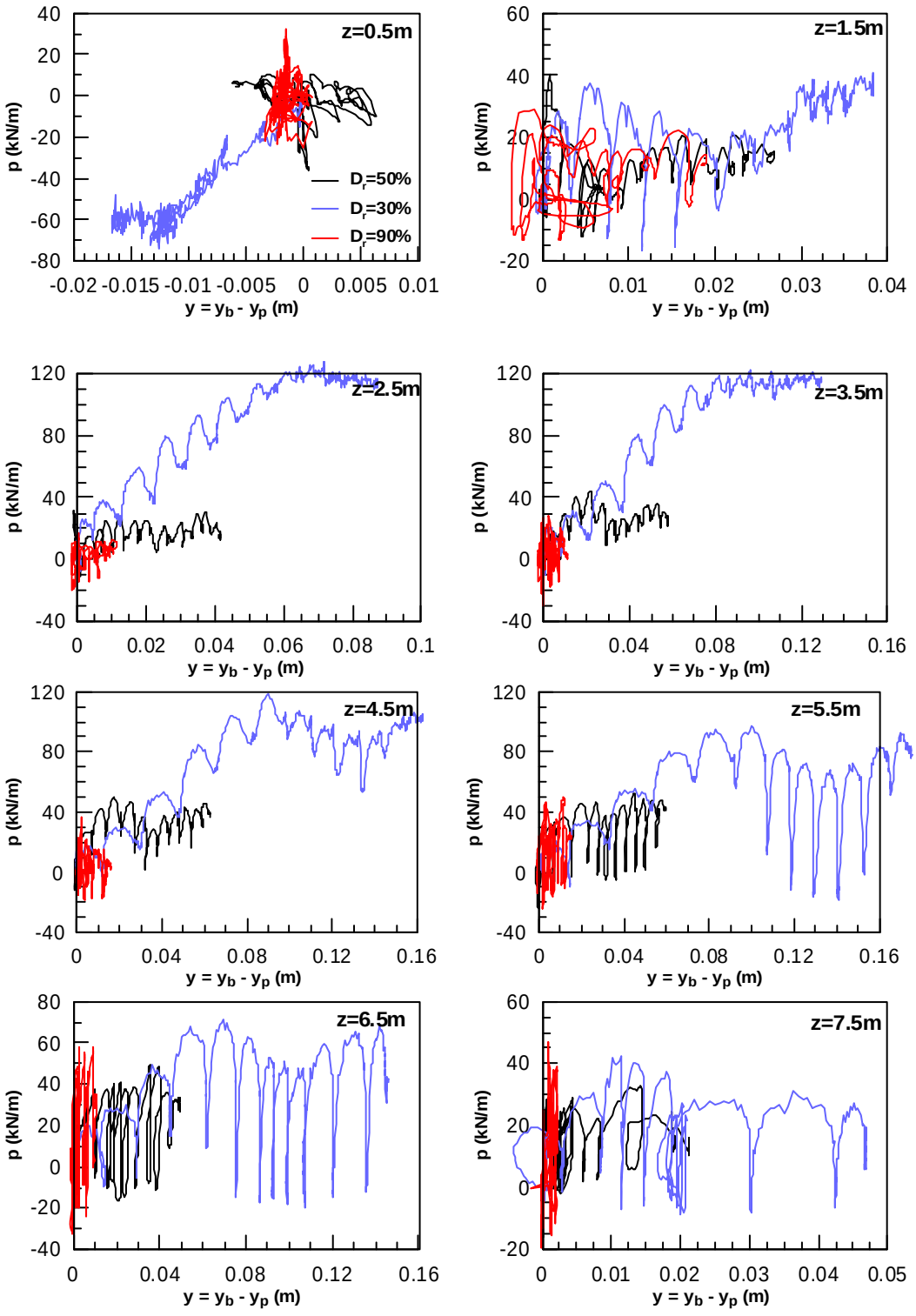

Figure 5.4: Effect of soil relative density on dynamic p-y curves throughout the soil layer (using boundary displacements)

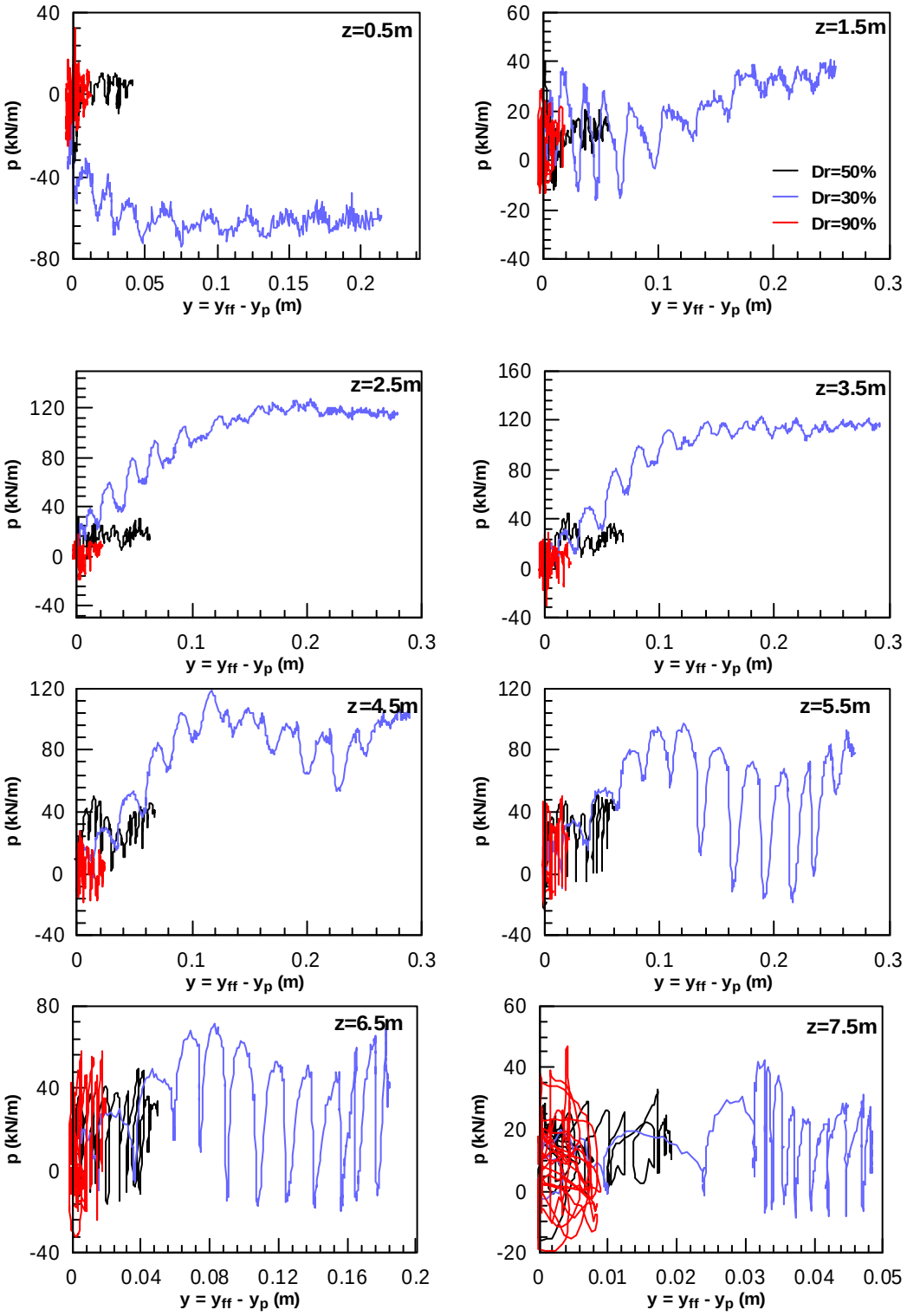

Figure 5.5: Effect of soil relative density on dynamic p-y curves throughout the soil layer (using free-field displacements)

The normalized p-y curves are shown in **Figure 5.6** and **Figure 5.7**. As mentioned in chapter 4, in order to have a clearer view over the reduction multiplier, the cyclic component is filtered out as much as possible.

It can be seen from the figures that mostly in shallow depths, the values of the pressure are larger in the case of loose sand which can be a consequence of the aforementioned negative pore pressure build-up in the regions near the pile. In larger depths, however, the values are less predictable and are quite close to each other.

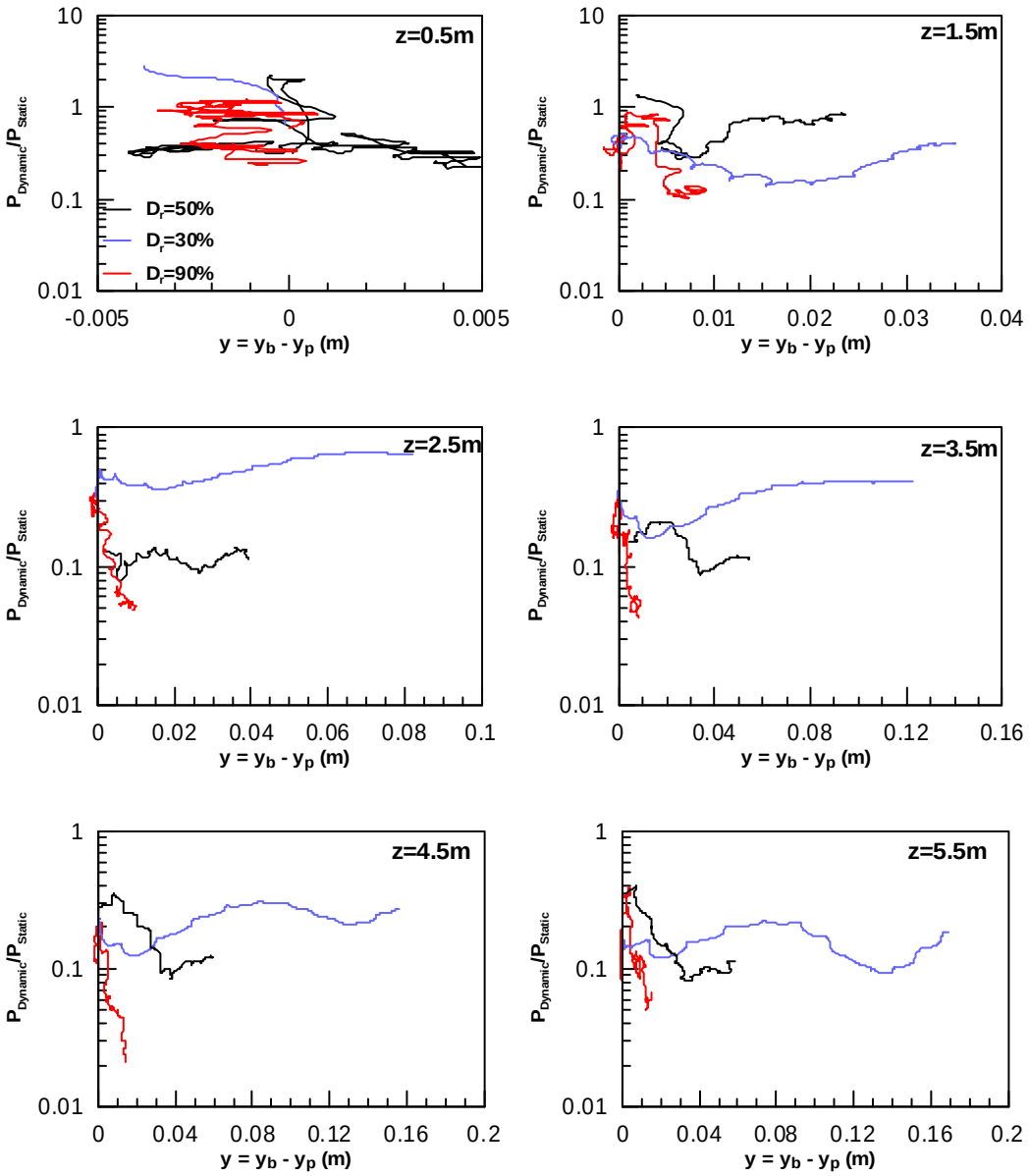

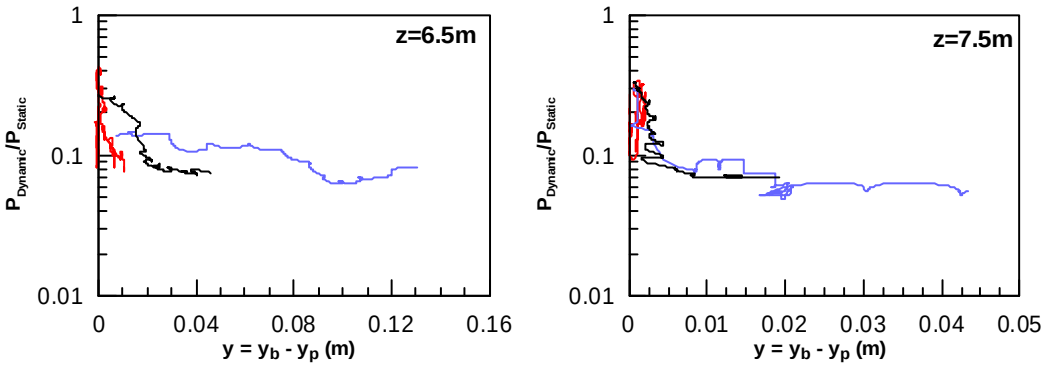

Figure 5.6: Effect of soil relative density on normalized p-y curves throughout the soil layer (using boundary displacements

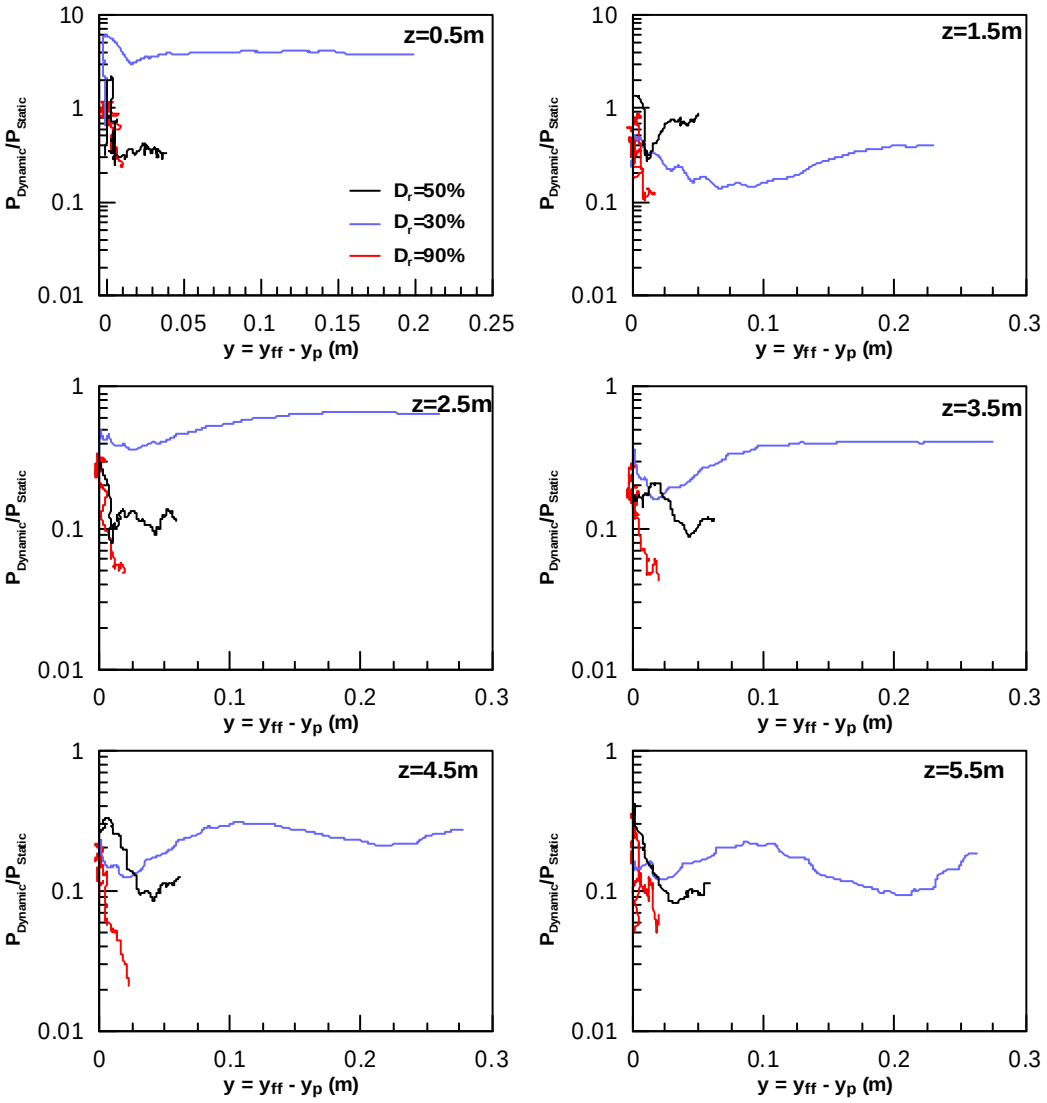

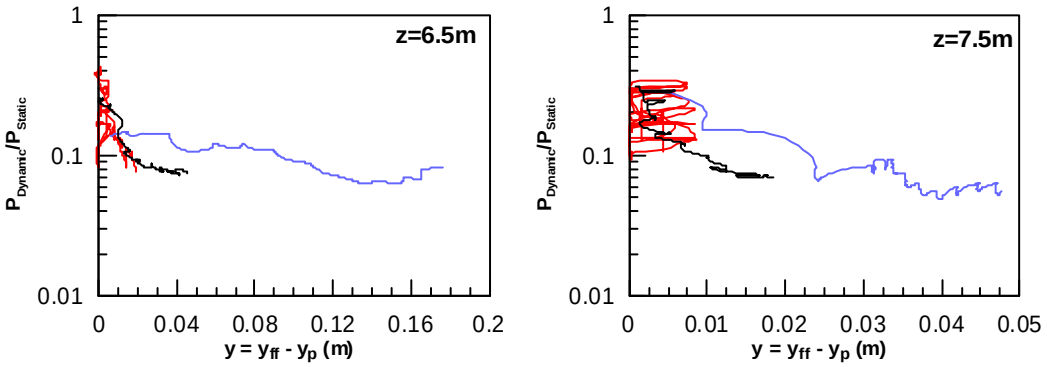

Figure 5.7: Effect of soil relative density on normalized p-y curves throughout the soil layer (using free-field displacements)

Overall, from the analyses regarding the effect of soil relative density the following observations are done:

- All the displacement components (pile, boundary and free-field) decrease with increase in soil relative density D_r.
- Complete liquefaction occurred in free-field in all of the analyses with dilation spikes that are more significant for models with larger relative density.
- The time-histories of excess pore pressure ratio near the pile indicate large dilation which is not reasonable especially for the model with D_r=30%.
- As a result of large dilation, soil reaction is large for D_r=30%, with D_r=50% following and D_r=90% yielding the smallest resistant almost in all relative displacement ranges.

5.3. Effect of permeability, k

In this paragraph the effect of soil permeability on the p-y response is evaluated. The permeability of soil in the basic analysis is equal to 6.1e-5 m/s. In order to see the effect of permeability four kinds of analyses have been done. Firstly, the undrained situation (k=0) has been analyzed in which the water is not allowed to be drained at all by switching off the flow of water in the numerical model. Secondly, the upper bound of k= 6.1e-4 m/s is applied and then the lower bound of k= 2.1e-5 m/s which is called the dynamic permeability is examined. It has been observed that when flow occurs in multiple directions, the permeability is decreased. The value $k = 6.1 \times 10^{-4} m/s$ reflects soil's characteristic property to increase its permeability as a result of pore pressure build-up. The specific value, which is ten times larger than the static, is based on recommendations by Shahir et al. (2010).

Finally, a different kind of analysis has been done in which the soil permeability varies as a function of excess pore pressure ratio, r_u based on Shahir et al. (2010). They performed finite element numerical analysis in order to simulate the centrifuge experiments done by Gonzalez et al. (2002) to define the appropriate assumption for the variation of permeability. The layout of the test and the finite element mesh are shown in **Figure 5.8.**

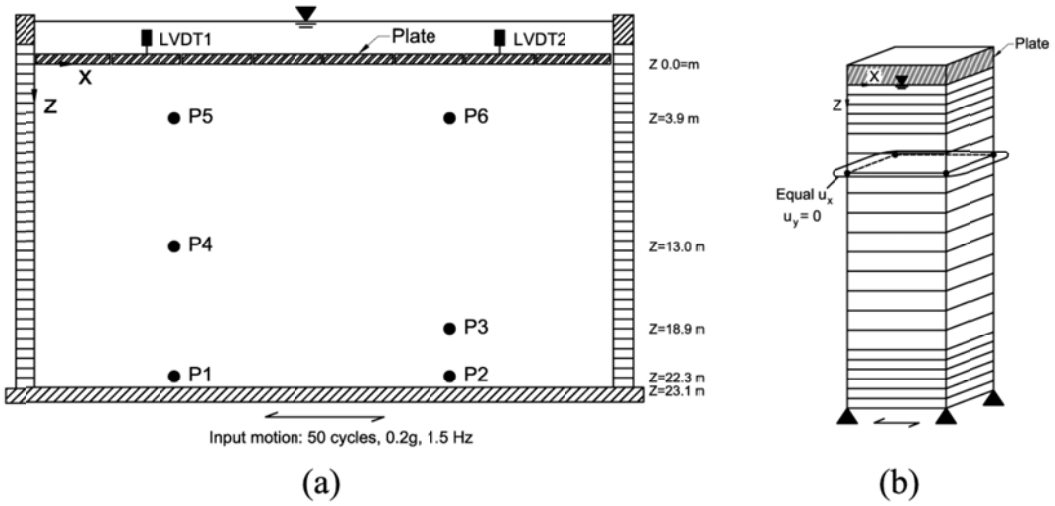

Figure 5.8: a) centrifuge test layout (Gonzalez et al., 2002) b) finite element mesh (Shahir et al., 2010)

Based on the results, the authors concluded that the best agreement is seen when permeability is expressed as a function of the excess pore pressure r_u. A simple power function was proposed for the increase in the permeability during the build-up state (i.e. before complete liquefaction $r_u < 1.0$):

$$\frac{k_b}{k_i} = 1 + (\alpha - 1) \times r_u^{\beta_1} \tag{5.2}$$

For the decrease in permeability during dissipation phase two cases were considered: **a)** Permeability drops immediately after the full liquefaction is finished; and **b)** it starts to decrease during the time of full liquefaction. Expressions (5.3) and (5.4) were proposed according to assumptions **a** and **b** respectively:

$$\frac{k}{k_{ini}} = \begin{cases} \alpha & in\ liquefied\ state\ (r_u = 1.0) \\ 1 + (\alpha - 1) \times r_u^{\beta_2} & in\ dissipation\ phase\ (r_u < 1.0) \end{cases} \tag{5.3}$$

$$\frac{k}{k_{ini}} = \begin{cases} \alpha & for\ t_1 < t < t_2 \\ 1 + (\alpha - 1)\left(\frac{t_3 - t}{t_3 - t_2}\right)^{\beta_2} & for\ t_2 < t < t_3 \\ 1.0 & for\ t_3 \leq t \end{cases} \tag{5.4}$$

A schematic representation of the proposed functions is shown in **Figure 5.9**. These functions have been implemented in the analysis through a FISH function which allowed the permeability to vary both in time and space.

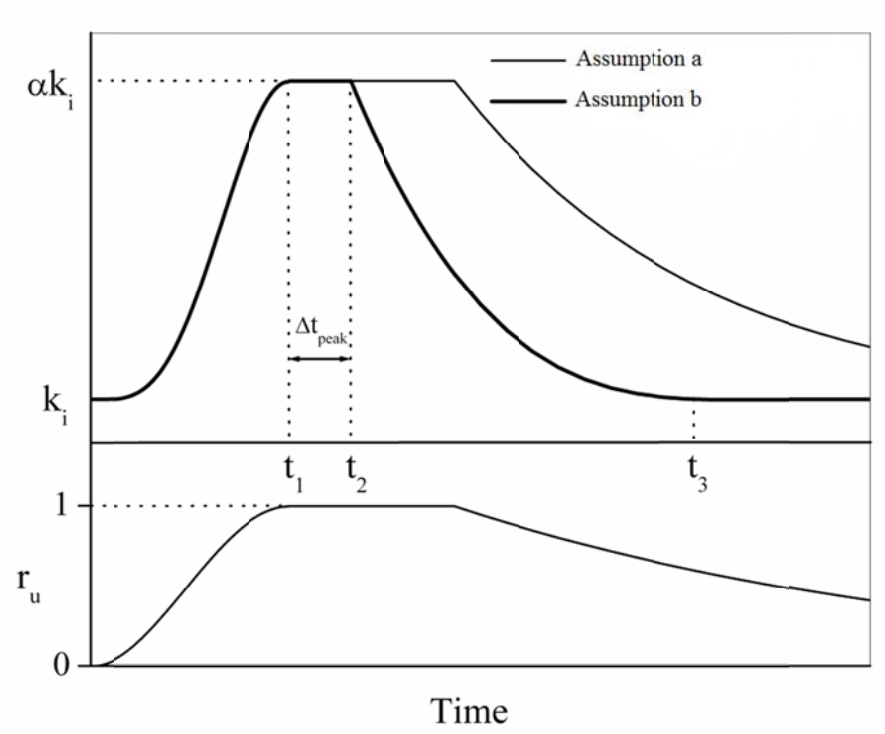

Figure 5.9: Schematic representation of the permeability as a function of excess pore pressure ratio r_u (after Shahir et al., 2010)

In the following, the comparative figures for different soil permeability are shown. **Figure 5.10** compares the lateral displacement for analyses with different permeability coefficients. It can be seen that the effect of permeability is not significant on the displacements. However, an increasing trend can be observed by decrease in permeability of the soil. In other words, the soil layer with the highest permeability (6.1e-5 m/s) has got the smallest displacements.

On the other hand, the results of the undrained analysis don't follow this pattern and lies between the basic and large permeable model which is not reasonable.

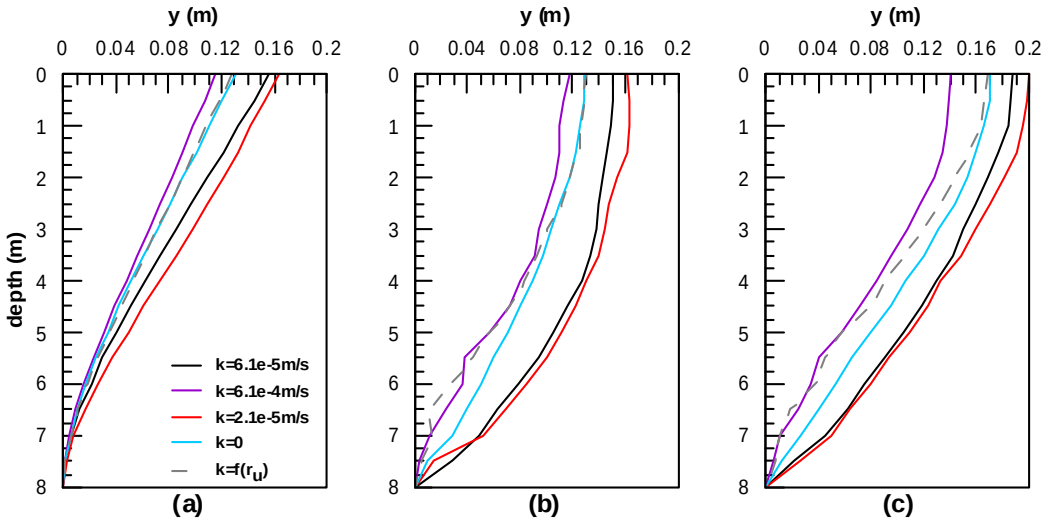

Figure 5.10: Effect of soil permeability on the profile of lateral displacement of a) pile, b) boundary and c) free-field

Figure 5.11 indicates the negative pore pressure build-up near the pile and a number of facts can be concluded from it.

In the analysis with smaller permeability, r_u gets larger negative values compared to the other analyses. This is mainly due to the fact that when permeability is larger, water can come from free-field to dissipate the negative pore pressure, whereas in the case of low permeable sample, this phenomenon does not occur and the excess pore pressure ratio continues to get larger negative values. Large negative excess pore pressure ratios are more significant at shallow depths and it is less considerable in larger depths.

Another interesting fact is that the results for the basic analysis are highly similar to the variable permeability analysis. Except for the shallow depth, the two figures are approximately identical which shows that taking into account the variable permeability does not alter the outcome significantly. Therefore, large computational cost of this kind of analysis is not justifiable.

The time-history of pore pressure ratio in the undrained analysis is not what we expect in some depths. Logically, it should have a downward trend towards large negative values due to large dilation as visible in some depths in **Figure 5.2**. But in the small depths, after reaching a dip at the beginning of shaking, it bounces back and starts to increase to values near 0 at the end of excitation. The reason might be the fact that

assuming zero permeability in soil does not illustrate the real behavior of the liquefied layer because minor flow of water exists even if the permeability is so small. In other words, in this case, minor flow of water throughout the layer is neglected, which is determinant in the pore pressure build-up and consequently the response of the pile. Based on these considerations, the results of this analysis are not shown in the comparative figures of the p-y curves.

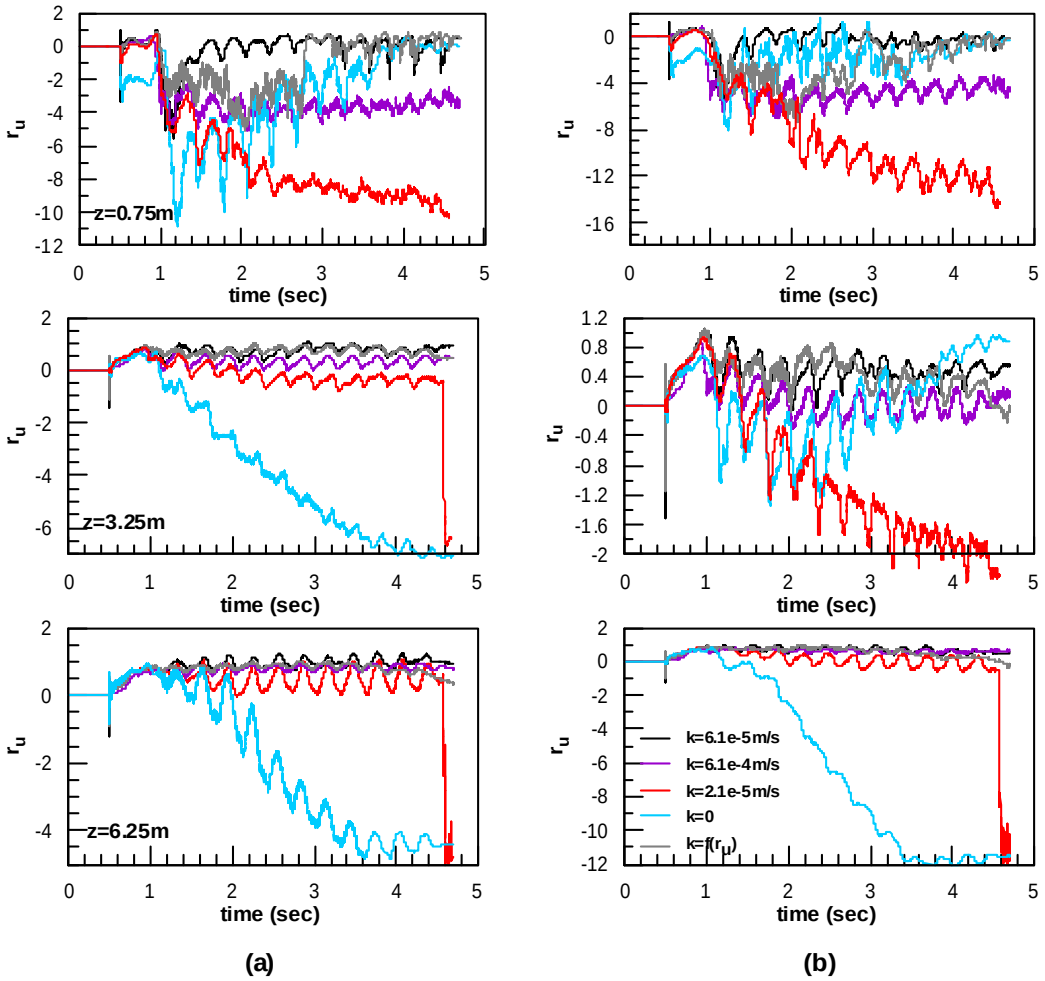

Figure 5.11: Effect of soil permeability on pore pressure build-up near the pile at a) upstream and b) downstream.

According to **Figure 5.12**, the difference in the excess pore pressure ratio in the free-field is less significant. However, large dilation spikes are observed in samples with low permeability especially in shallow depths due to larger displacements.

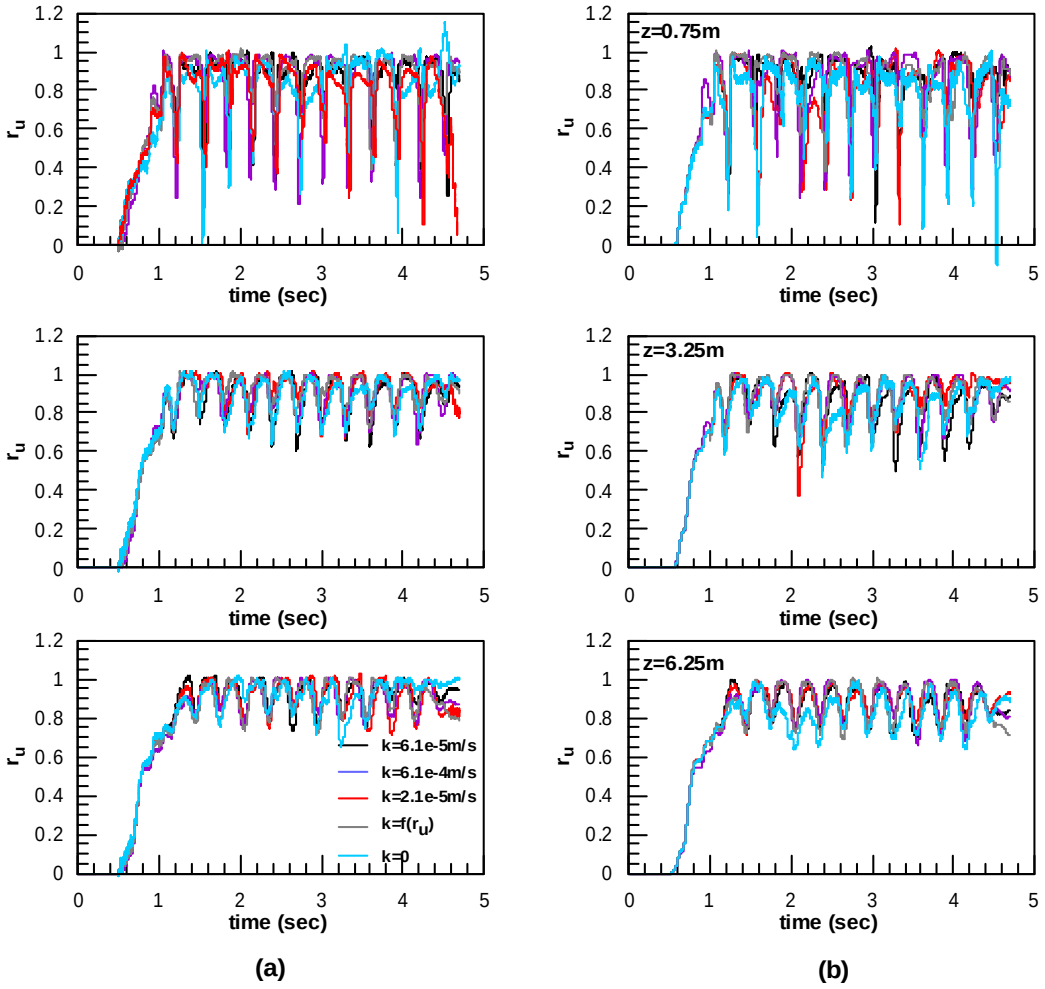

Figure 5.12: Effect of soil permeability on pore pressure build-up at free-field a) with pile and b) without pile.

As mentioned before, development of large negative pore pressure ratio in the low permeable soil causes large lateral resistance. Therefore, as indicated in **Figure 5.13** and **Figure 5.14**, the soil with lower permeability provides larger values in the p-y curves. The differences are significant in middle depths but negligible in very shallow and very large depths.

Apart from that, the lateral resistance of the sample with variable permeability is quite similar to the analysis with constant permeability coefficient in most of the depths measured while smaller relative displacement is observed.

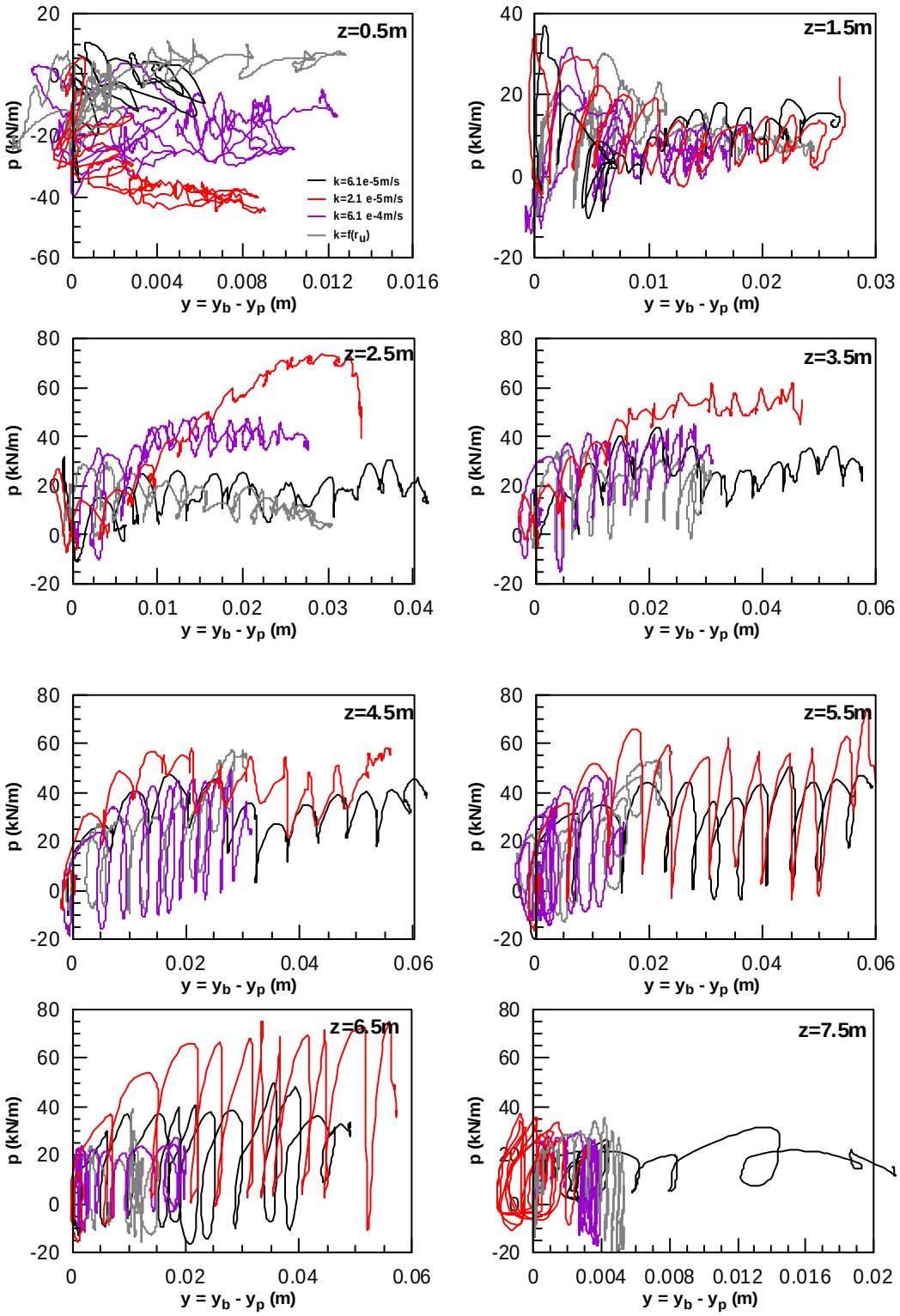

Figure 5.13: Effect of soil permeability on dynamic p-y curves throughout the soil layer (using boundary displacements)

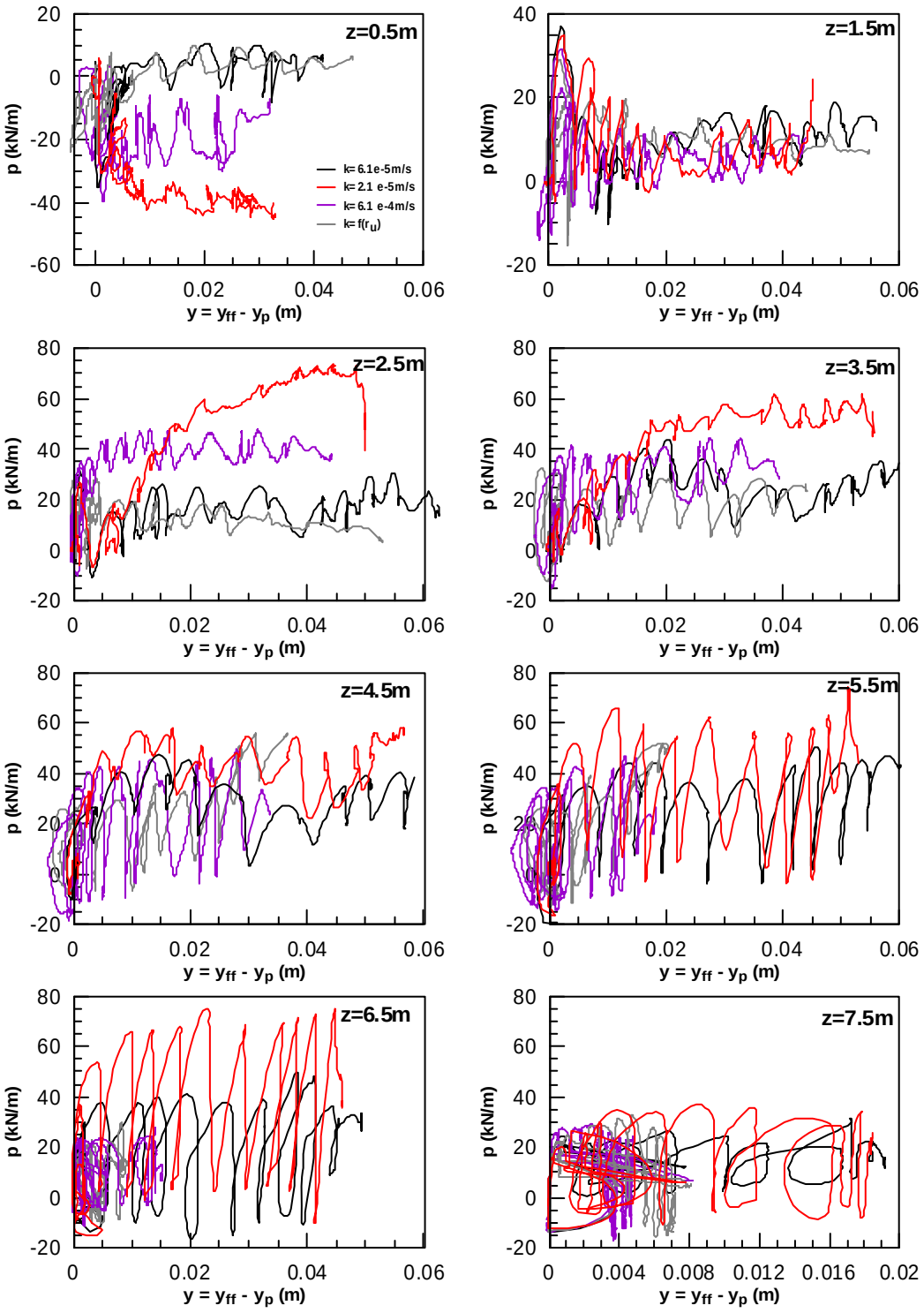

Figure 5.14: Effect of soil permeability on dynamic p-y curves throughout the soil layer (using free-field displacements)

Figure 5.15 and **Figure 5.16** show the p-y curves normalized with the static values which can be an indicator of the reduction multiplier m_p after filtering the cyclic components. It can be observed that the sample with small permeability yields larger normalized values compare to the others as a result of aforementioned negative pore pressure build-up. The difference with the other analyses is quite significant in most of the depths. Another important observation is close figures for variable and basic analysis in approximately all relative displacement ranges.

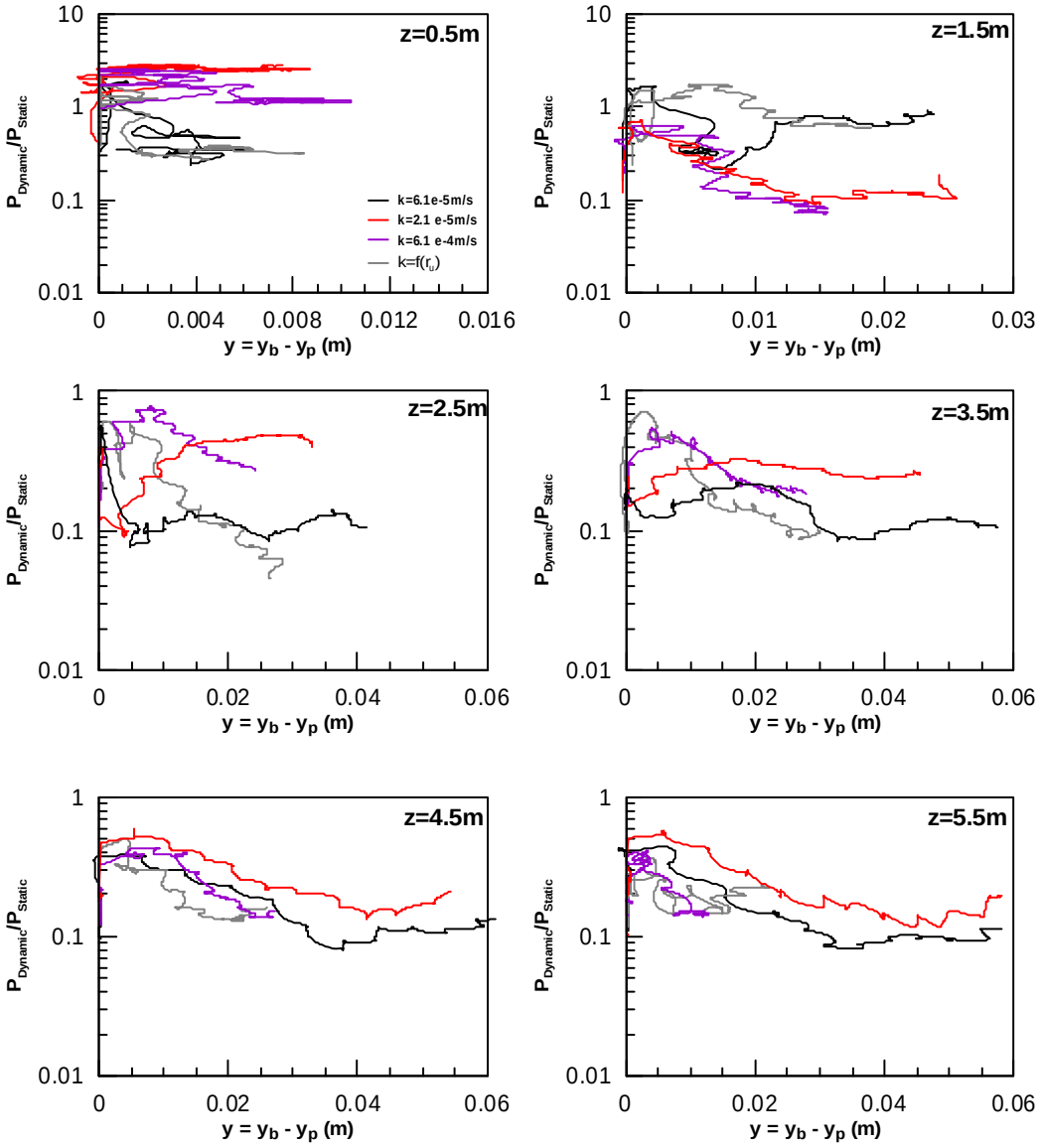

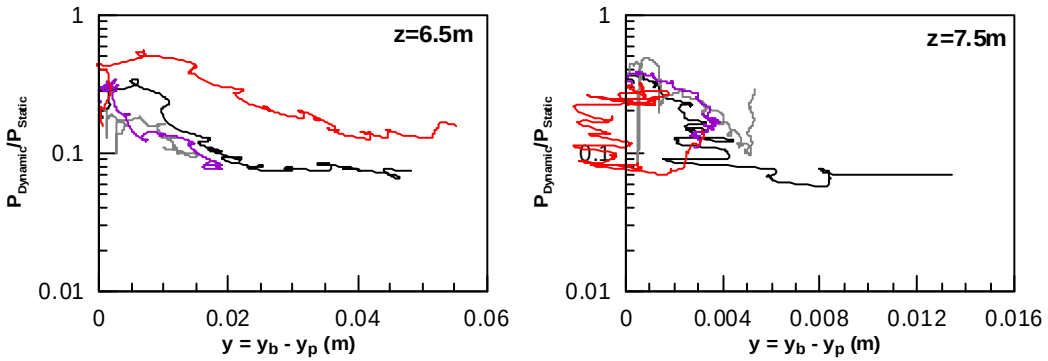

Figure 5.15: Effect of soil permeability on normalized p-y curves throughout the soil layer (using boundary displacements)

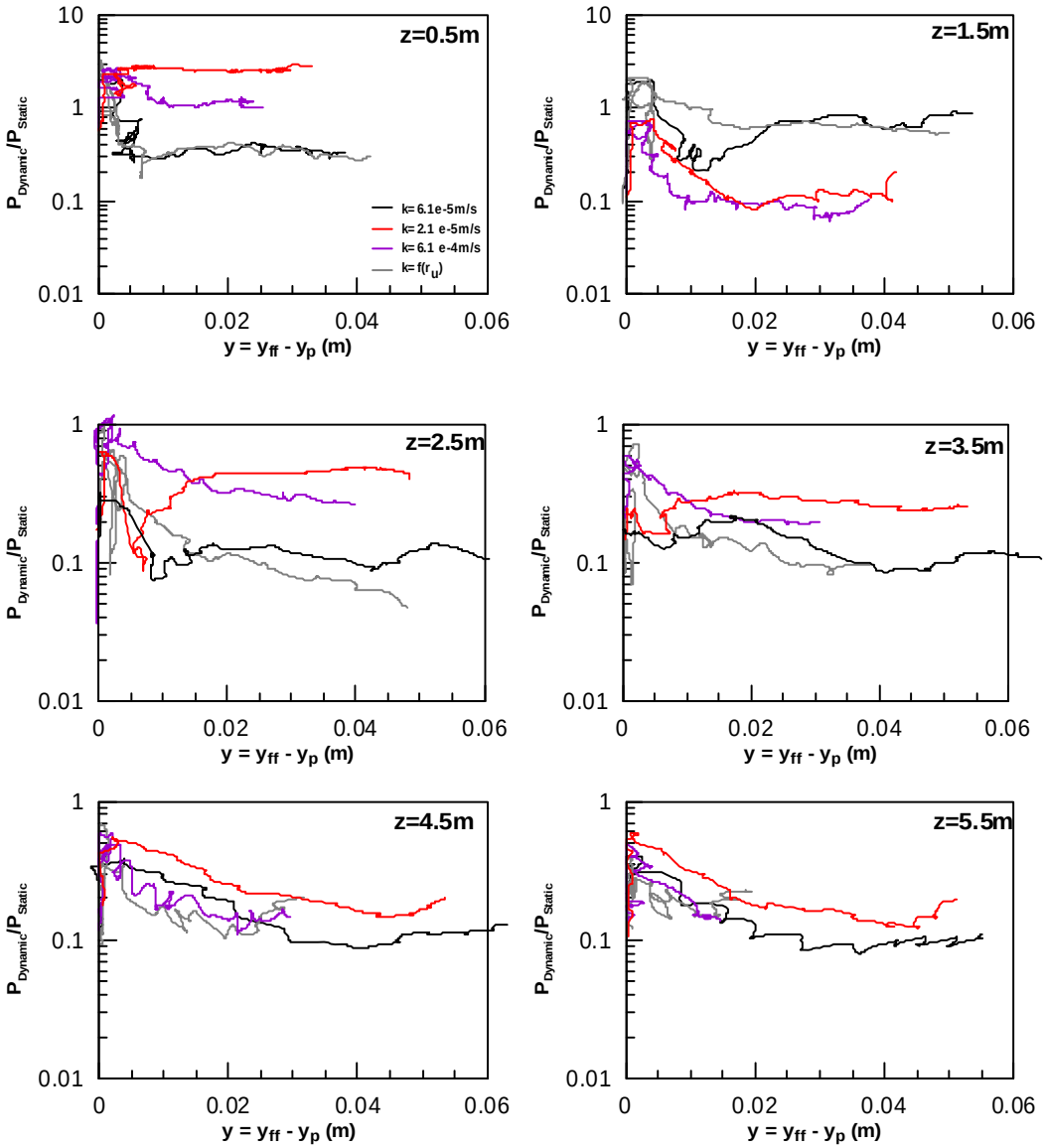

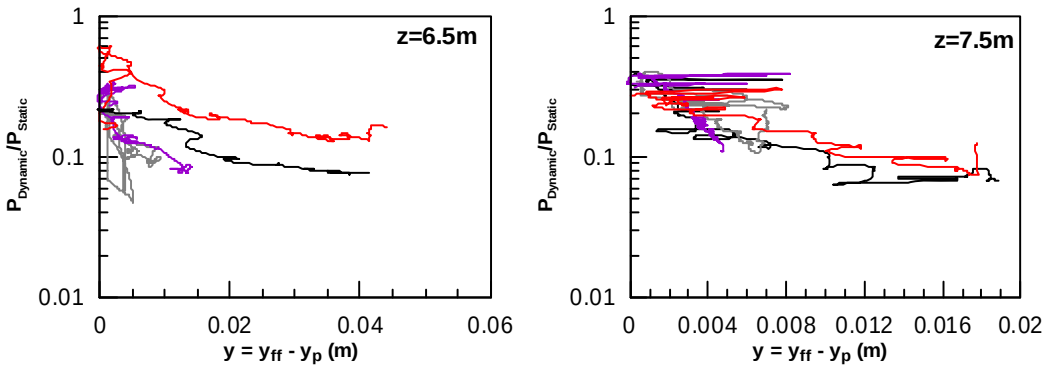

Figure 5.16: Effect of soil permeability on normalized p-y curves throughout the soil layer (using free-field displacements)

Overall, the following facts can be concluded from the analyses regarding the soil permeability:

- Permeability is quite determinant in the response of the pile in laterally spreading ground. In other words, piles embedded in low permeable liquefiable soil are subjected to larger lateral loading especially in middle depths.
- The lateral displacements in the liquefied soil and the pile are reversely related to permeability: the smaller the permeability, the larger the lateral displacements
- Applying the permeability as a function of excess pore pressure seems to have negligible effect on the response and is not recommended.
- Assigning zero permeability to soil (switching off the flow in the numerical analysis) are far from the reality and does not provide logical results since the inevitable flow of water throughout the liquefied soil layer during the excitation has significant impacts on the response and cannot be neglected.

5.4. Effect of excitation period

The effect of period of excitation on the liquefied p-y response has been evaluated by performing two different analyses with small and large period excitations, T=0.1s and T=0.5s respectively.

In the analysis for the T=0.1s, as the total duration for excitation with 14 cycles is equal to 1.9 sec which is relatively small for clear observation and comparison, the number of cycles has been increased to 42 cycles in order to reach the same overall duration of the excitation which is equal to 4.7 sec (by adding 0.5 seconds of no excitation at the beginning). However, after approximately 4 seconds the soil becomes unstable and responds strangely as **Figure 5.17** and **Figure 5.18** show. To be more precise, the excess pore pressure gets unacceptable large negative values after this time and the calculated p-y curves become unreasonably large (as shown in Appendix A).

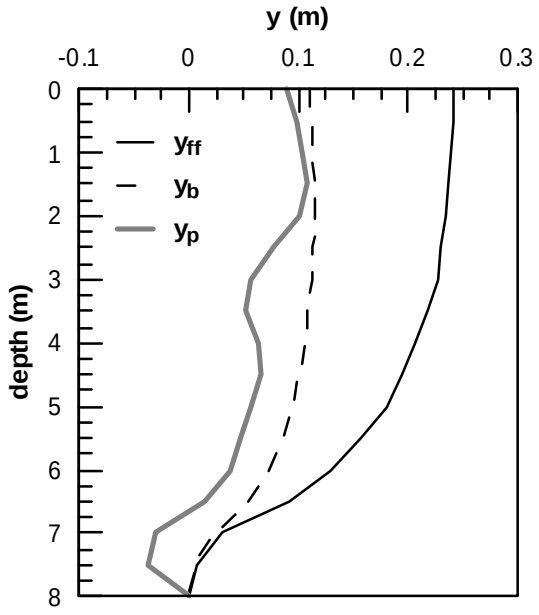

Figure 5.17: Profile of lateral displacements at the end of shaking

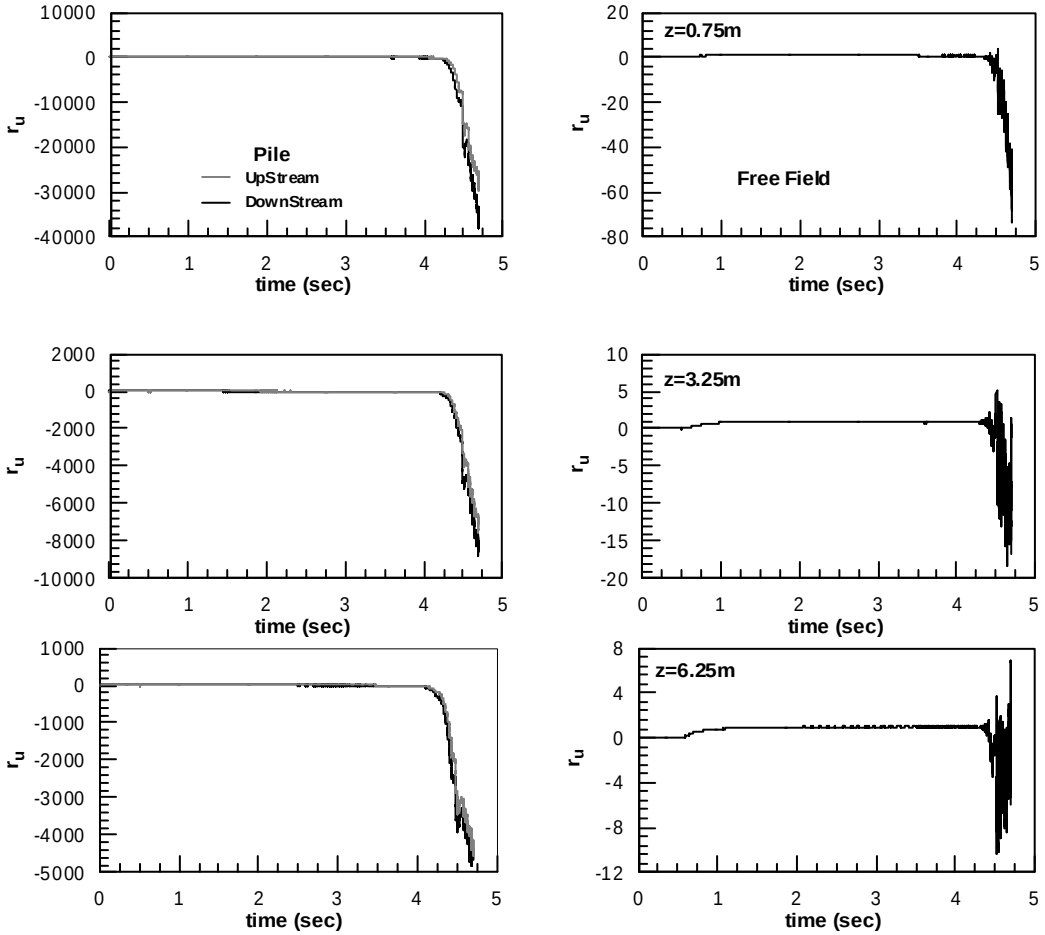

Figure 5.18: Time-histories of excess pore pressure ratio near the pile and at free-field

In the other analysis which is the evaluation of effect of large period (T=0.5s), the similar problem occurs after about 4 seconds as it is shown in **Figure 5.19** and **Figure 5.20**.

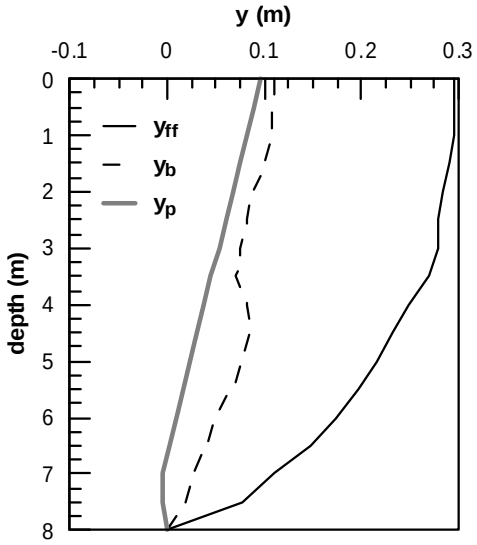

Figure 5.19: Profile of lateral displacements at the end of shaking

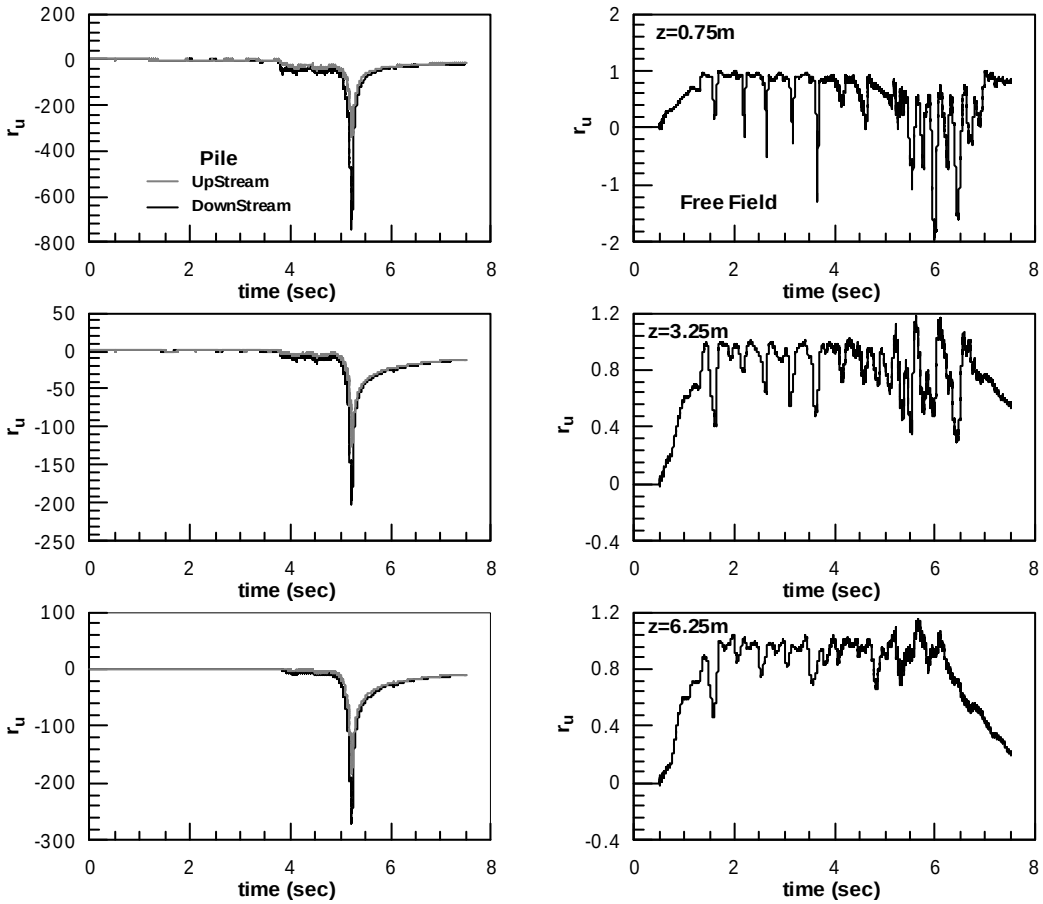

Figure 5.20: Time-histories of excess pore pressure ratio near the pile and at free-field

In order to make the comparison possible, all the figures – the time-histories of excess pore pressure and p-y curves and the profile of displacements – are plotted for the data in the first 3 seconds of the excitation and shown in the following figures. The reason is that at this moment the relative displacements are fairly equal for all of the analyses at corresponding depths as it is shown in **Figure 5.21**.

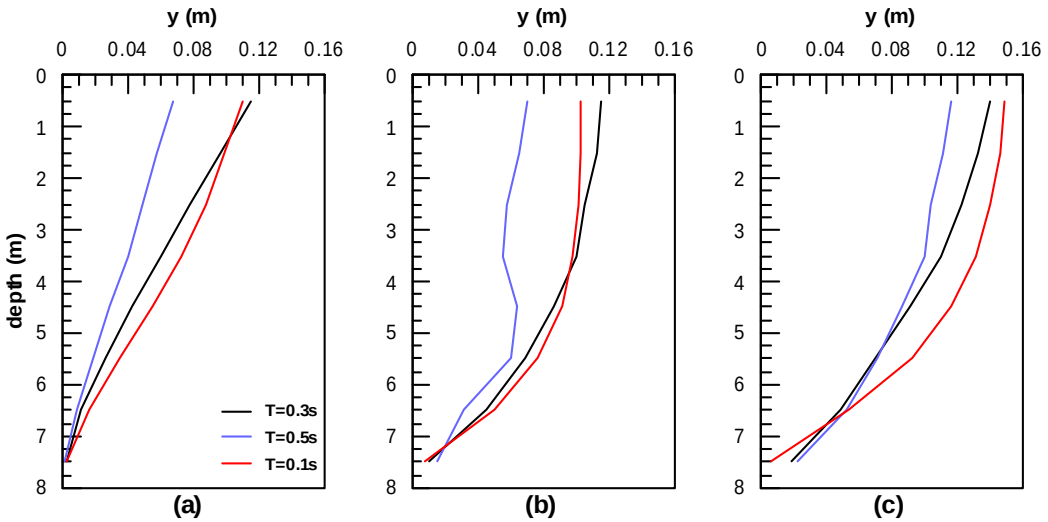

Figure 5.21: Effect of excitation period on the profile of lateral displacements of a) pile, b) boundary and c) free-field

Figure 5.22 which compares the excess pore pressure ratios near the pile, indicates that large negative excess pore pressure is developed in the low period excitation while the response for T=0.3s and 0.5s are similar. The reason seems to be based on the fact that when the loading rate is high, the water in the free-field does not find enough time to travel to the near the pile zone and dissipate the negative pressure which causes ever-increasing negative pore pressure beside the pile foundation. While in the other two analyses, the larger period allows the dissipation of negative pore pressure and makes the soil more homogenous. Again, the process is more significant at shallow depths where r_u gets values of the order of -10 at t=3 sec while in z=6.25 m it reaches zero only.

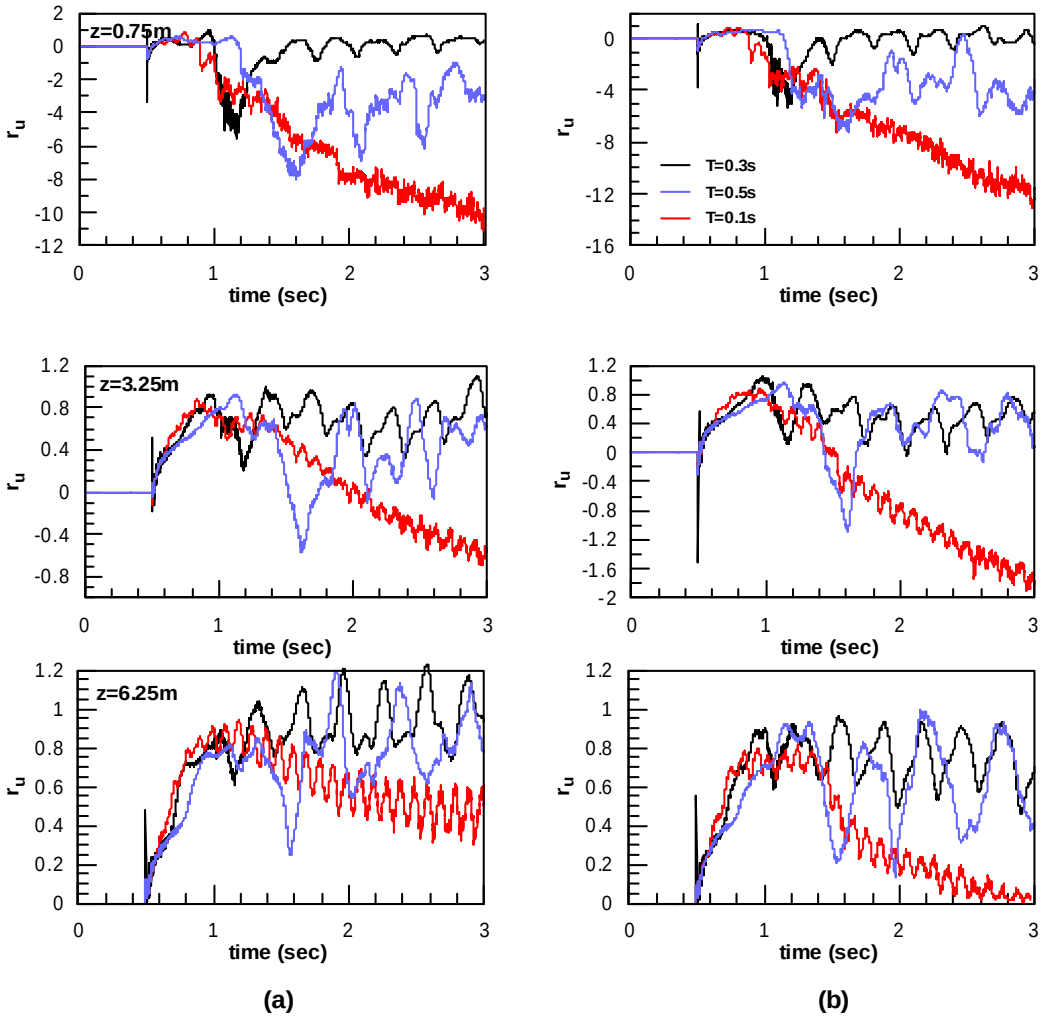

Figure 5.22: Effect of excitation period on pore pressure build-up near the pile at a) upstream and b) downstream

In the free-field, on the other hand, full liquefaction (i.e. r_u =1) occurs for T=0.1s with negligible dilation spikes while moderate and large spikes are observed for T=0.3s and 0.5s respectively (**Figure 5.23**). The reason is that when the period is larger, larger displacements occur in each cycle which lead to dilation and therefore, larger spikes.

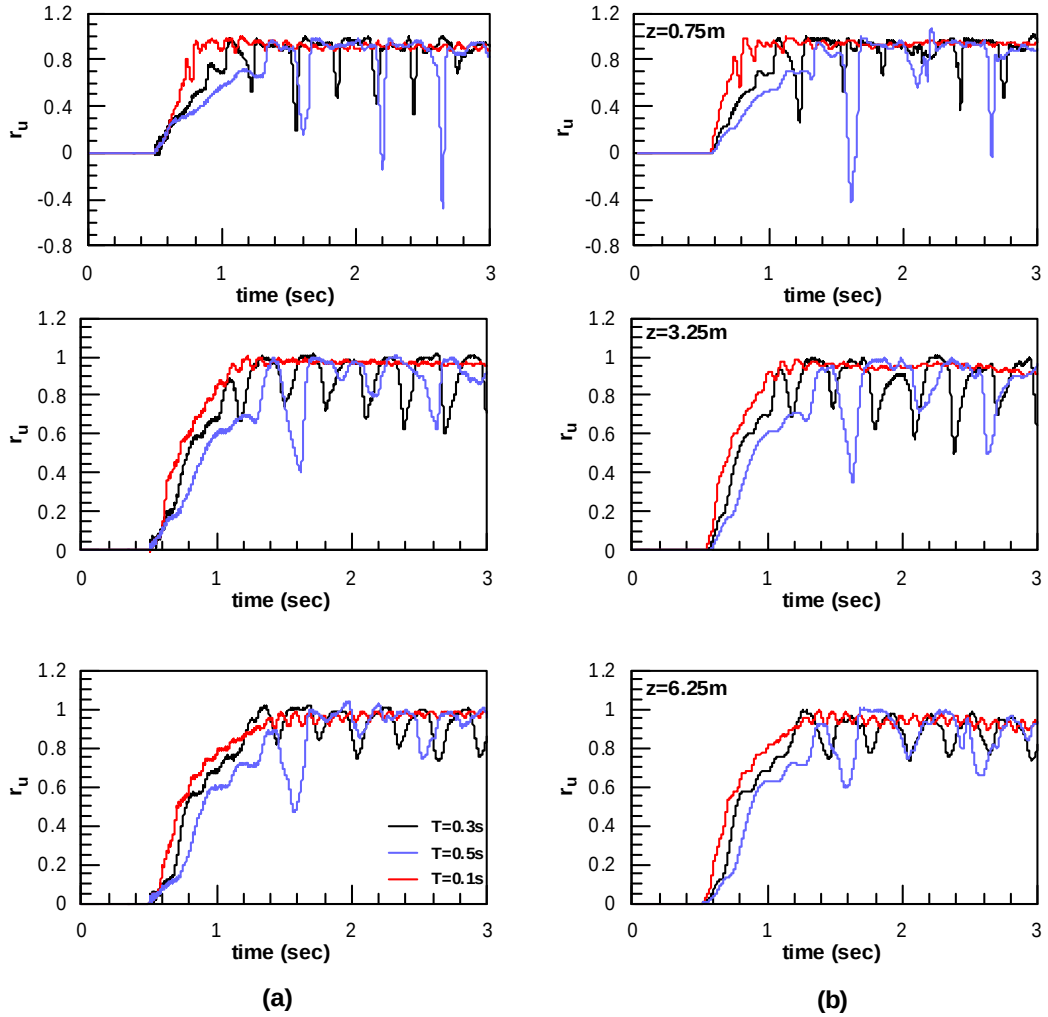

Figure 5.23: Effect of excitation period on pore pressure build-up at free-field a) with pile and b) without pile

Based on what was mentioned regarding the pore pressure build-up in the liquefied layer, the difference in the dynamic p-y curves can be explained. The large negative pore pressure developed in the analysis with T=0.1 sec makes soil stiffer and the stiffer soil provides stronger lateral resistance as shown in the following figures. The difference is more dramatic in shallow depths. Apart from that, the lateral force tends to increase continuously in this case while in the other two analyses, it reaches a plateau soon after the start of the excitation.

The results of the large period excitation are quite similar to the basic. It means that, the excess pore pressure either near the pile or in free-field are very close to each other at most of the places in these two analyses. Consequently, the p-y curves for both analyses are similar in corresponding depths.

It seems that at T=0.3s and the permeability coefficient equal to 6.1e-5 m/s, enough time exists for water to travel from free-field and dissipate the negative pore pressure. Therefore, in larger periods (in here T=0.5 s) the same phenomena occurs and the effect will be negligible.

Consequently, for a soil sample with specific permeability, there should be a threshold of the excitation period from which the influence becomes considerable. In other words, for instance, if the permeability coefficient was lower, T=0.5s could probably change the situation and help in the dissipation of the negative pore pressure, resulting in different p-y multiplier.

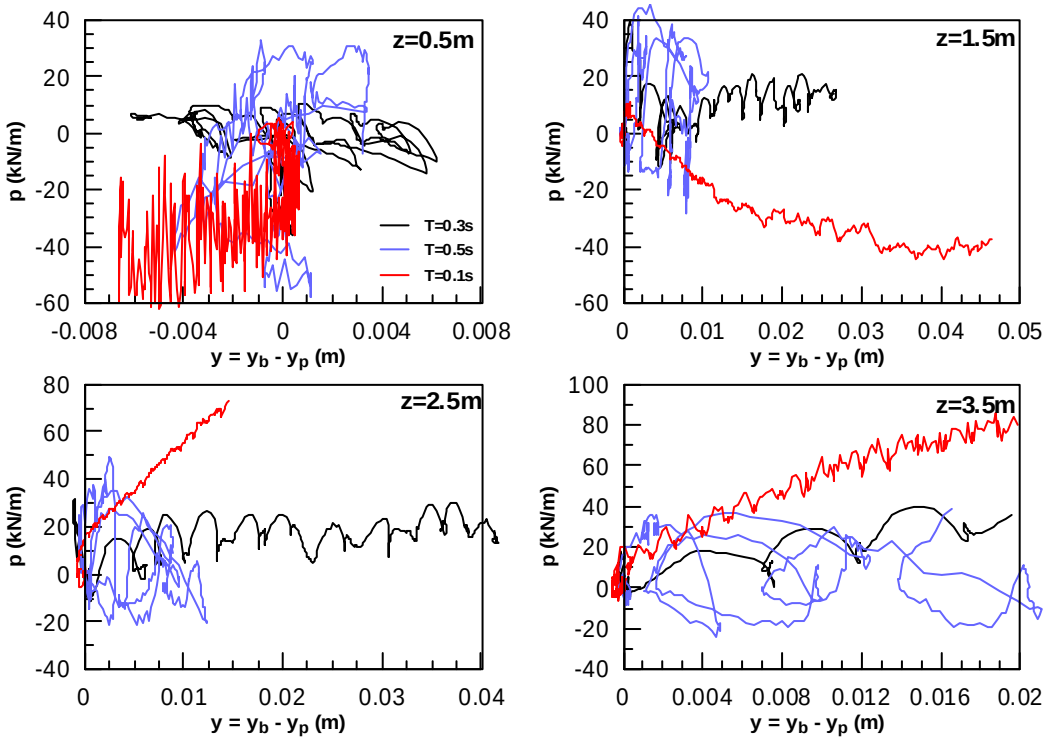

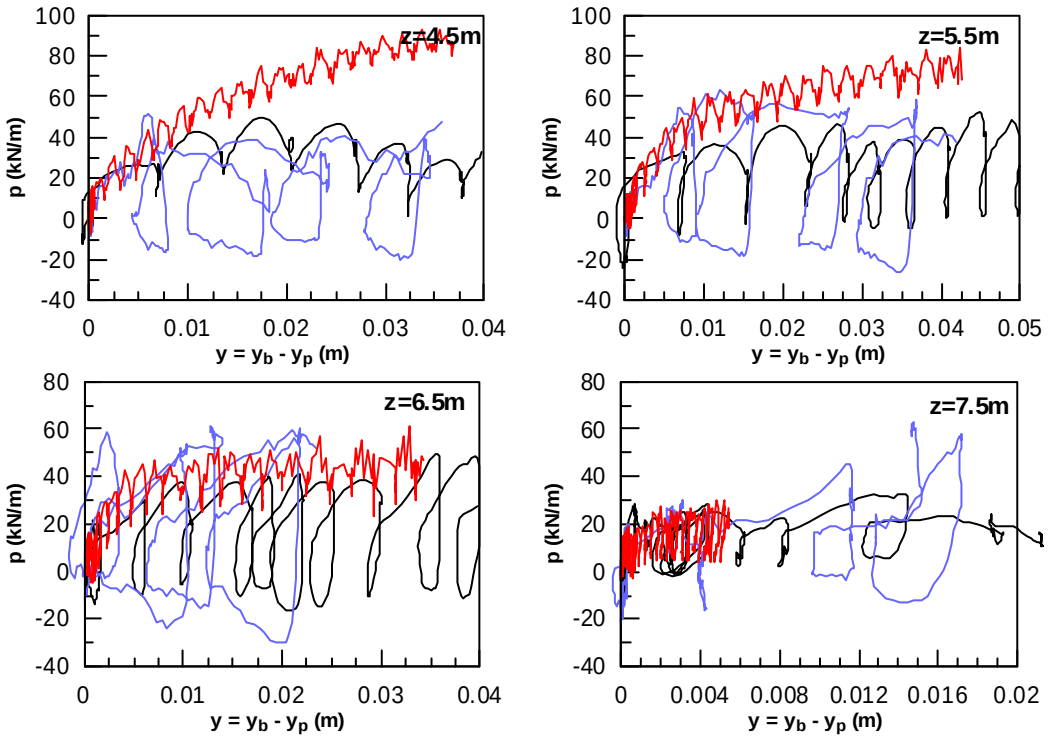

Figure 5.24: Effect of excitation period on dynamic p-y curves throughout the soil layer (using boundary displacements)

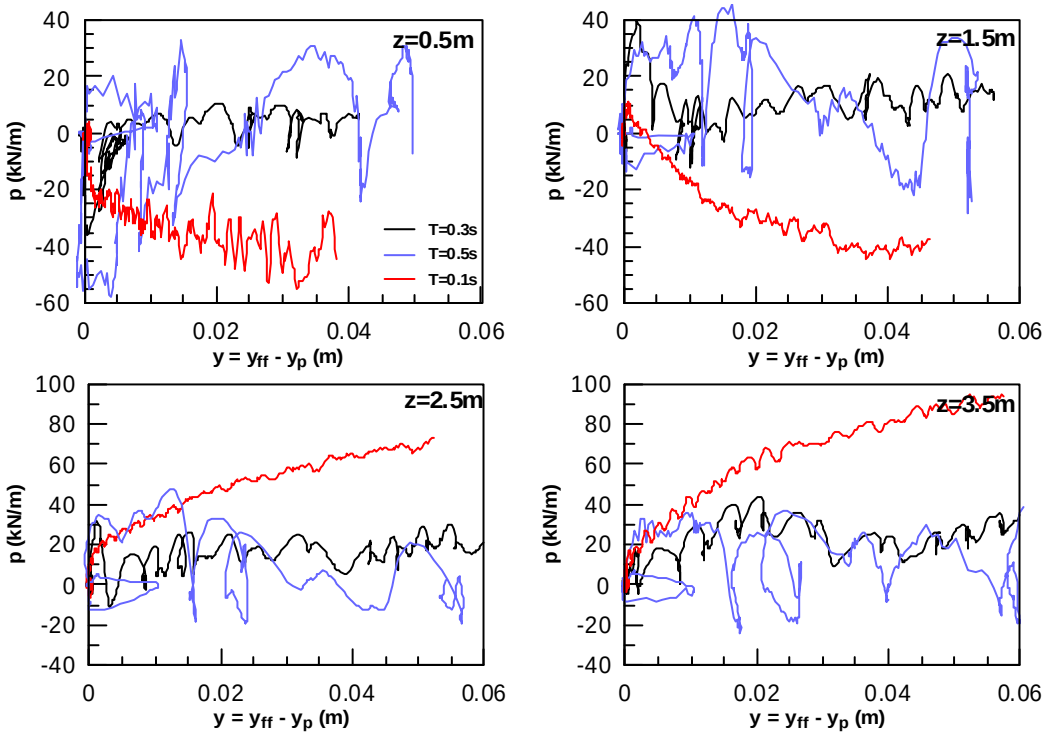

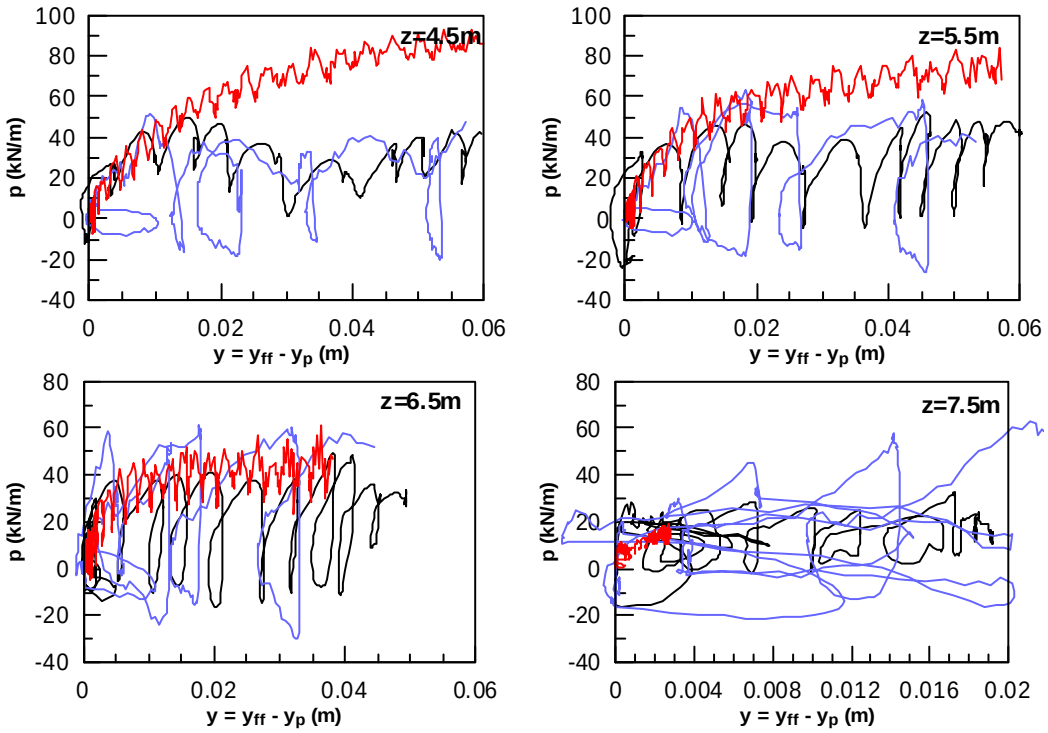

Figure 5.25: Effect of excitation period on dynamic p-y curves throughout the soil layer (using free-field displacements)

According to **Figure 5.26** and **Figure 5.27**, the normalized dynamic p-y curves get larger values for T=0.1s at smaller depths as a result of the aforementioned reasons while the two other figures give approximately similar results.

Another property of the normalized p-y curves is that for the smaller periods, the fluctuations are less. While in most of the depths, the figure for T=0.1s remains relatively stable during the excitation, moderate and large variations are observed for T=0.3s and T=0.5s respectively.

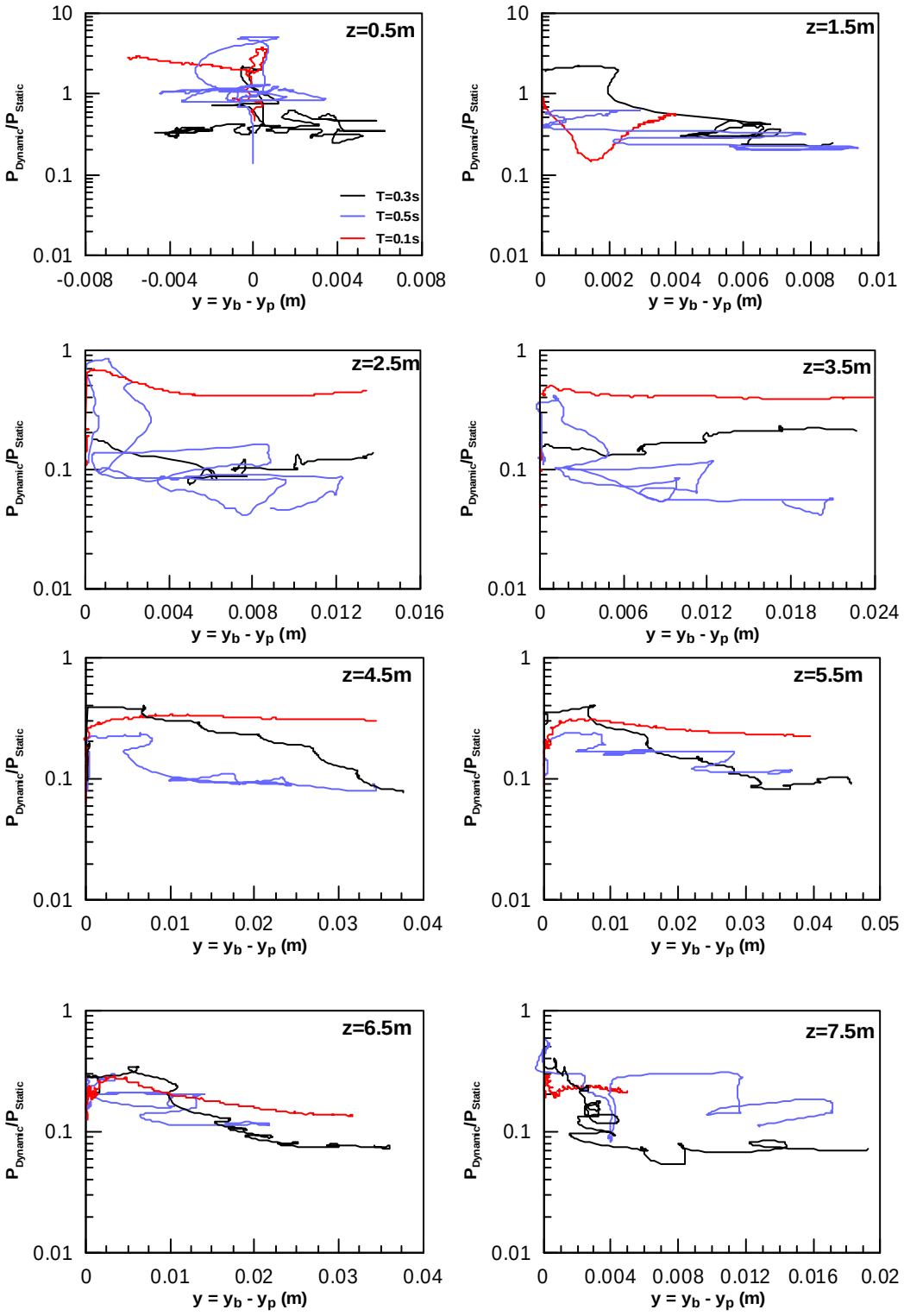

Figure 5.26: Effect of excitation period on normalized p-y curves throughout the soil layer (using boundary displacements)

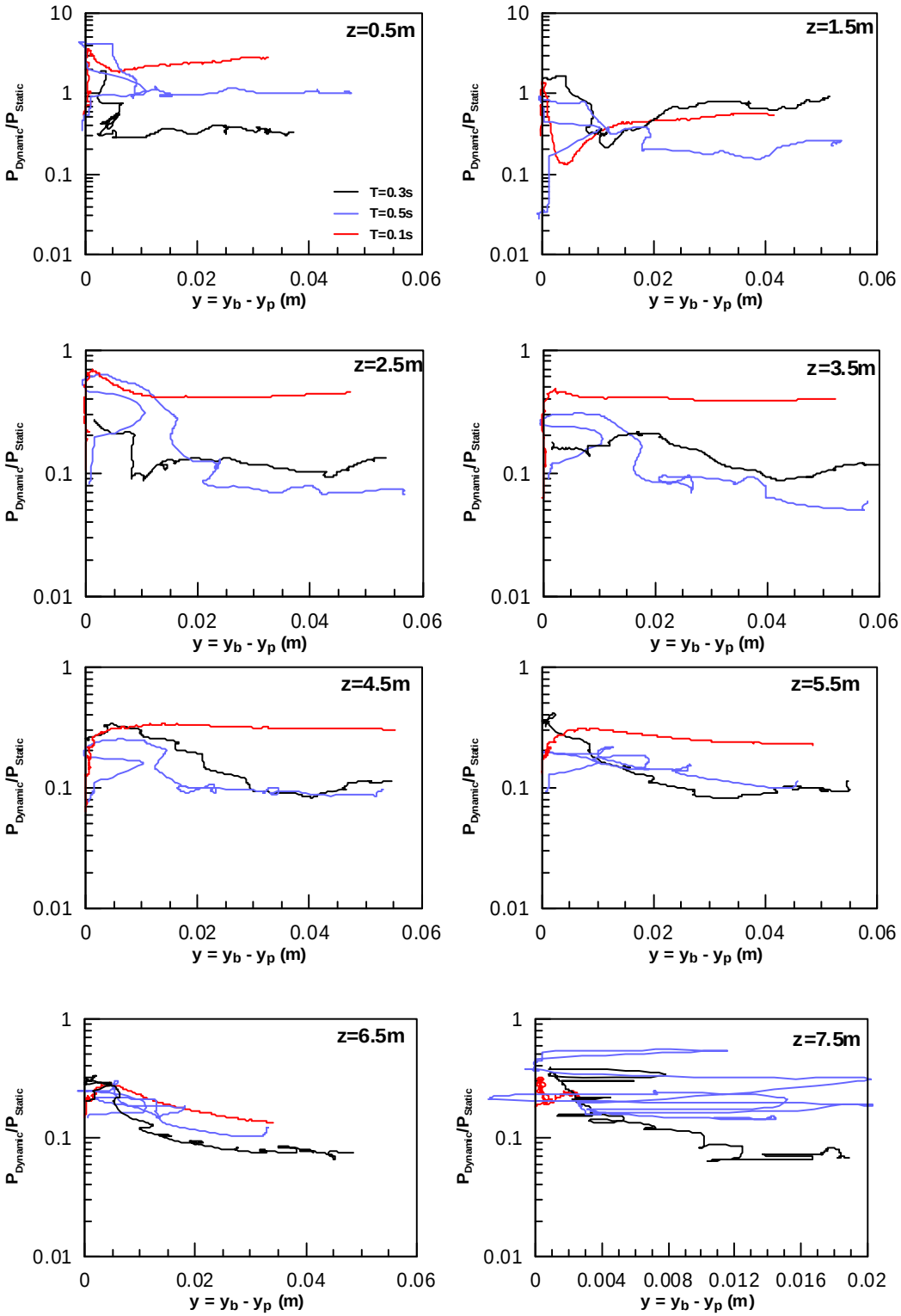

Figure 5.27: Effect of excitation period on normalized p-y curves throughout the soil layer (using free-field displacements)

Overall, the following facts can be obtained from studying the effect of excitation period:

- Large frequency excitation (i.e. small period) causes large negative pore pressure ratios in the vicinity of pile leading to an increase in the lateral force.
- Liquefiable soil subjected to large excitation period undergoes smaller lateral displacements. The same pattern is observed for the pile.
- There seems to be an upper bound to the excitation period's effect on the p-y response of the pile in liquefied soil which is a function of soil permeability. Therefore, the effect of shaking period and soil permeability are not independent and should be studied simultaneously.

Chapter 6

Effect of pile characteristics on liquefied p-y response

6.1. General

In this chapter the effects of parameters that correspond to pile are evaluated. These parameters are:

- Pile Diameter, D
- Pile Stiffness, EI
- Pile Installation Method
- Head Constraint

In the following, the results of analysis for each parameter will be discussed in separate paragraphs. Additionally, in each part, the modifications that should be done in the input file in order to take into account the effect of each parameter will be described clearly.

6.2. The effect of pile diameter

In this part, the effect of diameter of pile is evaluated by doing two analyses corresponding large and small diameter, 1 m and 0.4 m respectively.

In order to keep the ratios of the mesh size over the pile diameter constant, the length of pile and mesh dimensions have been changed by the same ratio. In other words, instead of 11 m* 5 m* 8 m finite difference mesh, in large and small diameter analyses the dimensions have changed to 18.5 m *8.3 m *13 m and 7.15 m * 3.25 m* 5 m respectively. Apart from that, the Young modulus of pile is changed in a way that the overall stiffness of pile (EI) is remained constant. As the diameter of pile changes the moment of inertia with a power of 4 in a circle ($I = \frac{\pi r^4}{4}$), for the large diameter the Young modulus is divided by $\left(\frac{1.0}{0.6}\right)^4 = 7.716$ and for the small diameter by $\left(\frac{0.4}{0.6}\right)^4 = 0.198$.

The depths, at which the time-histories of excess pore pressure ratio are kept, are also changed with the same ratios. The time-histories of lateral resistance and the displacements – that are used for the construction of p-y curves – are kept at each 1 meter throughout the layer for all of the analyses. Therefore, two type of comparison are made: one with comparing the same depths in each analysis, which is applicable for depths up to 4.5 m; and one with comparing depths with roughly the same z/h ratio. For instance, the depth of 2.5 m in the analysis of 0.4 m diameter pile is compared to 3.5 m in the basic and 6.5 m in the large diameter pile. The two sets of comparative figures are presented in the following pages.

The profiles of lateral displacements are shown in **Figure 6.1.** As it could be predicted, the displacements are larger for the larger samples. For free-field displacements, it is justifiable by many proposed empirical equations (Hamada et al., 1986, 1987; Aydan et al., 2005; Valsamis et al., 2010) which state that the thickness of the liquefied layer plays an important role in the final lateral displacement. Consequently, the displacements of pile follow the same pattern.

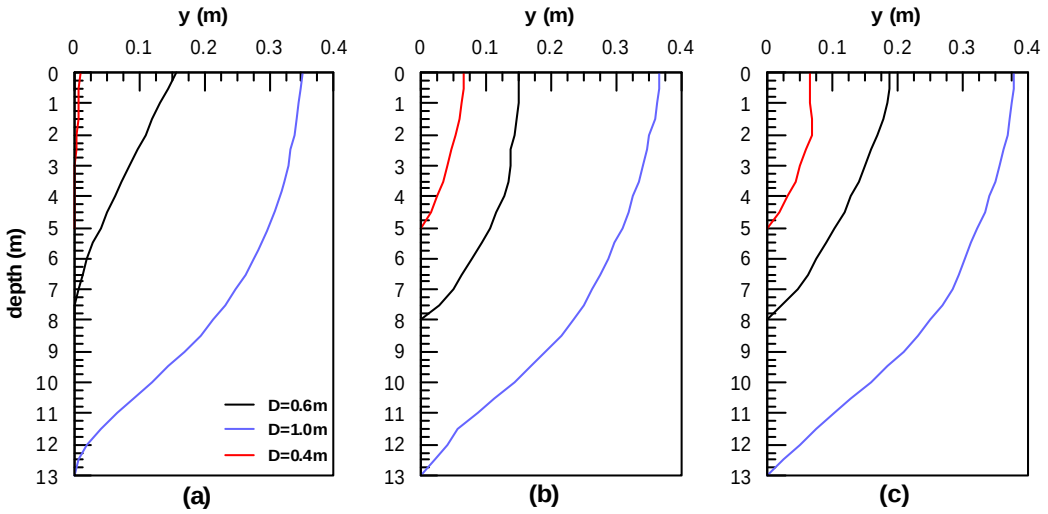

Figure 6.1: Effect of pile diameter on the profile of lateral displacements of a) pile, b) boundary and c) free-field

The time-histories of excess pore pressure ratio are near the pile and in the free-filed are shown in

Figure 6.2 and

Figure 6.3 respectively. Complete liquefaction has occurred in free-field for all of the analyses soon after the start of the excitation with moderate dilation spikes. On the other hand, different response is observed near the pile. The most significant point is the development of large negative excess pore pressure near the surface in the analysis with large diameter. It can be due to the fact that due to the large size of the pile, the travel distance of water is longer compared to the other analyses and cannot dissipate the negative pore pressure build-up in each cycle.

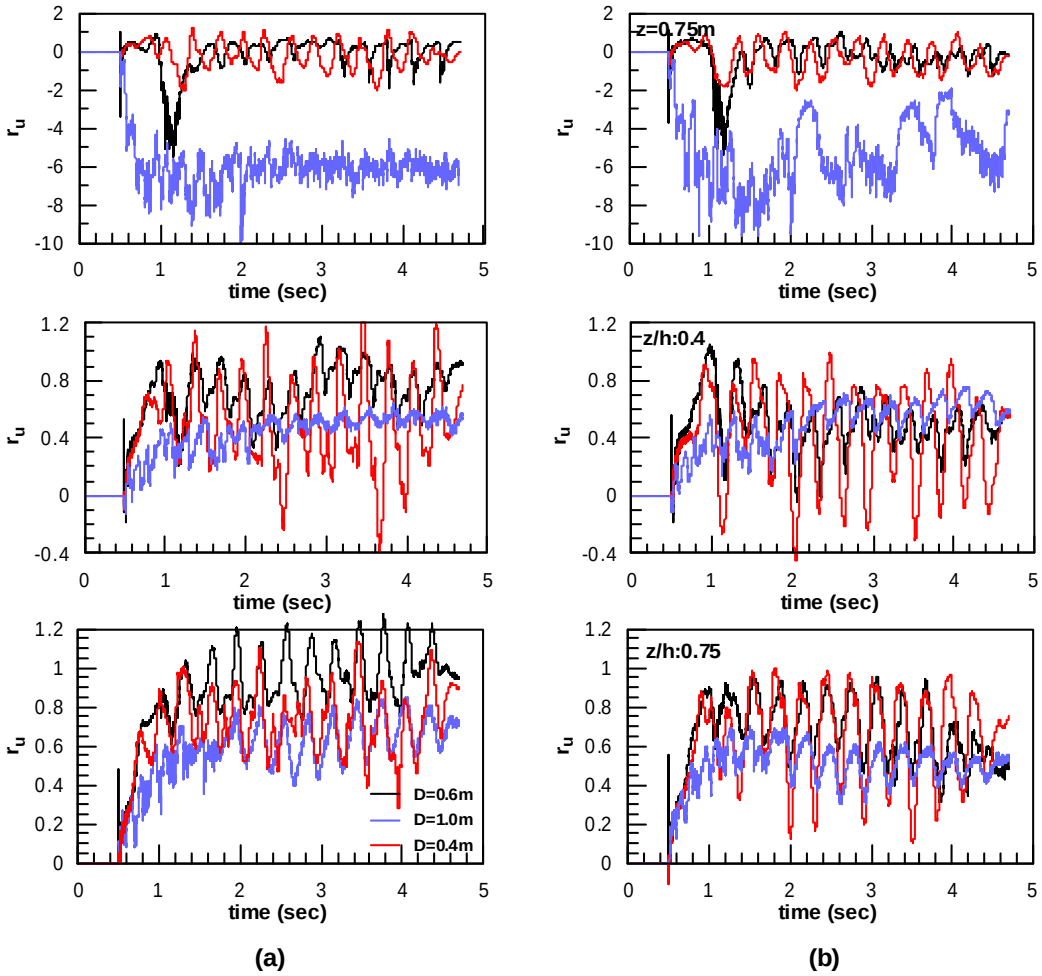

Figure 6.2: Effect of pile diameter on pore pressure build-up near the pile at a) upstream and b) downstream

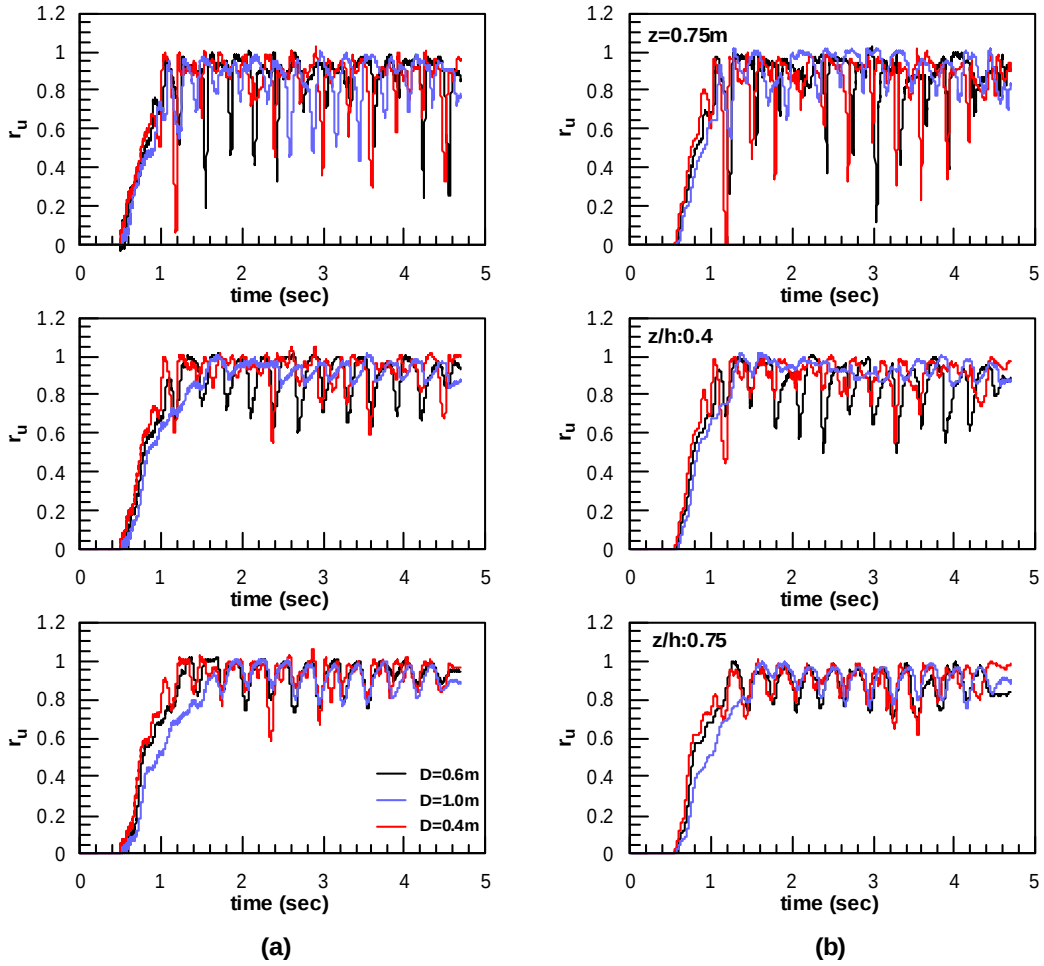

Figure 6.3: Effect of pile diameter on pore pressure build-up at free-field a) with pile and b) without pile

Figure 6.4 to **Figure 6.7** illustrate the dynamic p-y curves. It can be seen that different trends are observed for different depths. Therefore, no specific conclusions can be made regarding the effect of pile diameter on the response of the pile in the laterally spreading ground.

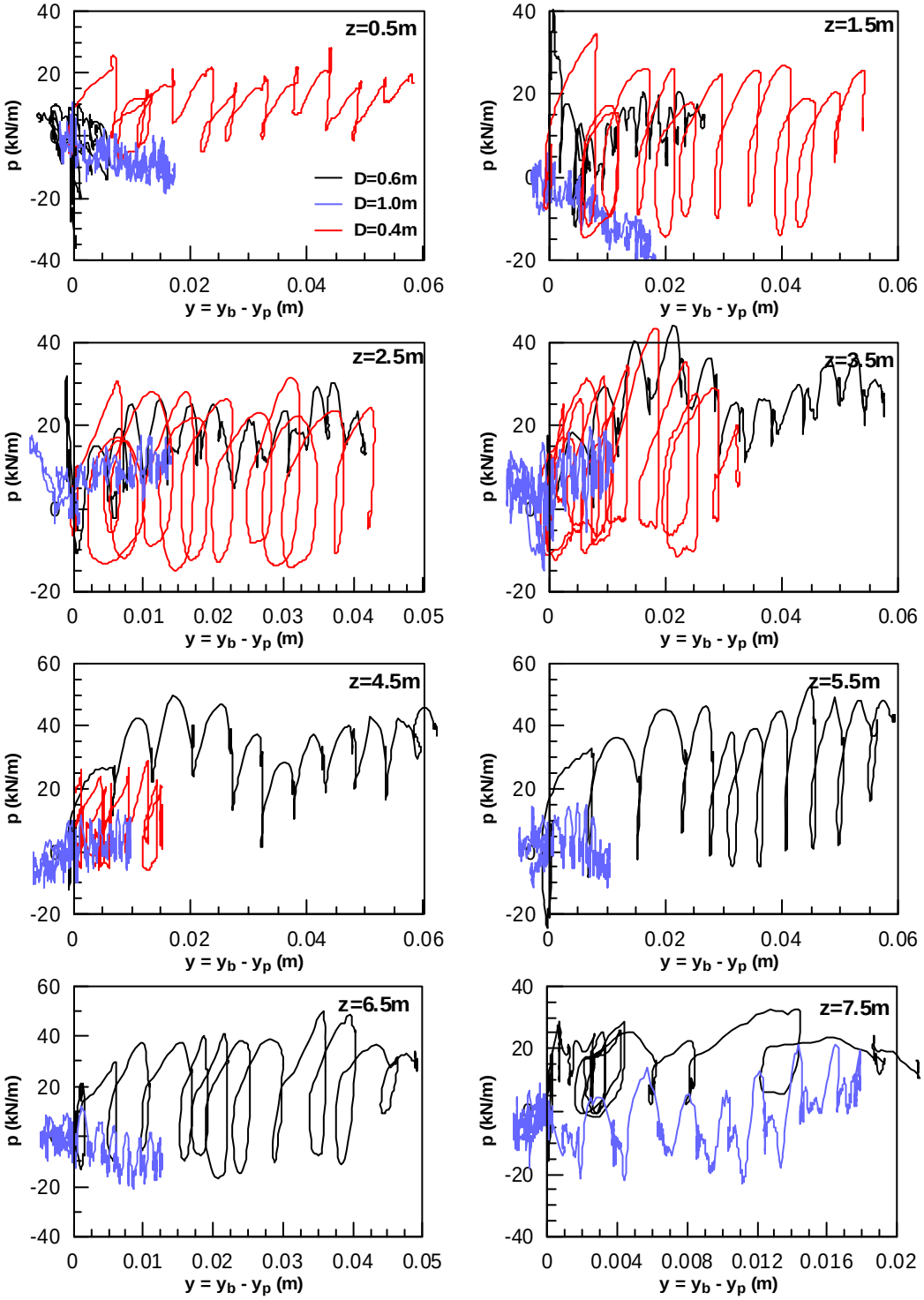

Figure 6.4: Effect of pile diameter on dynamic p-y curves with the same depth (using boundary displacements)

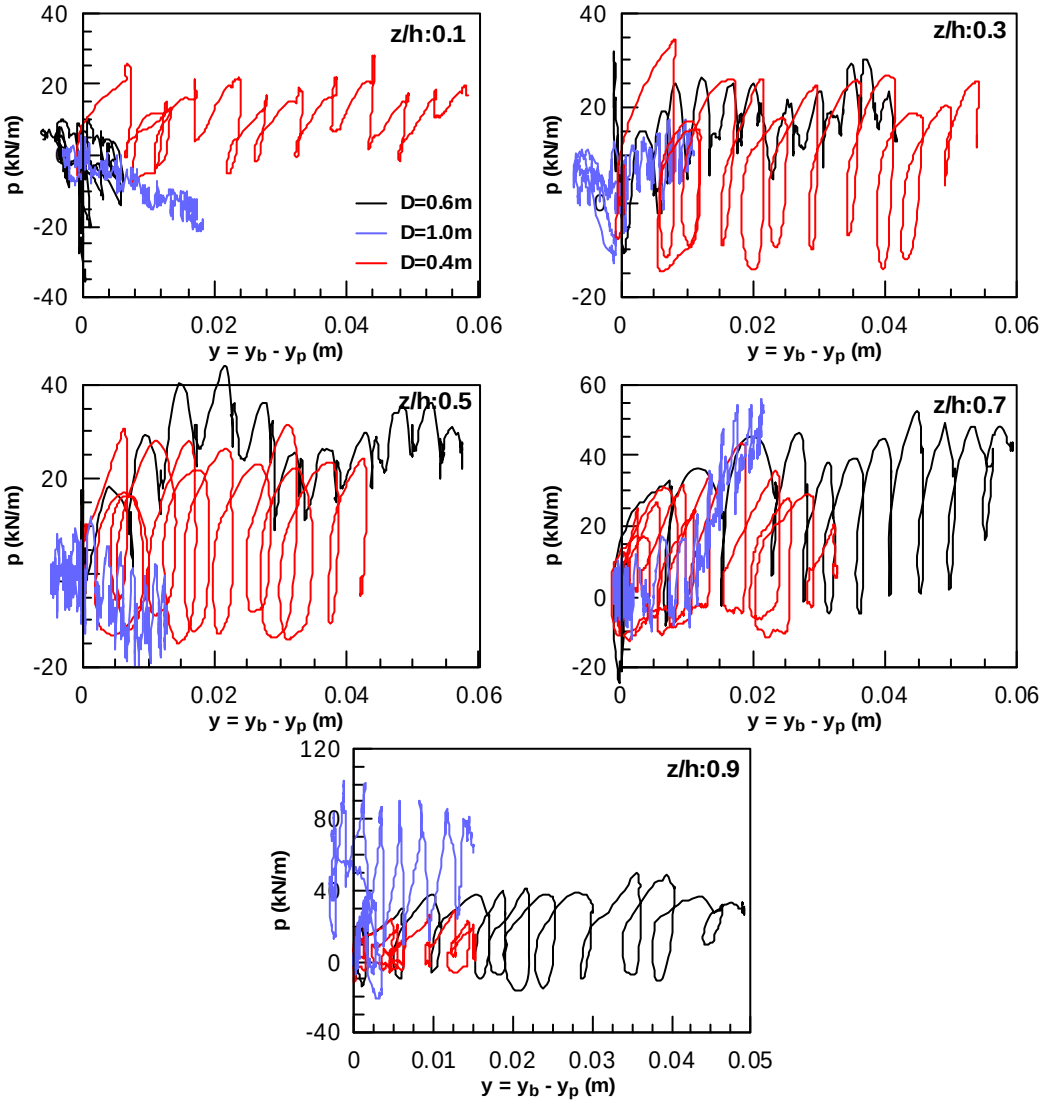

Figure 6.5: Effect of pile diameter on dynamic p-y curves throughout the soil layer with the same z/h ratio (using boundary displacements)

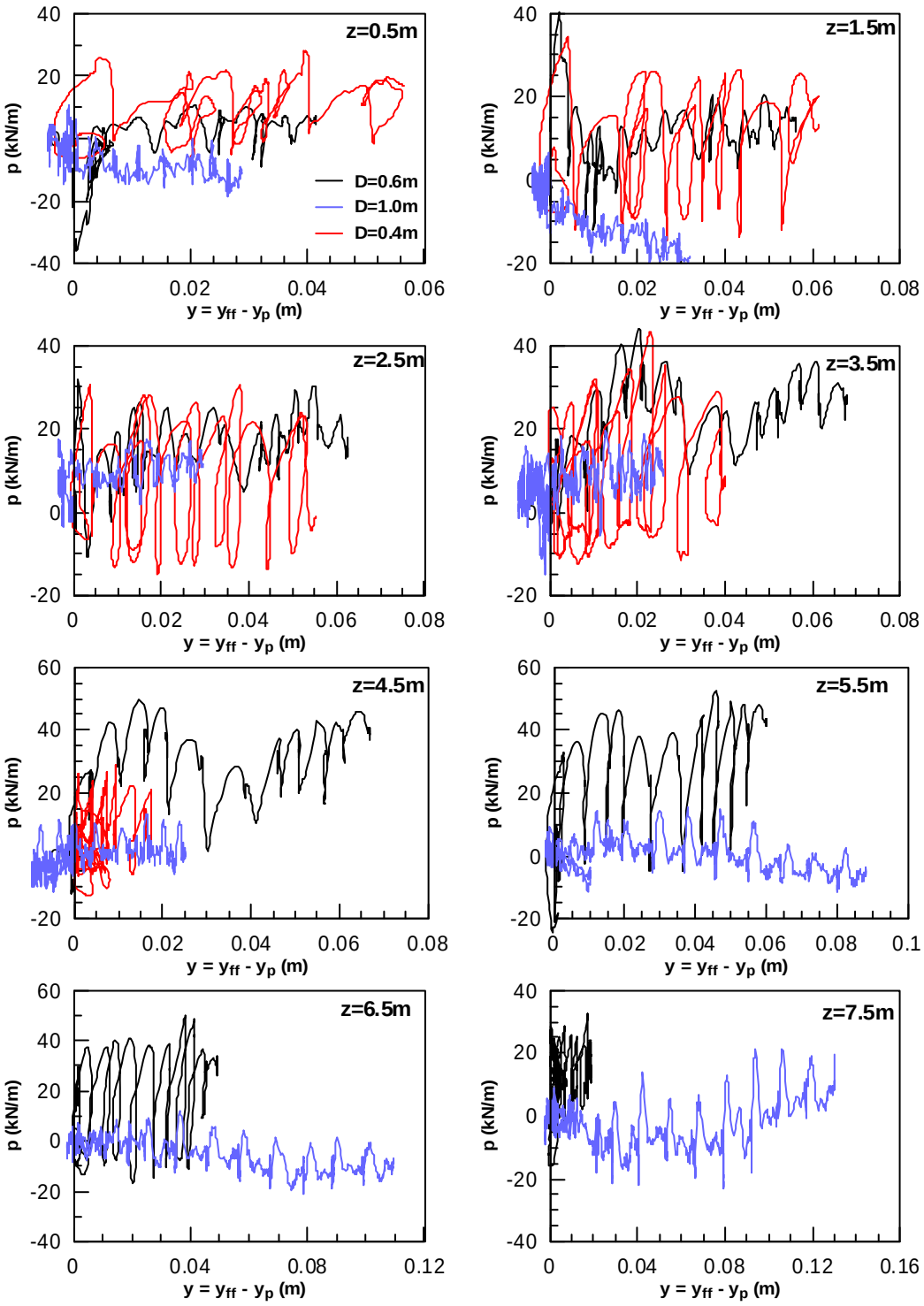

Figure 6.6: Effect of pile diameter on dynamic p-y curves with the same depth (using free-field displacements)

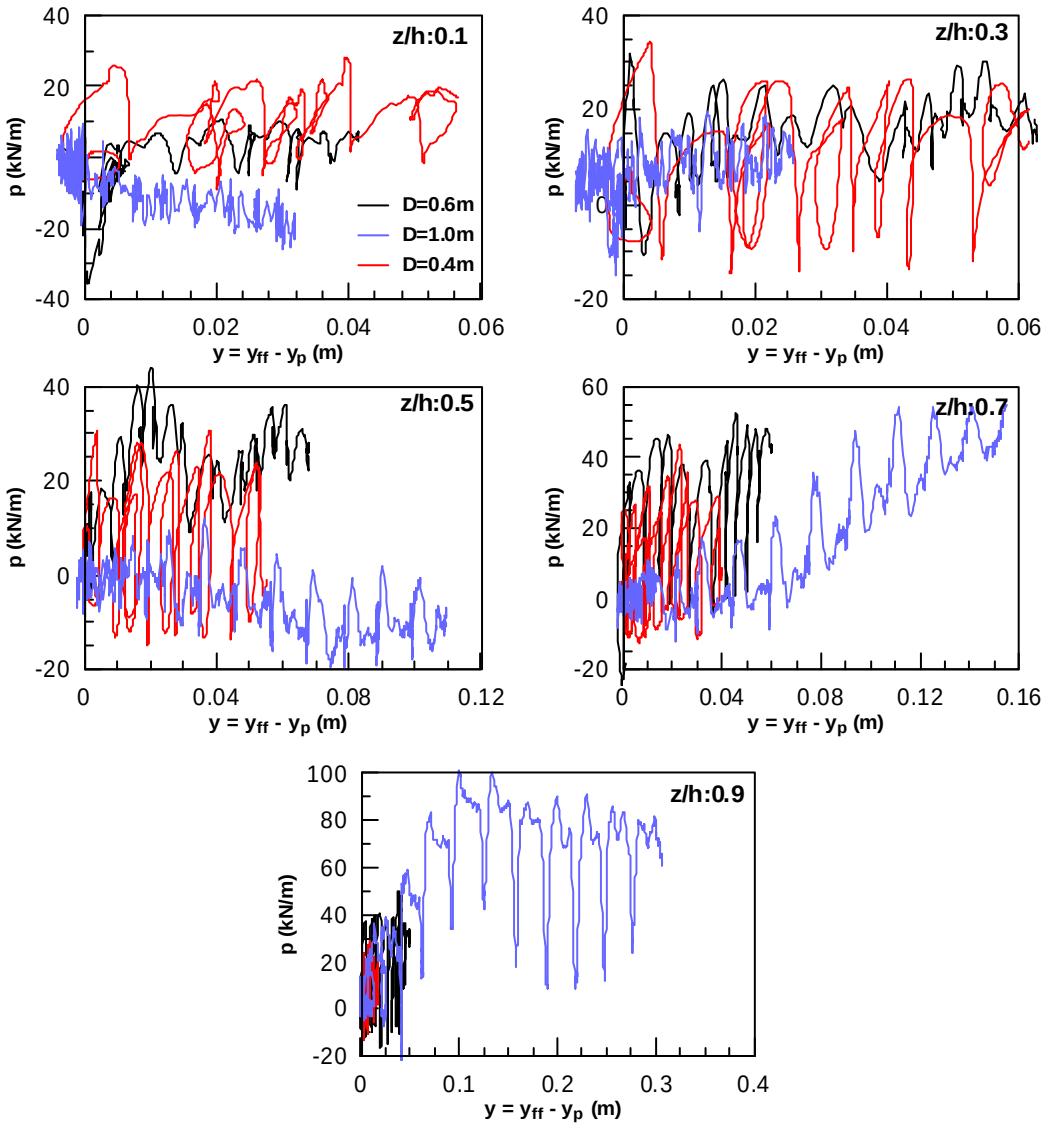

Figure 6.7: Effect of pile diameter on dynamic p-y curves throughout the soil layer with the same z/h ratio (using free-field displacements)

Figure 6.8 to **Figure 6.11** show the normalized p-y curves (i.e. the reduction multiplier). Again no specific trend is observed throughout the soil depth. In other words, while in shallow depths the analysis with $D = 0.4\,m$ yields larger degradation multiplier, a reversed pattern is observed in larger depths.

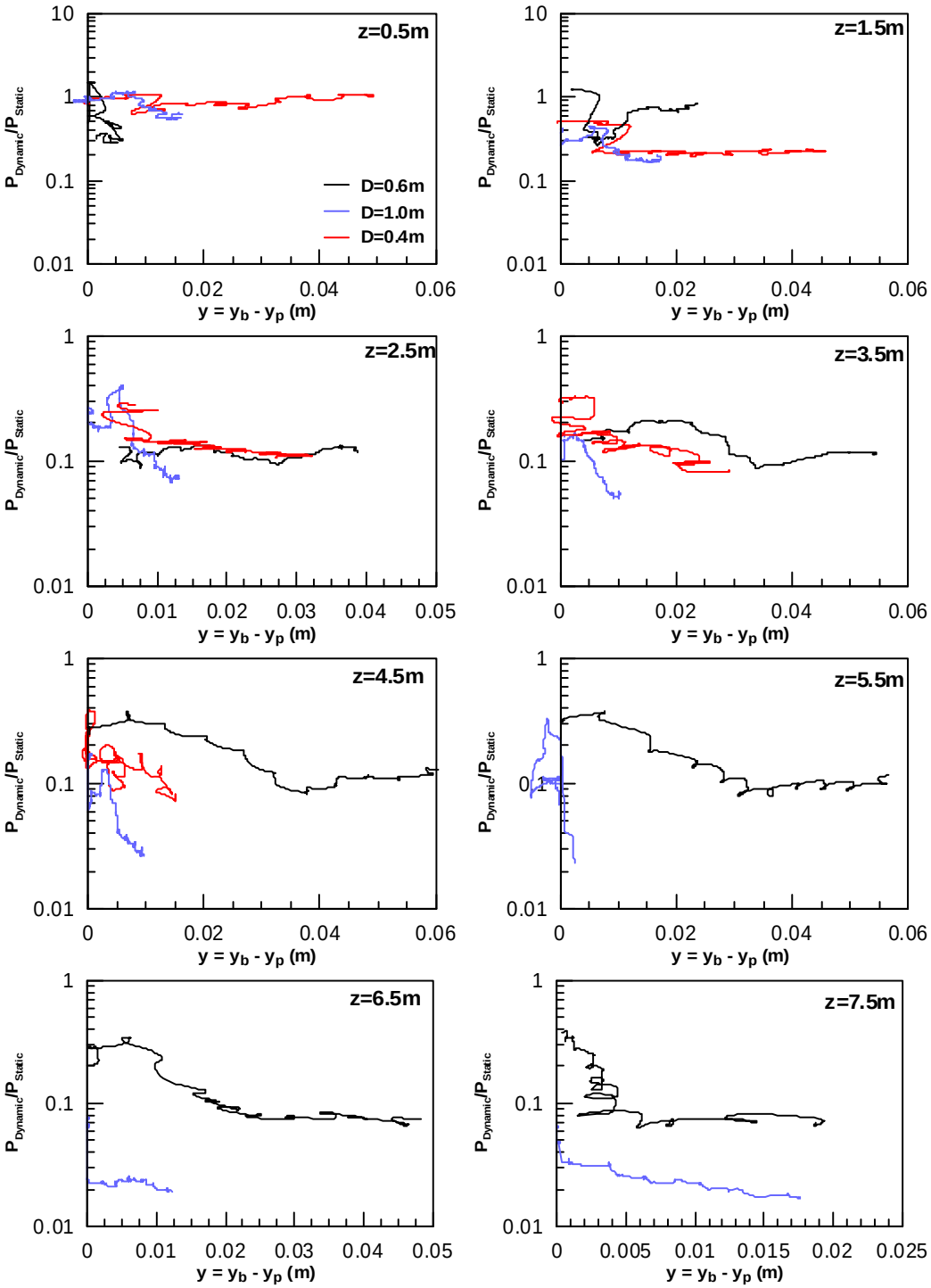

Figure 6.8: Effect of pile diameter on normalized p-y curves throughout the soil layer with the same depth (using boundary displacements)

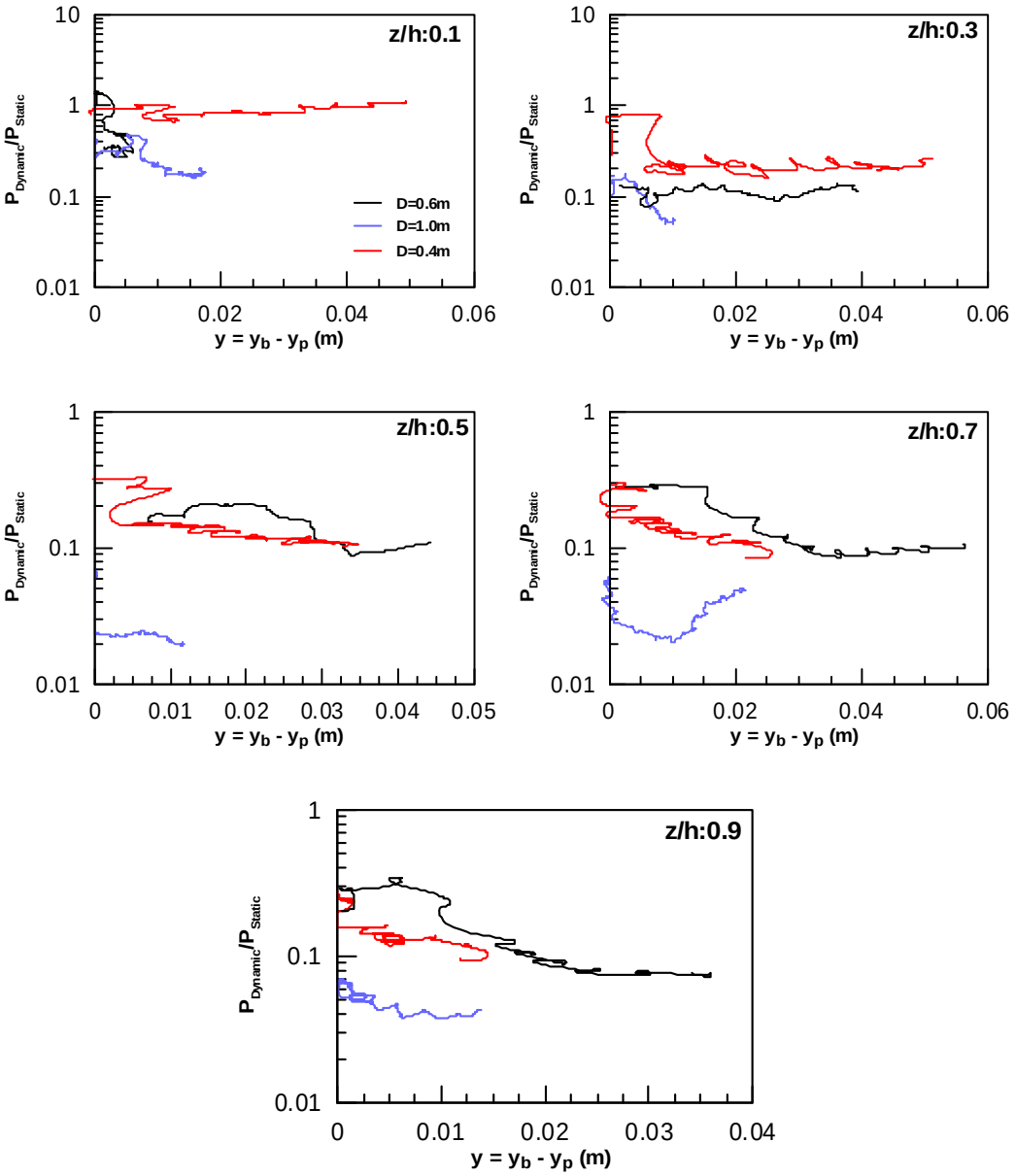

Figure 6.9: Effect of pile diameter on normalized p-y curves throughout the soil layer with the same z/h ratio (using boundary displacements)

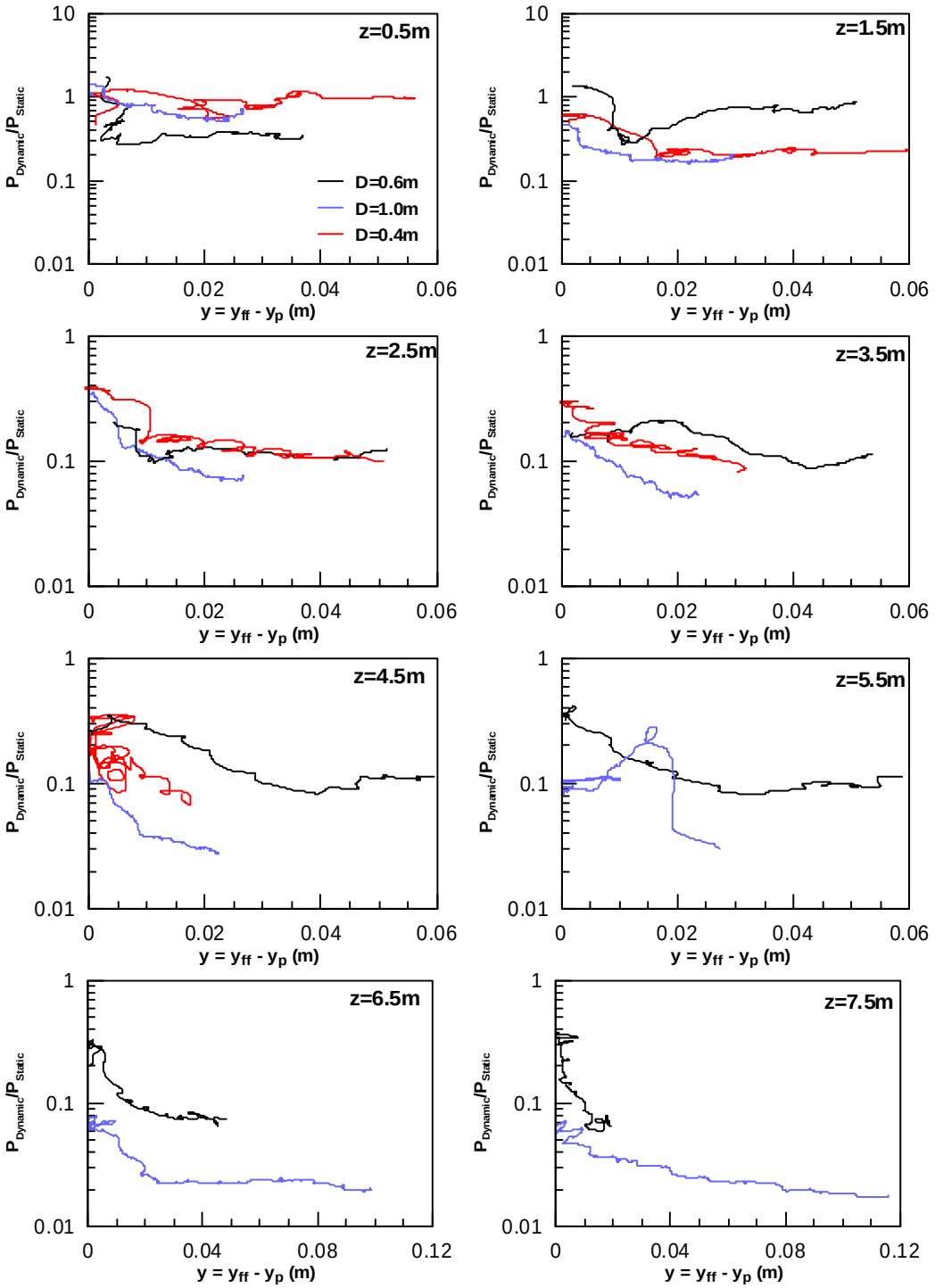

Figure 6.10: Effect of pile diameter on normalized p-y curves throughout the soil layer with the same depth (using free-field displacements)

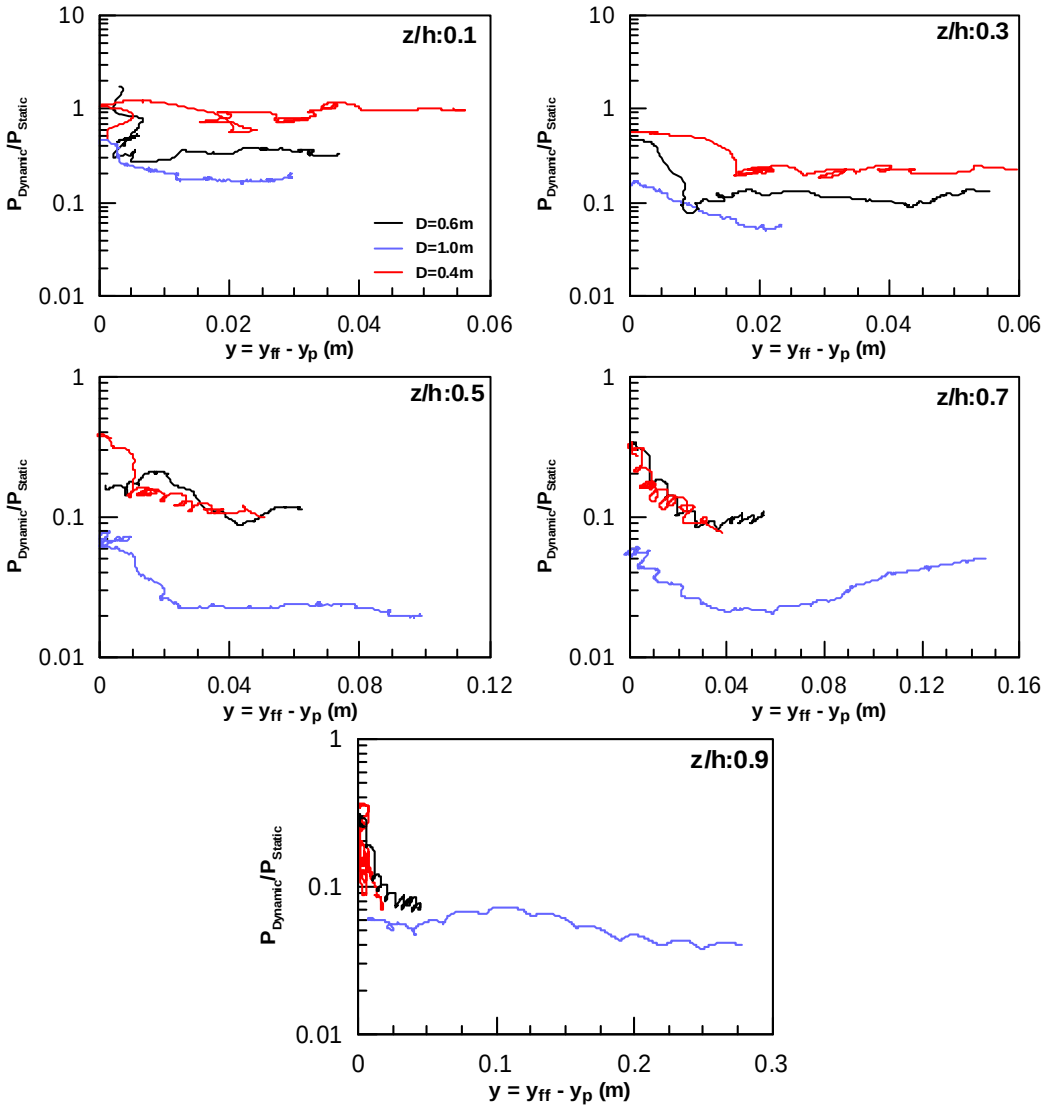

Figure 6.11: Effect of pile diameter on normalized p-y curves throughout the soil layer with the same z/h ratio (using free-field displacements)

By considering the previous figures, no specific trend is observed in r_u and the p-y curves and nothing can be said about the p-y curves and the multiplier. These unpredictable results can be caused by the following reasons:

- As the mesh size is changed with the same ratio of the diameters, the depth of the liquefied layer is changed which may lead to different situation. In other

words, thickness of the liquefied soil which may have an effect on the response of the pile is neglected in this type of analysis.

- As stated before, for different diameters the Young modulus of the section is modified in order to keep the value of "EI" unchanged. However, as they have different lengths, the stiffness of the pile (considered as a cantilever) differs significantly. Therefore, the response of the pile is different. For instance, the deflected shape of the pile with D=1.0 m is completely different from the others. In this case, the pile is more slender and follows the shape of the soil profile to some extent. Therefore, unlike the others, the curvature of the deflected pile changes.

6.3. The effect of pile stiffness

In order to see the effect of pile stiffness on the liquefied p-y response, an upper bound of practical pile stiffness is examined. To this end, a steel cylindrical pile with a thickness of 10 cm is chosen. Therefore, the stiffness is changed from 8,000 kNm^2 to 1,000,000 kNm^2.

As one could predict, the displacements of the stiff pile are smaller compared to the basic analysis as it is shown in **Figure 6.12 a**. This is true for the boundary displacements as well (**Figure 6.12 b**). It seems that the pinning effect of the stiffer pile is more profound compared to the basic one since the boundary displacement in the former is decreased from just under 19 cm to 7 cm, while in the basic analysis the fall is less significant (from 18.7 to 15 cm).

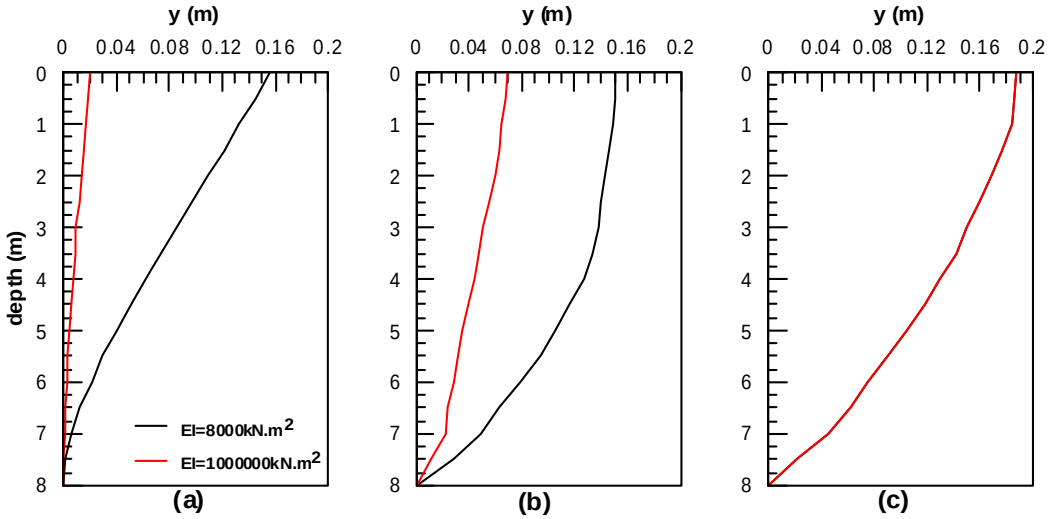

Figure 6.12: Effect of pile stiffness on the profile of lateral displacement of a) pile, b) boundary and c) free-field

As **Figure 6.13** depicts, large negative excess pore pressure is developed in the stiffer pile analysis near the pile foundation which is an indicative of large dilation in the soil in this region. It is due to the large relative displacements developed in this analysis since the movement of the pile is very small compared to the basic analysis. Additionally, it shows that the values are more negative near the surface (at z=0.75m). This is justifiable according to Gonzalez et al. (2009) who described the situation as an inverted cone (as mentioned in section 3.3).

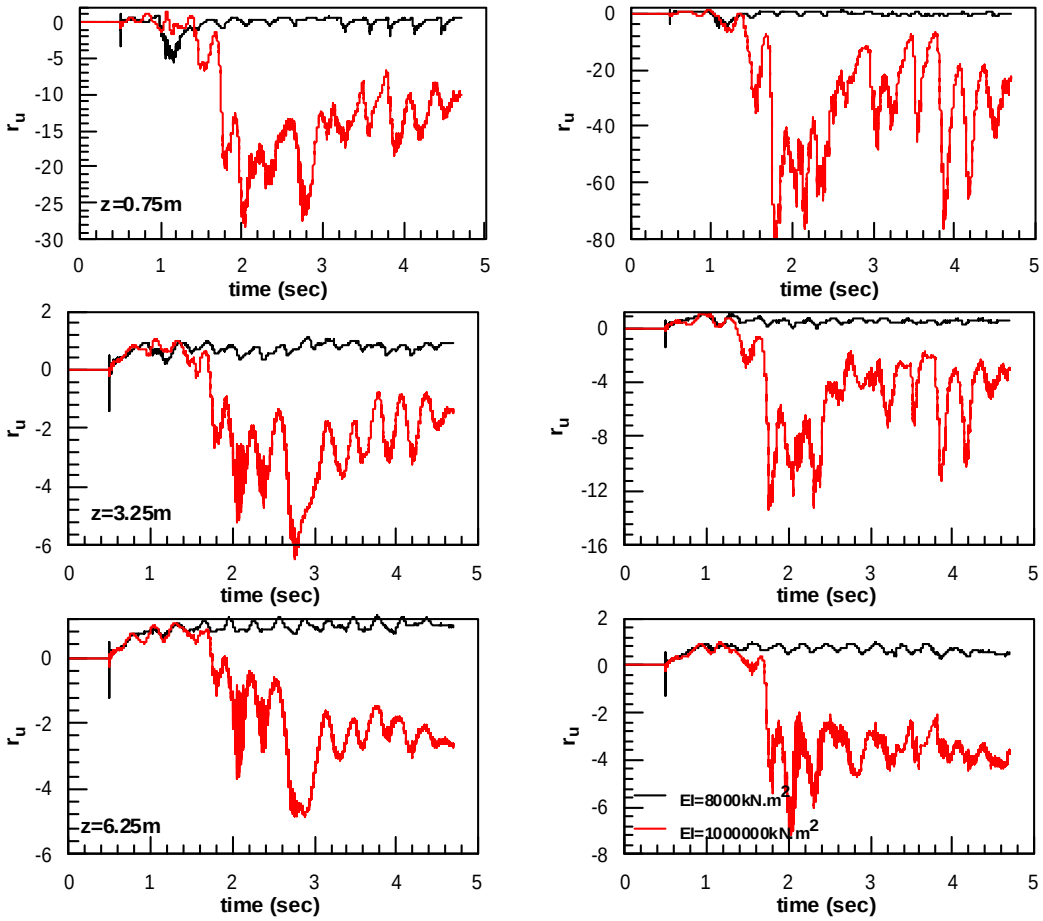

Figure 6.13: Effect of pile stiffness on pore pressure build-up near the pile at a) upstream and b) downstream.

In the free-field, however, this trend is not seen. The two figures are very similar and the only difference is the larger dilation spikes in the basic analysis which are due to the larger displacements. (**Figure 6.14**)

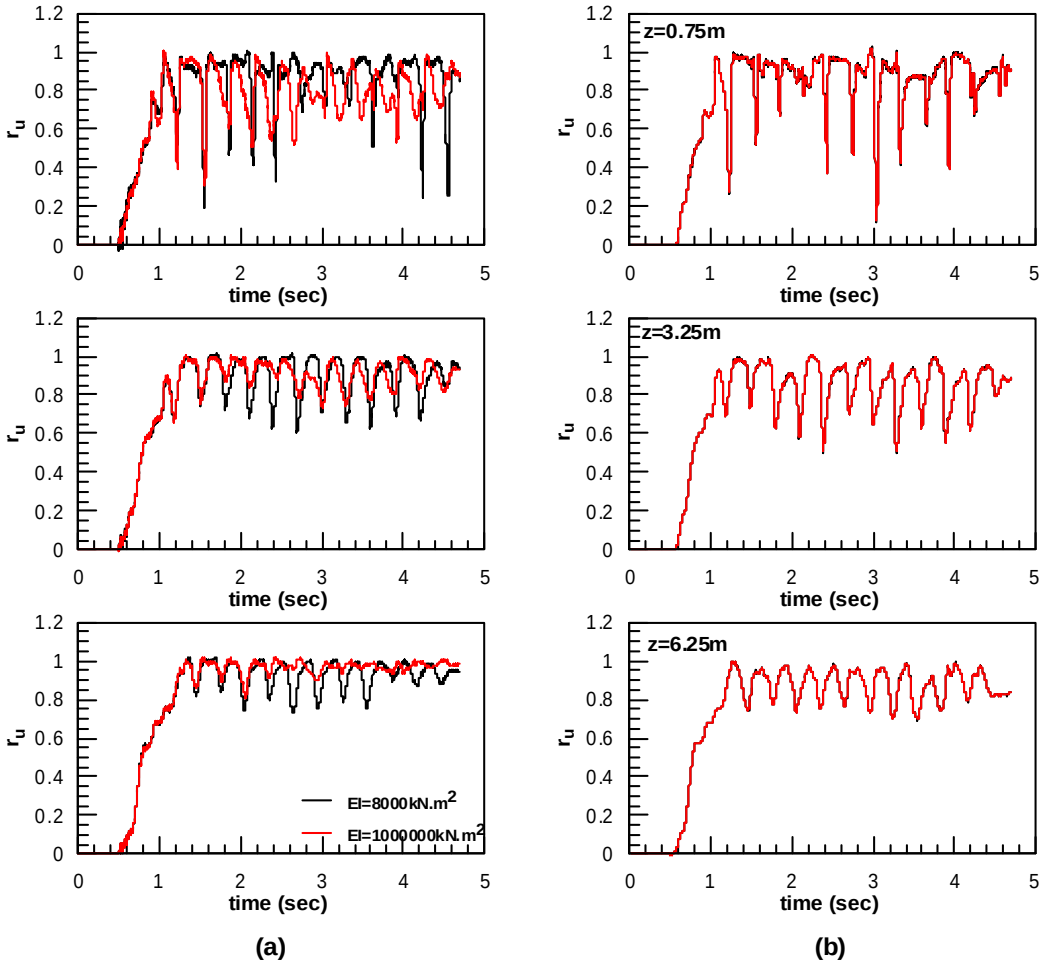

Figure 6.14: Effect of pile stiffness on pore pressure build-up at free-field a) with pile and b) without pile.

As mentioned before, large negative excess pore pressure ratios in soil near the stiff pile causes large lateral resistance compared to the basic ones as it is shown in **Figure 6.15** and **Figure 6.16**. The difference is more considerable at smaller depths due to the larger dilation and negative excess pore pressure ratios at this region and it becomes less considerable with increase in the depth of soil.

It should be noted that the relative displacements in **Figure 6.15** are smaller for the stiff pile while in **Figure 6.16** it is the opposite. This is due to the fact that, in basic analysis, except in small depths, boundary displacements are quite larger compared to the pile displacements whereas for the stiff pile analysis the differences are less significant. On the other hand, the free-field displacements are the same for the two analyses which cause "$y_{ff} - y_p$" to be larger for the stiffer pile.

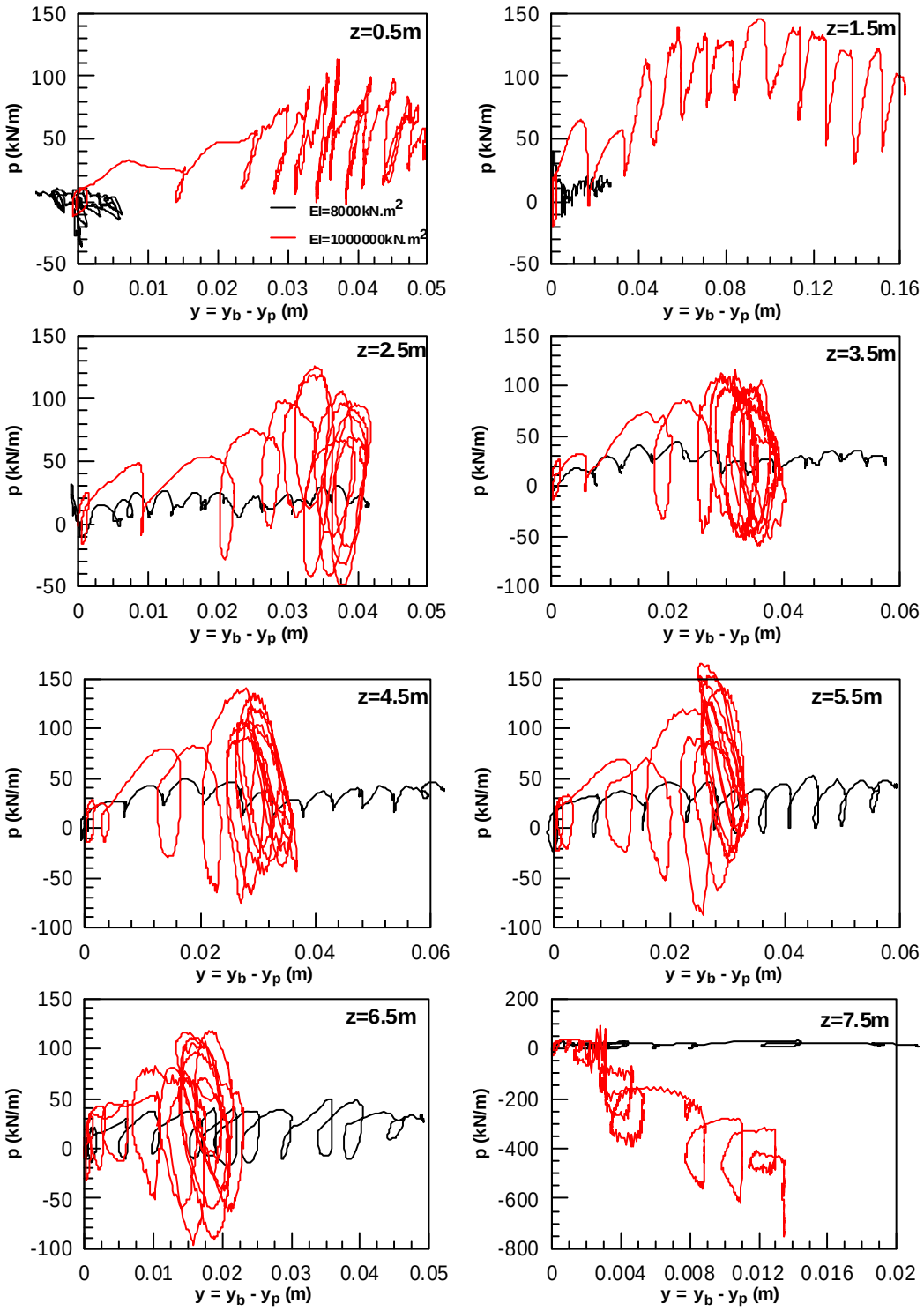

Figure 6.15: Effect of pile stiffness on dynamic p-y curves throughout the soil layer (using boundary displacements)

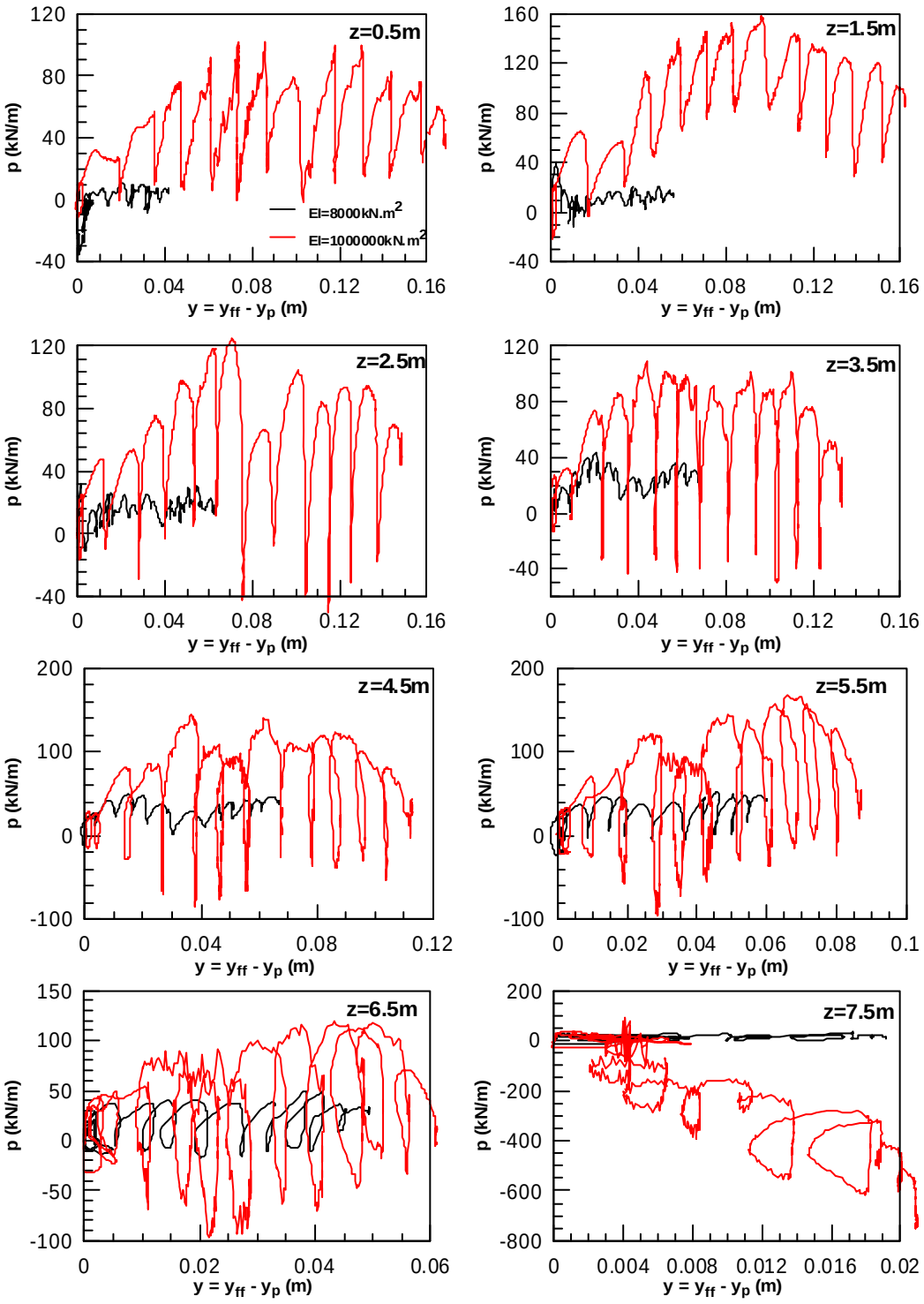

Figure 6.16: Effect of pile stiffness on dynamic p-y curves throughout the soil layer (using free-field displacements)

Figure 6.17 and **Figure 6.18** compare the degradation multiplier for the two analyses as a function of relative displacement. In the first figure, the relative displacement is calculated by the use of boundary displacements of the analyses with the pile. While in the second one the free-filed displacement obtained from the analyses without pile are utilized.

Considerable difference is observed between the two analyses, which is more profound at shallow depths as discussed previously as a consequence of large negative excess pore pressure build-up near the pile.

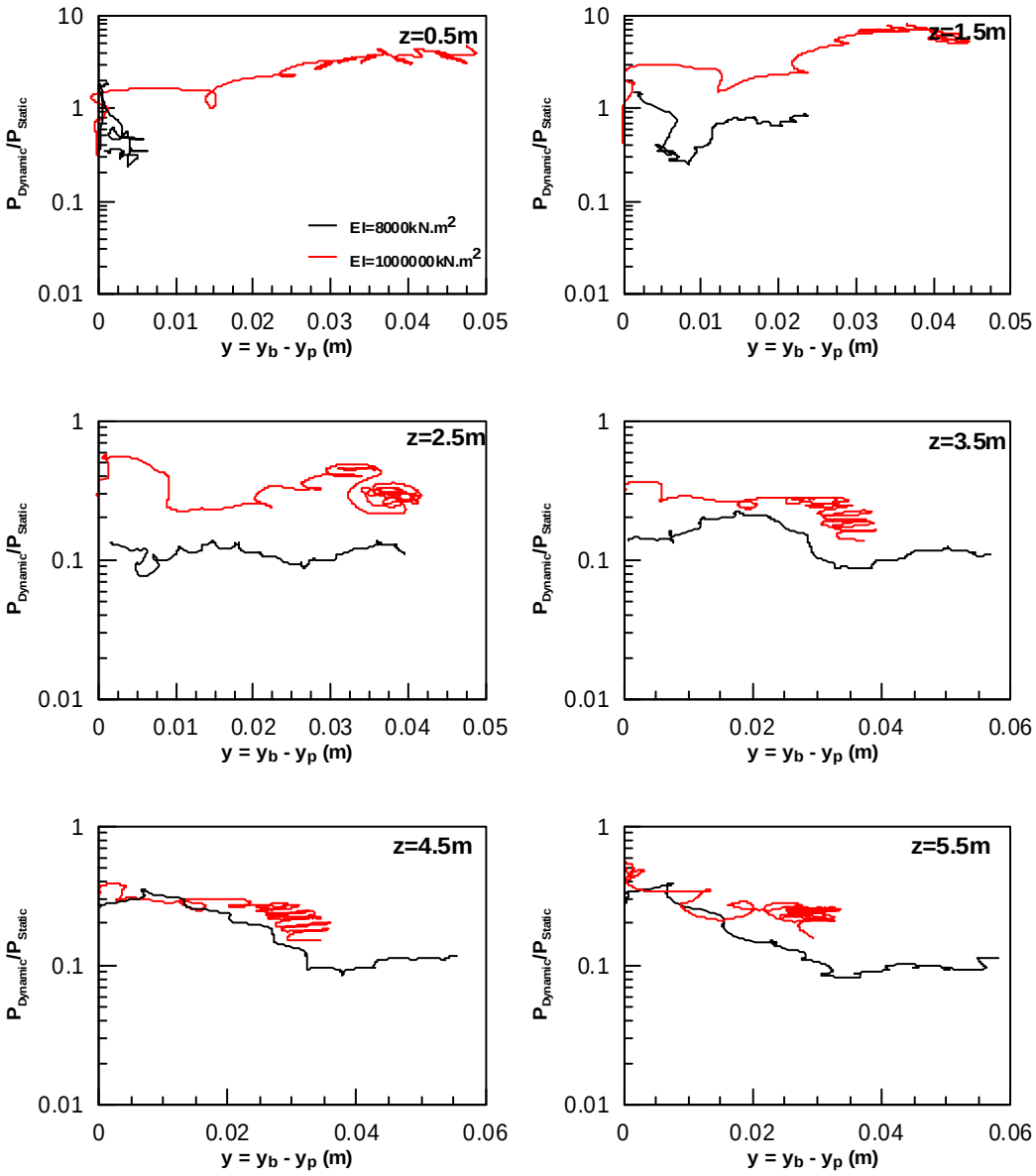

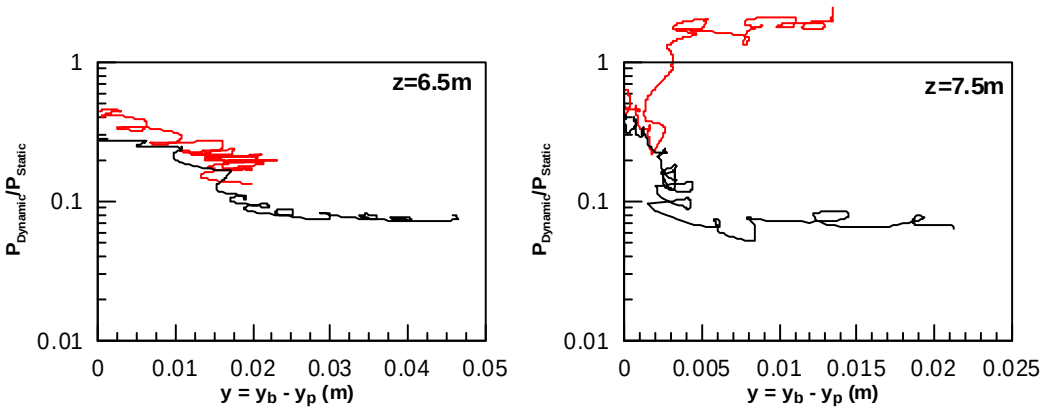

Figure 6.17: Effect of pile stiffness on normalized p-y curves throughout the soil layer (using boundary displacements)

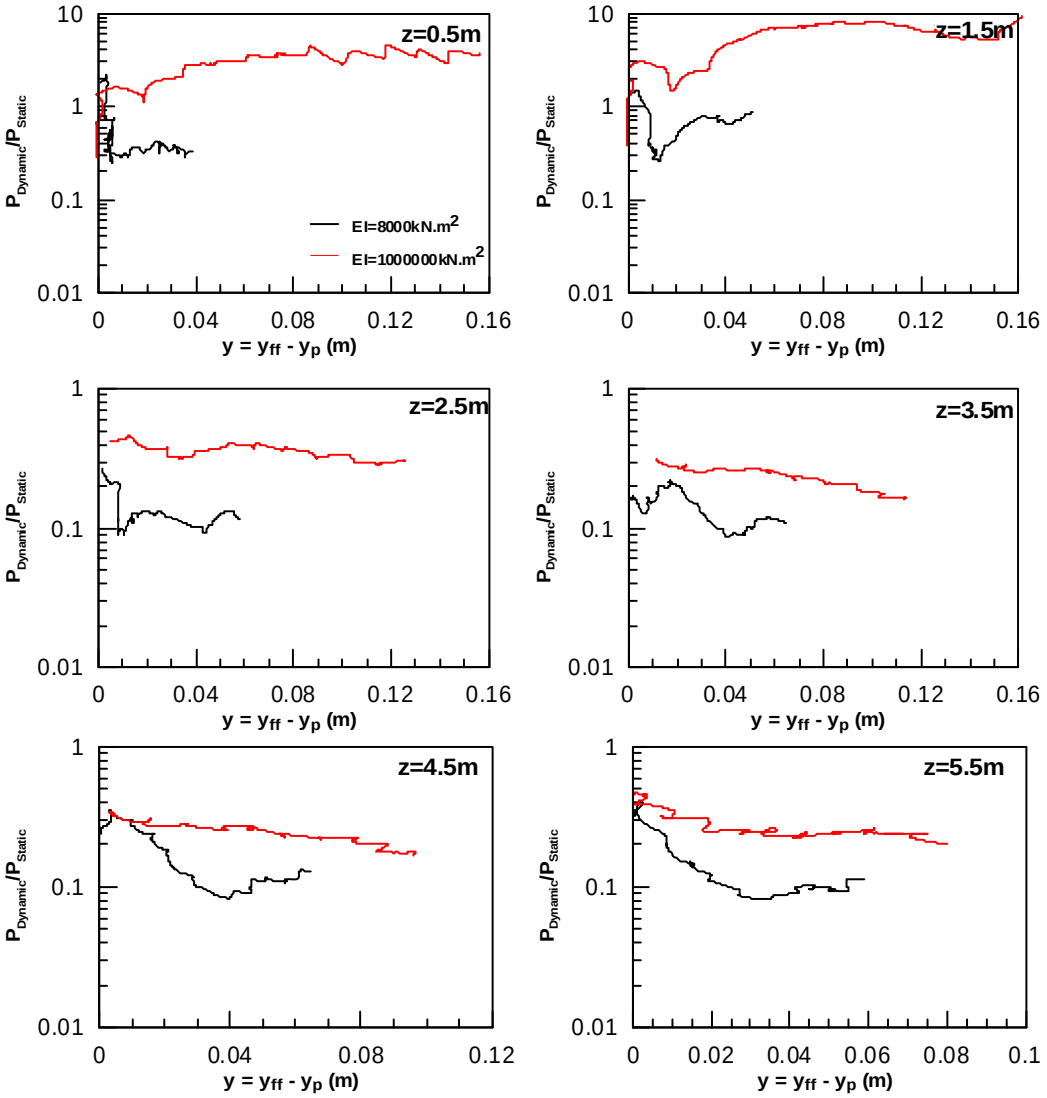

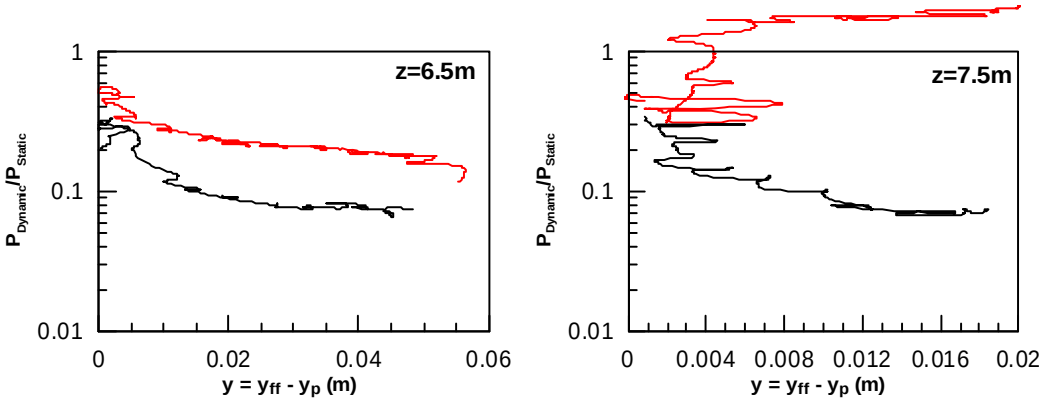

Figure 6.18: Effect of pile stiffness on normalized p-y curves throughout the soil layer (using free-field displacements)

Overall, it can be understood from this section that:

- As the pile with larger stiffness undergoes smaller lateral displacement, it causes the whole mesh to displace less as a result of more significant pinning effect.
- Large negative excess pore pressure is developed in the vicinity of stiff pile due to large relative displacement which cause larger lateral forces applied on the pile.
- The aforementioned influence in the p-y curve is considerably large which indicate that stiffness is one of the important parameters in the response of the pile.

6.4. The effect of Installation Method

In this part, the situation of a driven pile is examined, which changes the stress filed in soil surrounding the pile. This phenomenon is modeled in the numerical analysis using mechanism of expansion of cylindrical cavities which has been solved analytically by Vesic (1972). It was used in the analysis by developing a subroutine written in FISH which manually assigns modified stress values before the shaking and was developed in diploma thesis of Vassilis Papadopoulos (2010).

Some selected results of the analysis for the driven pile are shown in Figure 6.19 and **Figure 6. 20**.

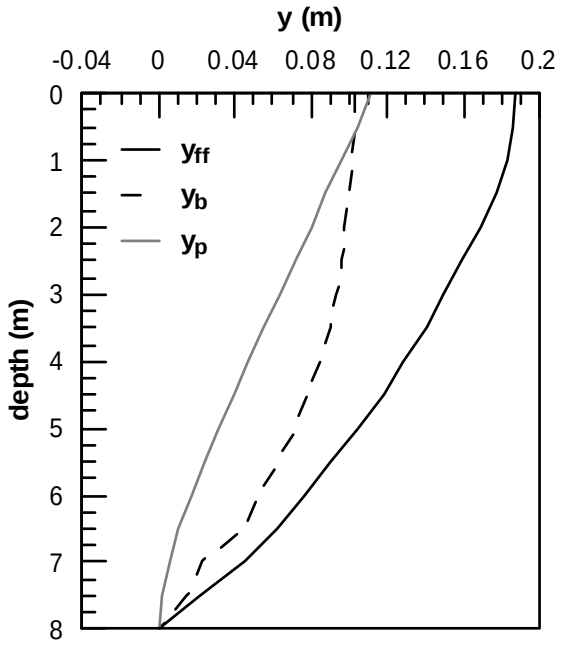

Figure 6.19: Profile of lateral displacements at the end of shaking

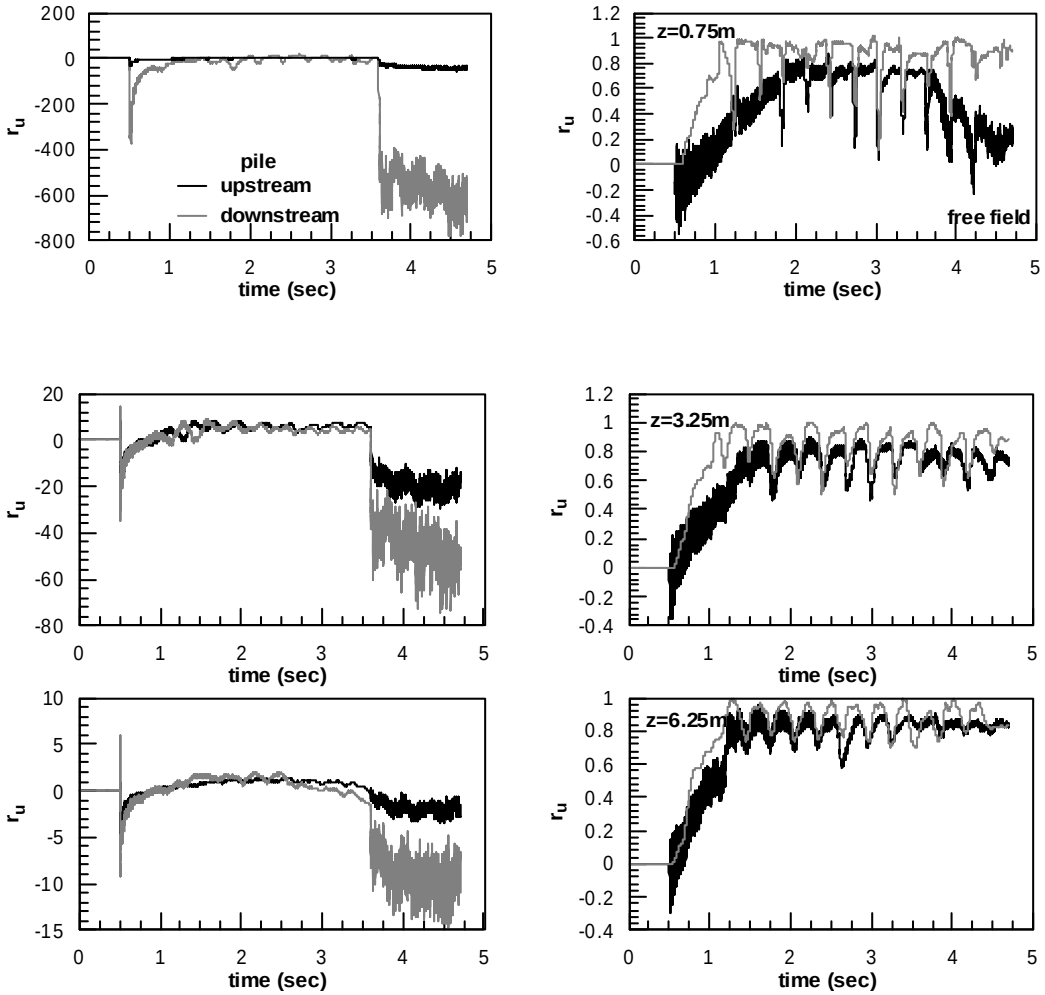

Figure 6. 20: Time-histories of excess pore pressure ratio near the pile and at free-filed

It can be clearly seen in **Figure 6. 20** that, strange results are developed after 3.5 sec which is indicative of soil instability at that moment. Therefore, the results of the first 3.5 sec are taken into account and compared to the basic analysis as shown in the following figures. The results at t=3.5s are shown hereafter:

Figure 6.21 shows that the displacements of pile and boundary are smaller for the driven pile compared to the basic analysis. It can be due to the fact that soil around the pile is stiffer in this case which prevents the excess movement of the pile and consequently the boundary.

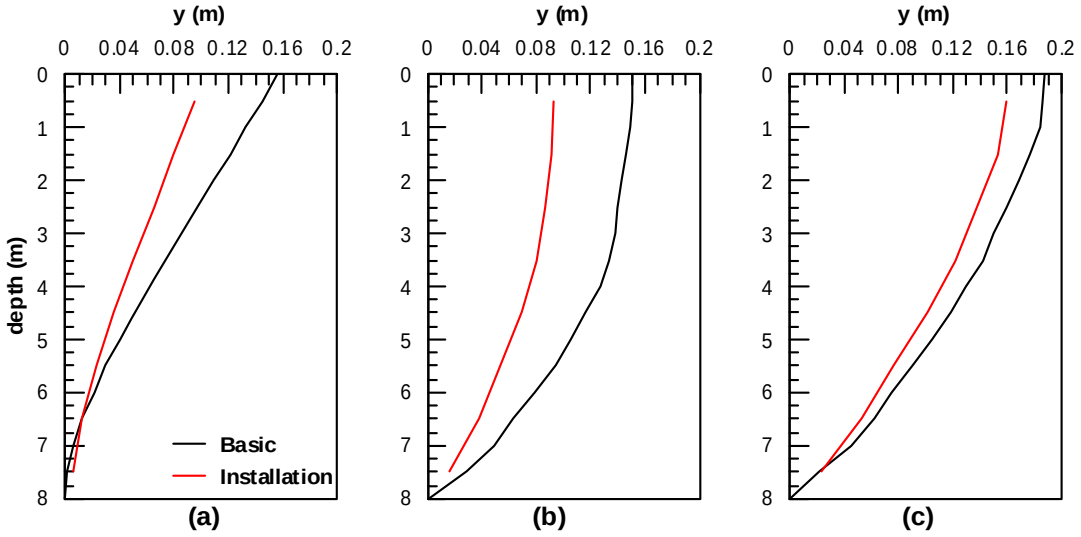

Figure 6.21: Effect of installation method on the profile of lateral displacements of a) pile, b) boundary and c) free-field

According to **Figure 6.22** and **Figure 6.23** which show the pore pressure build-up near the pile and in free field, the liquefaction in the driven-pile-analysis is not complete (r_u does not reach 1.0) especially in the areas near the pile due to large confining stresses. However, the overall trend is similar in the two analyses.

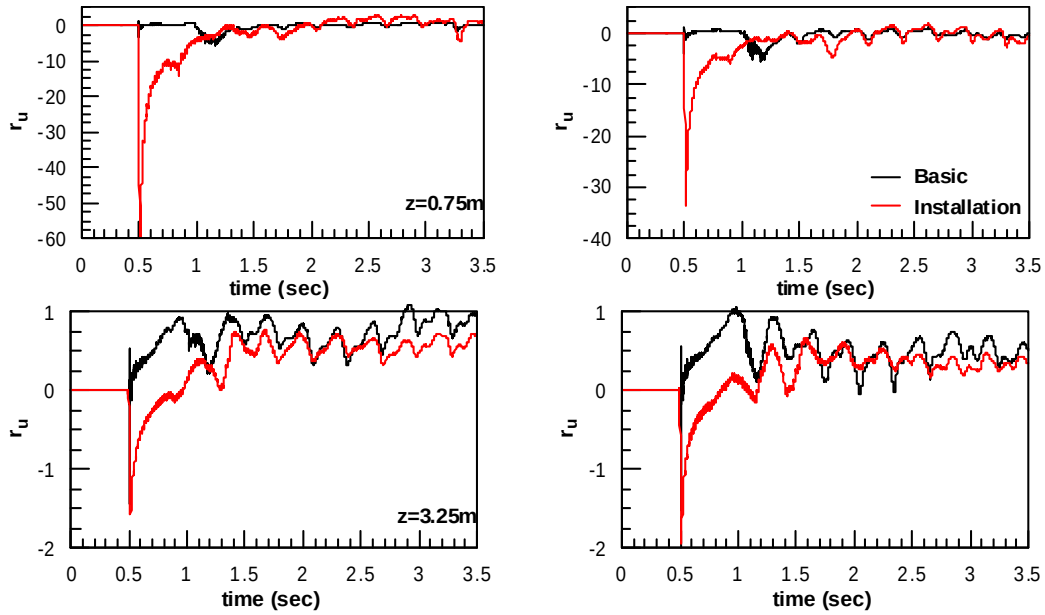

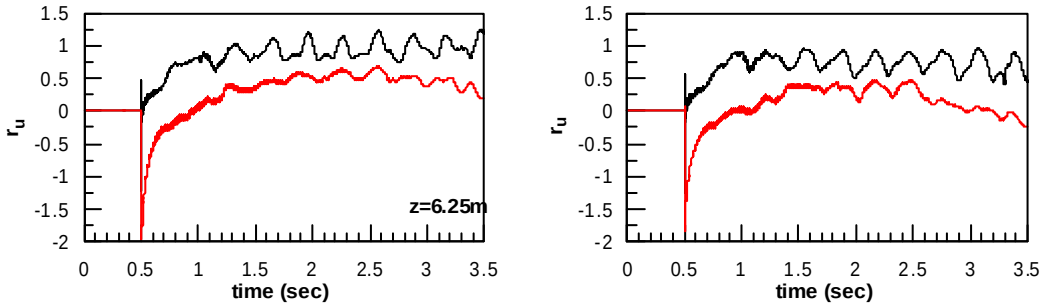

Figure 6.22: Effect of installation method on pore pressure build-up near the pile at a) upstream and b) downstream

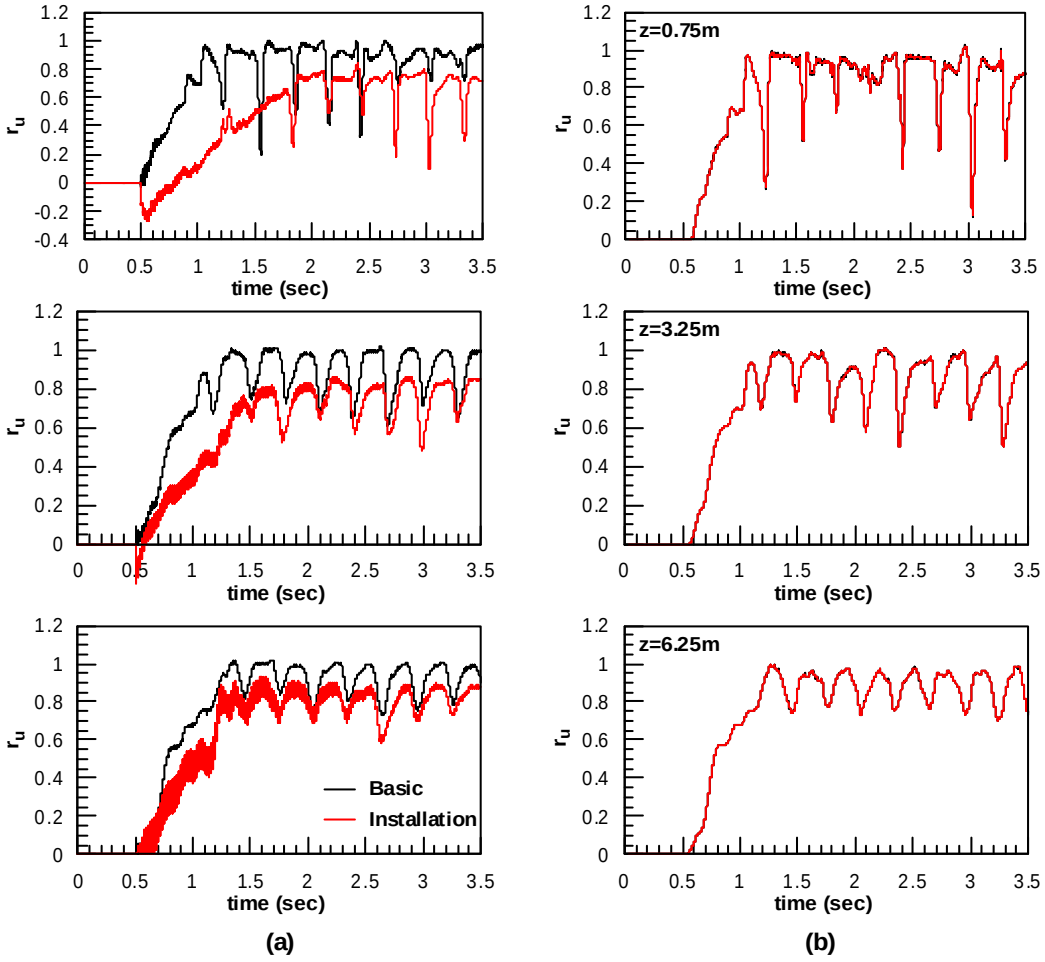

Figure 6.23: Effect of installation method on pore pressure build-up at free-field a) with pile and b) without pile

According to the dynamic p-y curves which are shown in **Figure 6.24** and **Figure 6.25**, the response of the soil is not considerably changes as a result of the change in

the installation method. Although the displacements are slightly smaller for the driven pile, in most of the places, the values of the pressure are quite close to each other indicating negligible effect of this parameter on the p-y response of the soil.

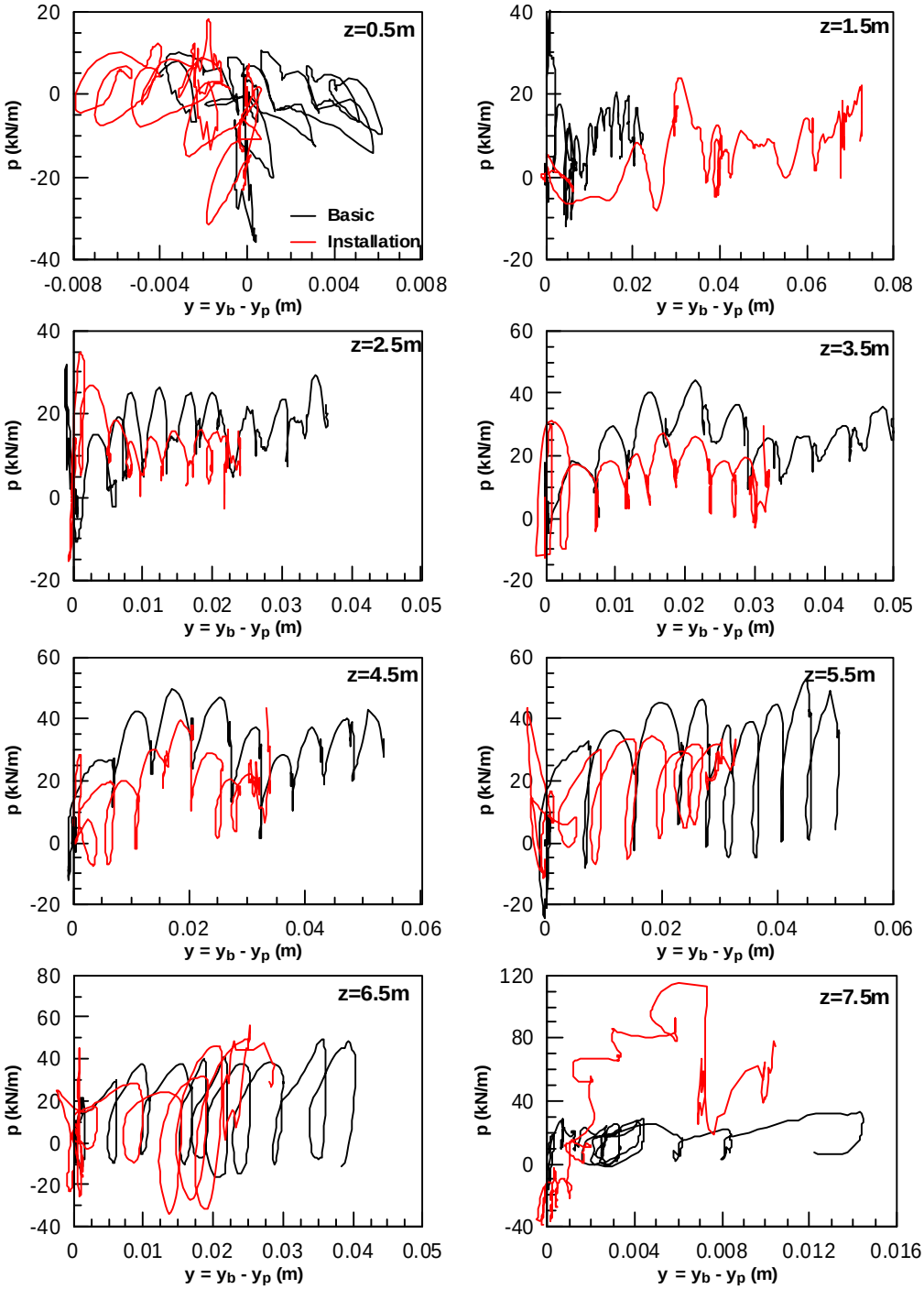

Figure 6.24: Effect of installation method on dynamic p-y curves throughout the soil layer (using boundary displacements)

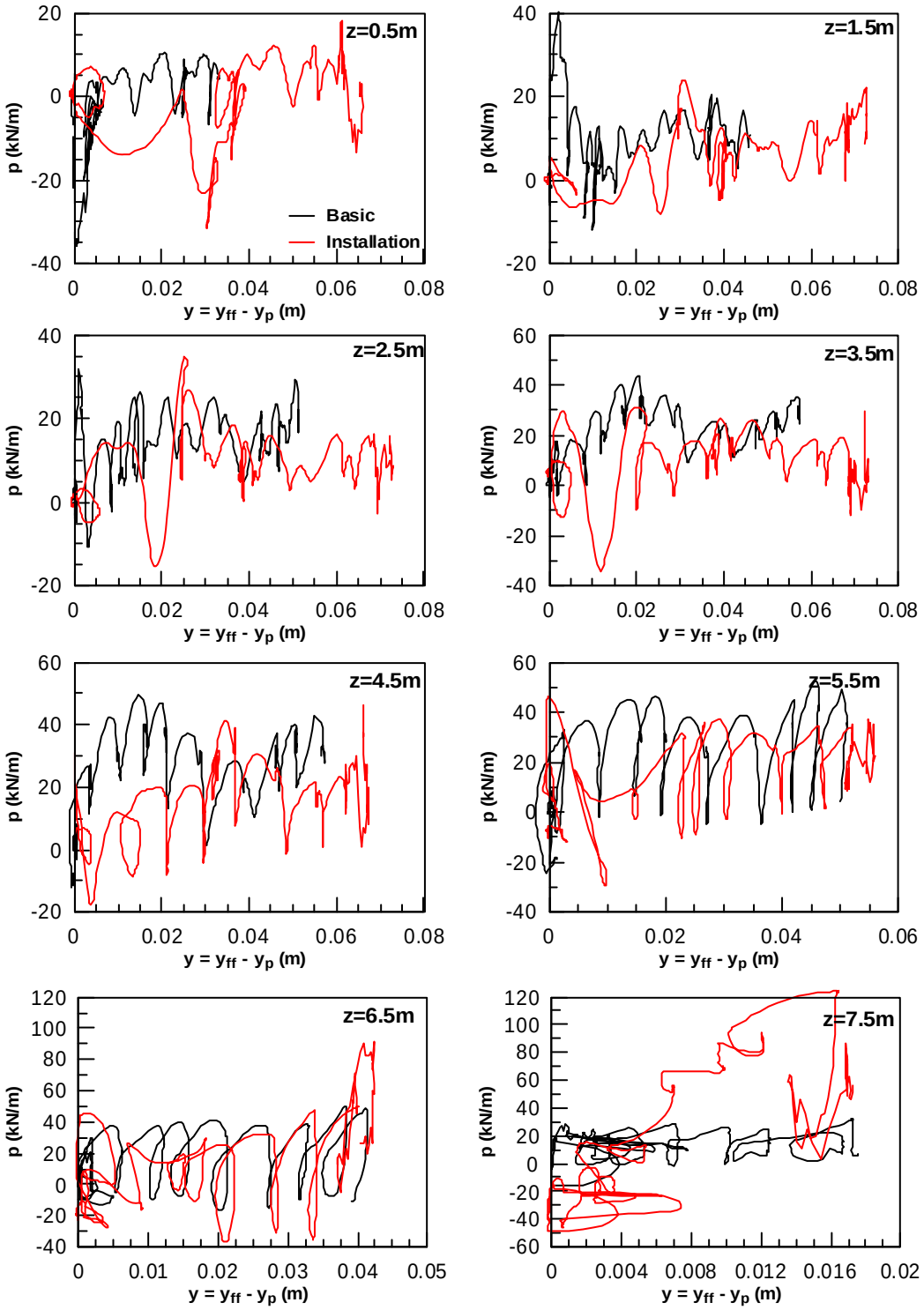

Figure 6.25: Effect of installation method on dynamic p-y curves throughout the soil layer (using free-field displacements)

The normalized p-y curves are shown in **Figure 6.26** and **Figure 6.27** for boundary and free-field displacements respectively. It should be noted that the cyclic component of the results are filtered out as much as possible in order to have a better view over the results. As stated before, apart from some ups and downs, the overall response of the two analyses are minor indicating that installation effect does not affect the resistance of the liquefied soil significantly.

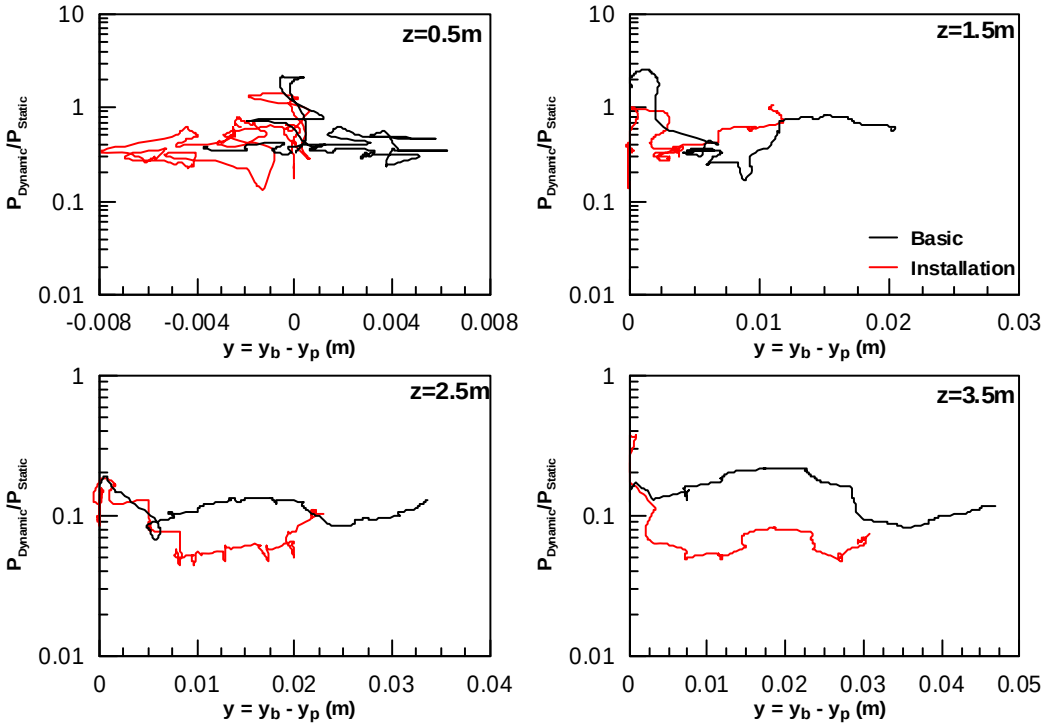

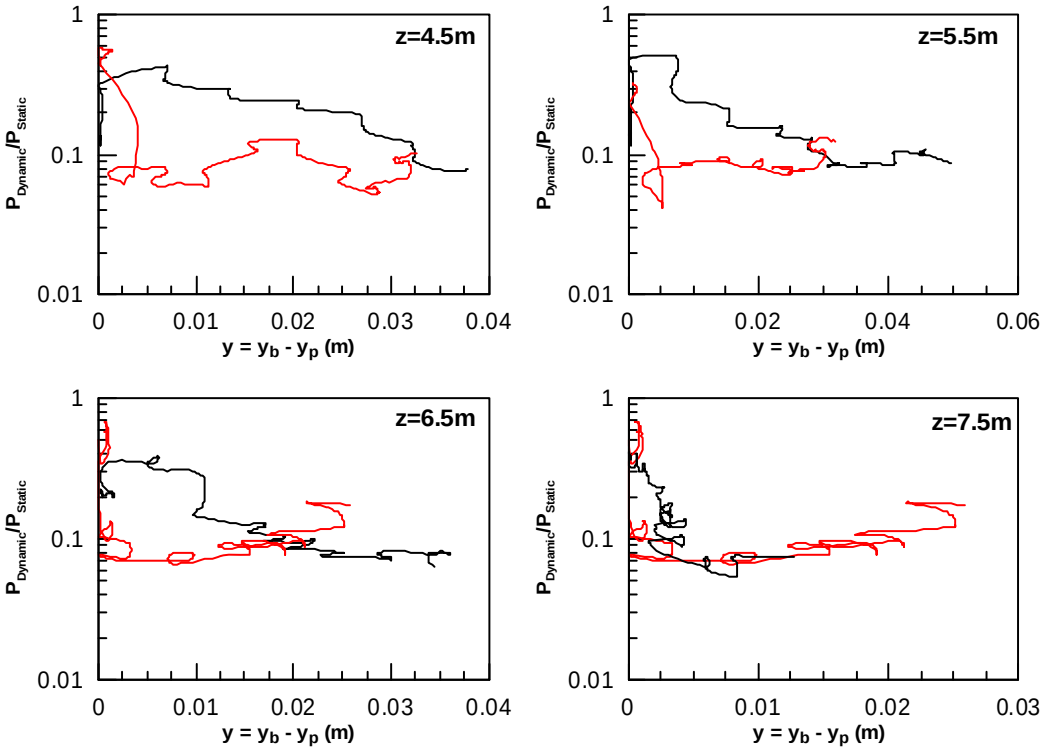

Figure 6.26: Effect of installation method on normalized p-y curves throughout the soil layer (using boundary displacements)

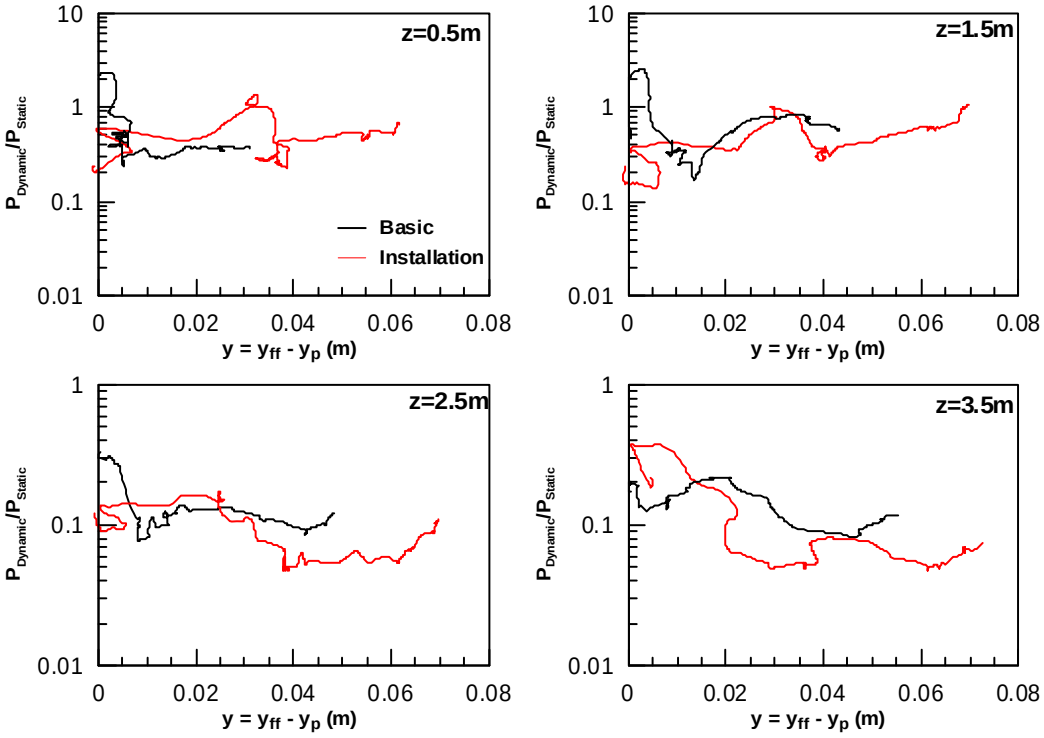

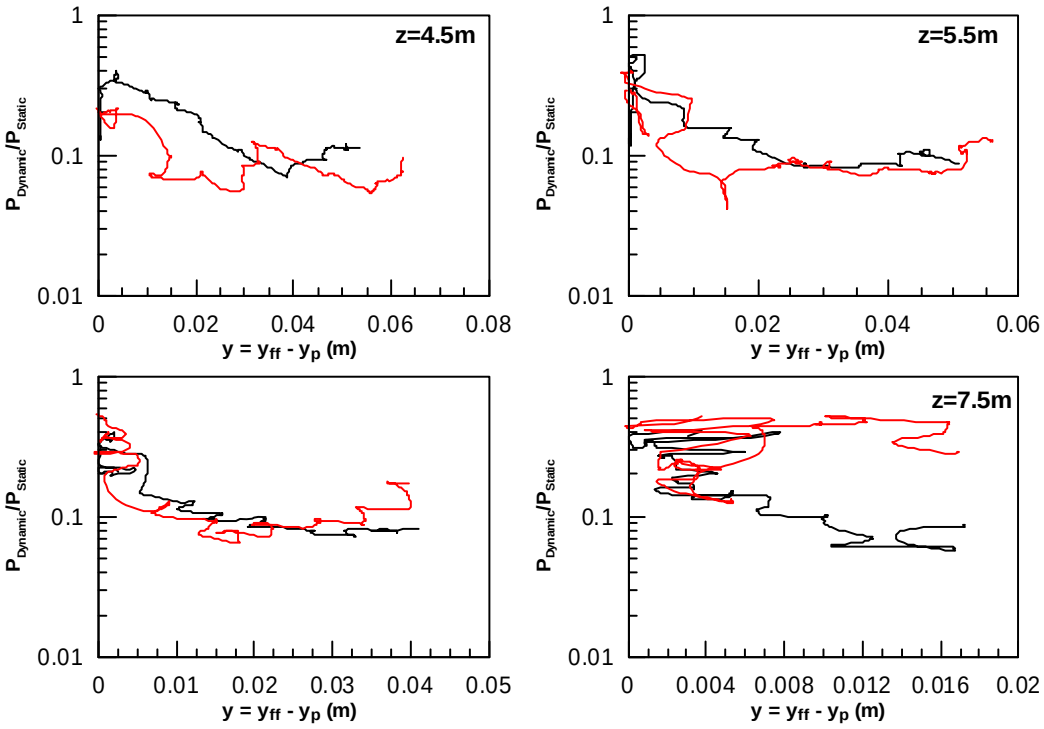

Figure 6.27: Effect of installation method on normalized p-y curves throughout the soil layer (using free-field displacements)

Overall, after studying the effect of installation pile method, following conclusions can be drawn:

- In a driven pile case, the lateral displacements are smaller due to the increased effective stresses around the pile.
- Apart from that, this parameter has negligible effects on the p-y response of the soil and can be neglected in the design of the pile foundations in liquefied soil.

6.5. The effect of Head Constraint

In this part, the pile head is fixed and the results are evaluated in order to see the effects of head condition. In order to simulate this situation, in the input file the head of the pile is fixed in X and Z directions. The results are presented in the following figures.

Figure 6.28 shows that the displacement profile of the pile is quite different from the basic analysis. While the pile with free-head behaves like a cantilever, the fixed-head pile deflects similar to a simply supported beam subjected to lateral distributed loading from the liquefied soil. Therefore, the displacements are significantly smaller in this case.

The behavior of the boundary is quite interesting in terms of lateral displacements: as we can see from **Figure 6.28 b,** when looking at the profile from down to the surface, the displacements tend to increase until about z=6 m, while it remains relatively constant for the rest of the soil layer. It seems that, this is due to the pinning effect of the pile with fixed head which is predictably larger that the free-head pile of the basic analysis.

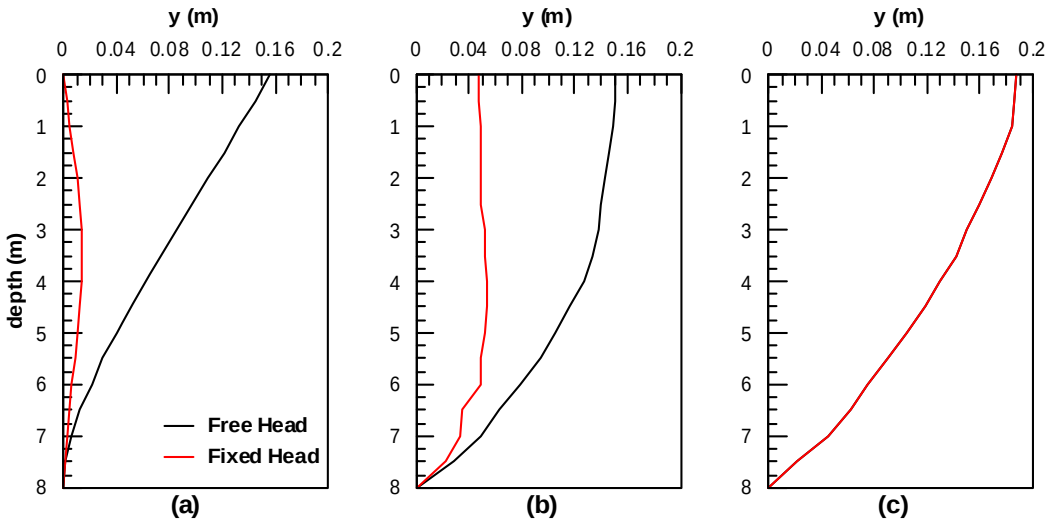

Figure 6.28: Effect of pile head constraint on the profile of lateral displacements of a) pile, b) boundary and c) free-field

From **Figure 6.29** we can see that large negative r_u is developed near the pile in the fixed pile analysis. This parameter gets larger negative values in lower depths like the previous sections which is an indicative of large dilation. The reason is that while the pile undergoes very small displacements, the soil undergoes considerable displacement. Consequently, the relative displacement between the pile and soil is considerable in each cycle. These large transient relative displacements cause large dilation and therefore, r_u tends to move towards negative values. As one could predict, these values are more significant in lower depths since the relative displacement are larger.

However, in the free-filed the r_u values are similar for the two analyses. The only difference is the dilation spikes of the basic analysis which are larger compared to the fixed-head pile analysis. It is due to the fact that the lateral displacements of soil are larger at the boundary for the free-head conditions as discussed in the previous paragraph and shown in **Figure 6.28**.

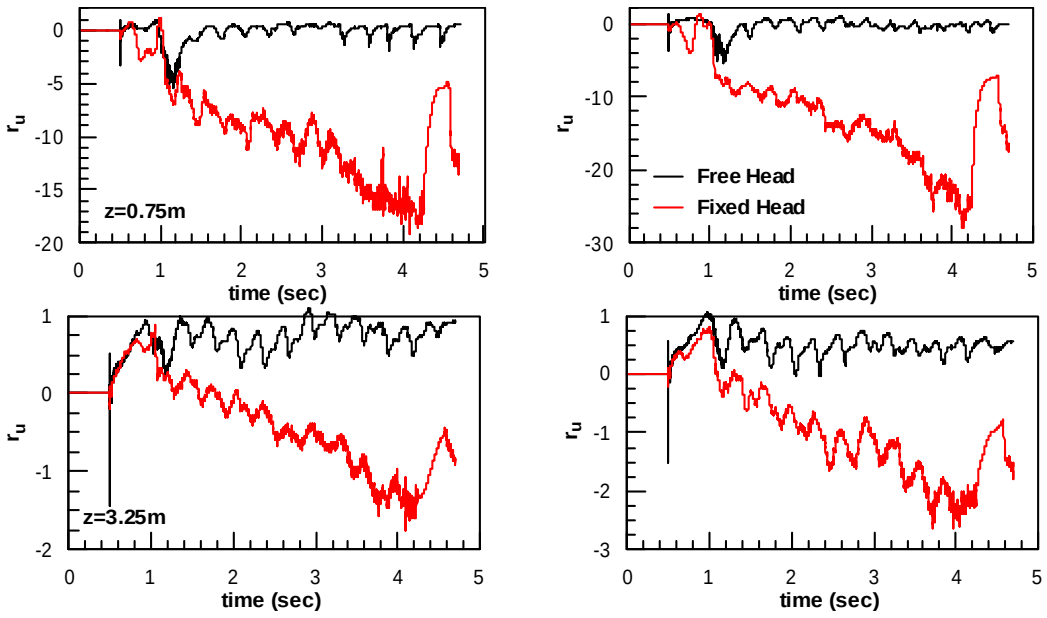

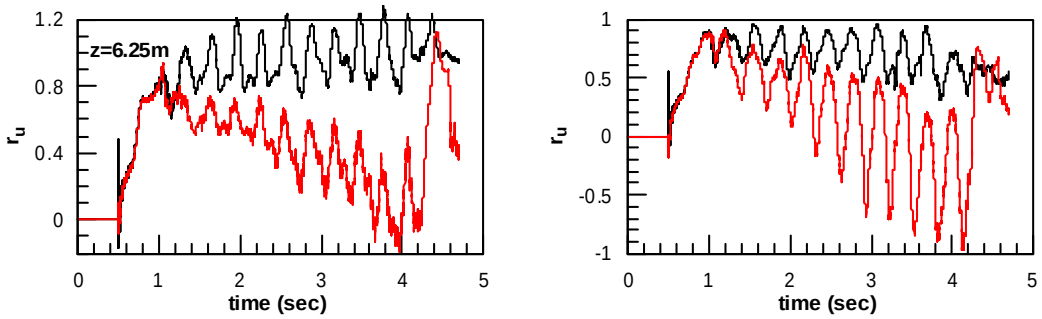

Figure 6.29: Effect of pile head constraint on pore pressure build-up near the pile at a) upstream and b) downstream

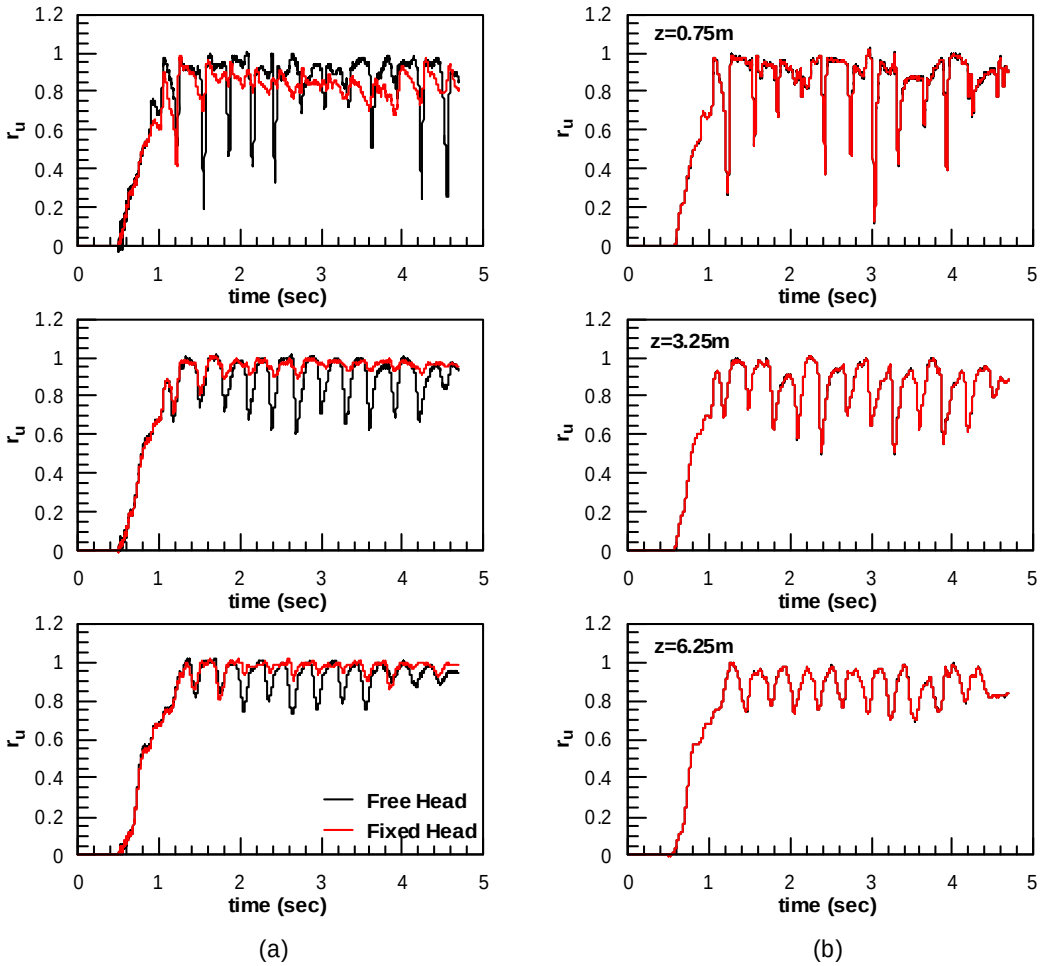

Figure 6.30: Effect of pile head constraint on pore pressure build-up at free-field a) with pile and b) without pile

As a result of the aforementioned phenomenon, as can be obviously seen in **Figure 6.31** and **Figure 6.32**, there is an increase in the lateral resistance of soil for the fixed-head pile analysis compared to the basic analysis. It should be considered that, this

increase in the resistance is more dramatic in shallow depths. In other words, head fixity affects regions near the surface significantly. But its effect decreases with depth which is quite reasonable.

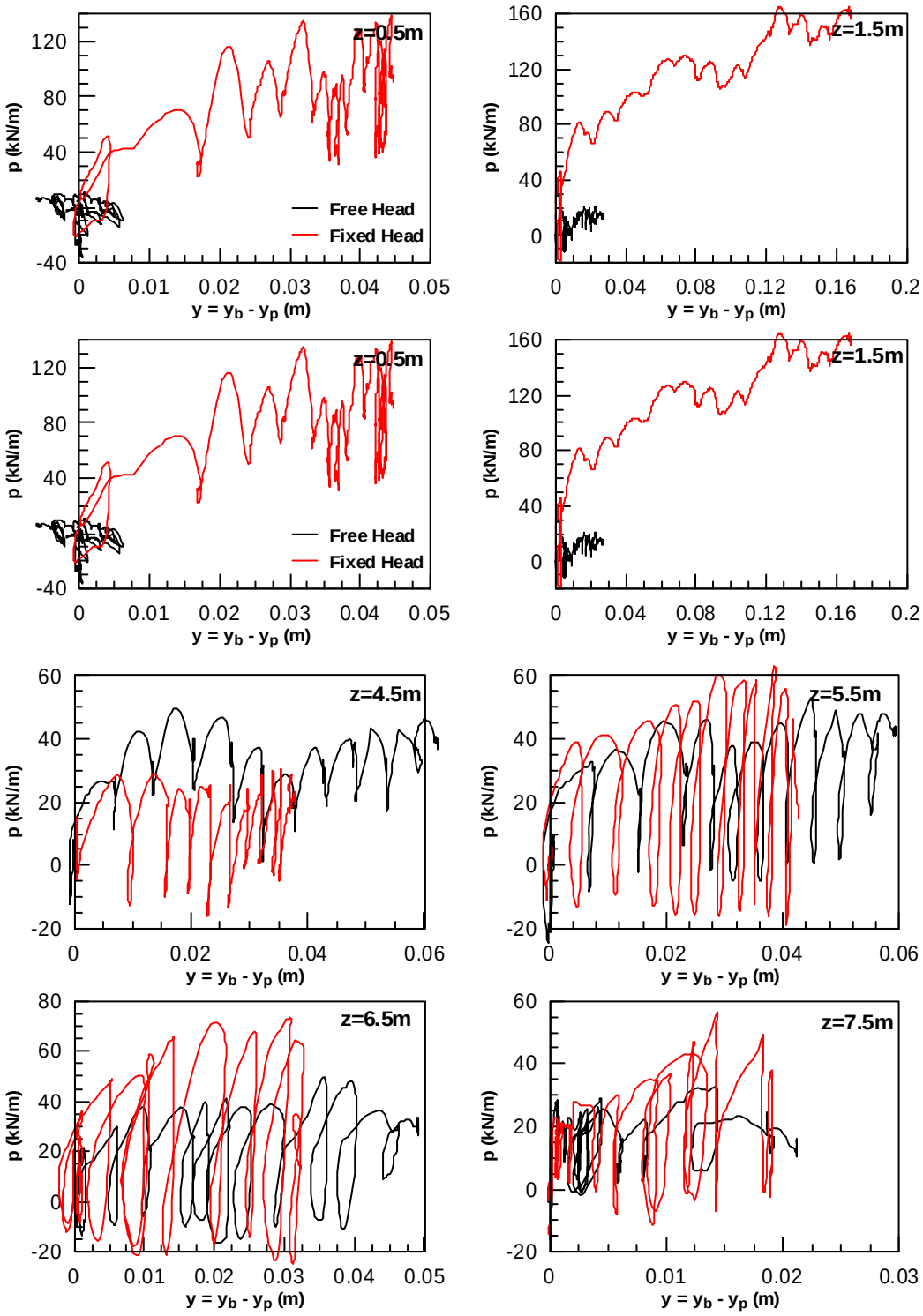

Figure 6.31: Effect of pile head constraint on dynamic p-y curves throughout the soil layer (using boundary displacements)

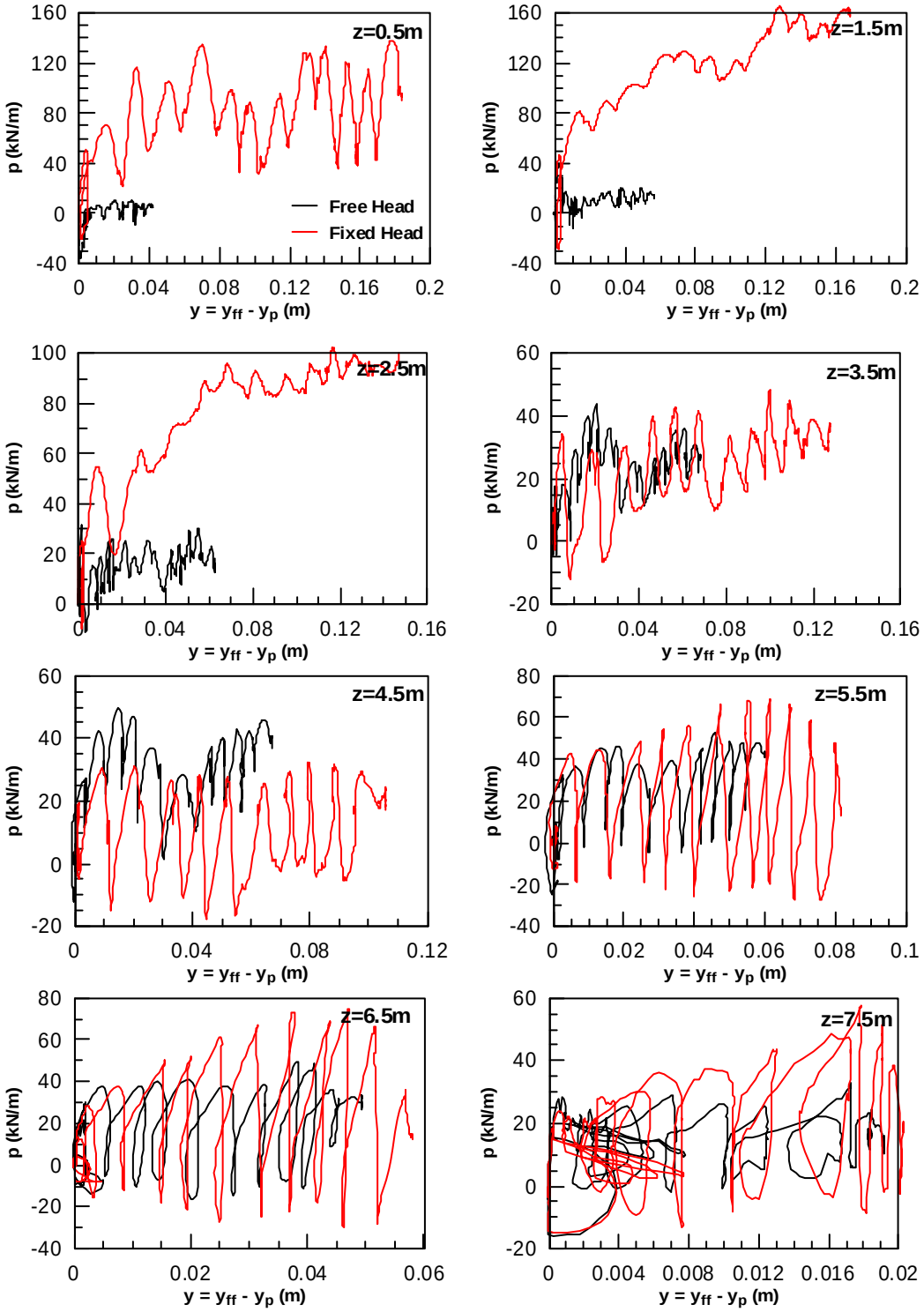

Figure 6.32: Effect of pile head constraint on dynamic p-y curves throughout the soil layer (using free-field displacements)

Figure 6.33 and **Figure 6.34** depict the p-y curves normalized with the static values after filtering the cyclic component. It can be seen that in shallow depths, the values of the dynamic p-y curves in the fixed head pile are even larger than the static ones where they change from 2 to 10 times larger than the static ones in depths 0.5 m and 1.5 m due to the aforementioned large dilations. This values decrease with depth considerably and reach a value of 0.1 to 0.2 in depths 3.5 m and 4.5 m. Therefore, in larger depths there is no large difference between the two analyses and the effect of head fixity is mostly limited to shallow depths.

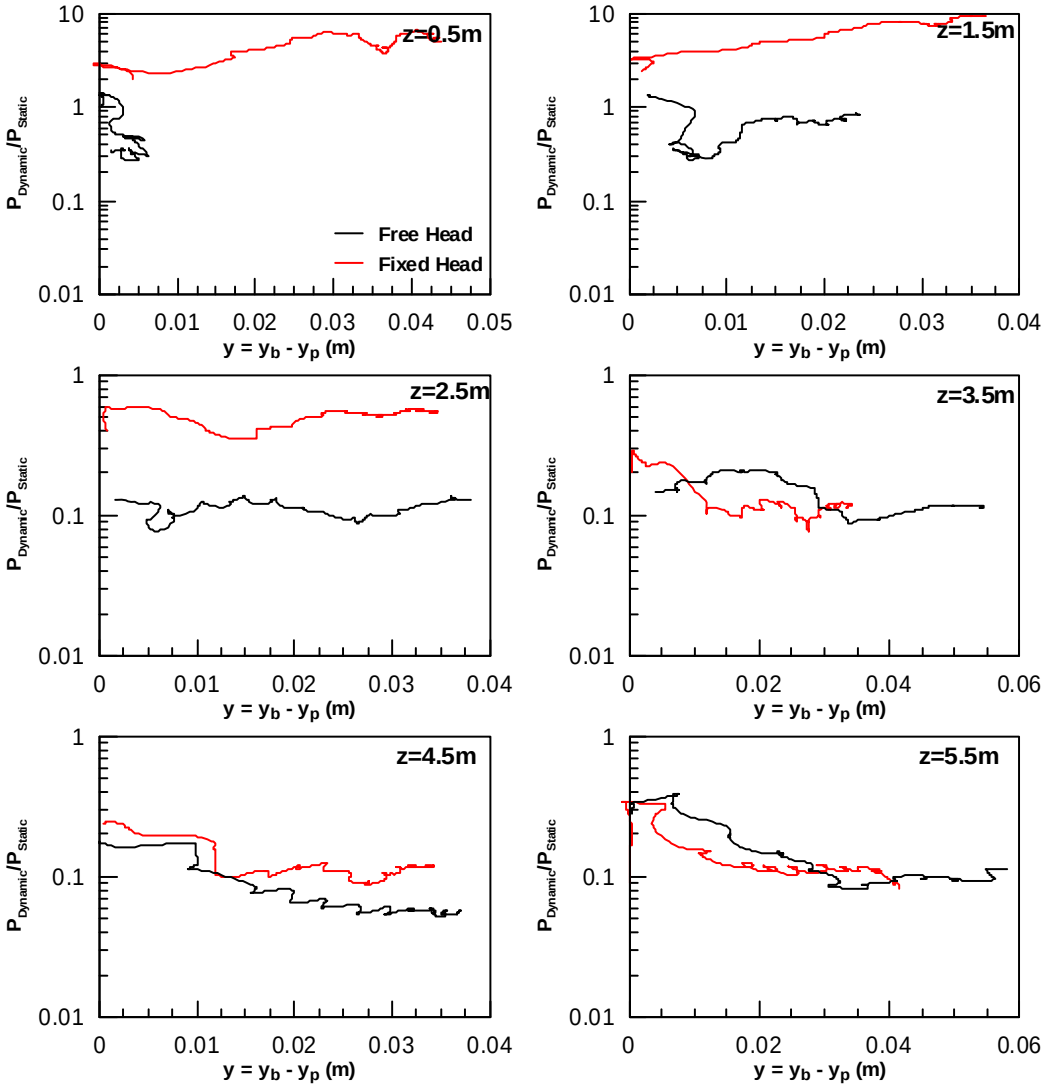

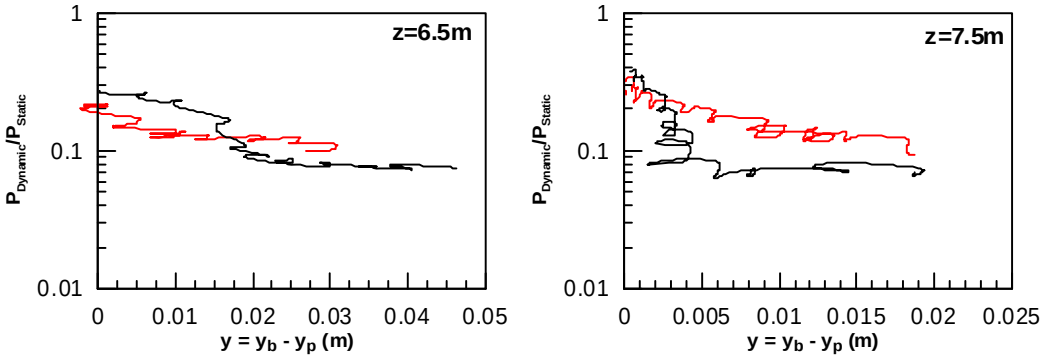

Figure 6.33: Effect of pile head constraint on normalized p-y curves throughout the soil layer (using boundary displacements)

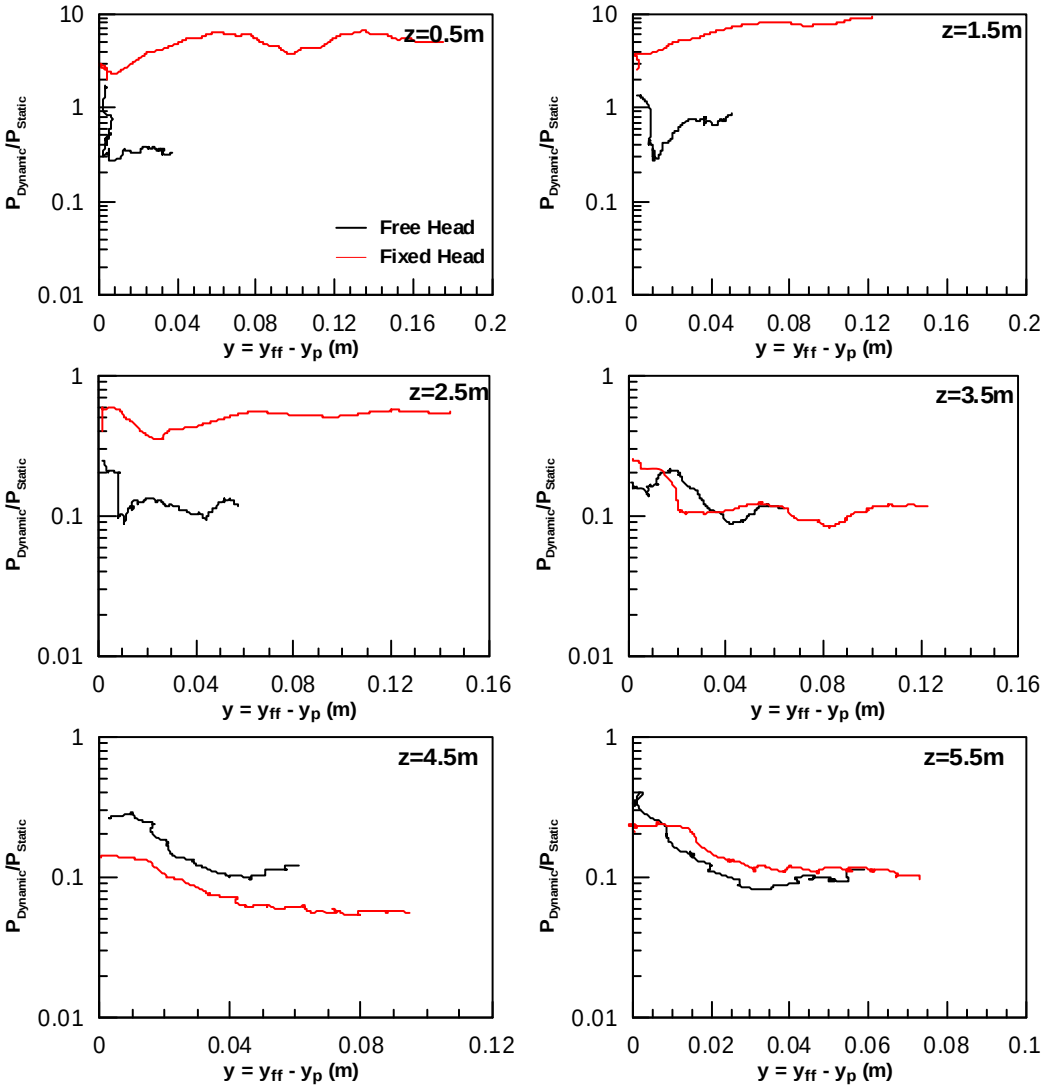

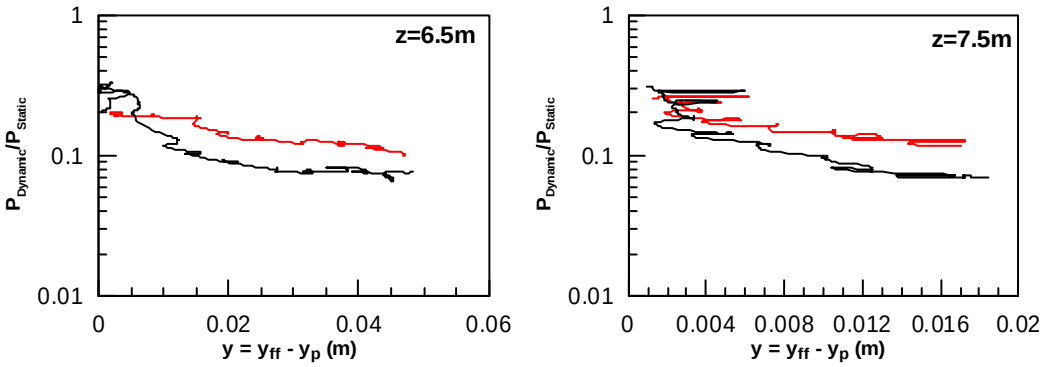

Figure 6.34: Effect of pile head constraint on normalized p-y curves throughout the soil layer (using free-field displacements)

To sum up, it can be obtained from these analyses that:

- The displacements of the boundary are smaller in the fixed-head pile compared to the basic one.
- Large negative excess pore pressure values are developed at areas near the pile especially at shallow depths.
- As a result of the previous, larger lateral loads are exerted from soil in fixed-head pile analysis compared to the basic one. These values are significantly higher in shallow depths and are not negligible.
- The effect of pile head constraint is limited to shallow depths and the response is quite similar to the basic analysis in depths larger than half the length of the pile.

Chapter 7

Conclusions

7.1. General

In this thesis, the effect of a number of parameters on the response of a pile embedded in laterally spreading ground is investigated through numerical analysis in finite difference code; FLAC3D. The results are extensively presented in the preceding chapters and the effect of each parameter is discussed separately. One important overall conclusion based on the analyses is that the assumption that at the fixed-end of springs the free-filed displacements are applied might be over-conservative since the pinning effect of the pile is significant. Apart from that, the effect of each parameter in the behavior of the model is summarized in the following paragraphs.

7.2. Effect of Soil Relative Density, D_r

As one could predict, the sample with larger relative density undergoes less lateral displacement. This is completely seen in the analyses in all displacement components (pile, boundary and relative displacements). However, the results are quite strange in terms of soil lateral resistance; the resistance of soil increases with decreased relative density and vice versa. It is speculated that this is due to large negative pore pressure build-up near the pile in the analysis with small relative density, which is in turn a consequence of the large relative displacement developed.

7.3. Effect of Soil Permeability, k

It was observed that permeability is quite determinant in the response of the pile in laterally spreading ground. The following conclusions can be drawn:

- Lateral displacement of the soil is reversely related to the permeability. It was observed that the larger the permeability, the less the lateral displacement of the soil (and consequently the pile).
- The lateral resistance of the soil is increased when the permeability is decreased. The reason is large and cumulative negative excess pore pressure which is developed near the pile due to the fact that water cannot find enough time to travel from free-field and dissipate the negative pore pressure in each cycle.
- Introduction of permeability as a function of excess pore pressure, r_u did not have significant effects on the response.

7.4. Effect of Excitation Period, T

From the free-field analyses it is shown that as T increases, soil displacements also increase. From the "pile" analyses you cannot draw safe conclusions with regard to displacement because of instability. In order to have equivalent and comparable displacements you should have the same number of cycles. However, the effect is quite complicated on the lateral resistance of the soil. To be more precise, when the model is shaken by an excitation which has a period of 0.5 seconds, no considerable difference is observed compared to the basic analysis which has a period of 0.3 seconds. On the other hand, when the excitation with T=0.1 sec is applied, large lateral resistance is observed.

According to the above observations, it can be concluded that a threshold may exist for excitation period to be determinant based on the current permeability of the soil. In other words, in the sample with k=6.2e-5 m/s, water finds enough time in each cycle to dissipate the negative pore pressure near the pile even when period is equal to 0.3

seconds. Therefore, increasing the period does not change the situation to a great extent. However, if T is decreased, there comes a time when water cannot dissipate negative r_u in each cycle, leading to large negative pore pressure ratios and therefore, large lateral resistance of the liquefied soil.

7.5. Effect of Pile Diameter

Larger lateral displacement of the liquefied layer and consequently the pile is observed in model with larger diameter and vice versa. This is due to the fact that the thickness of the soil layer is larger in this analysis, a determinant factor in lateral displacement of soil.

Apart from that, no specific pattern is observed in the lateral resistance of soil with the change in pile diameter. It might be due to the following reasons:

- The models have different soil thickness which may have significant effects on the response of the pile. To be more precise, the effect of soil thickness might have interfered with the effect of pile diameter.
- In different analyses, as the Young modulus of the section is modified in order to have the same value of “EI”, the ratio of the length of the pile over the stiffness of the section is significantly changed. It may have led to different response of the pile.

Overall, it should be mentioned that further investigation is needed in order to determine the effect of the pile diameter on the response of the pile in laterally spreading ground. However, assuming that this specific type of investigation is correct, it seems that the effect of pile diameter is not very significant. However, results indicate smaller degradation for piles of smaller diameter.

7.6. Effect of Pile Stiffness

Increasing the pile stiffness lead to the following:

- Decrease in the lateral displacement of the pile and consequently, a fall in the boundary displacements of the mesh due to the pinning effect.
- Larger lateral forces are exerted on the pile. The reason is large negative pore pressure ratios near the pile.

It can be concluded that stiffness of the pile is an important factor and should not be overlooked. However, further investigations are needed in order to quantify the results.

7.7. Effect of Installation Method

The stress field around the pile is changes in this analysis in order to simulate the situation of a driven pile. Justifiably, smaller lateral displacements in pile and boundary are observed because of denser soil around the pile. However, the effect on the p-y curves is minor. In other words, the lateral load exerted on pile is not affected considerably by the change in the installation method.

7.8. Effect of Head Constraint

As one would expect, significantly smaller lateral displacement of the boundary is observed in the fixed-head pile due to more profound pinning effect of the pile in this case.

Additionally, large negative pore pressure is developed near the pile, especially in shallow depth. Consequently, the lateral resistance of the soil is increased considerably, increasing the degradation multiplier. This effect is limited to shallow depth and becomes negligible in the lower half of the pile length.

Appendix A

Results of the Parametric Numerical Analysis

The results of the parametric analysis are presented hereafter based on the numbers of analyses indicated in **Table A.1**. The first analysis is the basic one and in other analyses, the parameter that has been changed from the basic analysis is shaded in the table.

Table A.1: The layout of the parametric analyses

No	D_r (%)	D (m)	EI (kNm^2)	T (sec)	Driven	k (m/sec)	Head Fixity
1	50	0.6	8000	0.3	NO	6.10E-05	NO
2	30	0.6	8000	0.3	NO	6.10E-05	NO
3	90	0.6	8000	0.3	NO	6.10E-05	NO
4	50	0.4	8000	0.3	NO	6.10E-05	NO
5	50	1	8000	0.3	NO	6.10E-05	NO
6	50	0.6	1000000	0.3	NO	6.10E-05	NO
7	50	0.6	8000	0.1	NO	6.10E-05	NO
8	50	0.6	8000	0.5	NO	6.10E-05	NO
9	50	0.6	8000	0.3	YES	6.10E-05	NO
10	50	0.6	8000	0.3	NO	6.10E-04	NO
11	50	0.6	8000	0.3	NO	2.10E-05	NO
12	50	0.6	8000	0.3	NO	0	NO
13	50	0.6	8000	0.3	NO	$k(r_u)$	NO
14	50	0.6	8000	0.3	NO	6.10E-05	YES

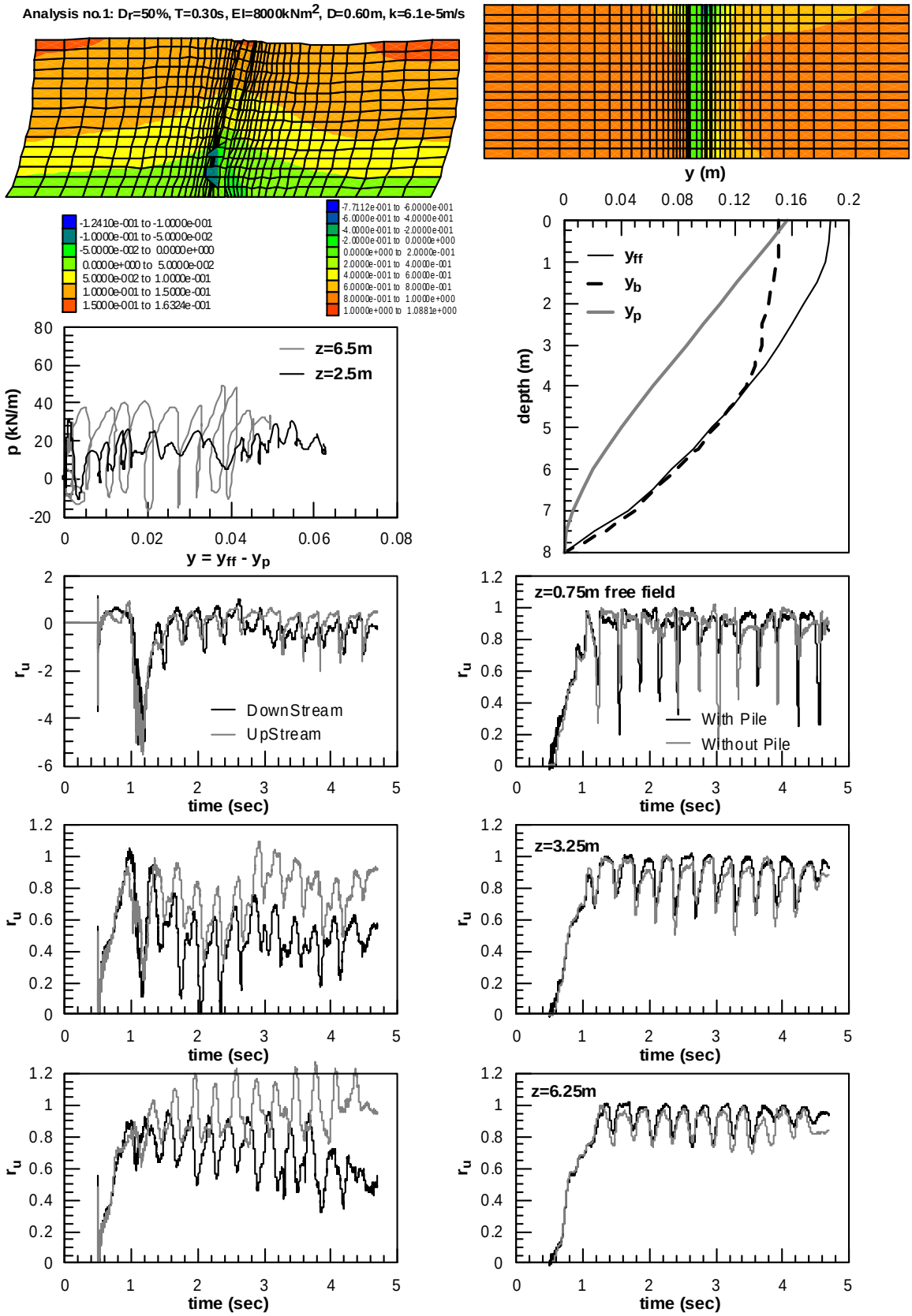
Analysis no.1: Dr=50%, T=0.30s, EI=8000kNm2, D=0.60m, k=6.1e-5m/s
-1.2410e-001 to -1.0000e-001
-1.0000e-001 to -5.0000e-002
-5.0000e-002 to 0.0000e+000
0.0000e+000 to 5.0000e-002
5.0000e-002 to 1.0000e-001
1.0000e-001 to 1.5000e-001
1.5000e-001 to 1.6324e-001
-7.7112e-001 to -6.0000e-001
-6.0000e-001 to -4.0000e-001
-4.0000e-001 to -2.0000e-001
-2.0000e-001 to 0.0000e+000
0.0000e+000 to 2.0000e-001
2.0000e-001 to 4.0000e-001
4.0000e-001 to 6.0000e-001
6.0000e-001 to 8.0000e-001
8.0000e-001 to 1.0000e+000
1.0000e+000 to 1.0881e+000
y (m)
0 0.04 0.08 0.12 0.16 0.2
p (kN/m)
z=6.5m
z=2.5m
y = yff - yp
depth (m)
yff
yb
yp
ru
DownStream
UpStream
time (sec)
z=0.75m free field
With Pile
Without Pile
z=3.25m
z=6.25m

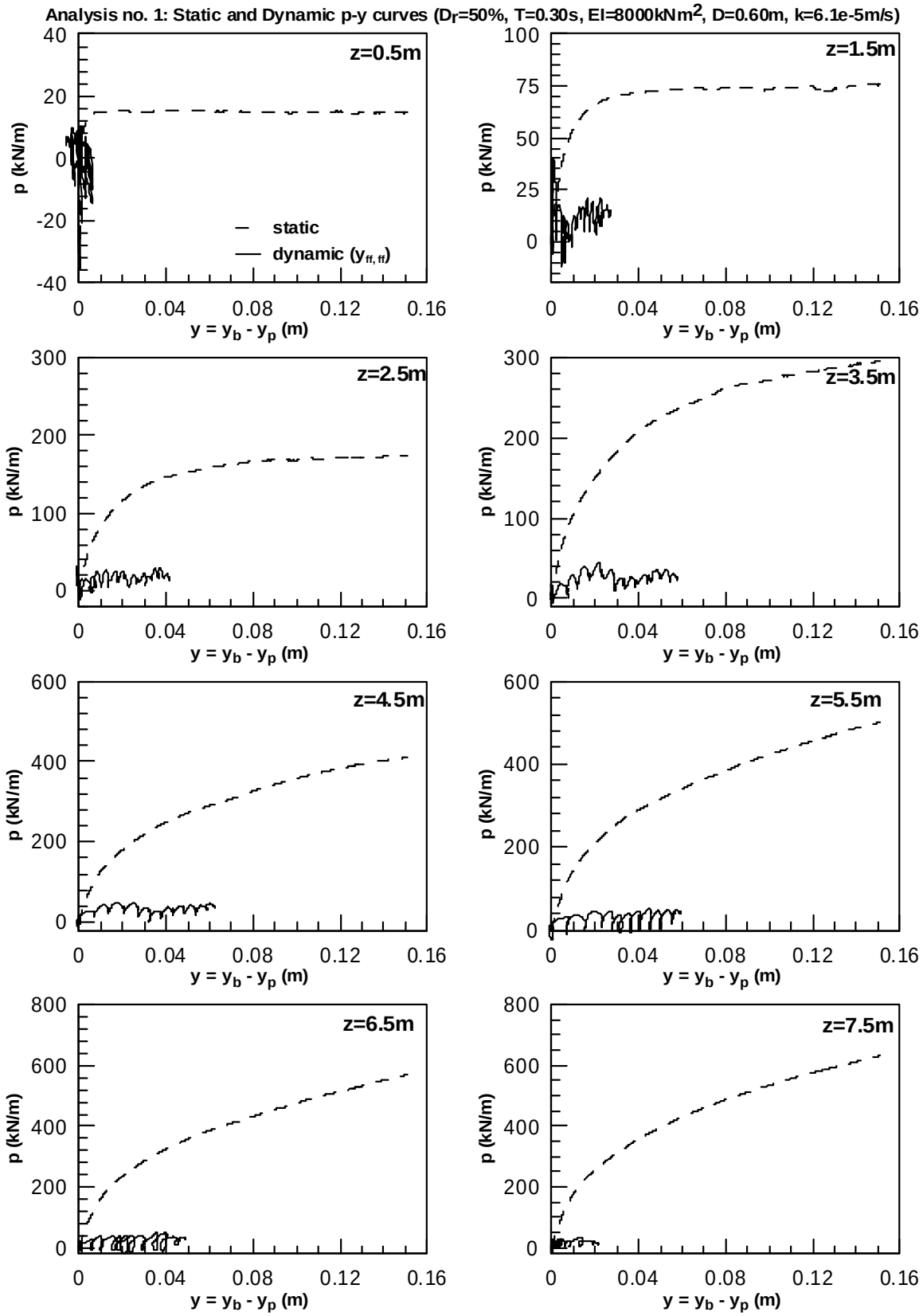
Analysis no. 1: Static and Dynamic p-y curves (Dr=50%, T=0.30s, EI=8000kNm2, D=0.60m, k=6.1e-5m/s)
z=0.5m
z=1.5m
z=2.5m
z=3.5m
z=4.5m
z=5.5m
z=6.5m
z=7.5m
p (kN/m)
y = yb - yp (m)
static
dynamic (yff, ff)

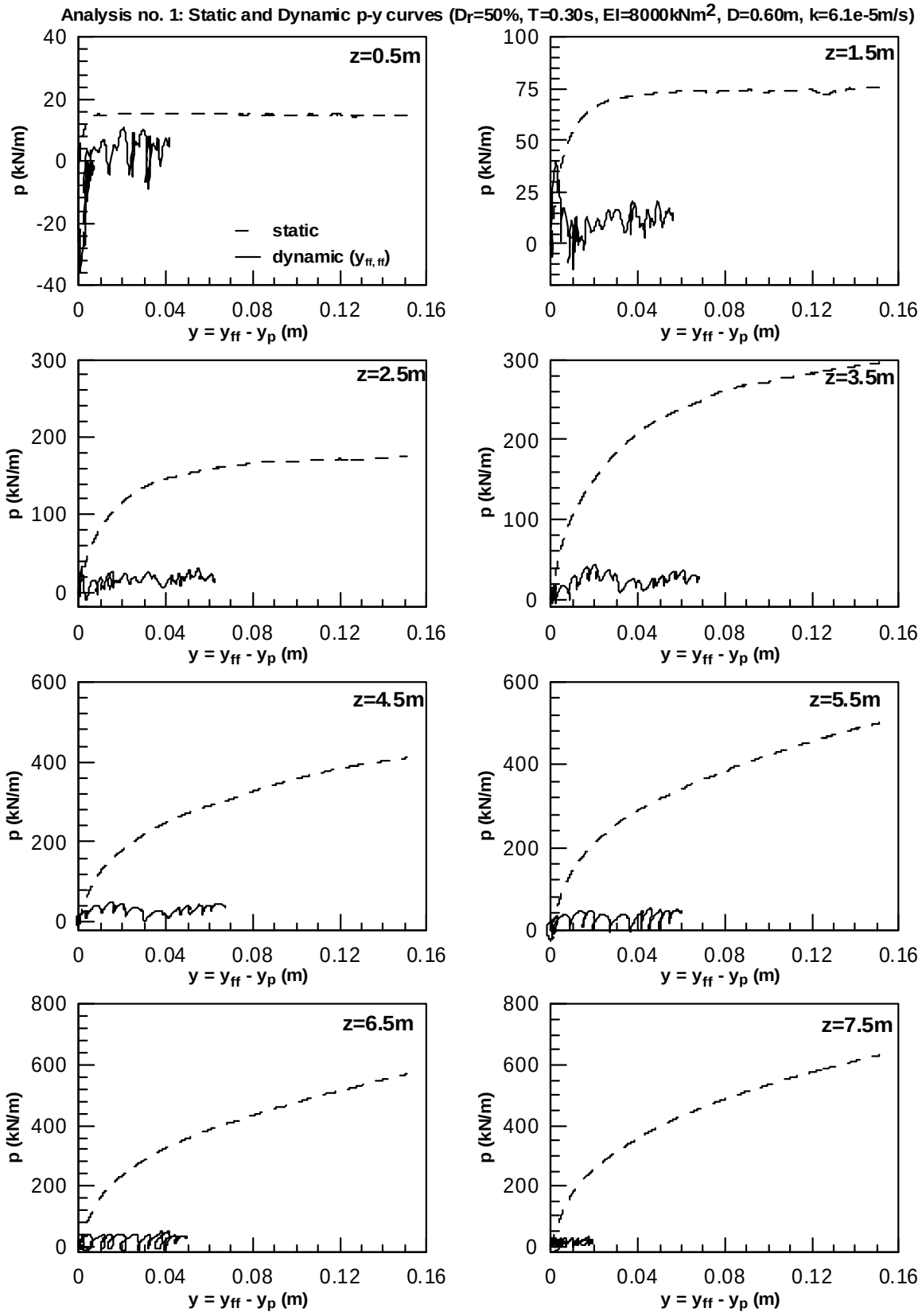
Analysis no. 1: Static and Dynamic p-y curves (Dr=50%, T=0.30s, EI=8000kNm2, D=0.60m, k=6.1e-5m/s)
z=0.5m
z=1.5m
z=2.5m
z=3.5m
z=4.5m
z=5.5m
z=6.5m
z=7.5m
static
dynamic (yff, ff)
p (kN/m)
y = yff - yp (m)

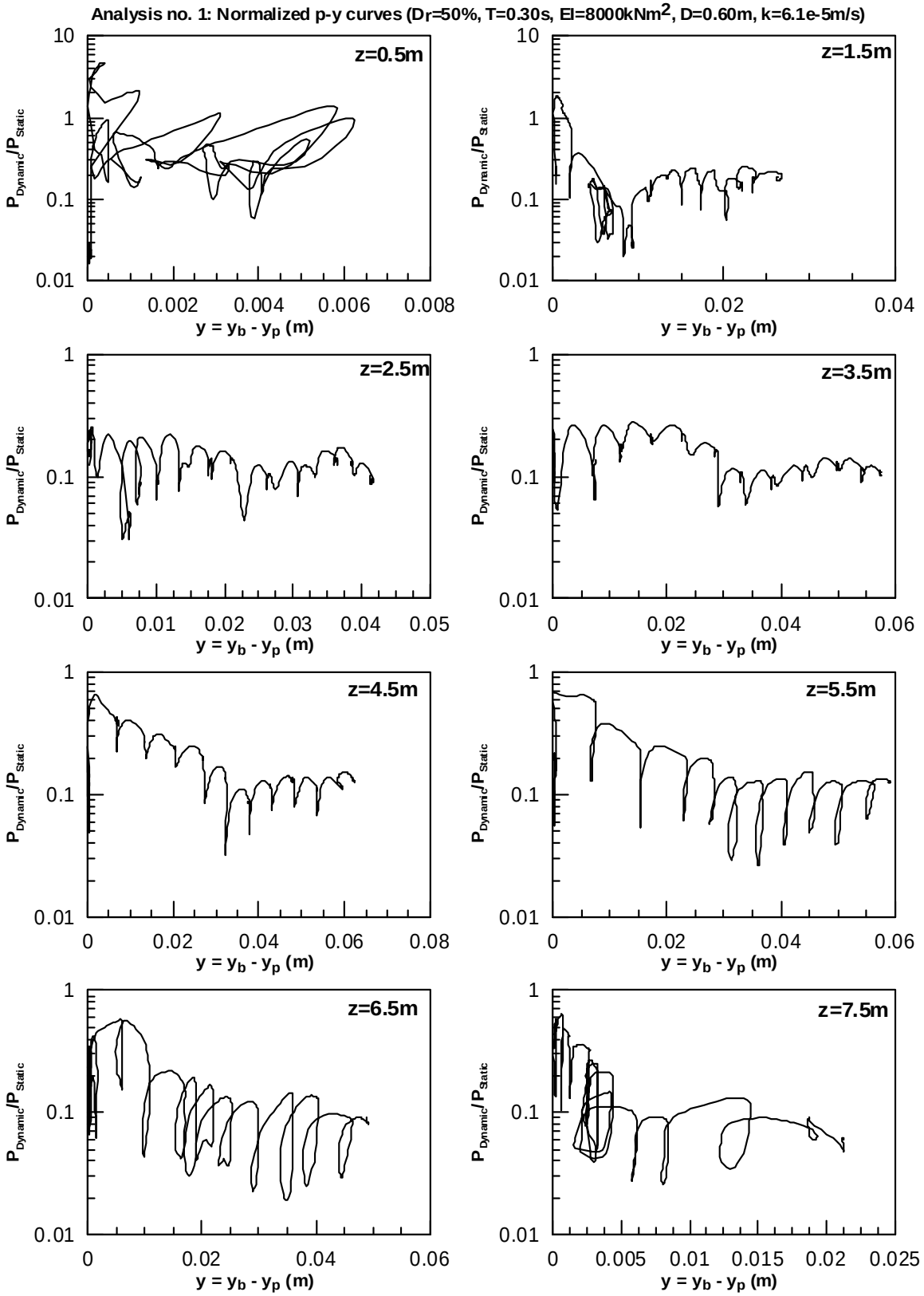
Analysis no. 1: Normalized p-y curves (Dr=50%, T=0.30s, EI=8000kNm2, D=0.60m, k=6.1e-5m/s)
z=0.5m
z=1.5m
z=2.5m
z=3.5m
z=4.5m
z=5.5m
z=6.5m
z=7.5m
P_Dynamic/P_Static
y = y_b - y_p (m)

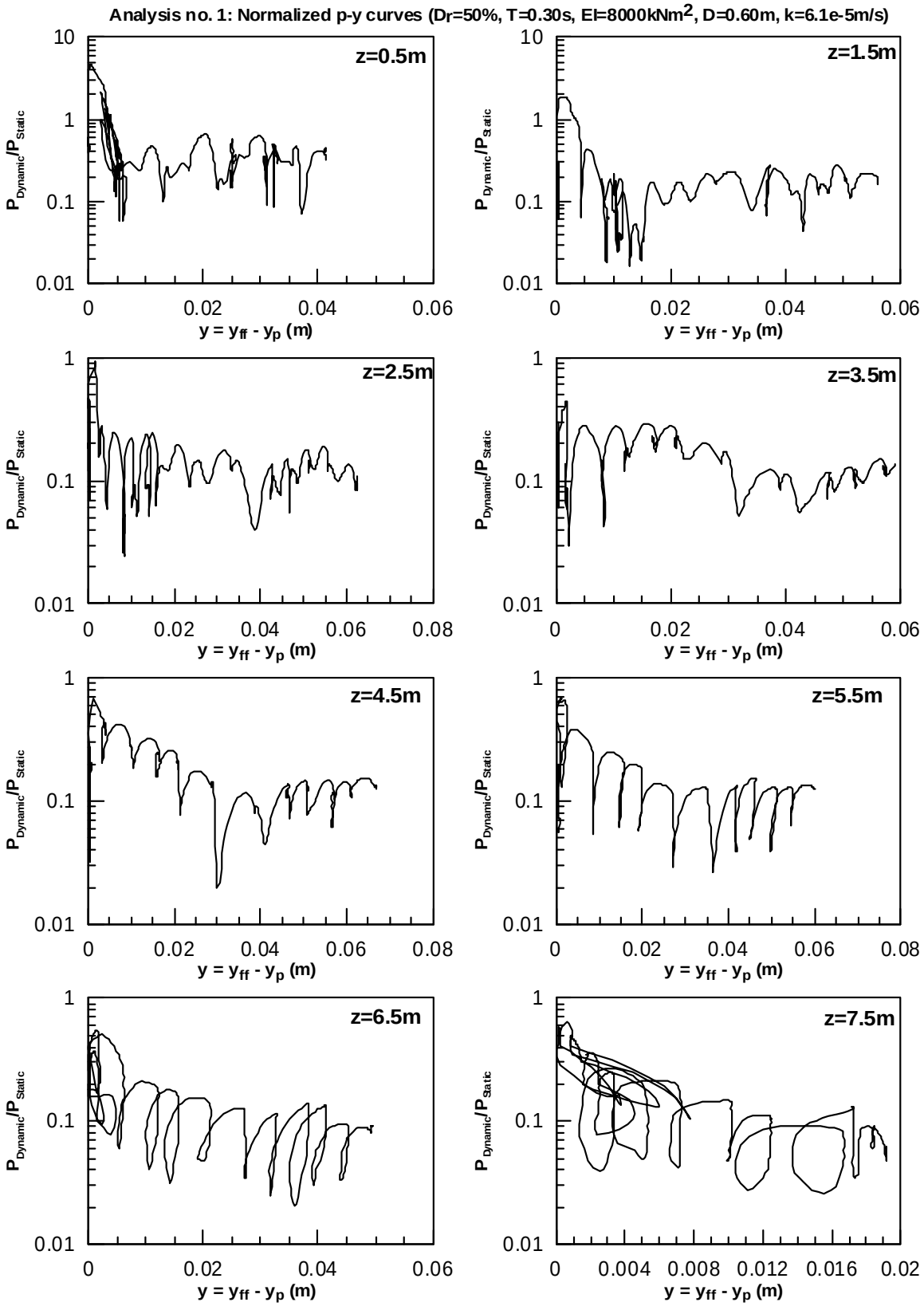
Analysis no. 1: Normalized p-y curves (Dr=50%, T=0.30s, EI=8000kNm2, D=0.60m, k=6.1e-5m/s)
z=0.5m
z=1.5m
z=2.5m
z=3.5m
z=4.5m
z=5.5m
z=6.5m
z=7.5m
P Dynamic/P Static
y = yff - yp (m)

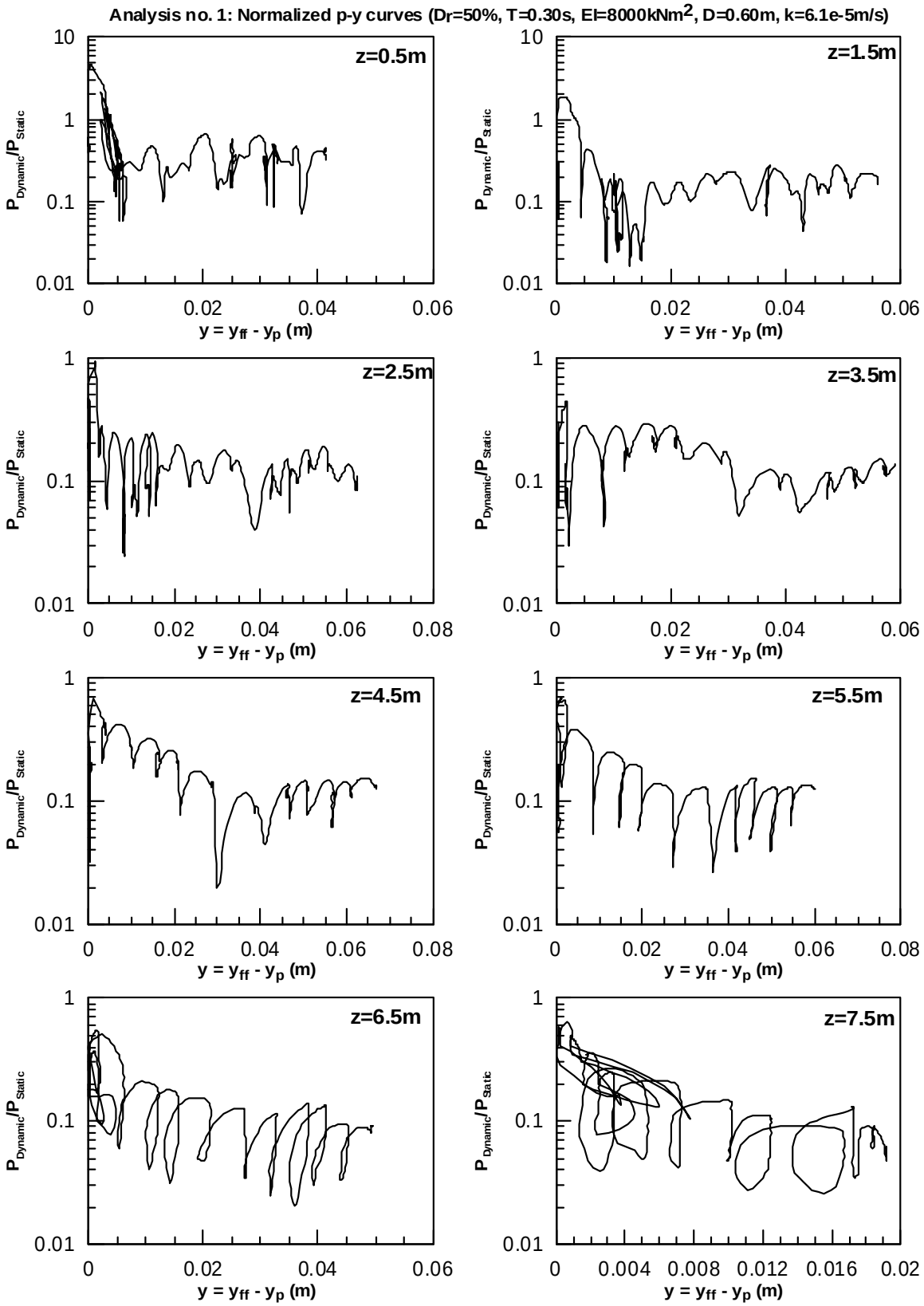
Analysis no. 1: Normalized p-y curves (Dr=50%, T=0.30s, EI=8000kNm2, D=0.60m, k=6.1e-5m/s)
z=0.5m
z=1.5m
z=2.5m
z=3.5m
z=4.5m
z=5.5m
z=6.5m
z=7.5m
P Dynamic/P Static
y = yff - yp (m)

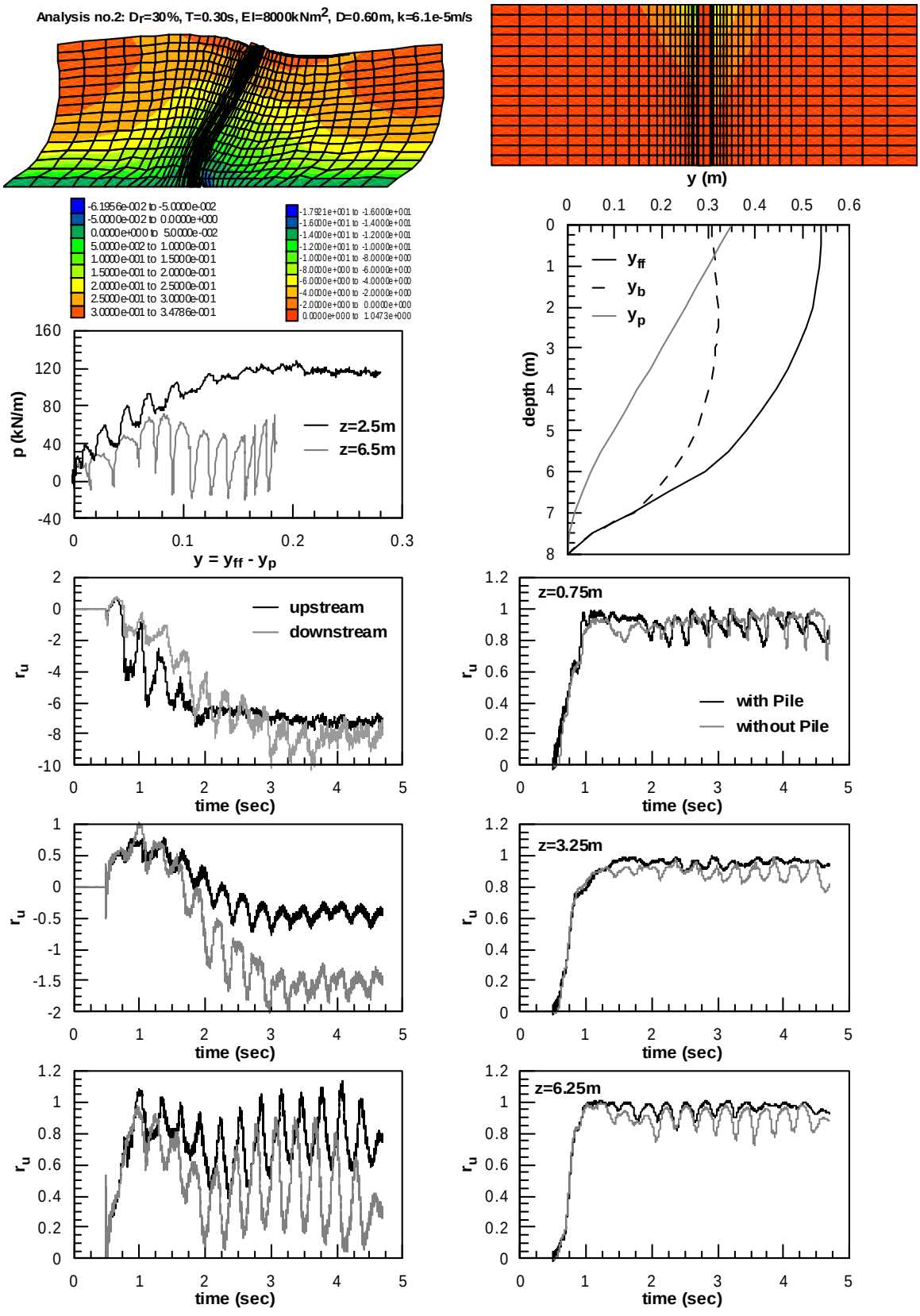
Analysis no.2: Dr=30%, T=0.30s, EI=8000kNm2, D=0.60m, k=6.1e-5m/s
y (m)
depth (m)
yff
yb
yp
p (kN/m)
z=2.5m
z=6.5m
y = yff - yp
ru
upstream
downstream
time (sec)
z=0.75m
with Pile
without Pile
z=3.25m
z=6.25m

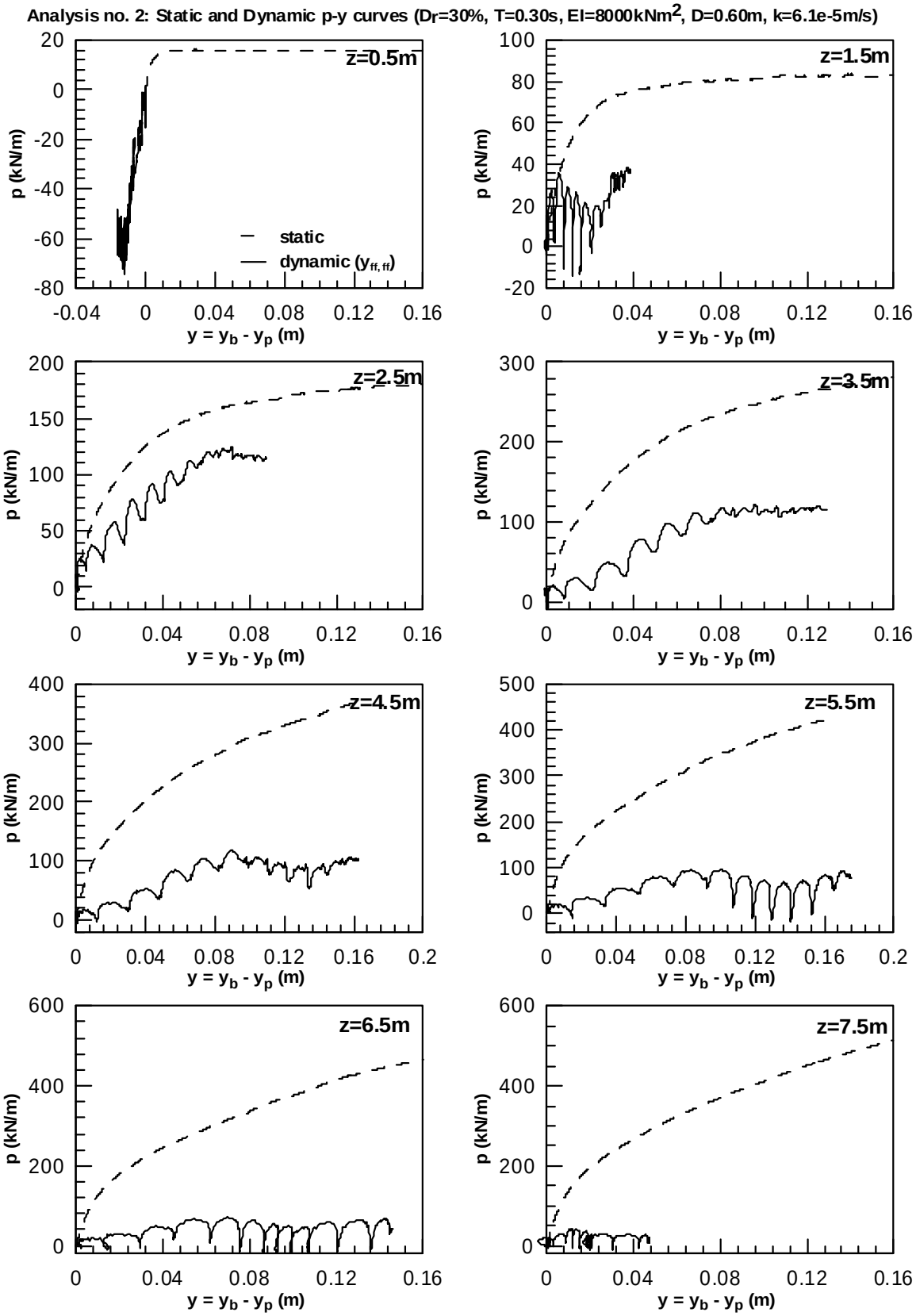
Analysis no. 2: Static and Dynamic p-y curves (Dr=30%, T=0.30s, EI=8000kNm2, D=0.60m, k=6.1e-5m/s)
z=0.5m
z=1.5m
z=2.5m
z=3.5m
z=4.5m
z=5.5m
z=6.5m
z=7.5m
static
dynamic (yff, rf)
p (kN/m)
y = yb - yp (m)

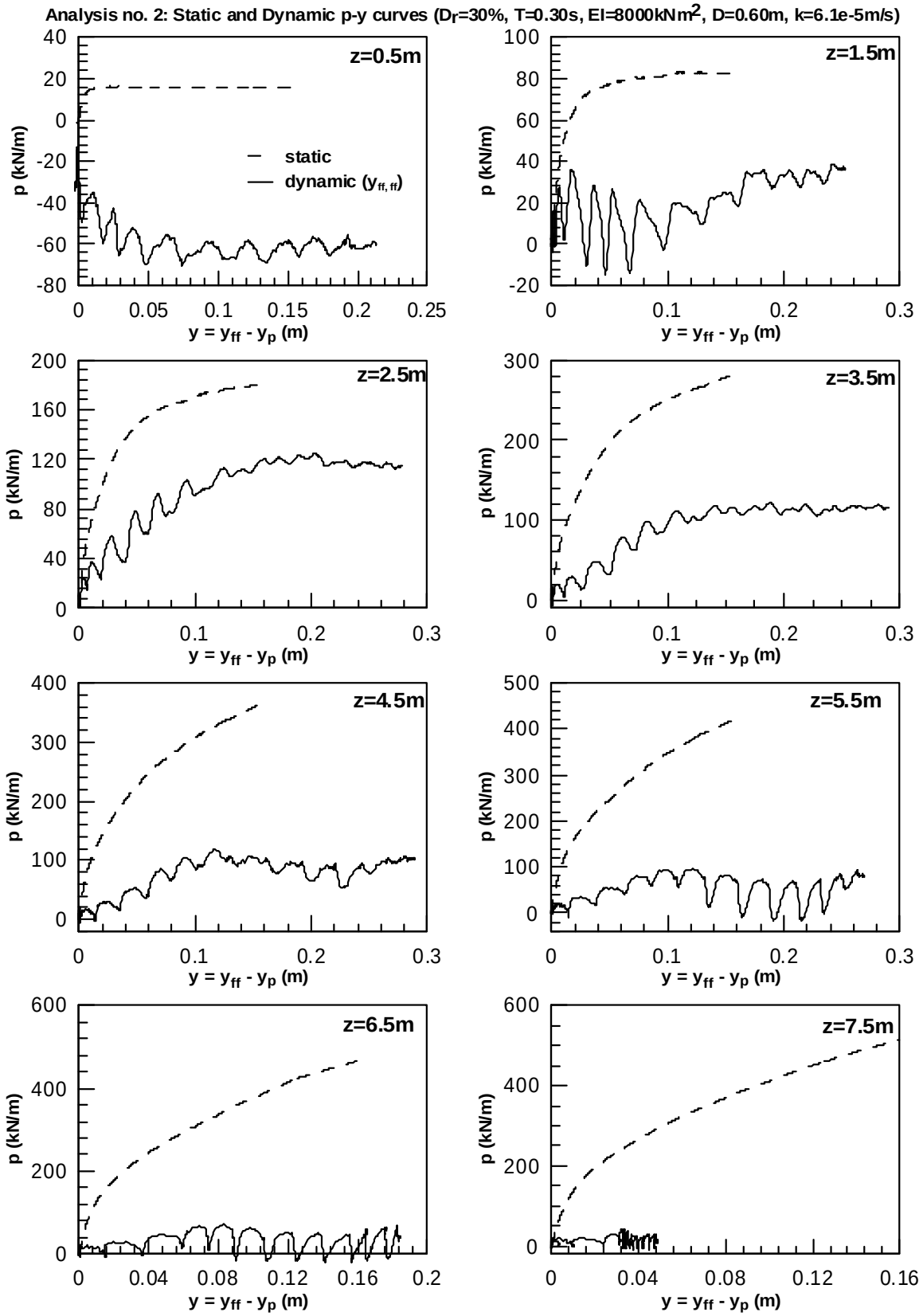
Analysis no. 2: Static and Dynamic p-y curves (Dr=30%, T=0.30s, EI=8000kNm2, D=0.60m, k=6.1e-5m/s)
z=0.5m
static
dynamic (yff, ff)
z=1.5m
z=2.5m
z=3.5m
z=4.5m
z=5.5m
z=6.5m
z=7.5m
p (kN/m)
y = yff - yp (m)

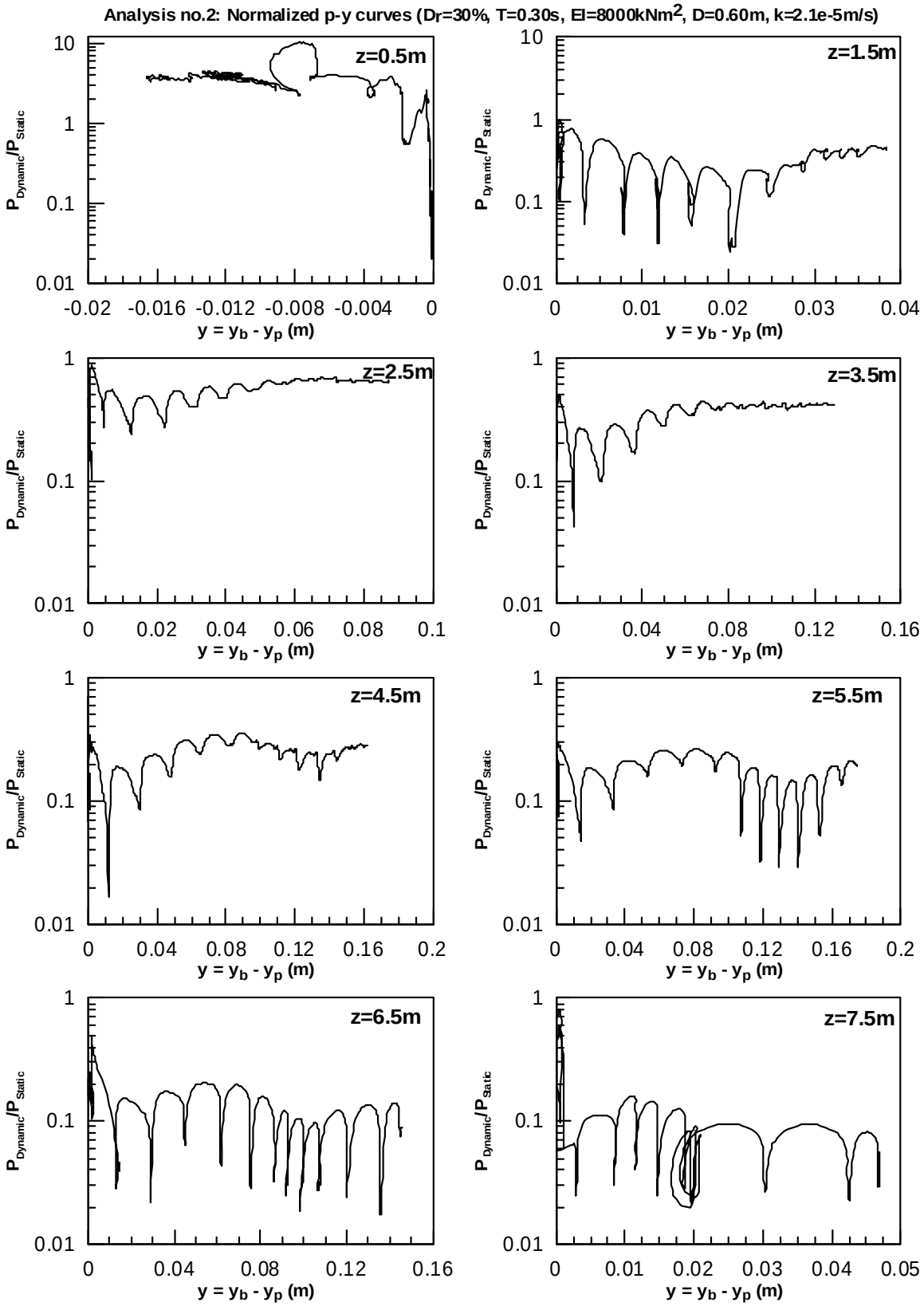
Analysis no.2: Normalized p-y curves (Dr=30%, T=0.30s, EI=8000kNm2, D=0.60m, k=2.1e-5m/s)
z=0.5m
z=1.5m
z=2.5m
z=3.5m
z=4.5m
z=5.5m
z=6.5m
z=7.5m
P Dynamic/P Static
y = yb - yp (m)

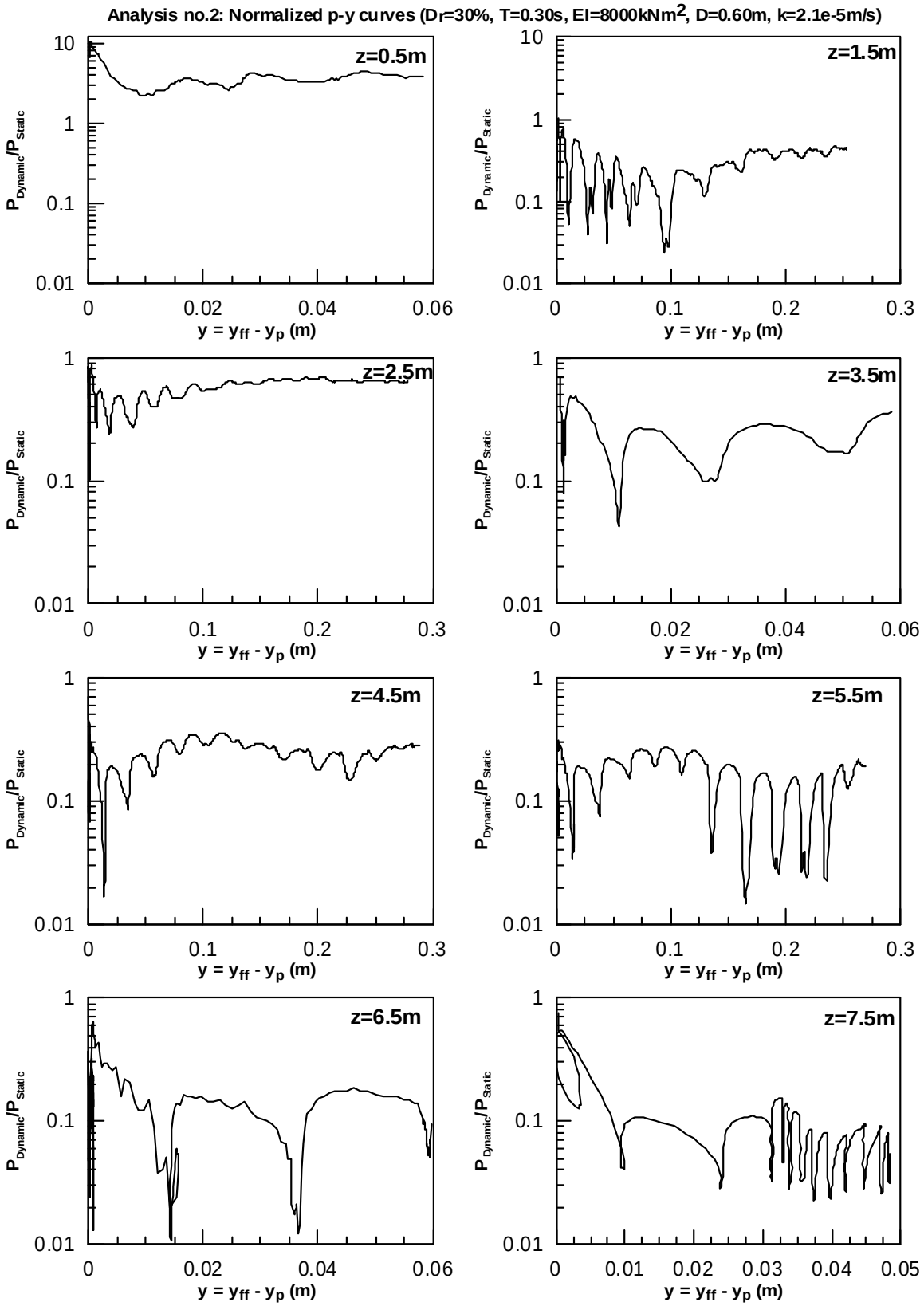
Analysis no.2: Normalized p-y curves (Dr=30%, T=0.30s, EI=8000kNm2, D=0.60m, k=2.1e-5m/s)
z=0.5m
z=1.5m
z=2.5m
z=3.5m
z=4.5m
z=5.5m
z=6.5m
z=7.5m
P Dynamic/P Static
y = yff - yp (m)

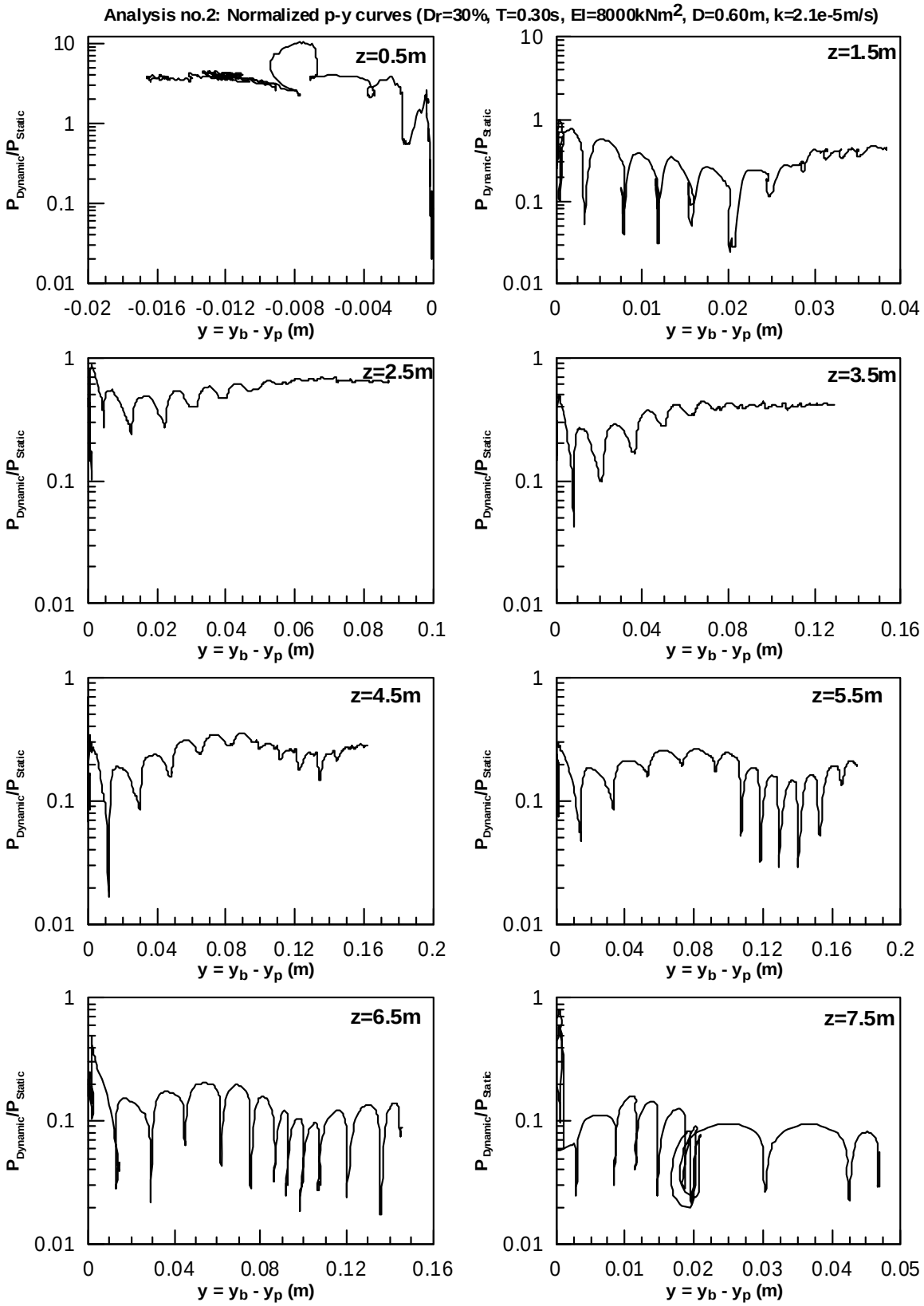
Analysis no.2: Normalized p-y curves (Dr=30%, T=0.30s, EI=8000kNm2, D=0.60m, k=2.1e-5m/s)
z=0.5m
z=1.5m
z=2.5m
z=3.5m
z=4.5m
z=5.5m
z=6.5m
z=7.5m
P Dynamic/P Static
y = yb - yp (m)

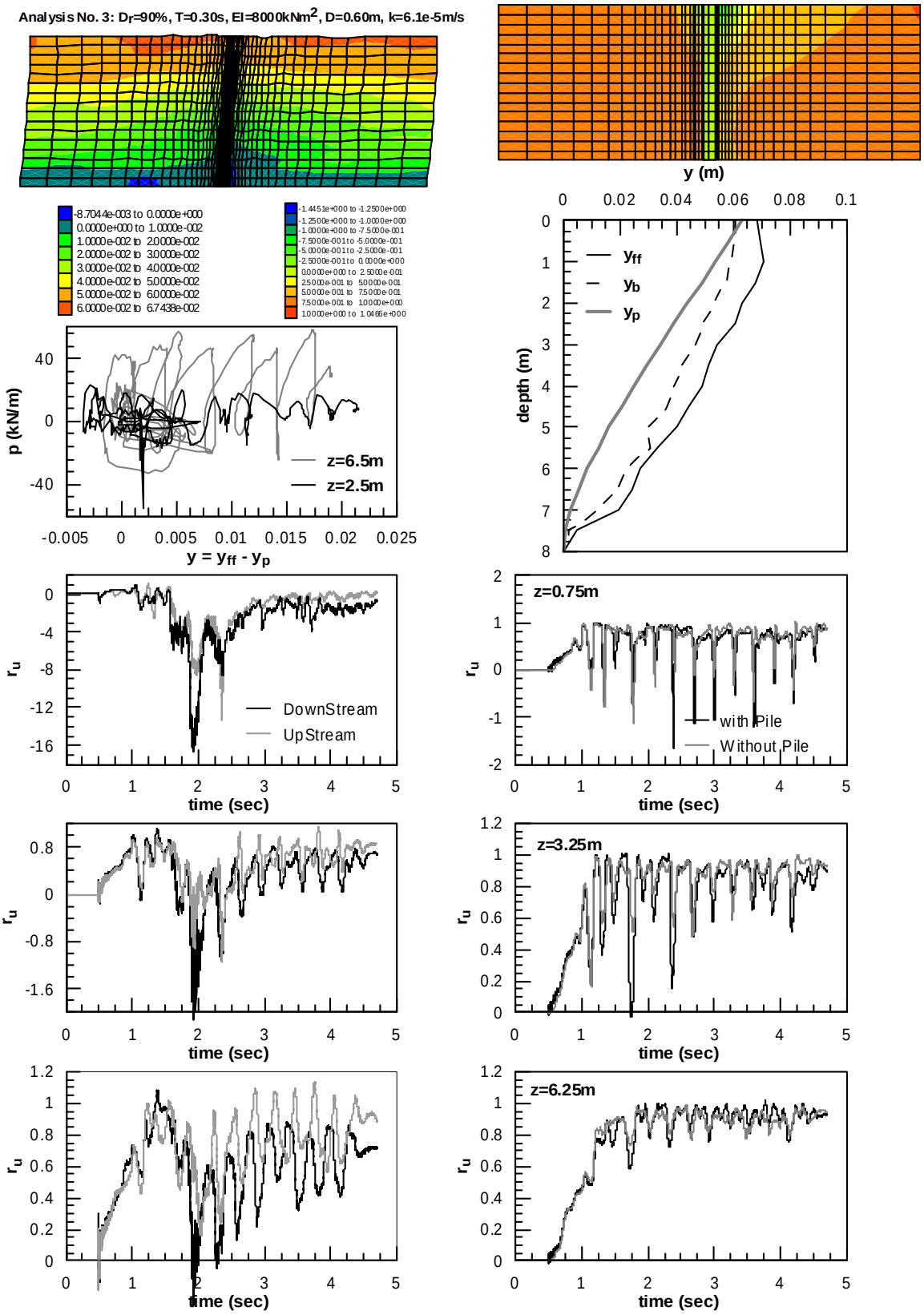
Analysis No. 3: Dr=90%, T=0.30s, EI=8000kNm2, D=0.60m, k=6.1e-5m/s
-8.7044e-003 to 0.0000e+000
0.0000e+000 to 1.0000e-002
1.0000e-002 to 2.0000e-002
2.0000e-002 to 3.0000e-002
3.0000e-002 to 4.0000e-002
4.0000e-002 to 5.0000e-002
5.0000e-002 to 6.0000e-002
6.0000e-002 to 6.7438e-002
-1.4451e+000 to -1.2500e+000
-1.2500e+000 to -1.0000e+000
-1.0000e+000 to -7.5000e-001
-7.5000e-001 to -5.0000e-001
-5.0000e-001 to -2.5000e-001
-2.5000e-001 to 0.0000e+000
0.0000e+000 to 2.5000e-001
2.5000e-001 to 5.0000e-001
5.0000e-001 to 7.5000e-001
7.5000e-001 to 1.0000e+000
1.0000e+000 to 1.0466e+000
y (m)
depth (m)
yff
yb
yp
p (kN/m)
z=6.5m
z=2.5m
y = yff - yp
ru
DownStream
UpStream
time (sec)
z=0.75m
with Pile
Without Pile
z=3.25m
z=6.25m

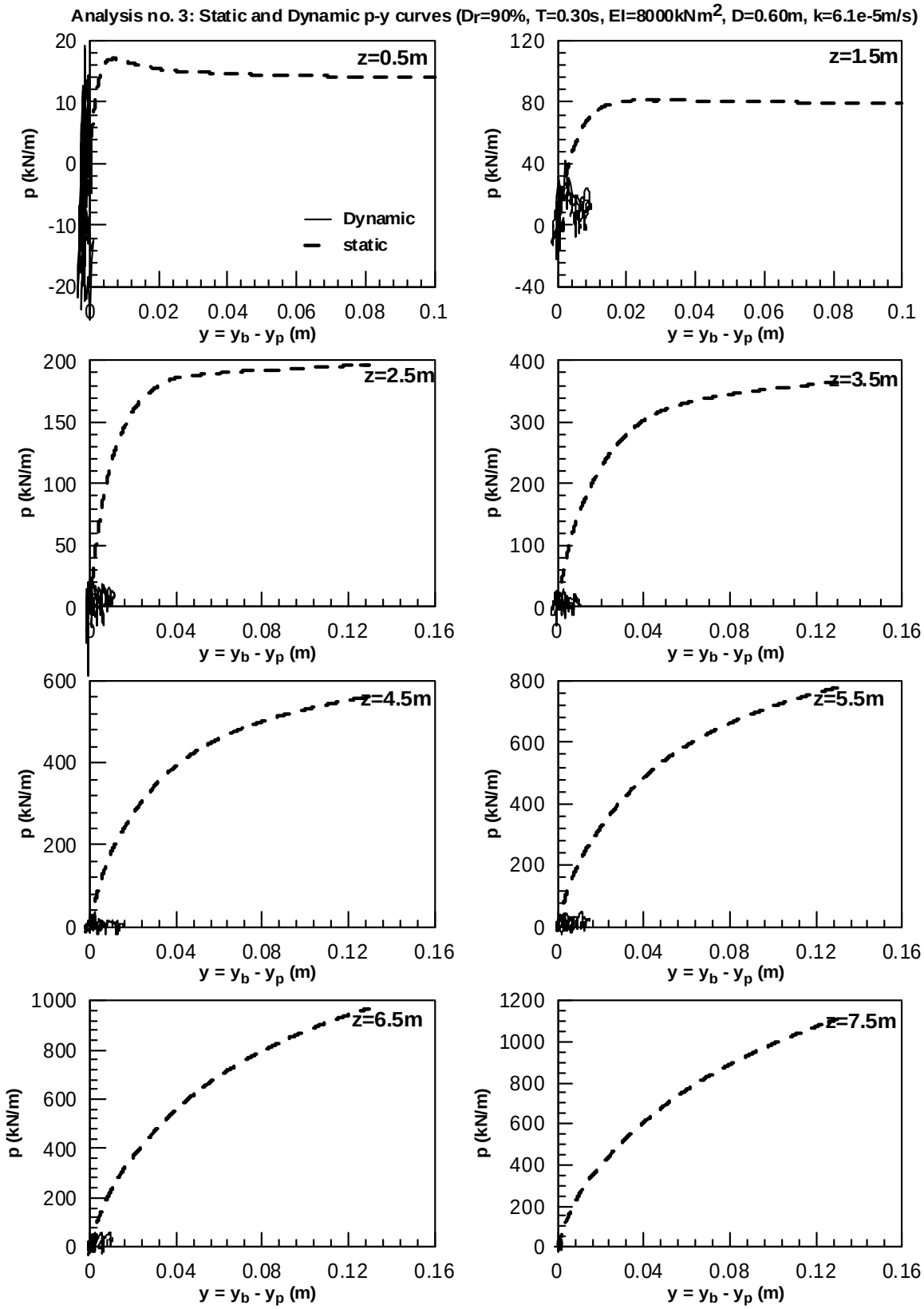
Analysis no. 3: Static and Dynamic p-y curves (Dr=90%, T=0.30s, EI=8000kNm2, D=0.60m, k=6.1e-5m/s)
z=0.5m
z=1.5m
z=2.5m
z=3.5m
z=4.5m
z=5.5m
z=6.5m
z=7.5m
Dynamic
static
p (kN/m)
y = yb - yp (m)

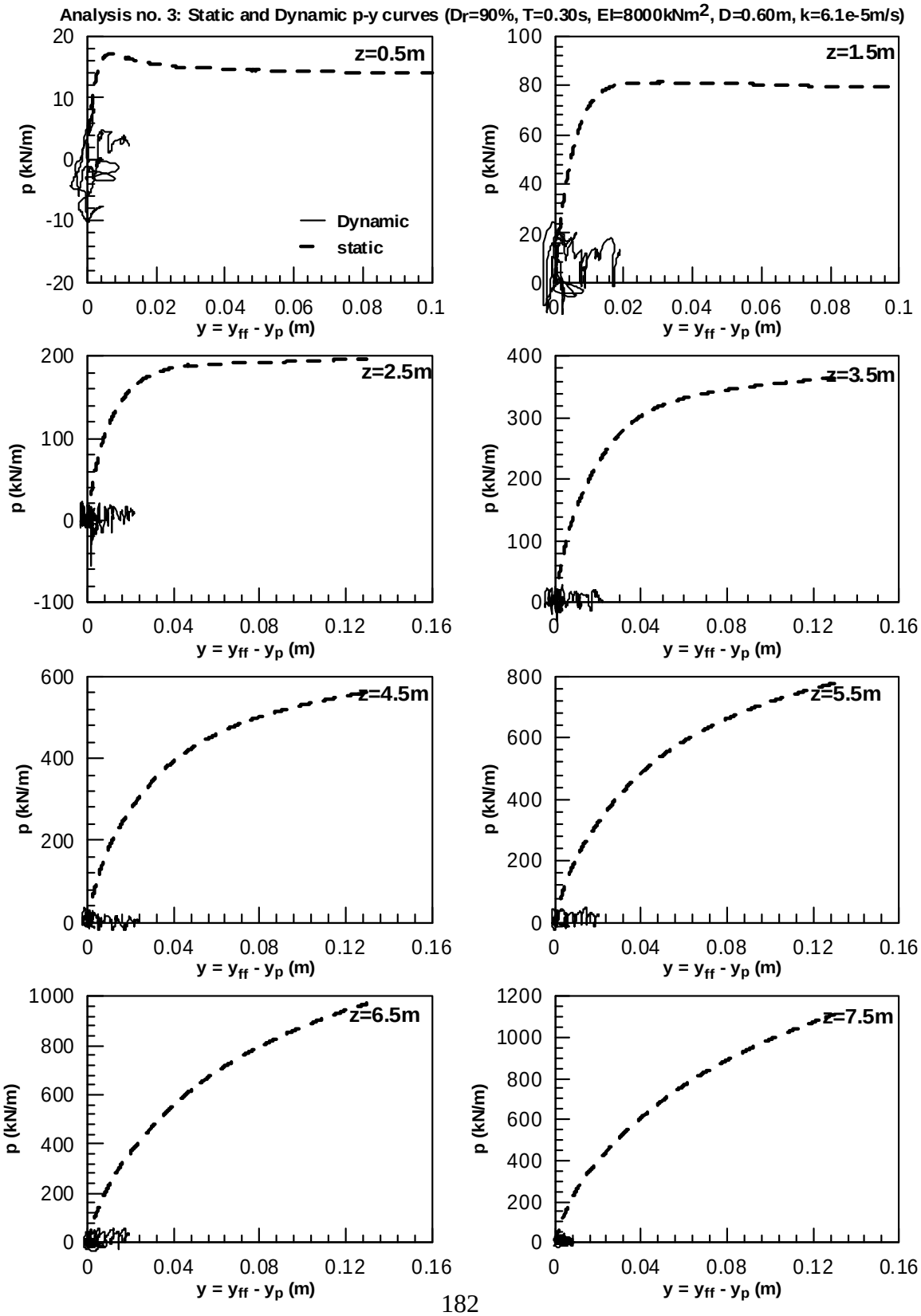
Analysis no. 3: Static and Dynamic p-y curves (Dr=90%, T=0.30s, EI=8000kNm2, D=0.60m, k=6.1e-5m/s)
z=0.5m
z=1.5m
z=2.5m
z=3.5m
z=4.5m
z=5.5m
z=6.5m
z=7.5m
Dynamic
static
p (kN/m)
y = yff - yp (m)

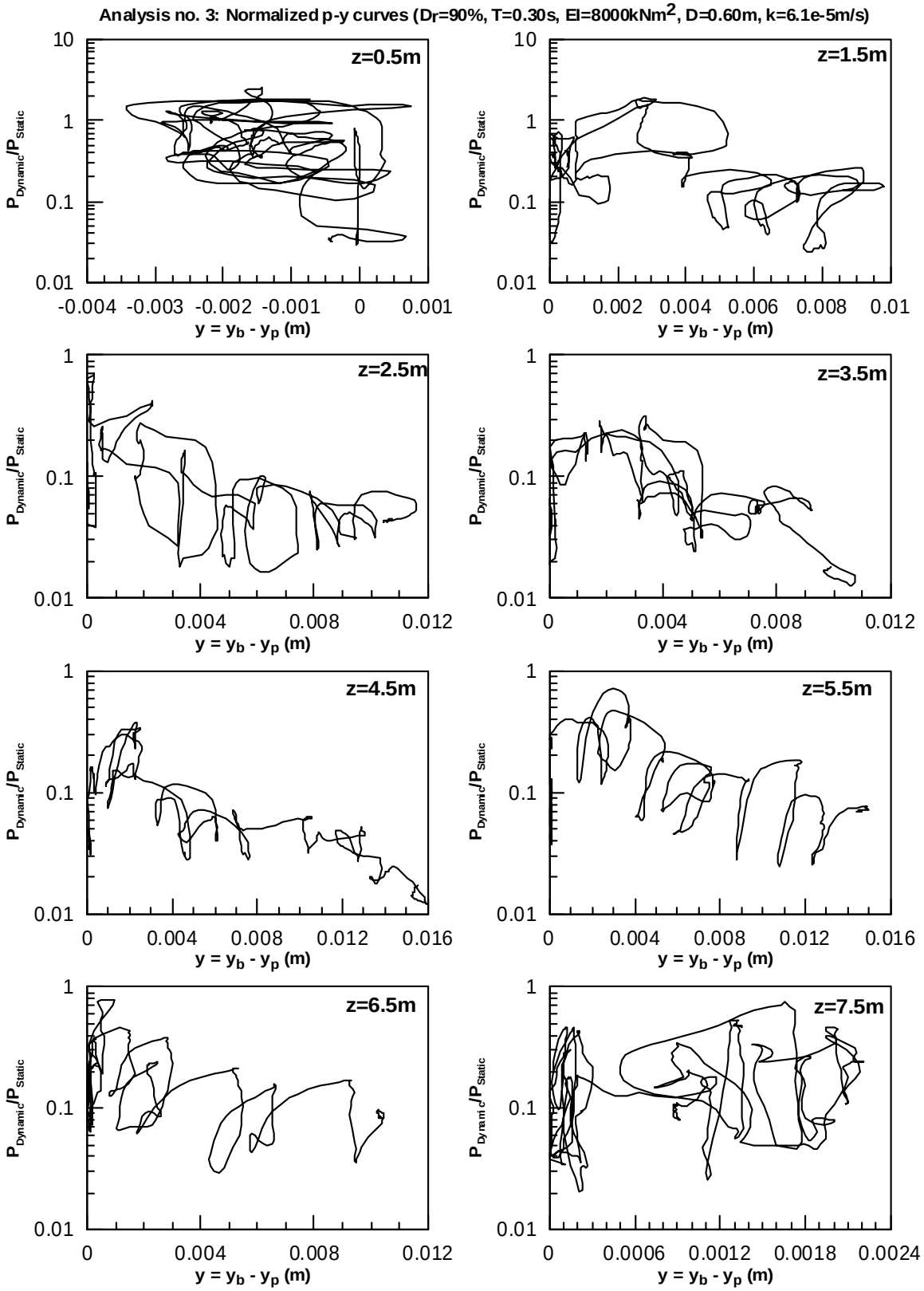
Analysis no. 3: Normalized p-y curves (Dr=90%, T=0.30s, EI=8000kNm2, D=0.60m, k=6.1e-5m/s)
z=0.5m
z=1.5m
z=2.5m
z=3.5m
z=4.5m
z=5.5m
z=6.5m
z=7.5m
P Dynamic/P Static
y = yb - yp (m)

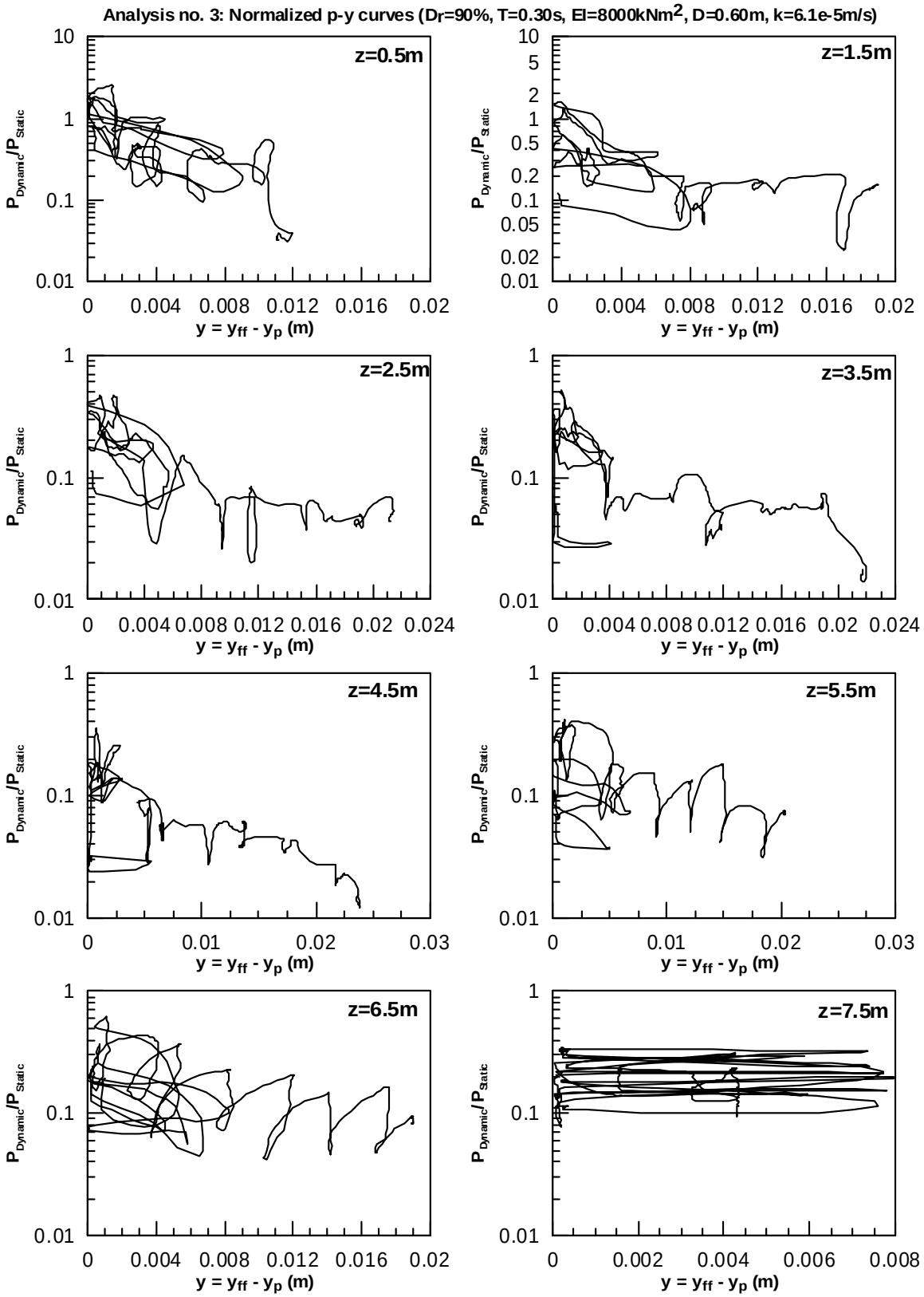
Analysis no. 3: Normalized p-y curves (Dr=90%, T=0.30s, EI=8000kNm2, D=0.60m, k=6.1e-5m/s)
z=0.5m
z=1.5m
z=2.5m
z=3.5m
z=4.5m
z=5.5m
z=6.5m
z=7.5m
P Dynamic/P Static
y = yff - yp (m)

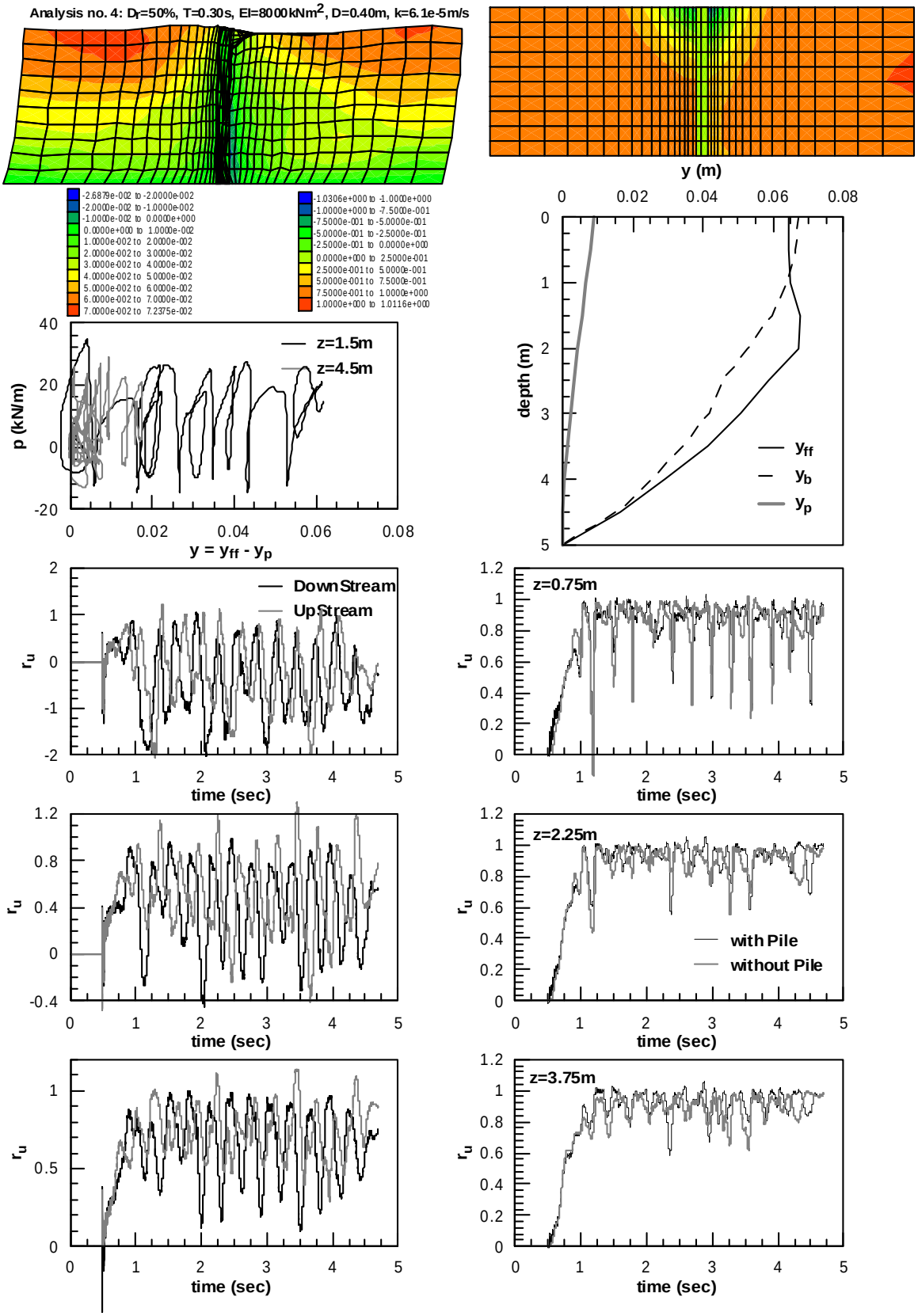
Analysis no. 4: Dr=50%, T=0.30s, EI=8000kNm2, D=0.40m, k=6.1e-5m/s
y (m)
depth (m)
yff
yb
yp
p (kN/m)
z=1.5m
z=4.5m
y = yff - yp
DownStream
UpStream
ru
time (sec)
z=0.75m
z=2.25m
with Pile
without Pile
z=3.75m

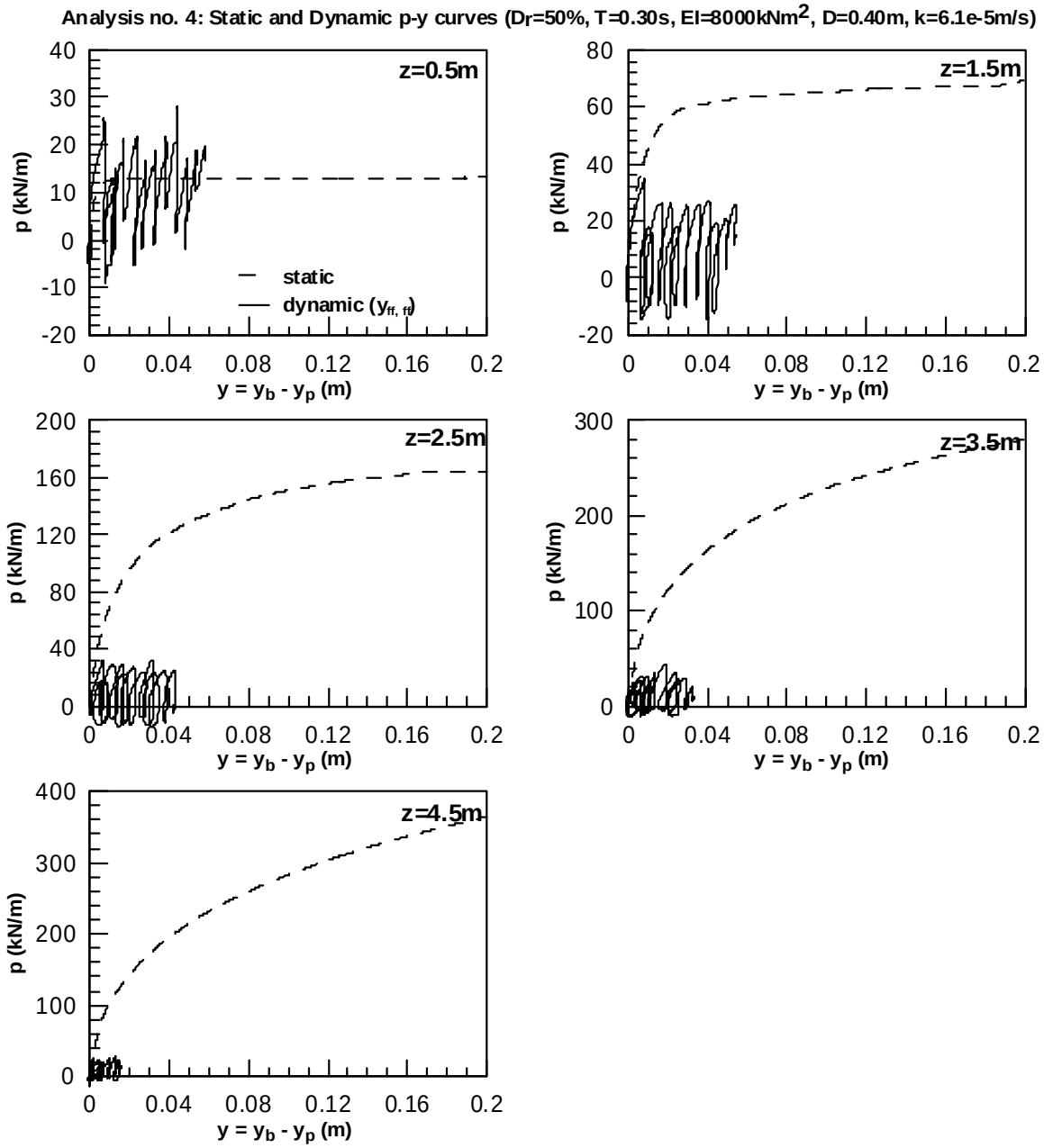
Analysis no. 4: Static and Dynamic p-y curves (Dr=50%, T=0.30s, EI=8000kNm2, D=0.40m, k=6.1e-5m/s)
z=0.5m
z=1.5m
z=2.5m
z=3.5m
z=4.5m
p (kN/m)
y = yb - yp (m)
static
dynamic (yff, ff)

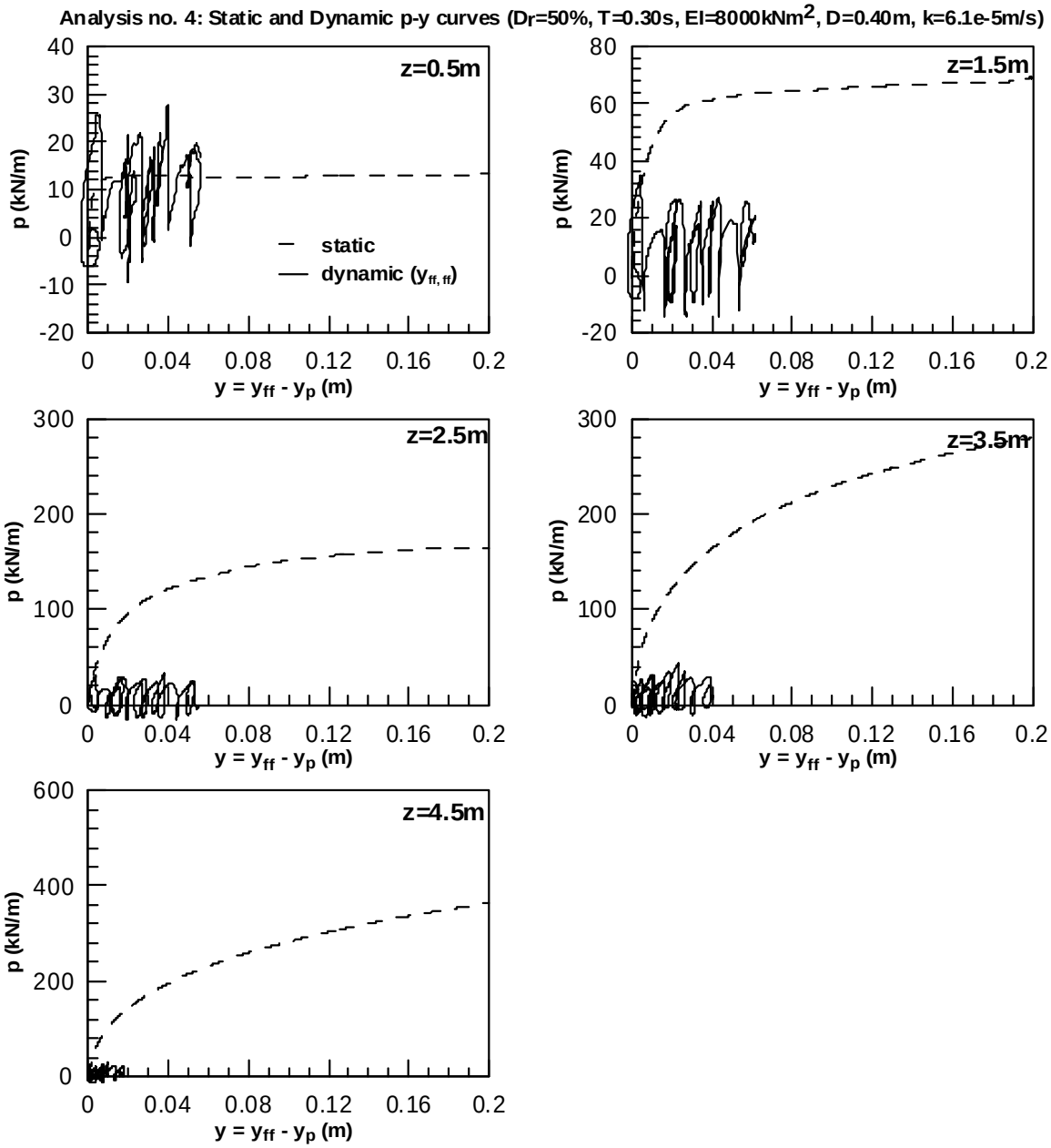
Analysis no. 4: Static and Dynamic p-y curves (Dr=50%, T=0.30s, EI=8000kNm2, D=0.40m, k=6.1e-5m/s)
z=0.5m
z=1.5m
z=2.5m
z=3.5m
z=4.5m
p (kN/m)
y = yff - yp (m)
static
dynamic (yff, ff)

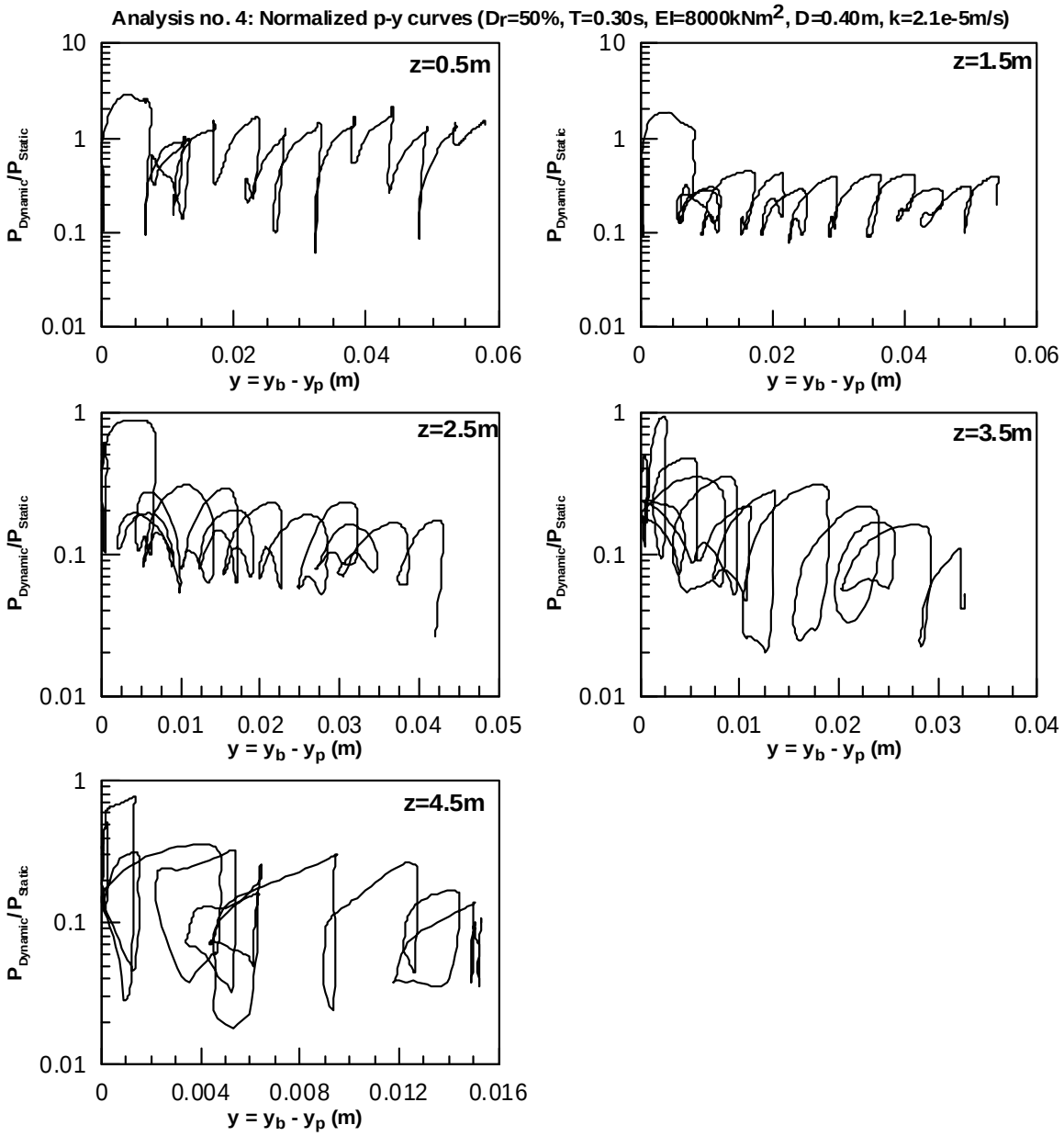
Analysis no. 4: Normalized p-y curves (Dr=50%, T=0.30s, EI=8000kNm2, D=0.40m, k=2.1e-5m/s)
z=0.5m
z=1.5m
z=2.5m
z=3.5m
z=4.5m
P Dynamic/P Static
y = yb - yp (m)

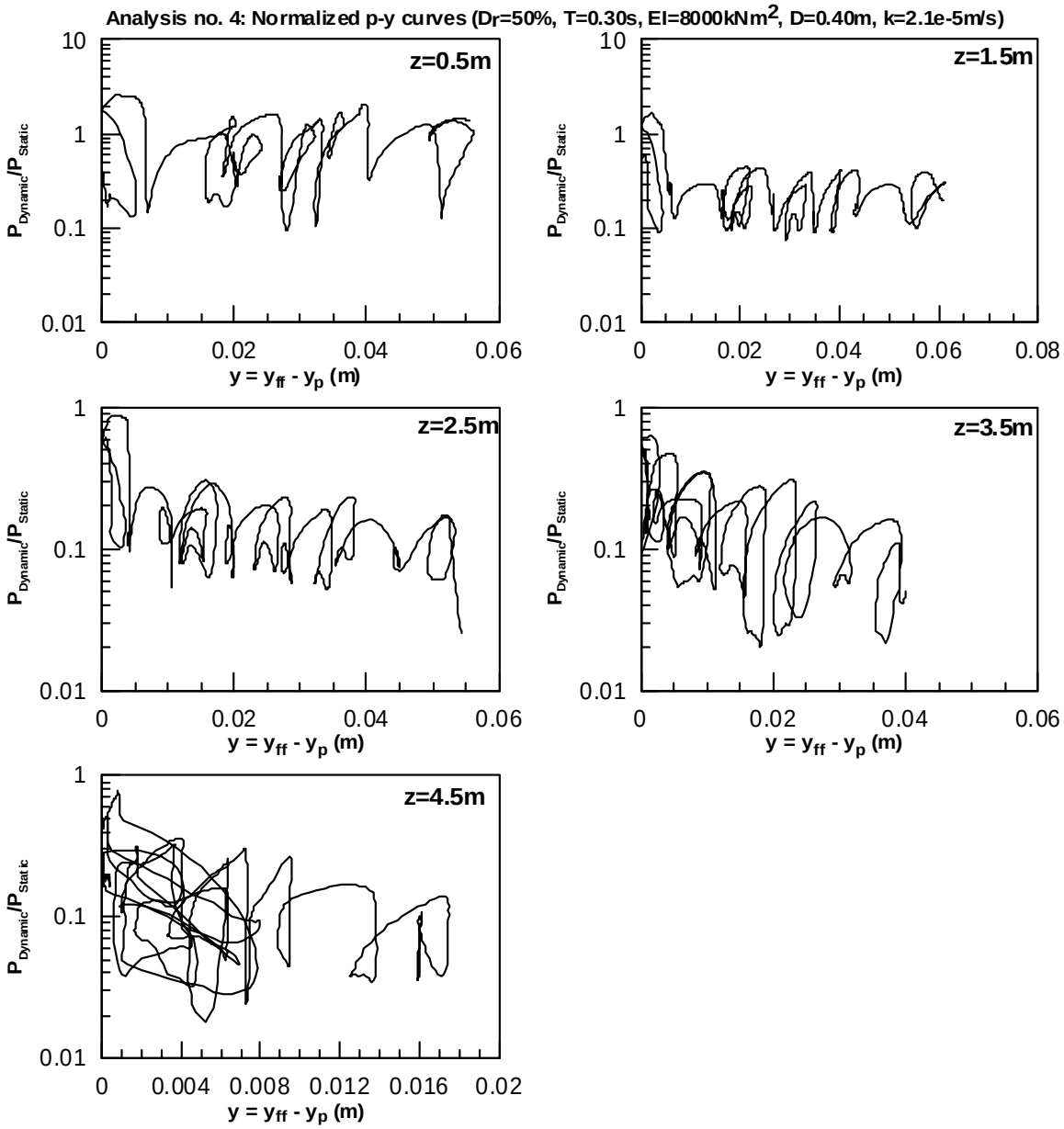
Analysis no. 4: Normalized p-y curves (Dr=50%, T=0.30s, EI=8000kNm2, D=0.40m, k=2.1e-5m/s)
z=0.5m
z=1.5m
z=2.5m
z=3.5m
z=4.5m
P_Dynamic/P_Static
y = y_ff - y_p (m)

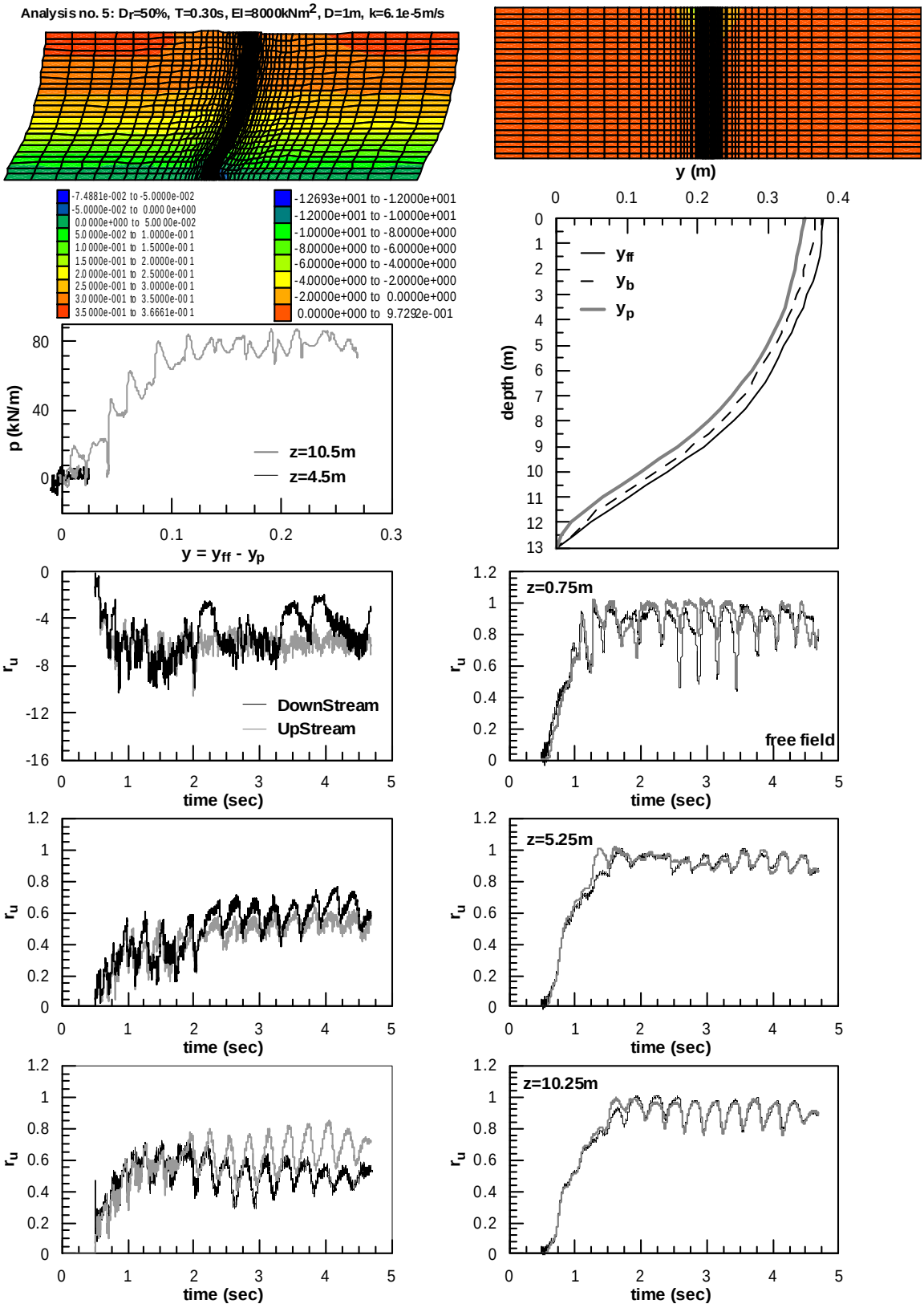
Analysis no. 5: D_r=50%, T=0.30s, EI=8000kNm^2, D=1m, k=6.1e-5m/s
y (m)
depth (m)
y_{ff}
y_b
y_p
p (kN/m)
z=10.5m
z=4.5m
y = y_{ff} - y_p
r_u
DownStream
UpStream
time (sec)
z=0.75m
free field
z=5.25m
z=10.25m

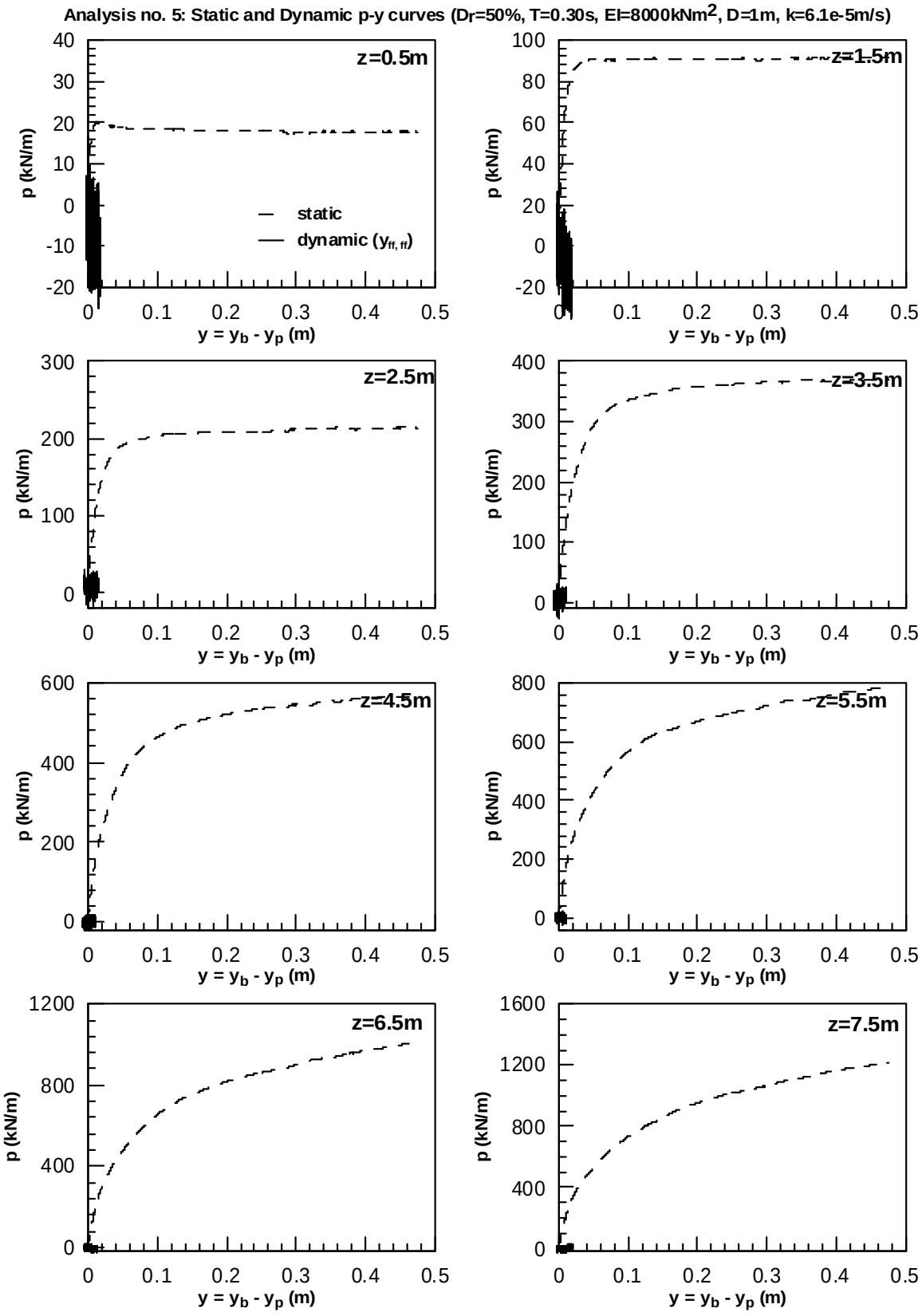
Analysis no. 5: Static and Dynamic p-y curves (Dr=50%, T=0.30s, EI=8000kNm2, D=1m, k=6.1e-5m/s)
z=0.5m
z=1.5m
z=2.5m
z=3.5m
z=4.5m
z=5.5m
z=6.5m
z=7.5m
static
dynamic (yff, ff)
p (kN/m)
y = yb - yp (m)

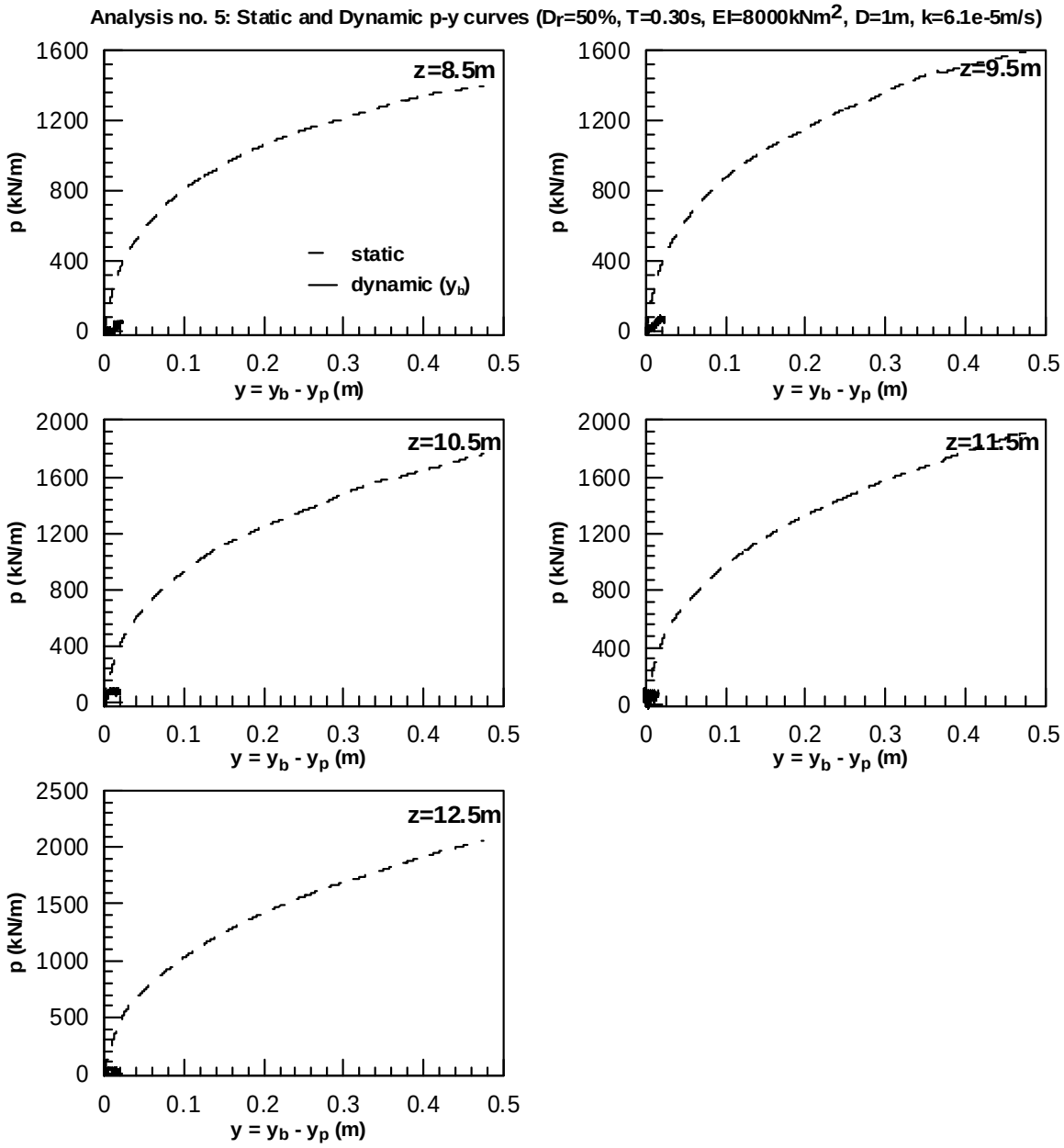
Analysis no. 5: Static and Dynamic p-y curves (Dr=50%, T=0.30s, EI=8000kNm2, D=1m, k=6.1e-5m/s)
z=8.5m
z=9.5m
z=10.5m
z=11.5m
z=12.5m
static
dynamic (yb)
p (kN/m)
y = yb - yp (m)

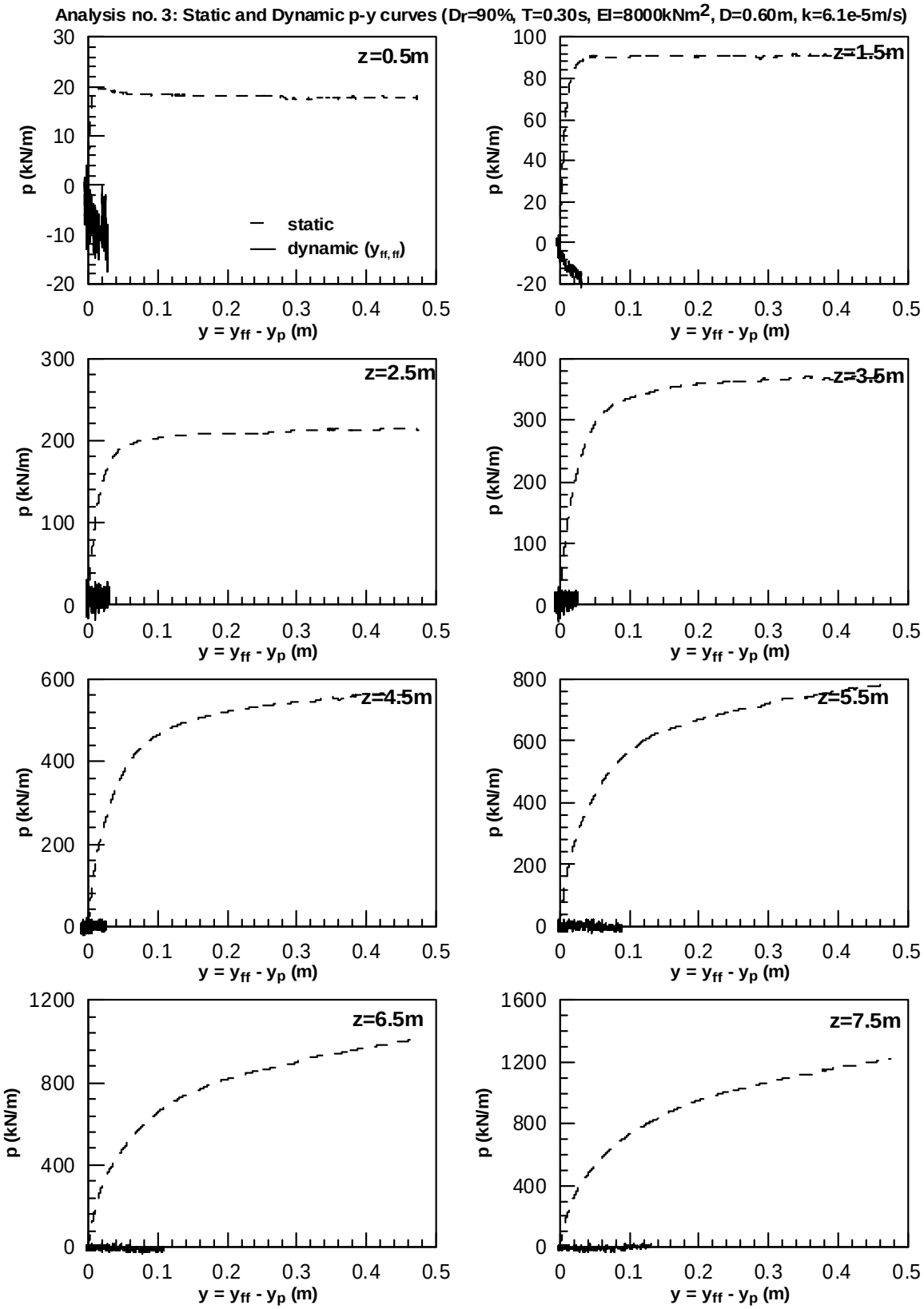
Analysis no. 3: Static and Dynamic p-y curves (Dr=90%, T=0.30s, EI=8000kNm2, D=0.60m, k=6.1e-5m/s)
z=0.5m
z=1.5m
z=2.5m
z=3.5m
z=4.5m
z=5.5m
z=6.5m
z=7.5m
static
dynamic (yff, ff)
p (kN/m)
y = yff - yp (m)

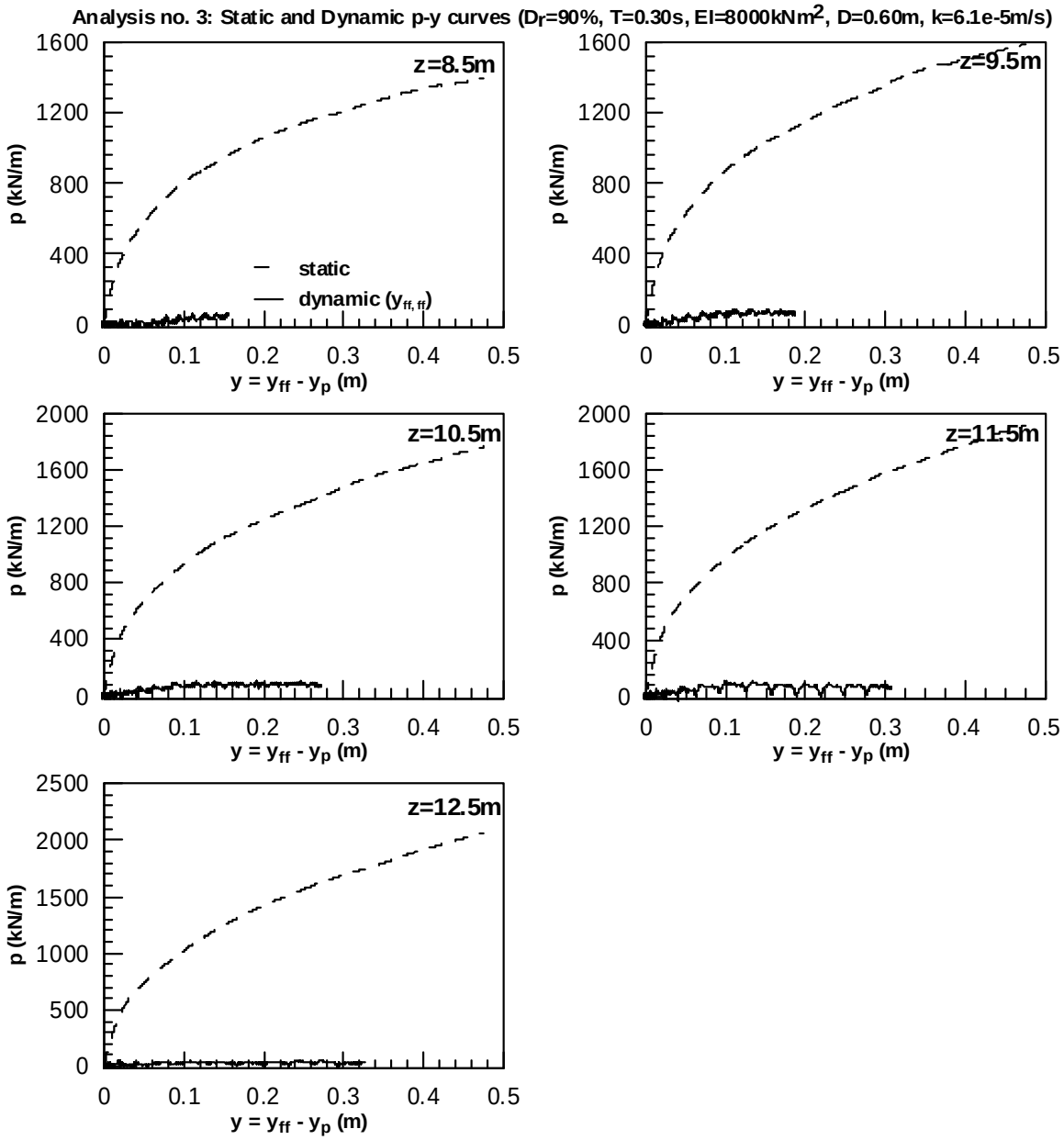
Analysis no. 3: Static and Dynamic p-y curves (D_r=90%, T=0.30s, EI=8000kNm^2, D=0.60m, k=6.1e-5m/s)
z=8.5m
z=9.5m
z=10.5m
z=11.5m
z=12.5m
static
dynamic ($y_{ff,ff}$)
p (kN/m)
y = y_{ff} - y_p (m)

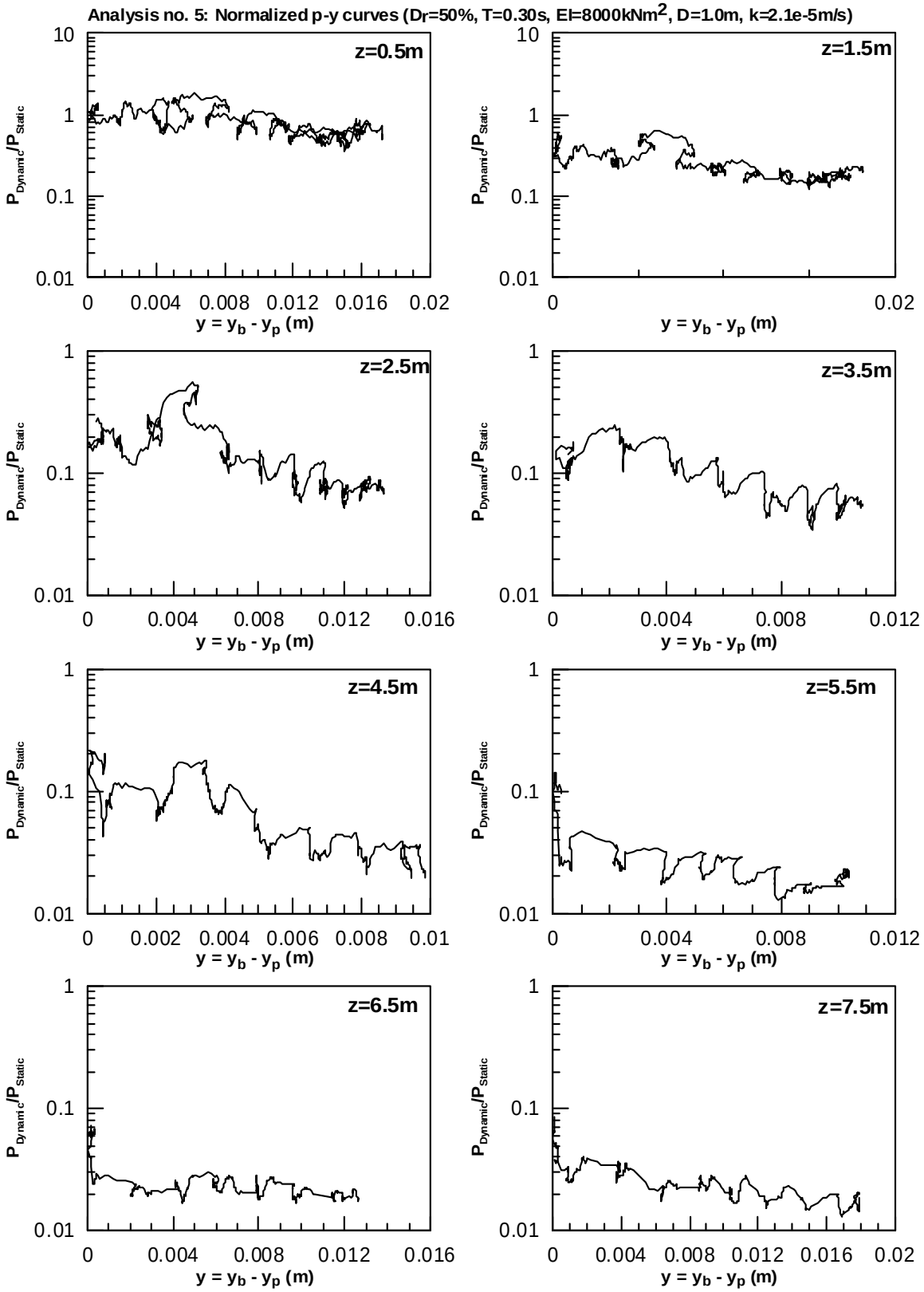
Analysis no. 5: Normalized p-y curves (Dr=50%, T=0.30s, EI=8000kNm2, D=1.0m, k=2.1e-5m/s)
z=0.5m
z=1.5m
z=2.5m
z=3.5m
z=4.5m
z=5.5m
z=6.5m
z=7.5m
P_Dynamic/P_Static
y = y_b - y_p (m)

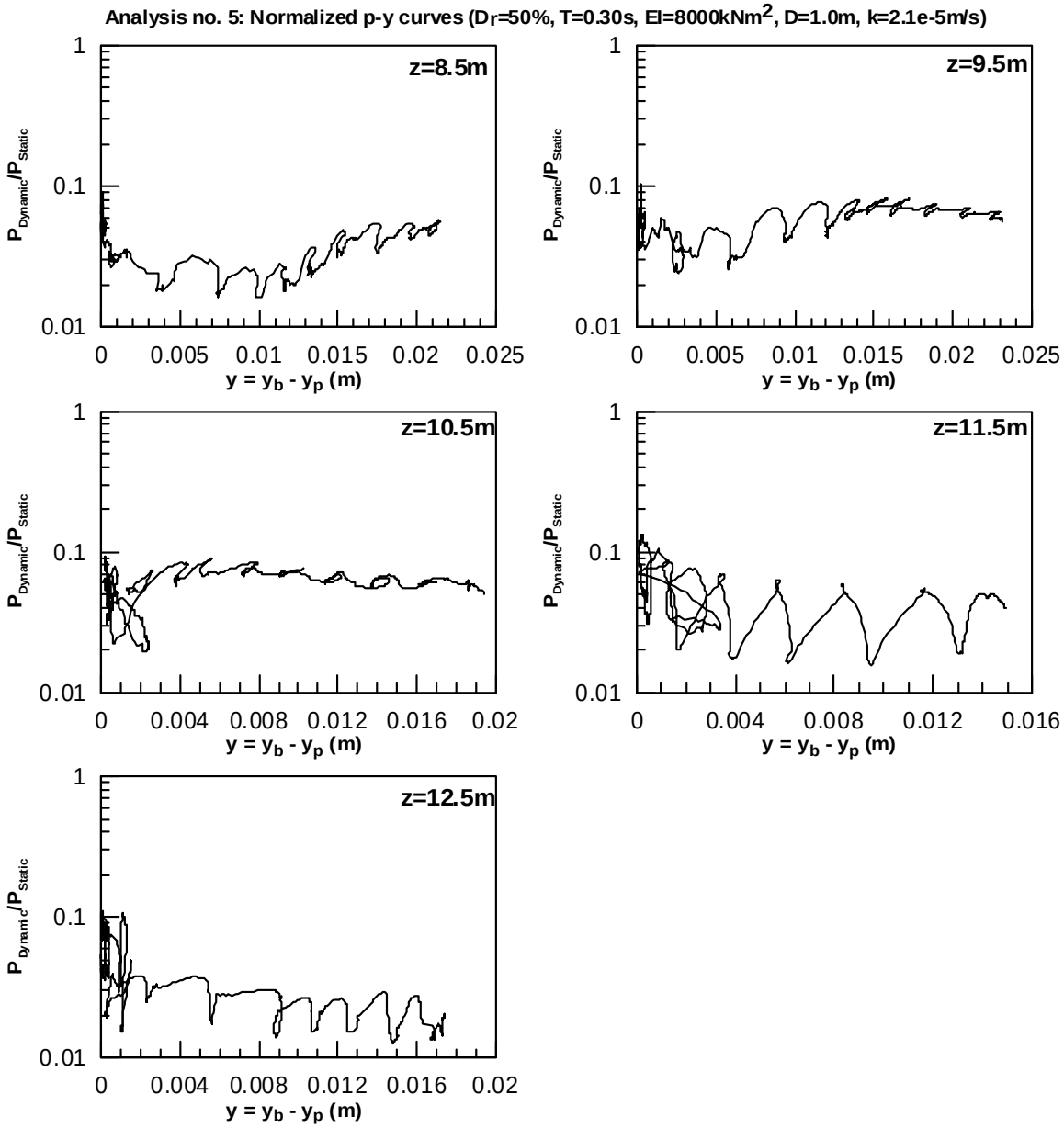
Analysis no. 5: Normalized p-y curves (Dr=50%, T=0.30s, EI=8000kNm2, D=1.0m, k=2.1e-5m/s)
z=8.5m
z=9.5m
z=10.5m
z=11.5m
z=12.5m
P Dynamic/P Static
y = yb - yp (m)
1
0.1
0.01
0
0.005
0.01
0.015
0.02
0.025
0.004
0.008
0.012
0.016

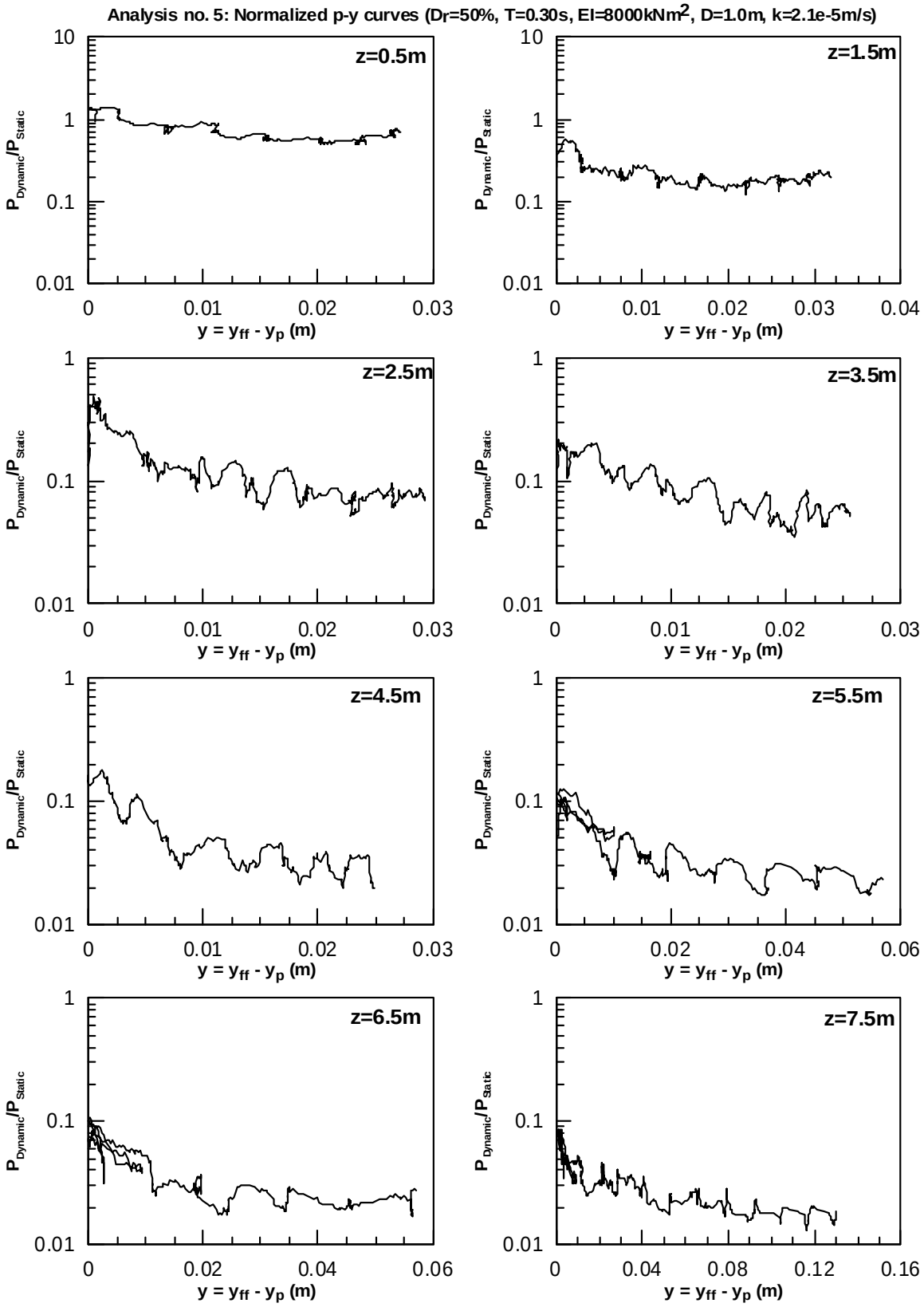
Analysis no. 5: Normalized p-y curves (Dr=50%, T=0.30s, EI=8000kNm2, D=1.0m, k=2.1e-5m/s)
z=0.5m
z=1.5m
z=2.5m
z=3.5m
z=4.5m
z=5.5m
z=6.5m
z=7.5m
P Dynamic/P Static
y = yff - yp (m)

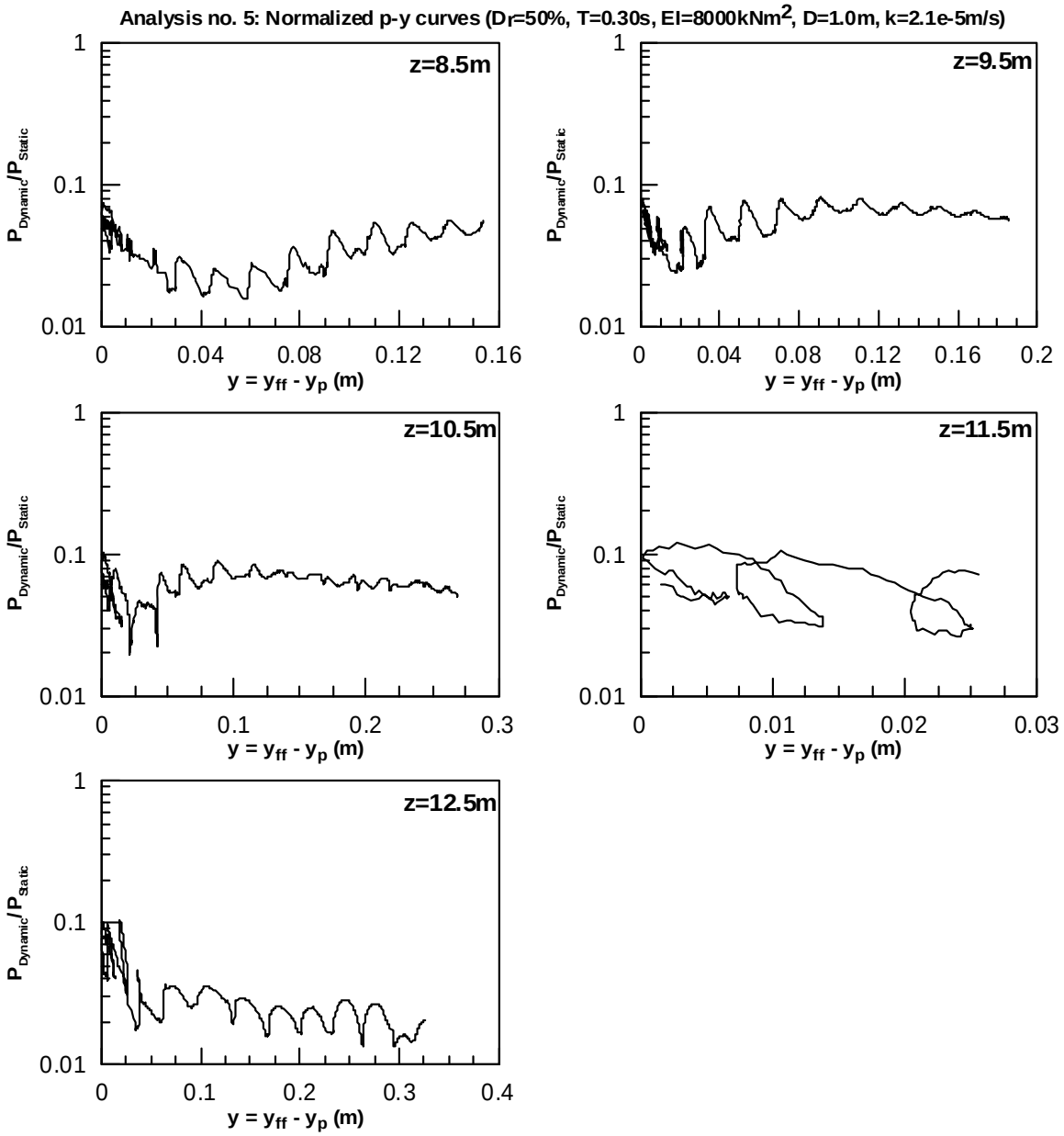
Analysis no. 5: Normalized p-y curves (Dr=50%, T=0.30s, EI=8000kNm2, D=1.0m, k=2.1e-5m/s)
z=8.5m
z=9.5m
z=10.5m
z=11.5m
z=12.5m
P_Dynamic/P_Static
y = y_ff - y_p (m)
1
0.1
0.01
0
0.04
0.08
0.12
0.16
0.2
0.3
0.4
0.01
0.02
0.03

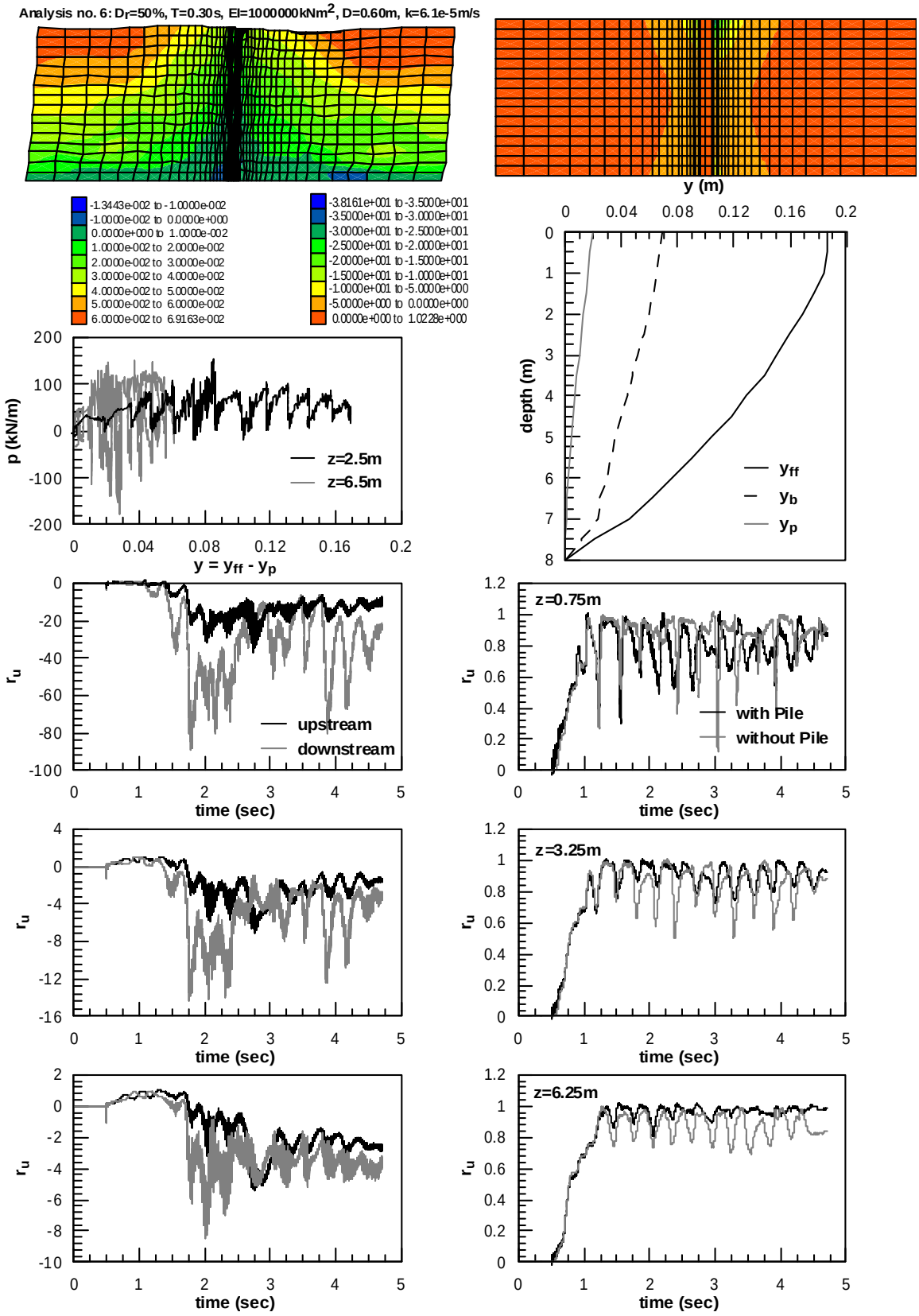
Analysis no. 6: D_r=50%, T=0.30s, EI=1000000kNm^2, D=0.60m, k=6.1e-5m/s
-1.3443e-002 to -1.0000e-002
-1.0000e-002 to 0.0000e+000
0.0000e+000 to 1.0000e-002
1.0000e-002 to 2.0000e-002
2.0000e-002 to 3.0000e-002
3.0000e-002 to 4.0000e-002
4.0000e-002 to 5.0000e-002
5.0000e-002 to 6.0000e-002
6.0000e-002 to 6.9163e-002
-3.8161e+001 to -3.5000e+001
-3.5000e+001 to -3.0000e+001
-3.0000e+001 to -2.5000e+001
-2.5000e+001 to -2.0000e+001
-2.0000e+001 to -1.5000e+001
-1.5000e+001 to -1.0000e+001
-1.0000e+001 to -5.0000e+000
-5.0000e+000 to 0.0000e+000
0.0000e+000 to 1.0228e+000
y (m)
depth (m)
y_{ff}
y_b
y_p
p (kN/m)
z=2.5m
z=6.5m
y = y_{ff} - y_p
r_u
upstream
downstream
z=0.75m
with Pile
without Pile
z=3.25m
z=6.25m
time (sec)

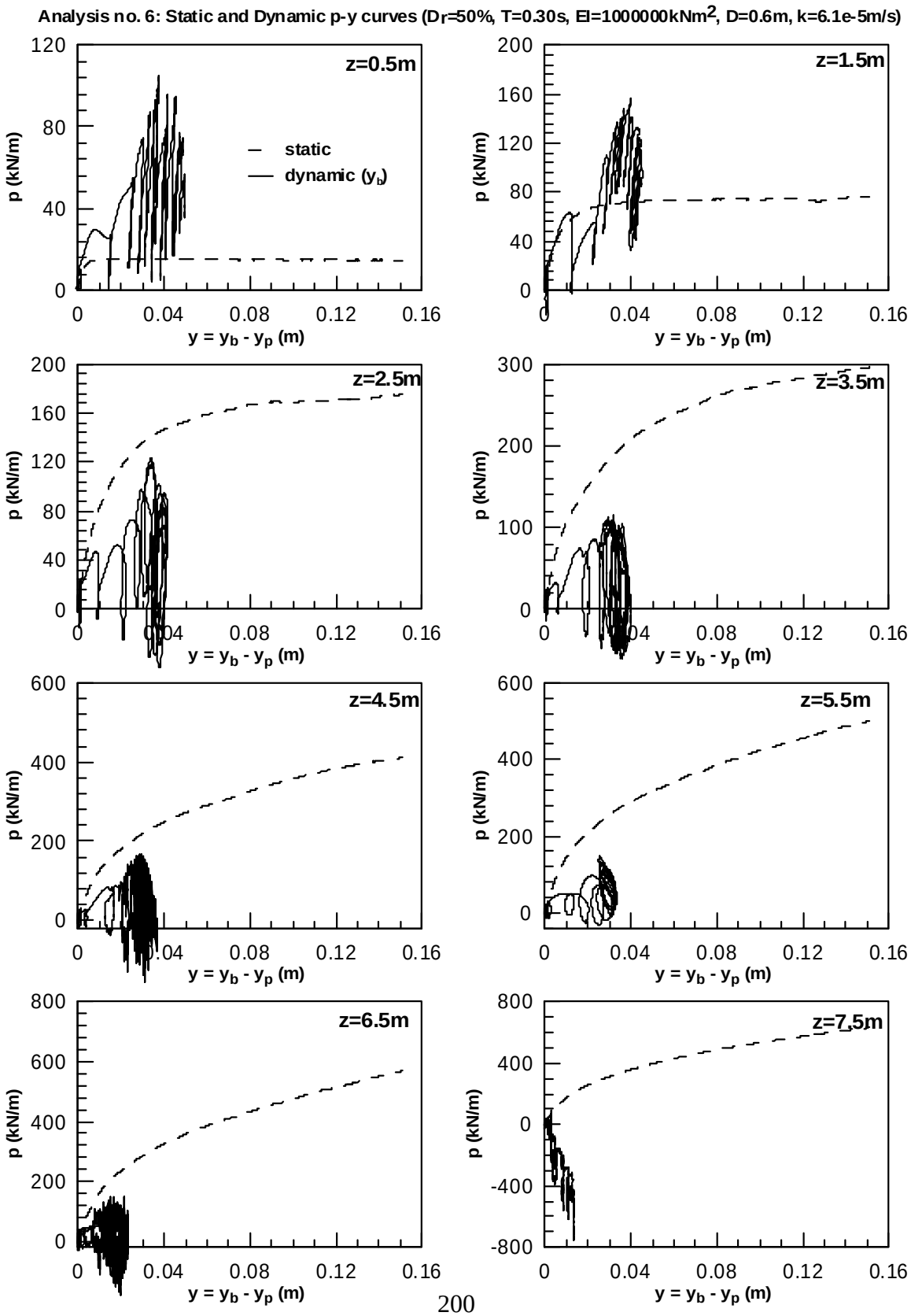
Analysis no. 6: Static and Dynamic p-y curves (Dr=50%, T=0.30s, EI=1000000kNm2, D=0.6m, k=6.1e-5m/s)
z=0.5m
z=1.5m
z=2.5m
z=3.5m
z=4.5m
z=5.5m
z=6.5m
z=7.5m
static
dynamic (yb)
p (kN/m)
y = yb - yp (m)

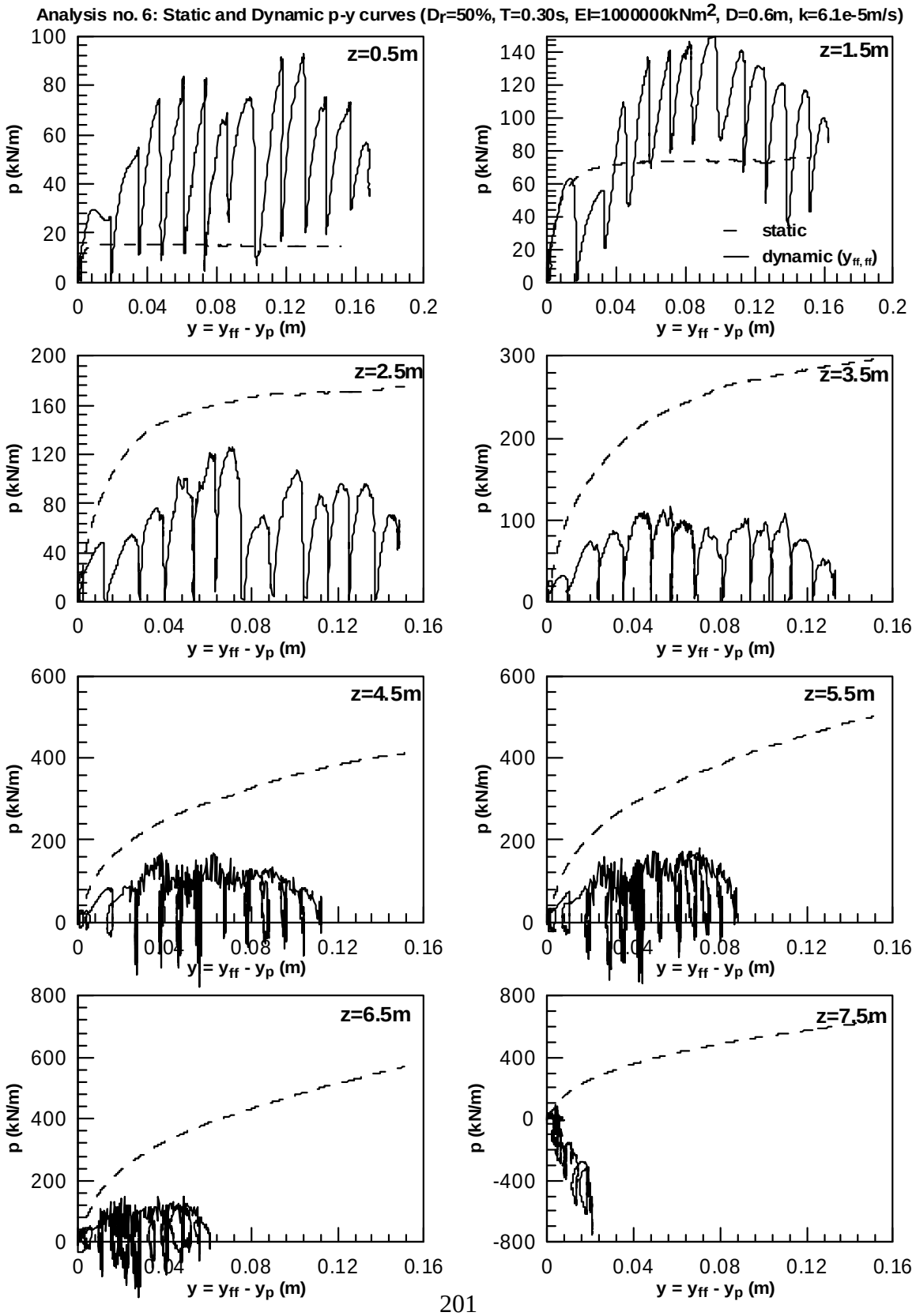
Analysis no. 6: Static and Dynamic p-y curves (Dr=50%, T=0.30s, EI=1000000kNm2, D=0.6m, k=6.1e-5m/s)
z=0.5m
z=1.5m
z=2.5m
z=3.5m
z=4.5m
z=5.5m
z=6.5m
z=7.5m
p (kN/m)
y = yff - yp (m)
static
dynamic (yff, ff)

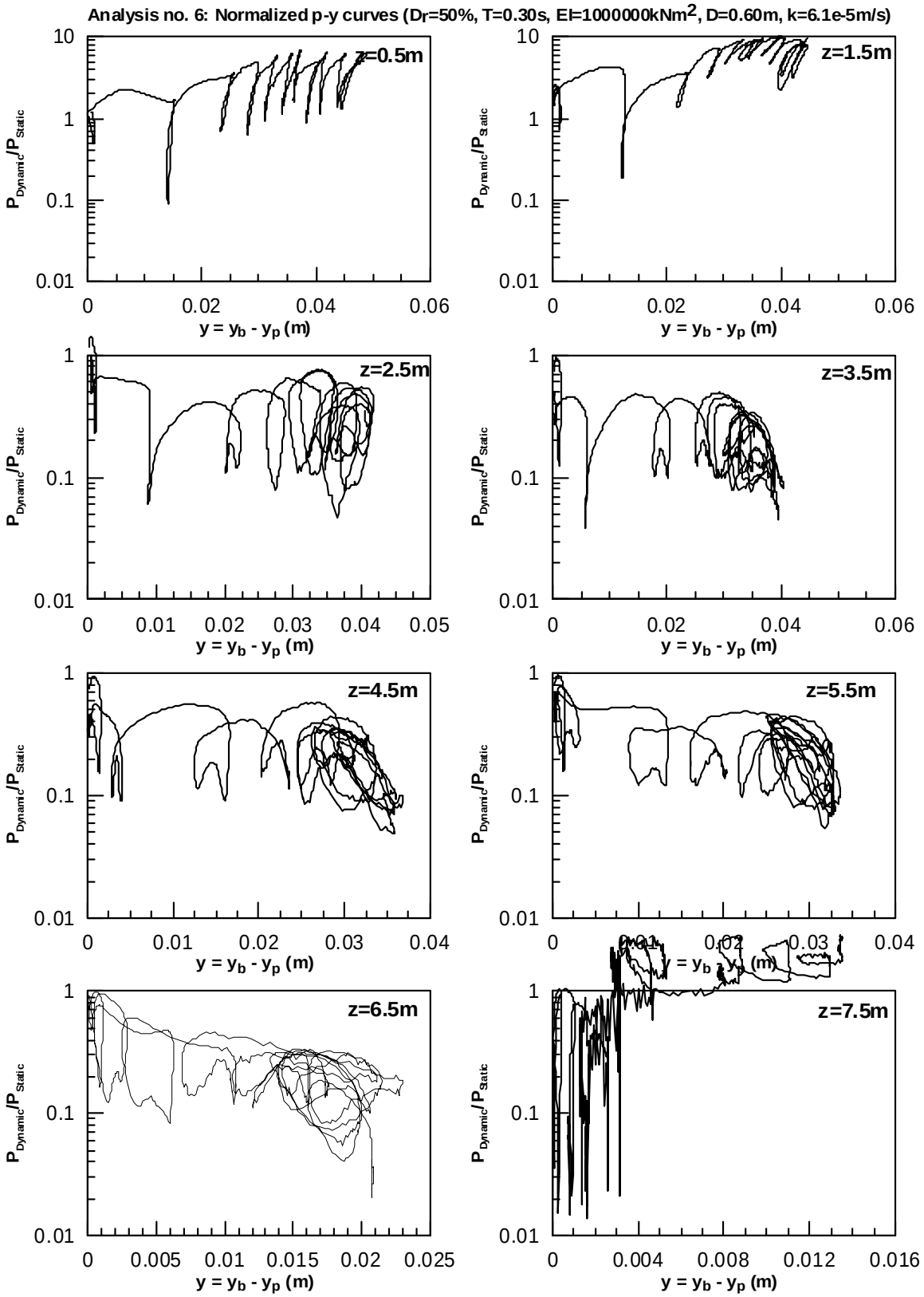
Analysis no. 6: Normalized p-y curves (Dr=50%, T=0.30s, EI=1000000kNm2, D=0.60m, k=6.1e-5m/s)
z=0.5m
z=1.5m
z=2.5m
z=3.5m
z=4.5m
z=5.5m
z=6.5m
z=7.5m
P Dynamic/P Static
y = yb - yp (m)

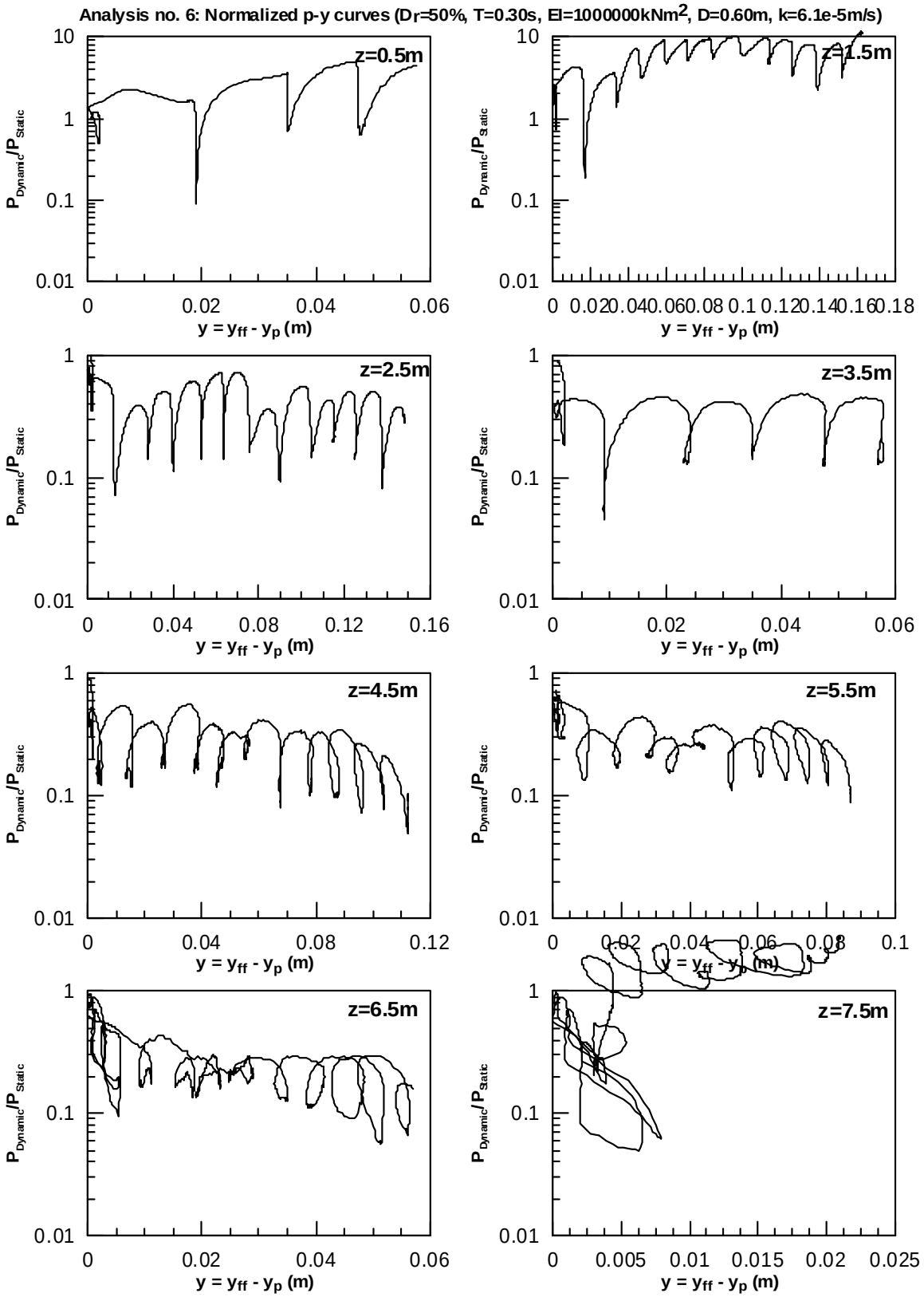
Analysis no. 6: Normalized p-y curves (Dr=50%, T=0.30s, EI=1000000kNm2, D=0.60m, k=6.1e-5m/s)
z=0.5m
z=1.5m
z=2.5m
z=3.5m
z=4.5m
z=5.5m
z=6.5m
z=7.5m
P Dynamic/P Static
y = yff - yp (m)

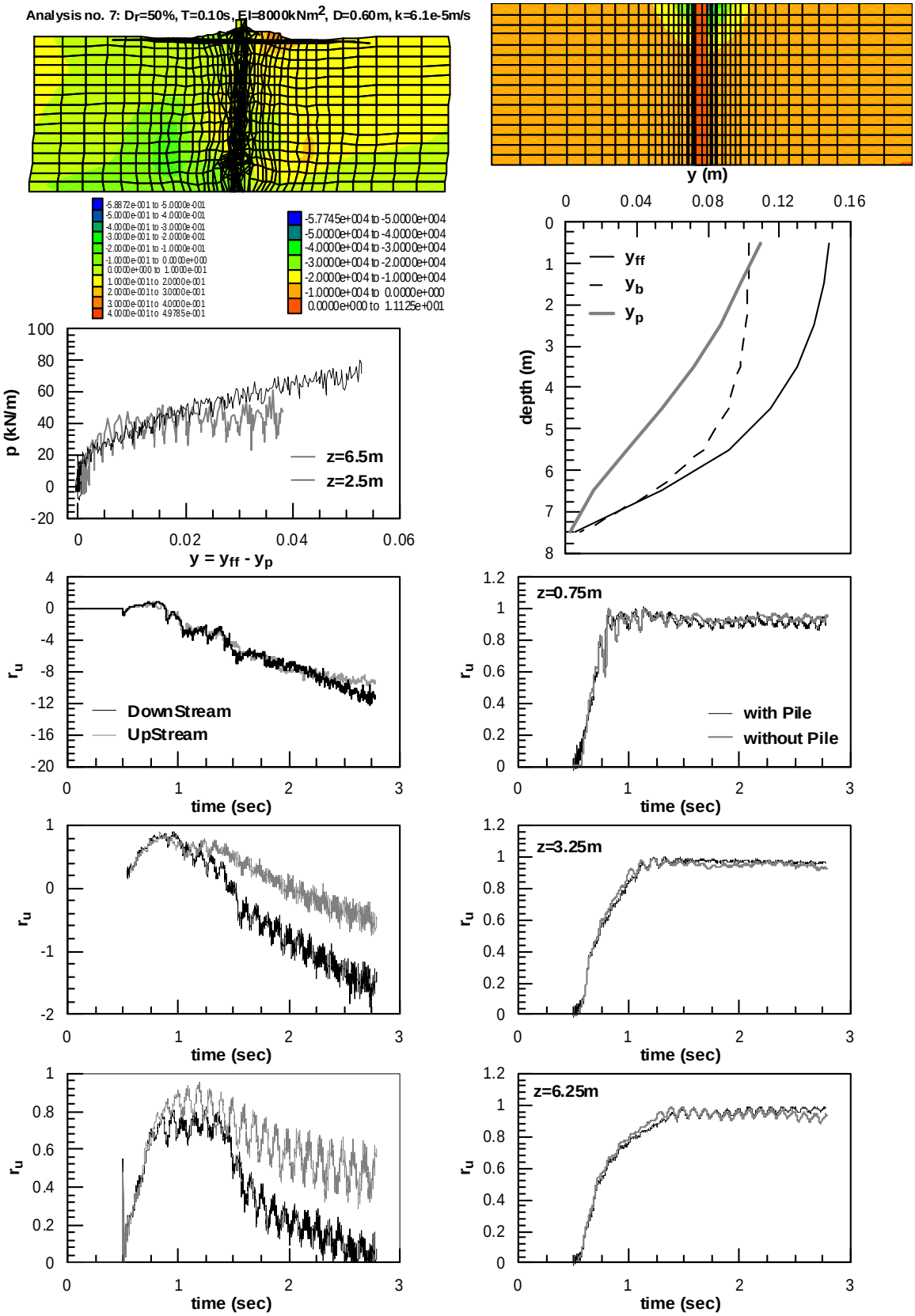
Analysis no. 7: D_r=50%, T=0.10s, EI=8000kNm^2, D=0.60m, k=6.1e-5m/s
-5.8872e-001 to -5.0000e-001
-5.0000e-001 to -4.0000e-001
-4.0000e-001 to -3.0000e-001
-3.0000e-001 to -2.0000e-001
-2.0000e-001 to -1.0000e-001
-1.0000e-001 to 0.0000e+000
0.0000e+000 to 1.0000e-001
1.0000e-001 to 2.0000e-001
2.0000e-001 to 3.0000e-001
3.0000e-001 to 4.0000e-001
4.0000e-001 to 4.9785e-001
-5.7745e+004 to -5.0000e+004
-5.0000e+004 to -4.0000e+004
-4.0000e+004 to -3.0000e+004
-3.0000e+004 to -2.0000e+004
-2.0000e+004 to -1.0000e+004
-1.0000e+004 to 0.0000e+000
0.0000e+000 to 1.1125e+001
y (m)
depth (m)
y_{ff}
y_b
y_p
p (kN/m)
z=6.5m
z=2.5m
y = y_{ff} - y_p
r_u
DownStream
UpStream
time (sec)
z=0.75m
with Pile
without Pile
z=3.25m
z=6.25m

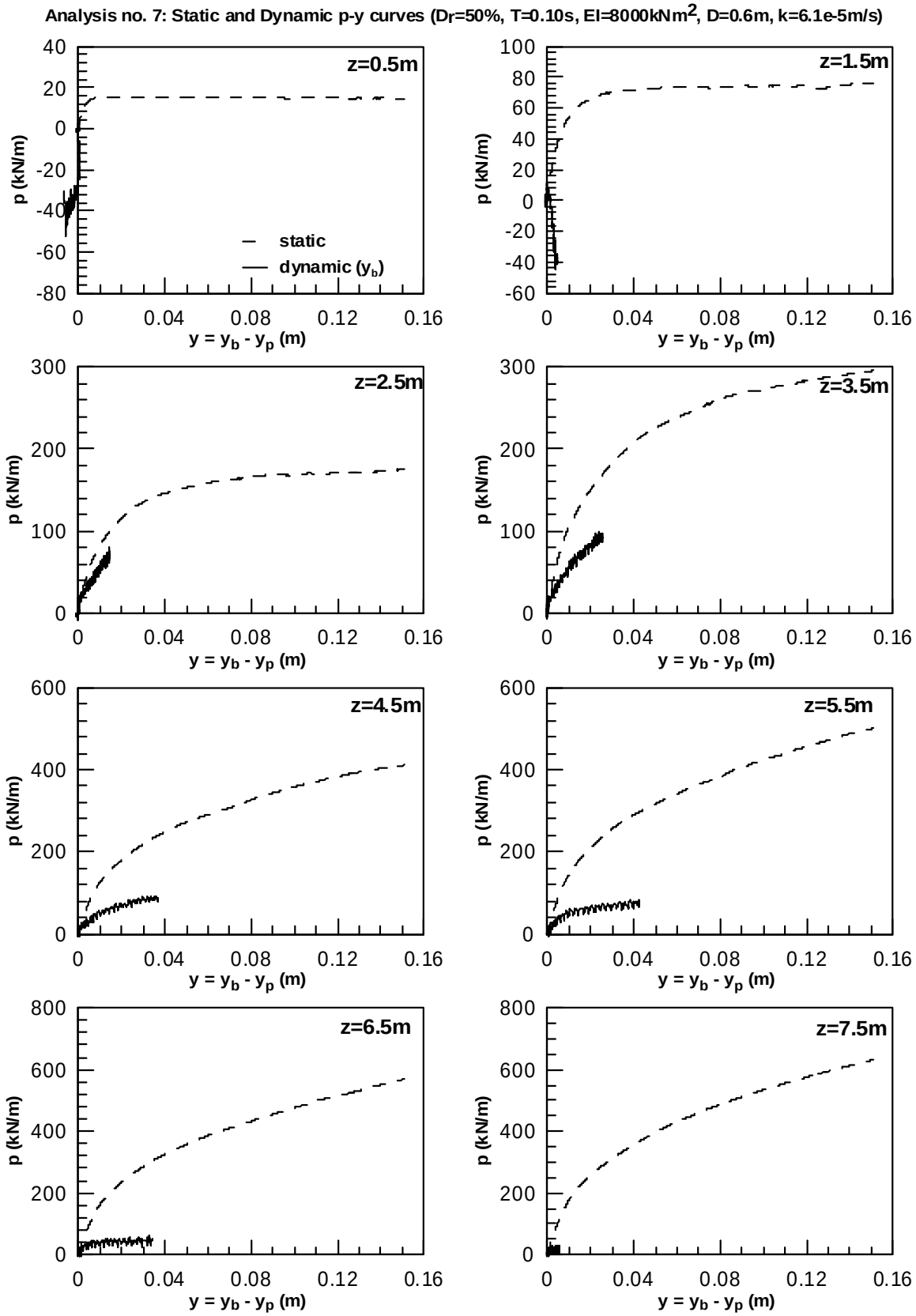
Analysis no. 7: Static and Dynamic p-y curves (Dr=50%, T=0.10s, EI=8000kNm2, D=0.6m, k=6.1e-5m/s)
z=0.5m
z=1.5m
z=2.5m
z=3.5m
z=4.5m
z=5.5m
z=6.5m
z=7.5m
static
dynamic (yb)
p (kN/m)
y = yb - yp (m)

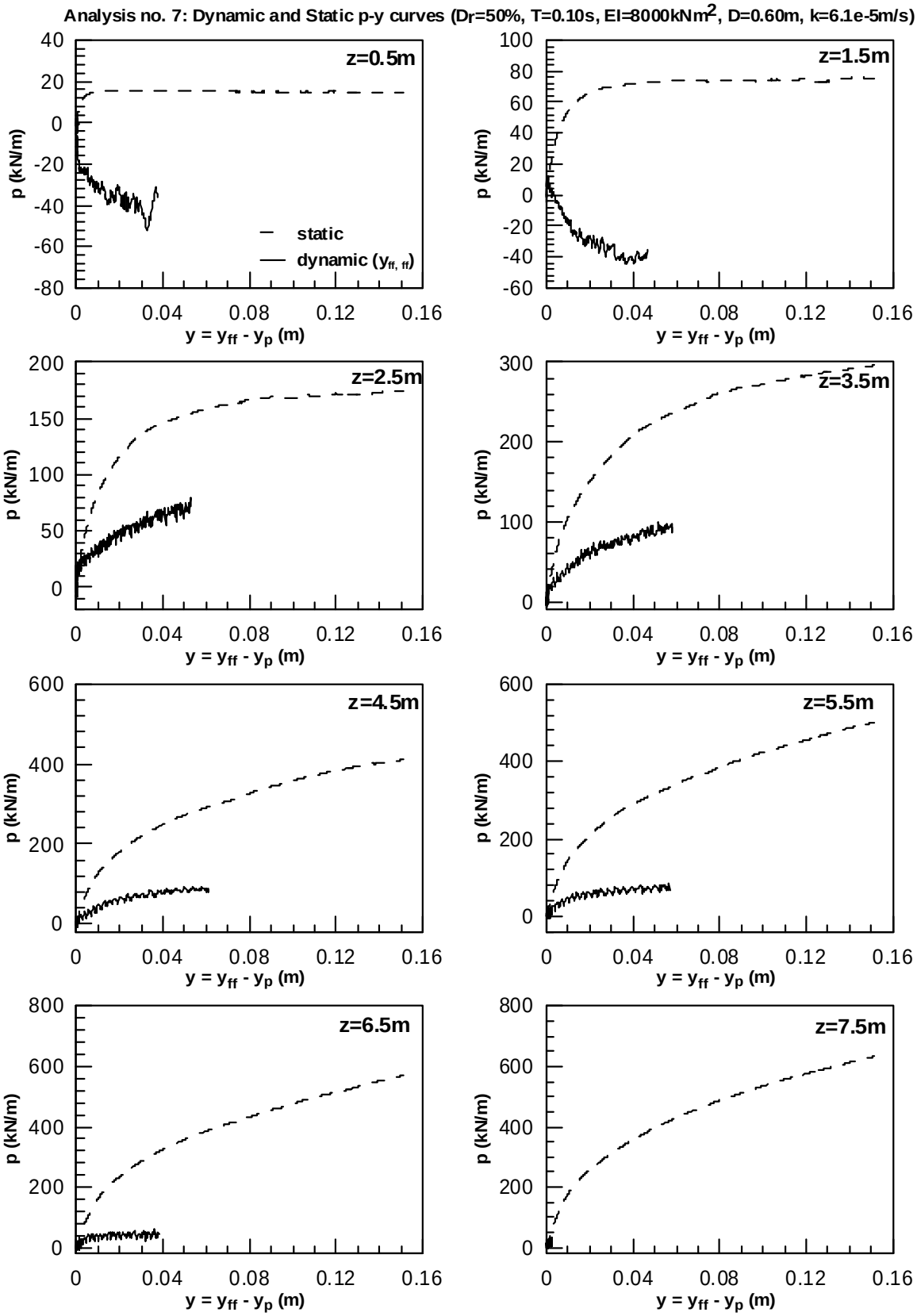
Analysis no. 7: Dynamic and Static p-y curves (Dr=50%, T=0.10s, EI=8000kNm2, D=0.60m, k=6.1e-5m/s)
z=0.5m
z=1.5m
z=2.5m
z=3.5m
z=4.5m
z=5.5m
z=6.5m
z=7.5m
static
dynamic (yff, ff)
p (kN/m)
y = yff - yp (m)

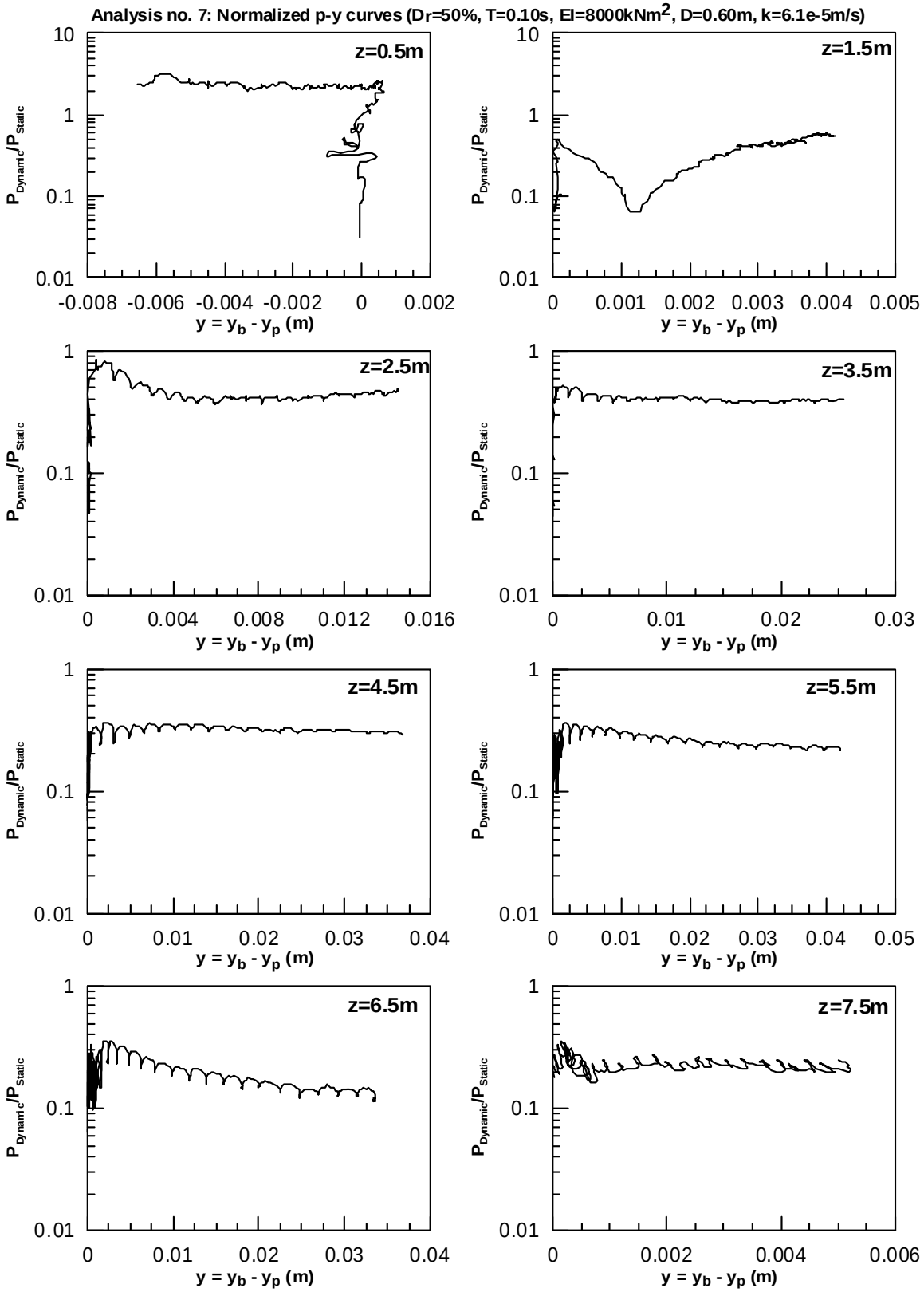
Analysis no. 7: Normalized p-y curves (Dr=50%, T=0.10s, EI=8000kNm2, D=0.60m, k=6.1e-5m/s)
z=0.5m
z=1.5m
z=2.5m
z=3.5m
z=4.5m
z=5.5m
z=6.5m
z=7.5m
P_Dynamic/P_Static
y = y_b - y_p (m)

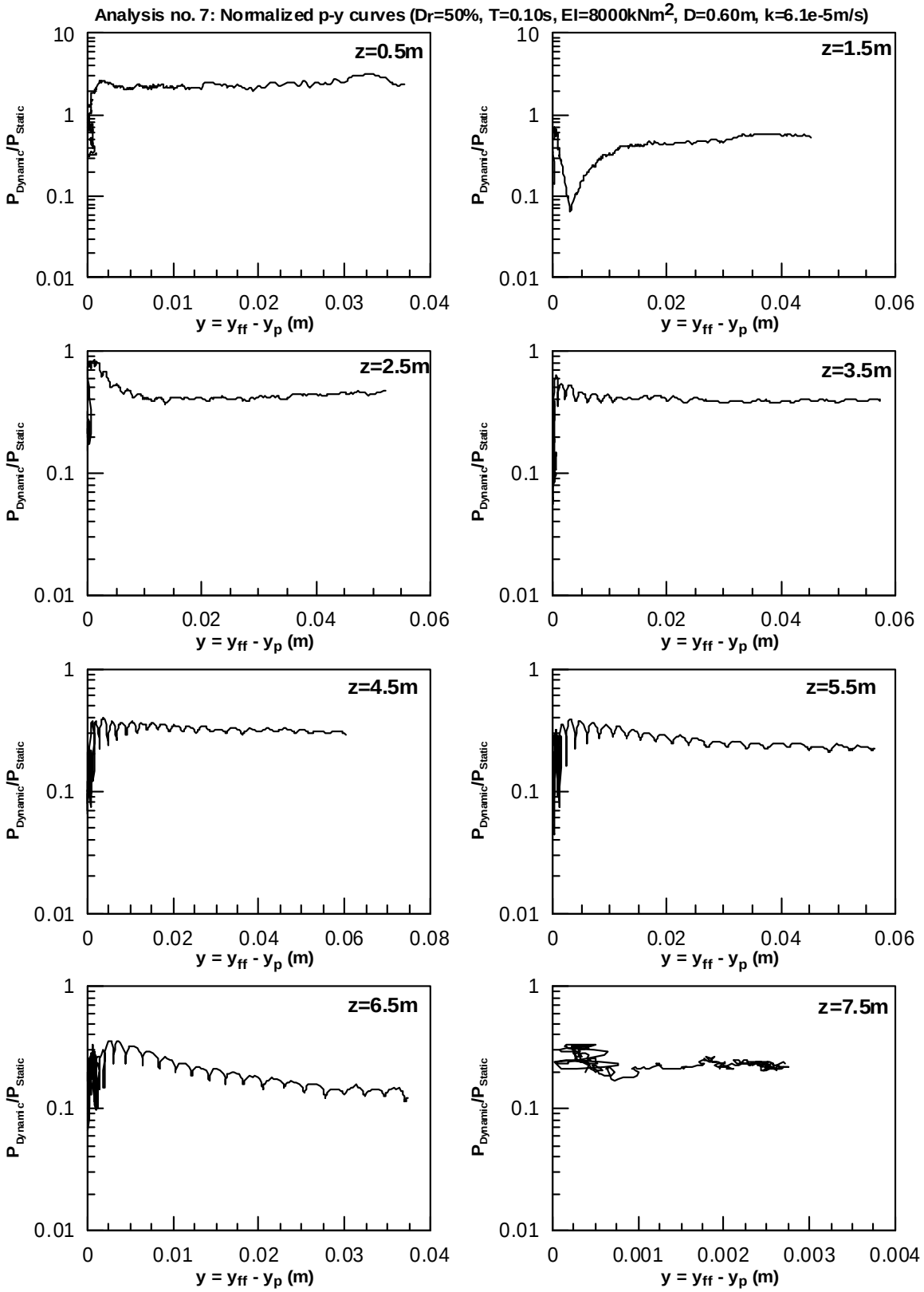
Analysis no. 7: Normalized p-y curves (Dr=50%, T=0.10s, EI=8000kNm2, D=0.60m, k=6.1e-5m/s)
z=0.5m
z=1.5m
z=2.5m
z=3.5m
z=4.5m
z=5.5m
z=6.5m
z=7.5m
P_Dynamic/P_Static
y = y_ff - y_p (m)

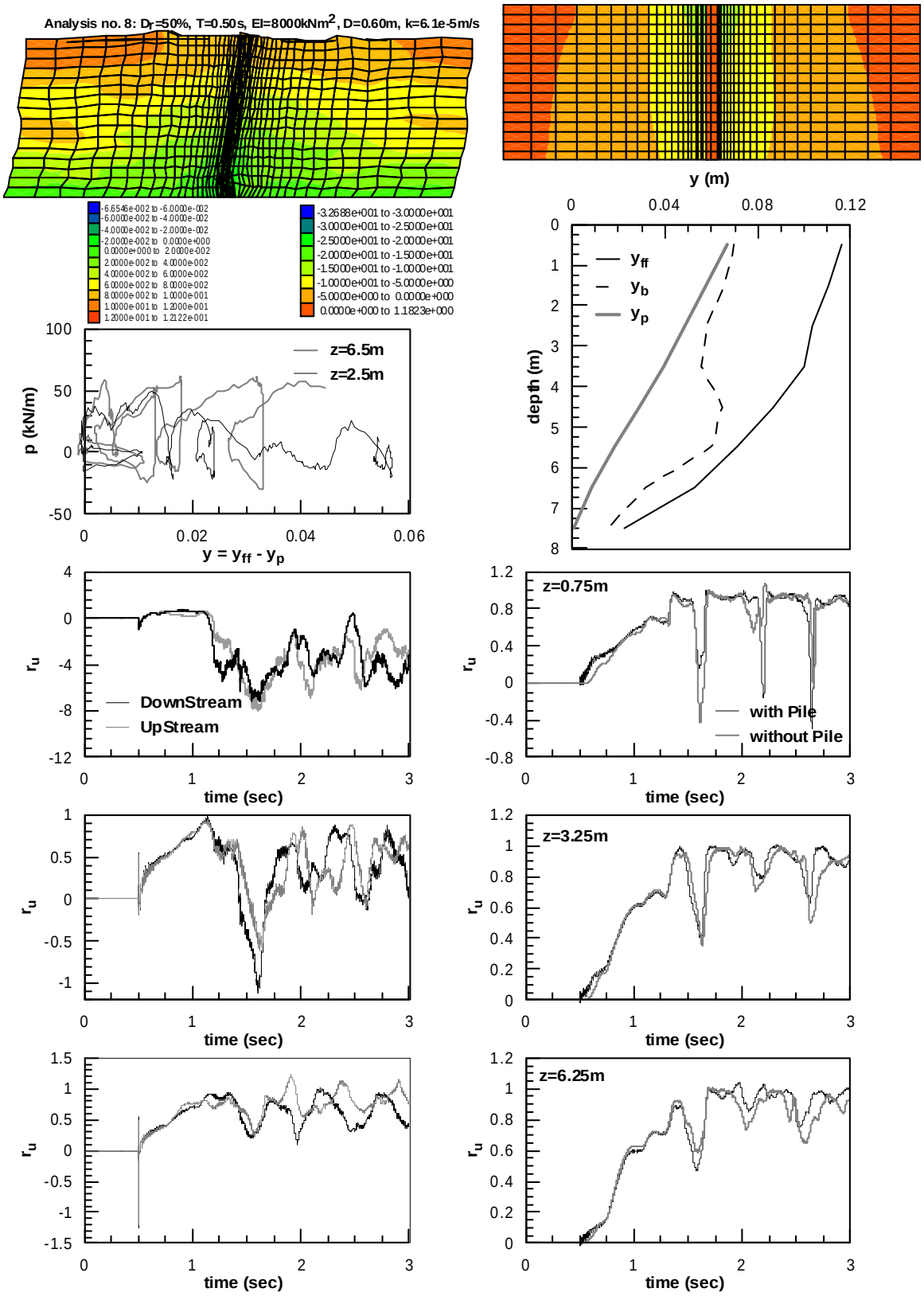
Analysis no. 8: Dr=50%, T=0.50s, EI=8000kNm2, D=0.60m, k=6.1e-5m/s
y (m)
depth (m)
yff
yb
yp
p (kN/m)
z=6.5m
z=2.5m
y = yff - yp
ru
DownStream
UpStream
time (sec)
z=0.75m
with Pile
without Pile
z=3.25m
z=6.25m

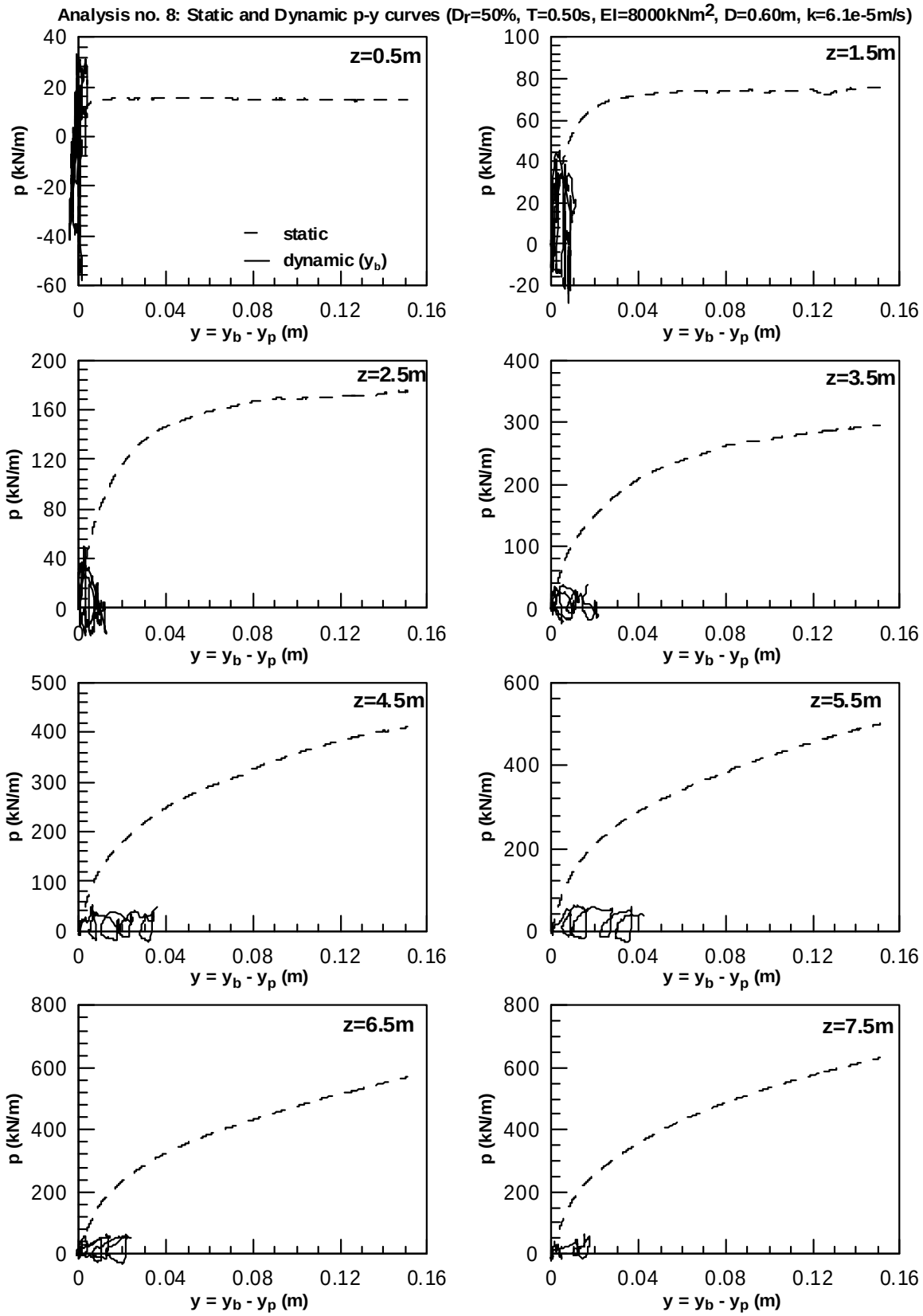
Analysis no. 8: Static and Dynamic p-y curves (Dr=50%, T=0.50s, EI=8000kNm2, D=0.60m, k=6.1e-5m/s)
z=0.5m
z=1.5m
z=2.5m
z=3.5m
z=4.5m
z=5.5m
z=6.5m
z=7.5m
static
dynamic (yb)
p (kN/m)
y = yb - yp (m)

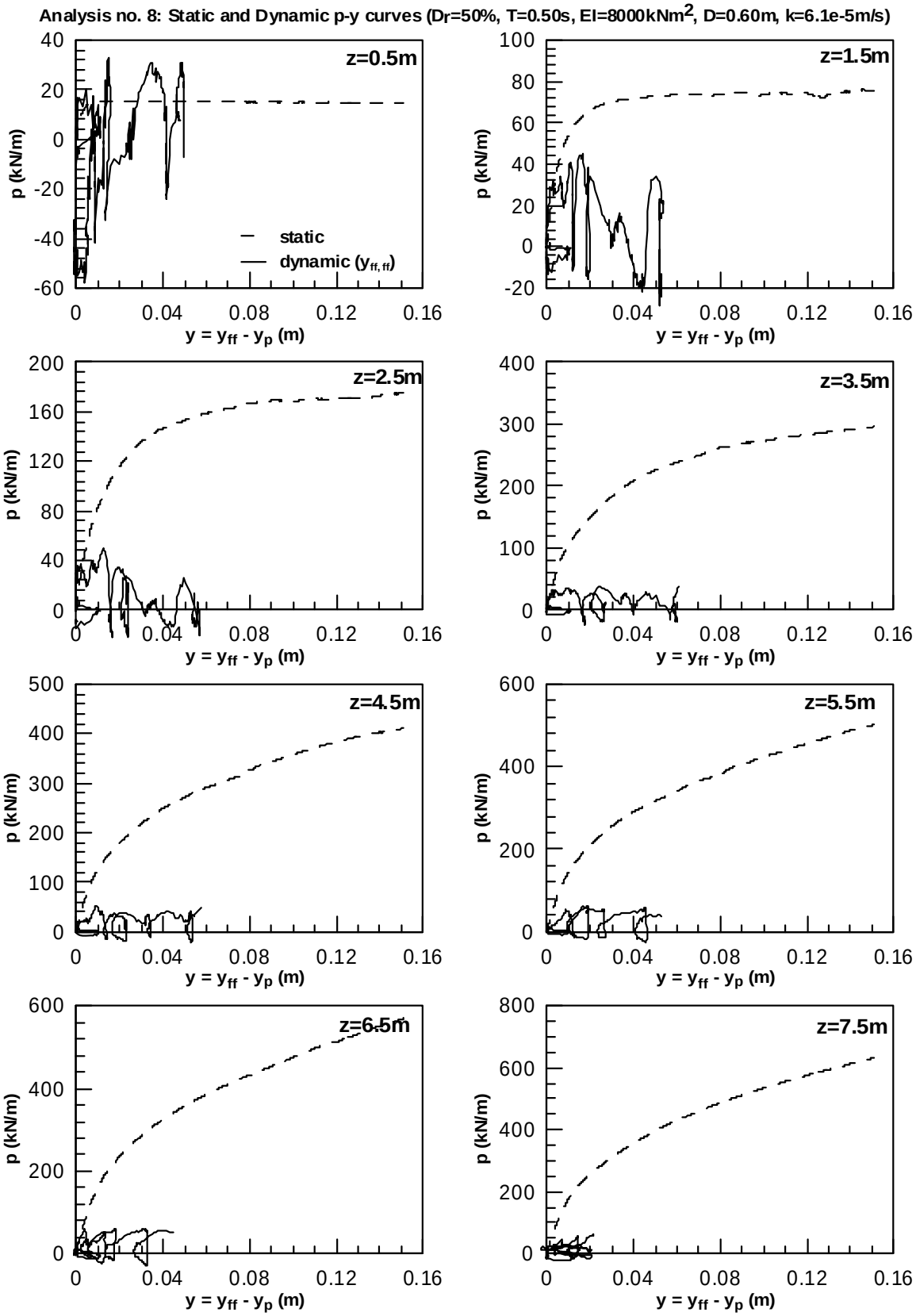
Analysis no. 8: Static and Dynamic p-y curves (Dr=50%, T=0.50s, EI=8000kNm2, D=0.60m, k=6.1e-5m/s)
z=0.5m
z=1.5m
z=2.5m
z=3.5m
z=4.5m
z=5.5m
z=6.5m
z=7.5m
static
dynamic (yff, ff)
p (kN/m)
y = yff - yp (m)

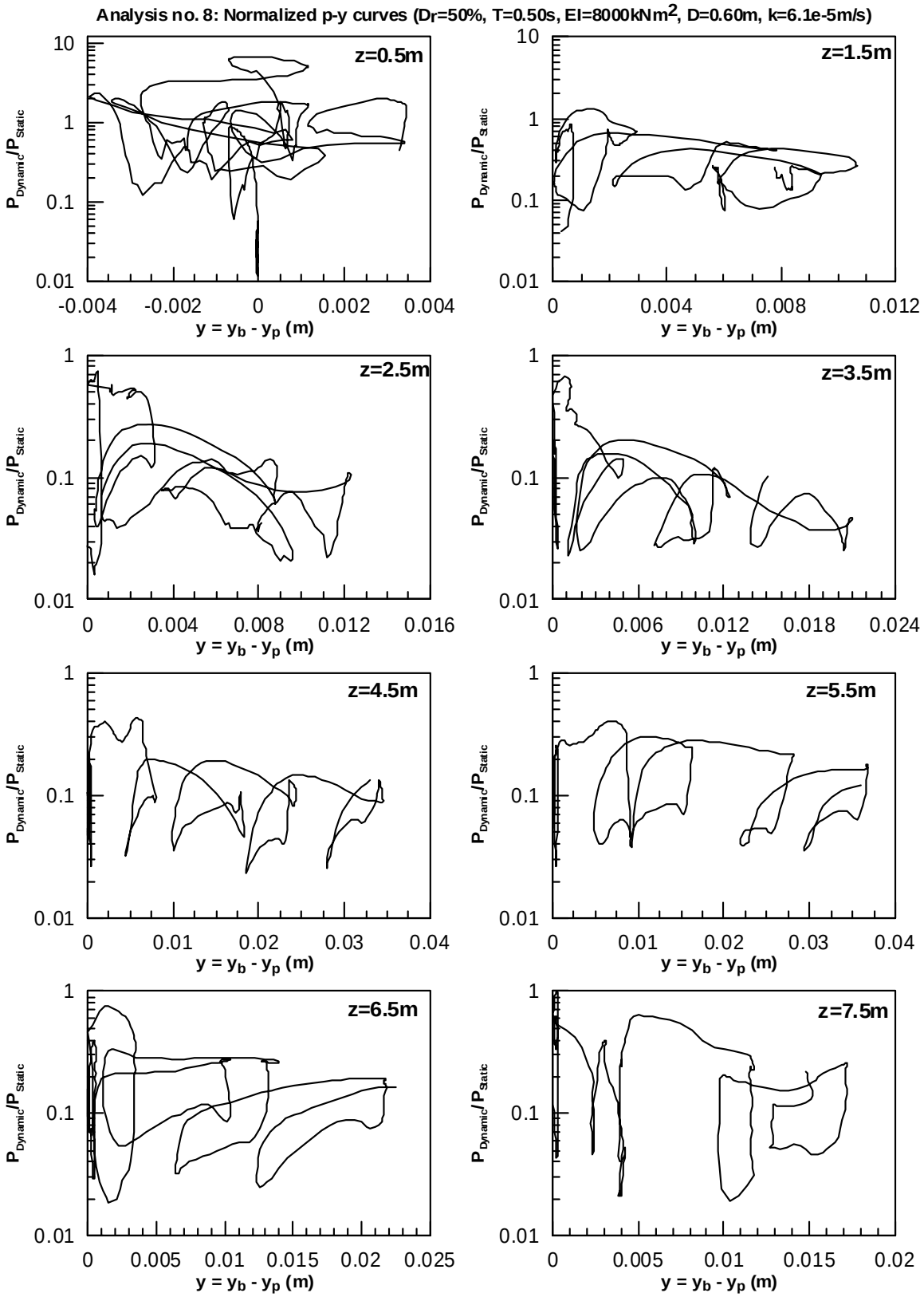
Analysis no. 8: Normalized p-y curves (Dr=50%, T=0.50s, EI=8000kNm2, D=0.60m, k=6.1e-5m/s)
z=0.5m
z=1.5m
z=2.5m
z=3.5m
z=4.5m
z=5.5m
z=6.5m
z=7.5m
P Dynamic/P Static
y = yb - yp (m)

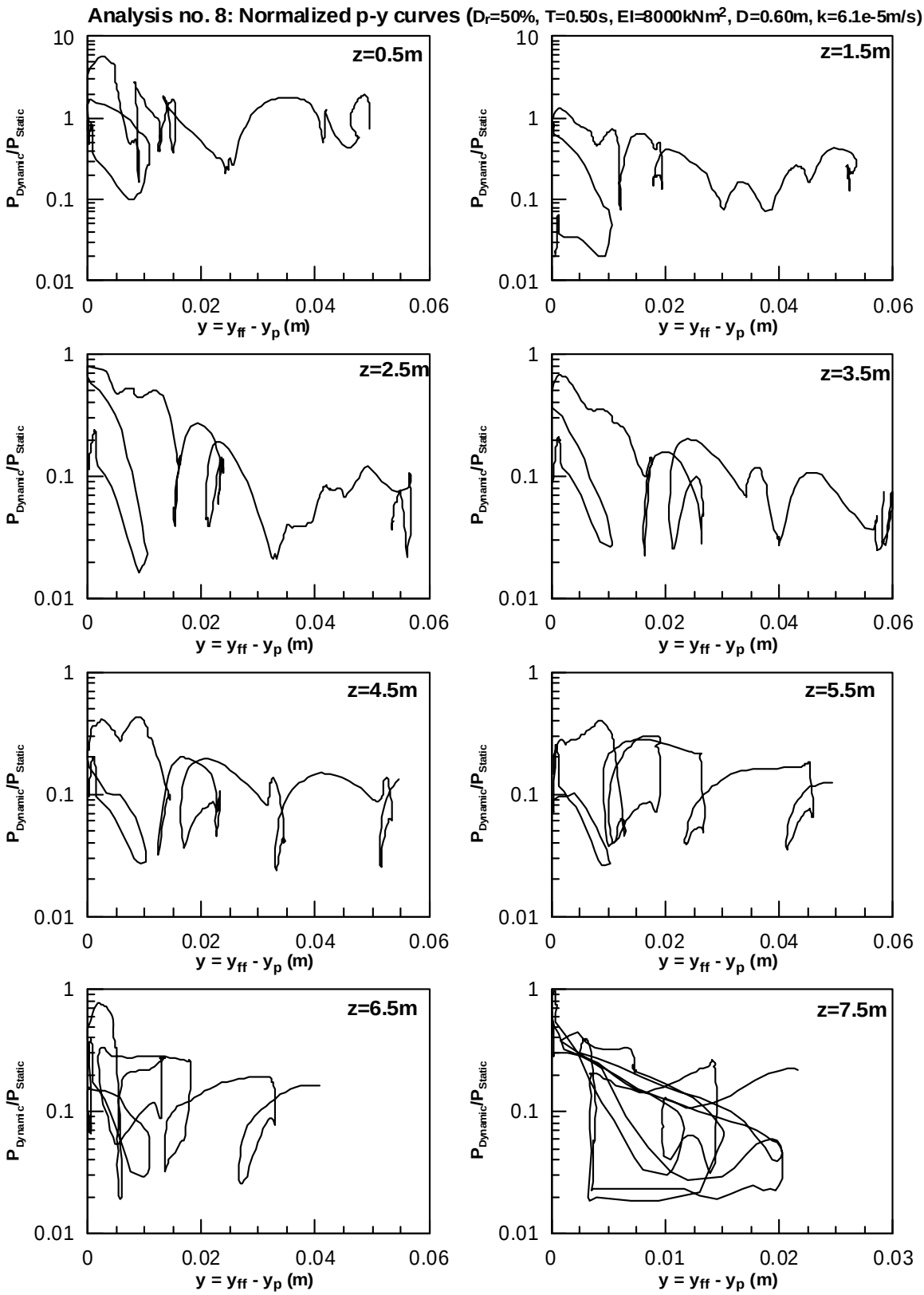
Analysis no. 8: Normalized p-y curves (Dr=50%, T=0.50s, EI=8000kNm2, D=0.60m, k=6.1e-5m/s)
z=0.5m
z=1.5m
z=2.5m
z=3.5m
z=4.5m
z=5.5m
z=6.5m
z=7.5m
P Dynamic/P Static
y = yff - yp (m)

D_r=50%, T=0.30s, EI=8000kNm^2, D=0.60m, k=6.1e-5m/s Installation

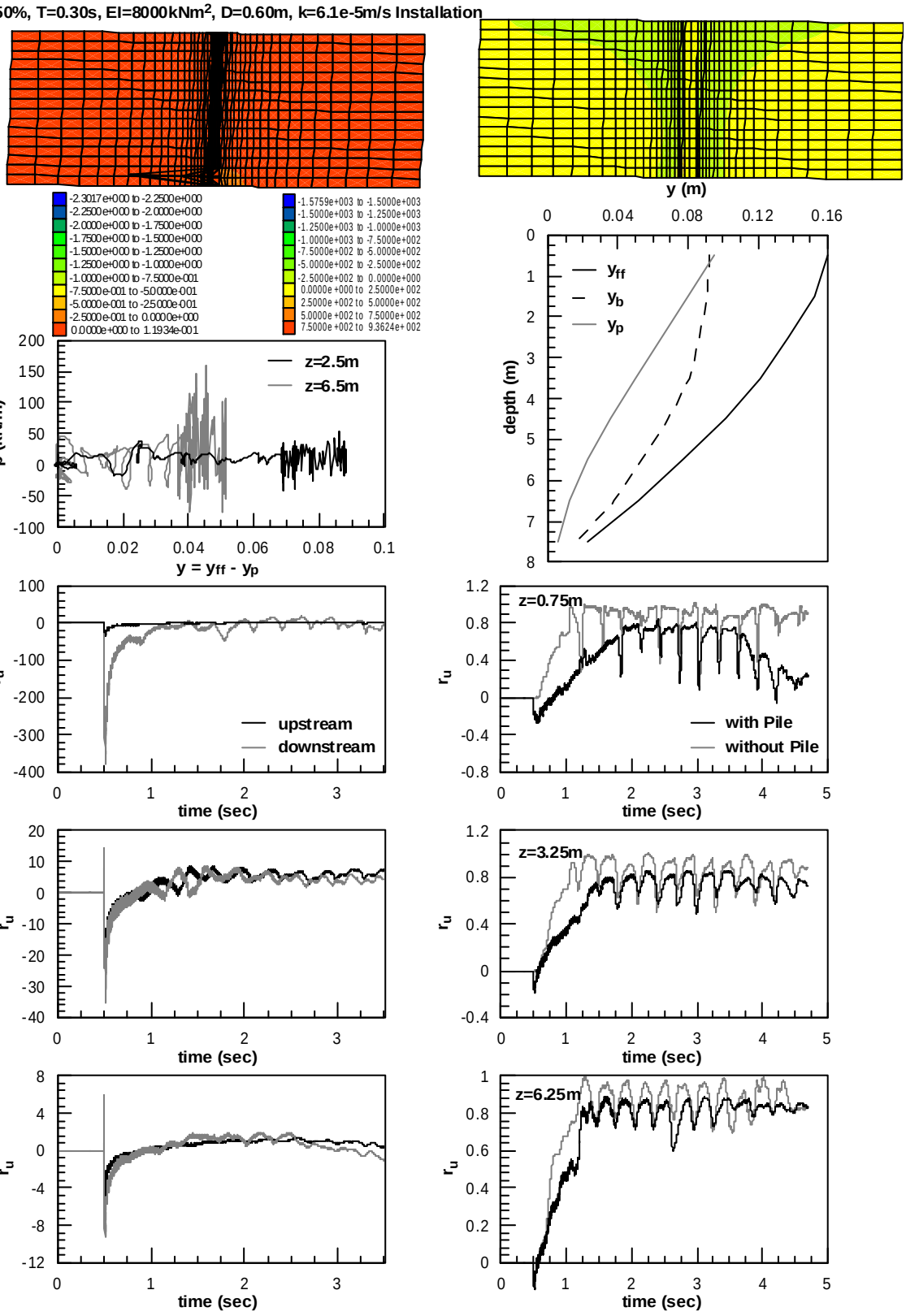

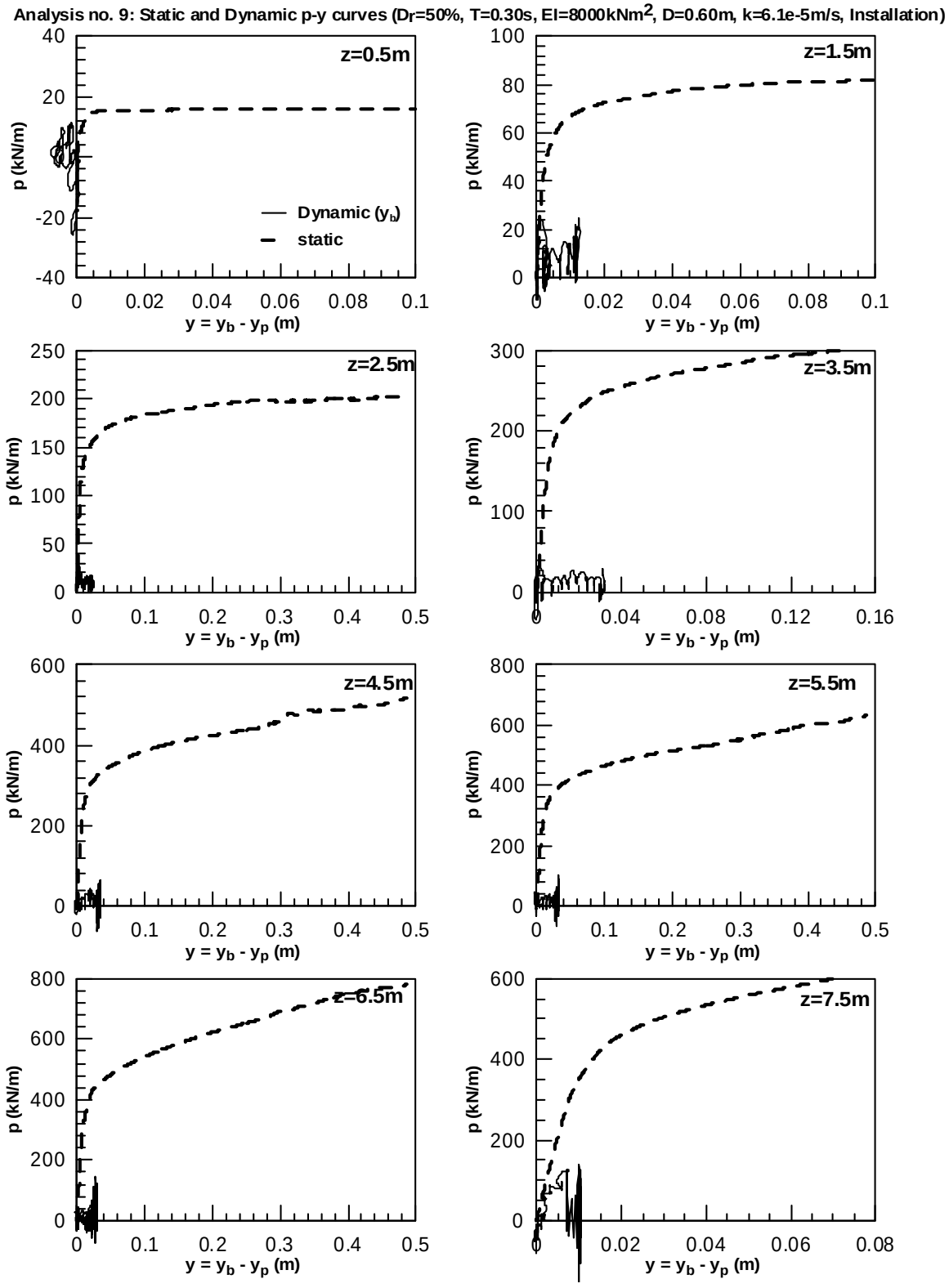
Analysis no. 9: Static and Dynamic p-y curves (Dr=50%, T=0.30s, EI=8000kNm2, D=0.60m, k=6.1e-5m/s, Installation)
z=0.5m
z=1.5m
z=2.5m
z=3.5m
z=4.5m
z=5.5m
z=6.5m
z=7.5m
Dynamic (yb)
static
p (kN/m)
y = yb - yp (m)

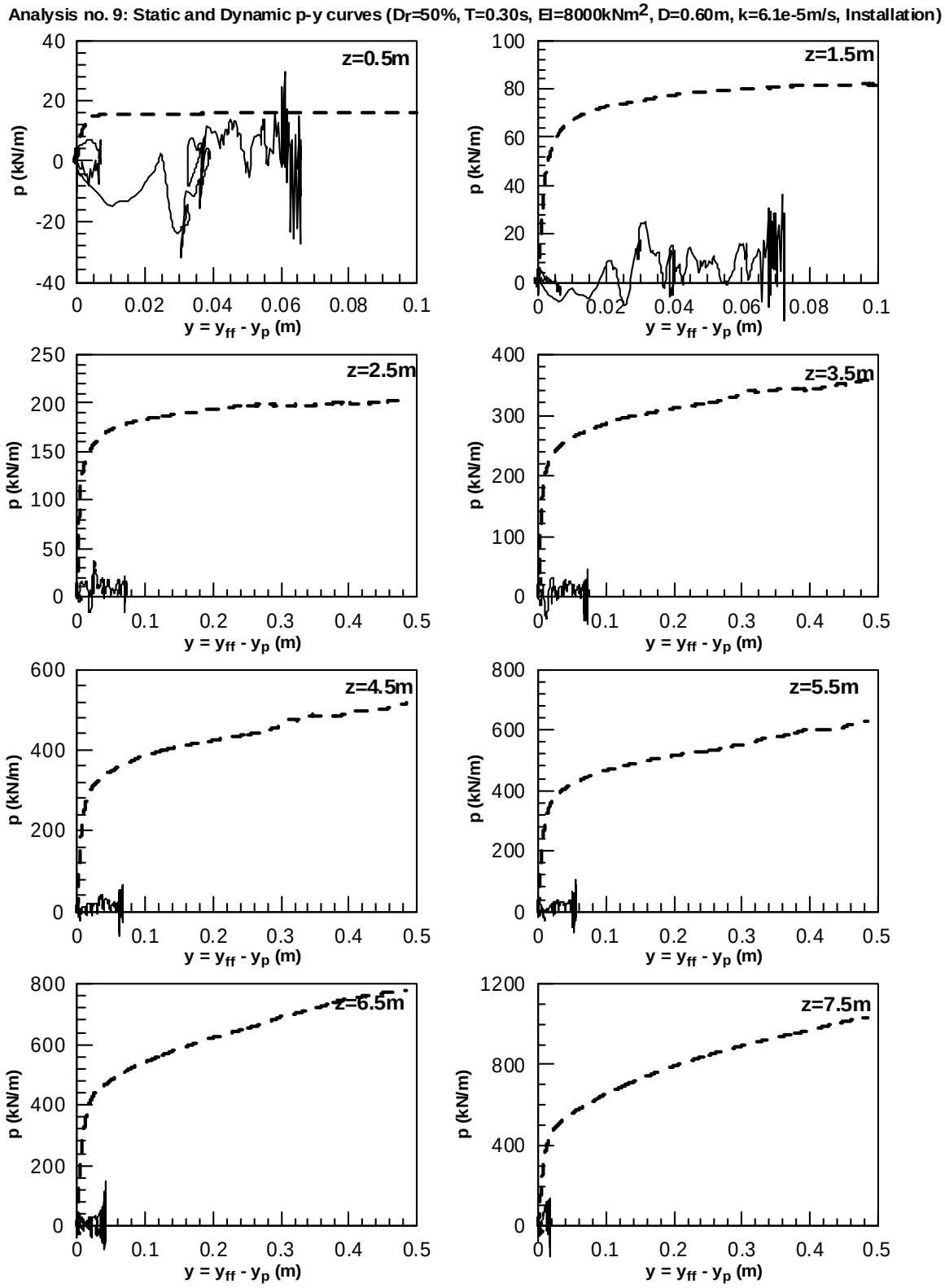
Analysis no. 9: Static and Dynamic p-y curves (Dr=50%, T=0.30s, EI=8000kNm2, D=0.60m, k=6.1e-5m/s, Installation)
z=0.5m
z=1.5m
z=2.5m
z=3.5m
z=4.5m
z=5.5m
z=6.5m
z=7.5m
p (kN/m)
y = yff - yp (m)

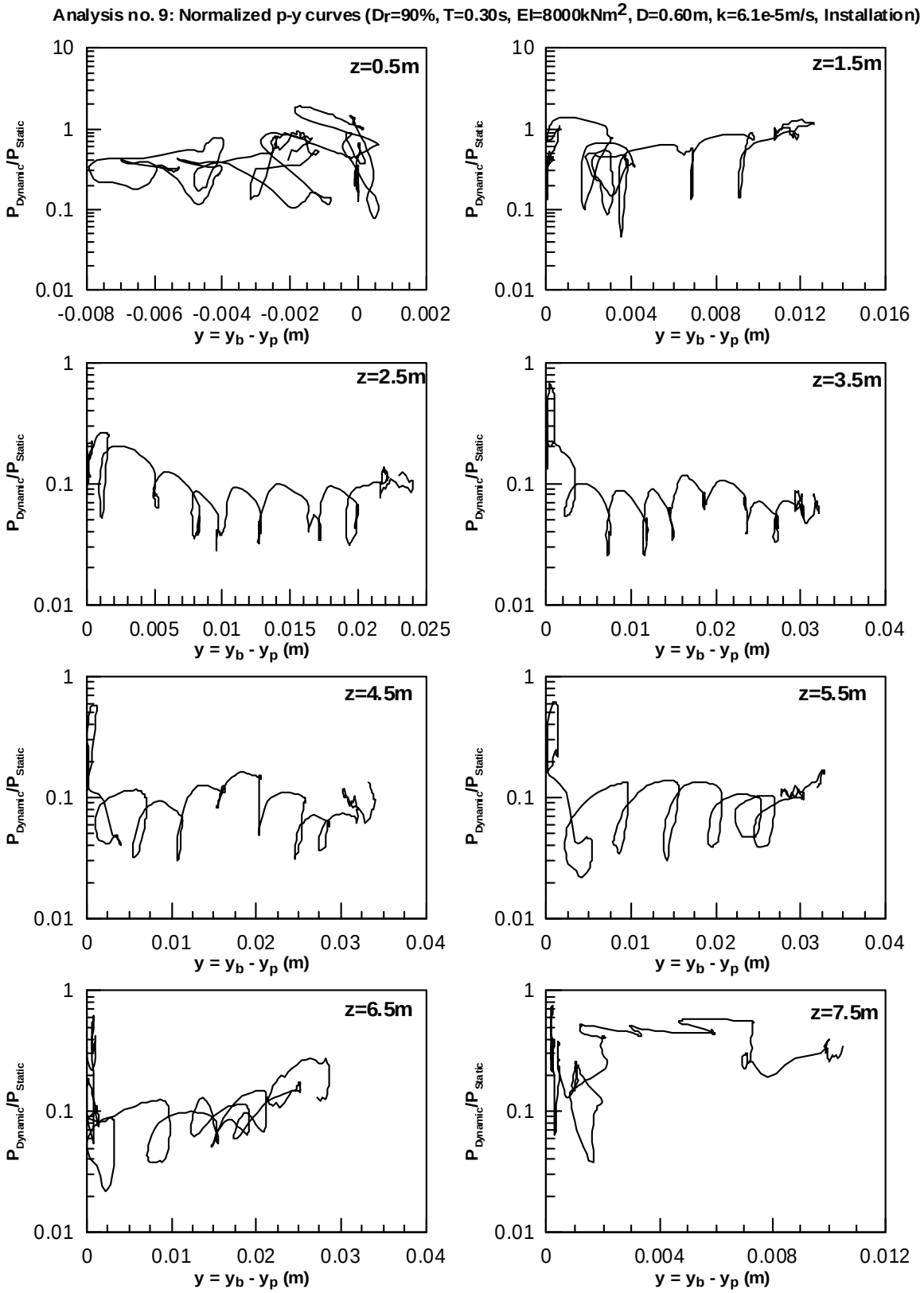
Analysis no. 9: Normalized p-y curves (Dr=90%, T=0.30s, EI=8000kNm2, D=0.60m, k=6.1e-5m/s, Installation)
z=0.5m
z=1.5m
z=2.5m
z=3.5m
z=4.5m
z=5.5m
z=6.5m
z=7.5m
P Dynamic/P Static
y = yb - yp (m)

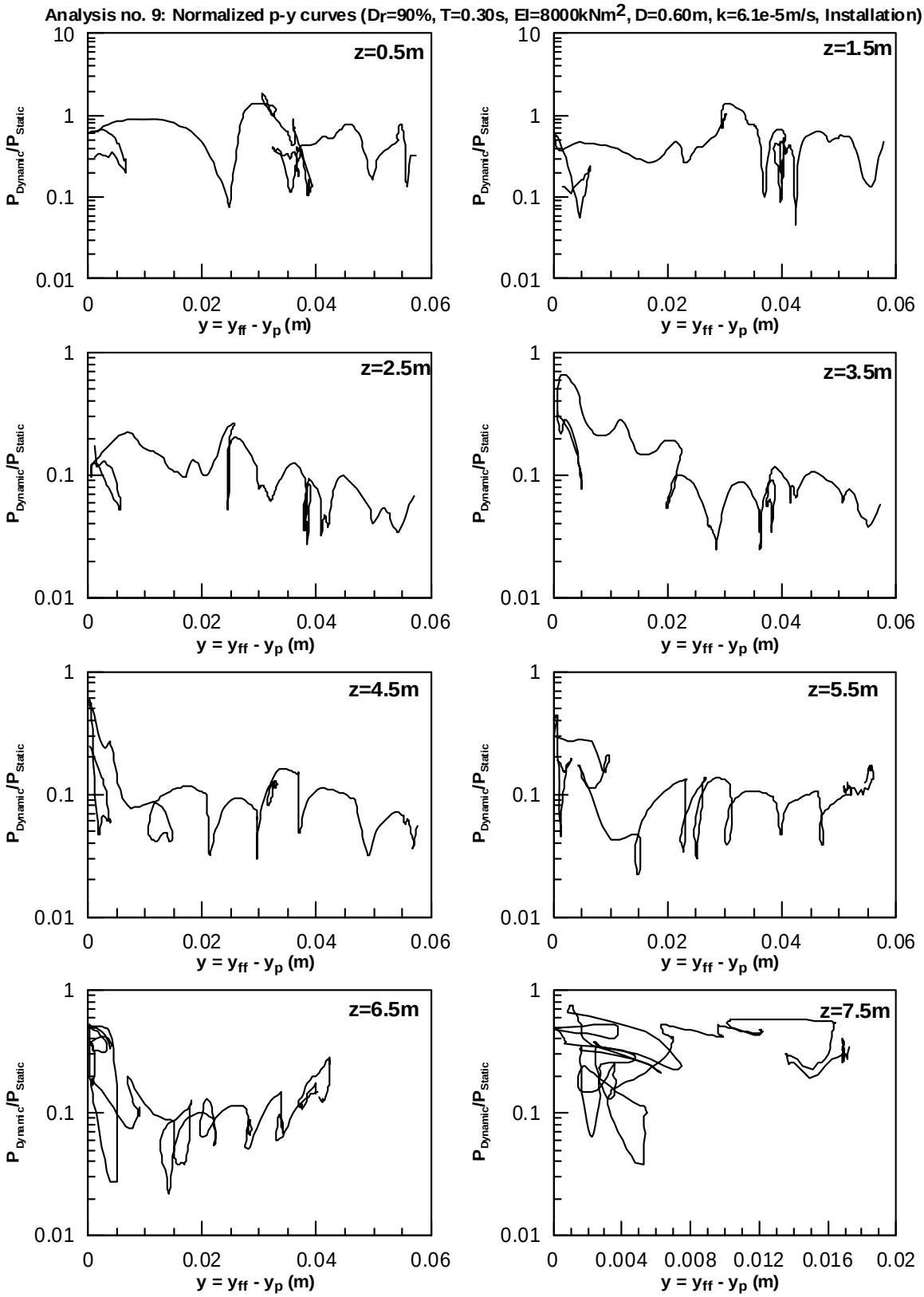
Analysis no. 9: Normalized p-y curves (Dr=90%, T=0.30s, EI=8000kNm2, D=0.60m, k=6.1e-5m/s, Installation)
z=0.5m
z=1.5m
z=2.5m
z=3.5m
z=4.5m
z=5.5m
z=6.5m
z=7.5m
P Dynamic/P Static
y = yff - yp (m)
10
1
0.1
0.01
0
0.02
0.04
0.06
0.004
0.008
0.012
0.016
0.02

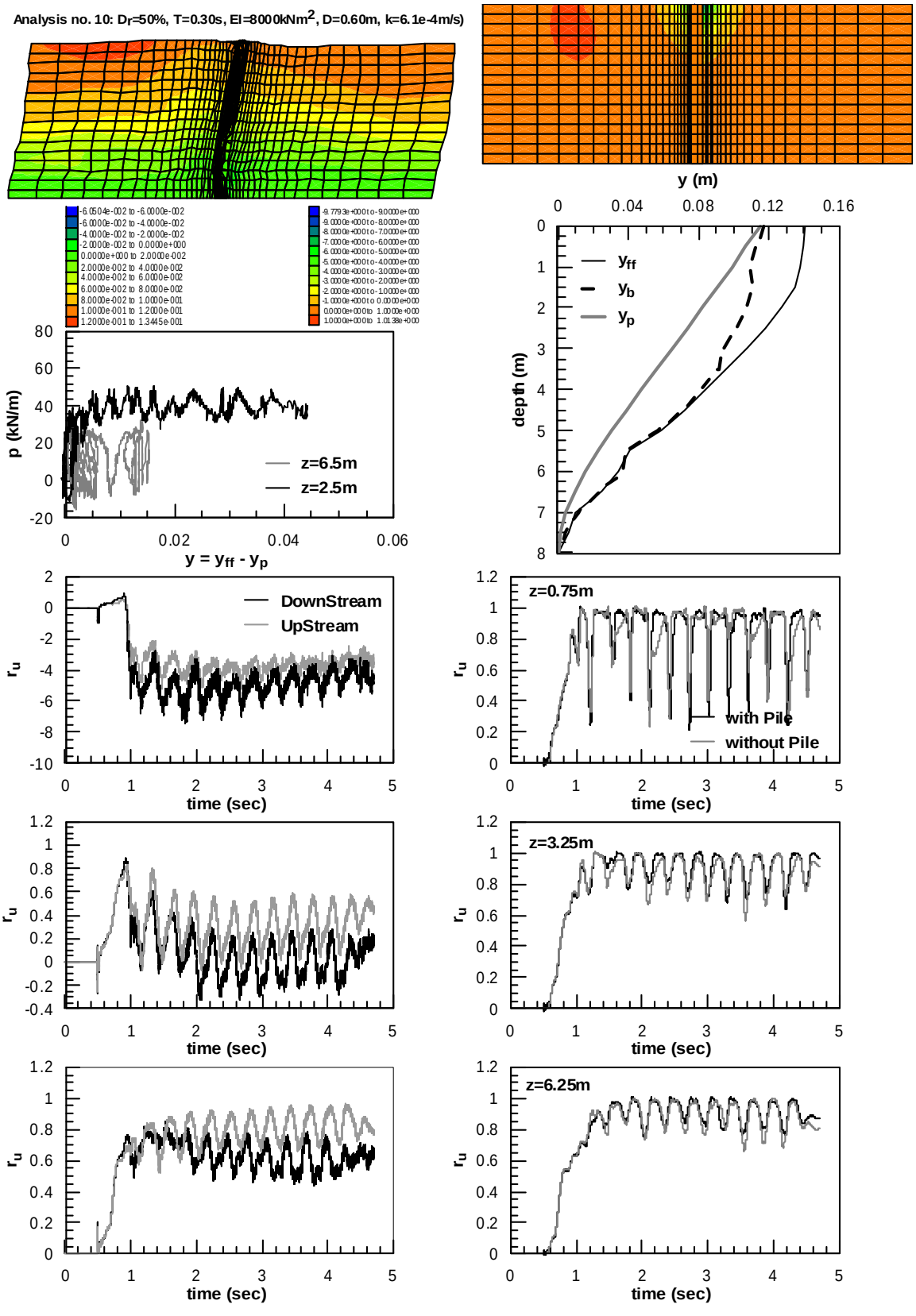
Analysis no. 10: Dr=50%, T=0.30s, EI=8000kNm2, D=0.60m, k=6.1e-4m/s)
y (m)
depth (m)
yff
yb
yp
p (kN/m)
z=6.5m
z=2.5m
y = yff - yp
ru
DownStream
UpStream
time (sec)
z=0.75m
with Pile
without Pile
z=3.25m
z=6.25m

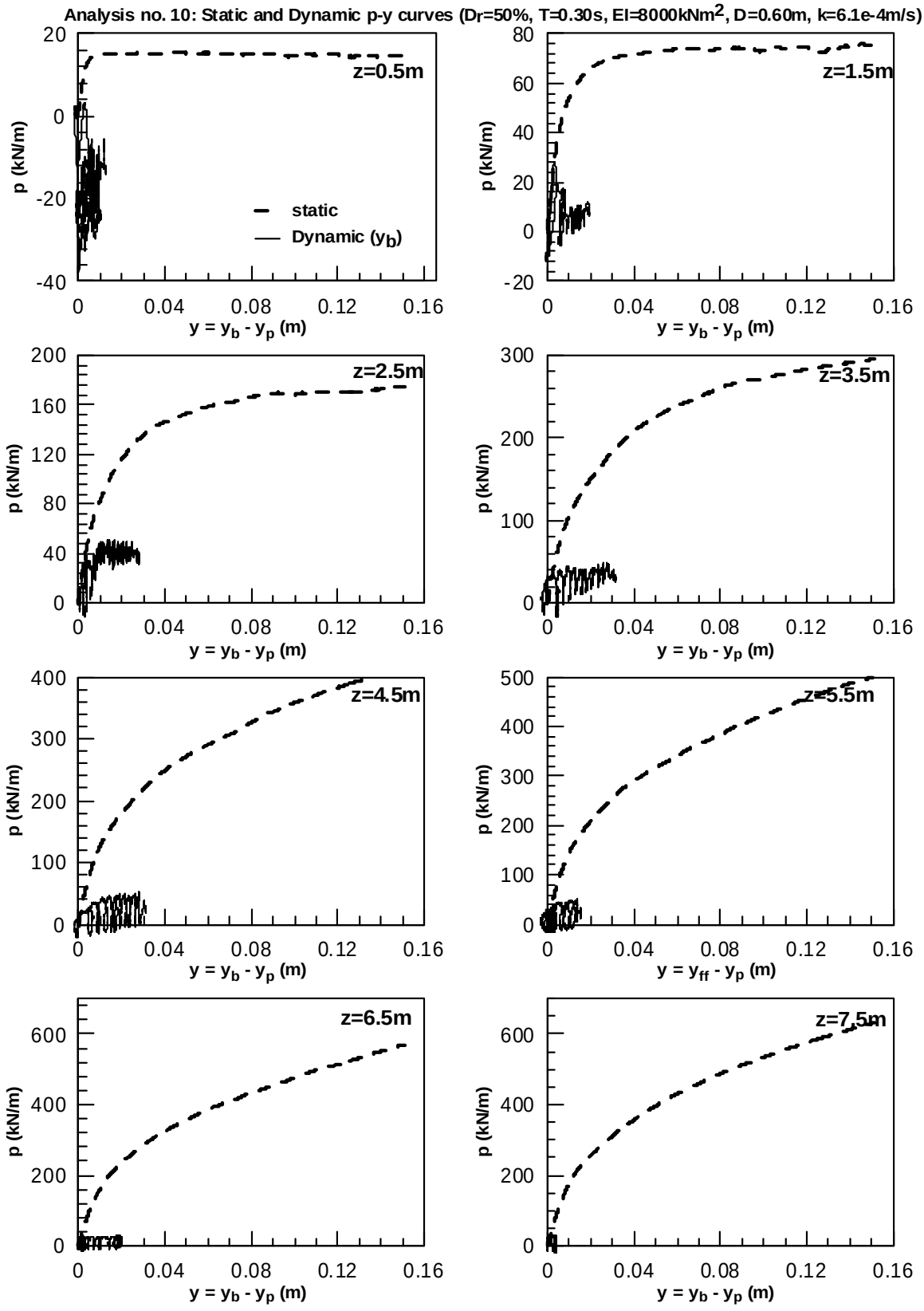
Analysis no. 10: Static and Dynamic p-y curves (Dr=50%, T=0.30s, EI=8000kNm2, D=0.60m, k=6.1e-4m/s)
z=0.5m
z=1.5m
z=2.5m
z=3.5m
z=4.5m
z=5.5m
z=6.5m
z=7.5m
static
Dynamic (yb)
p (kN/m)
y = yb - yp (m)
y = yff - yp (m)

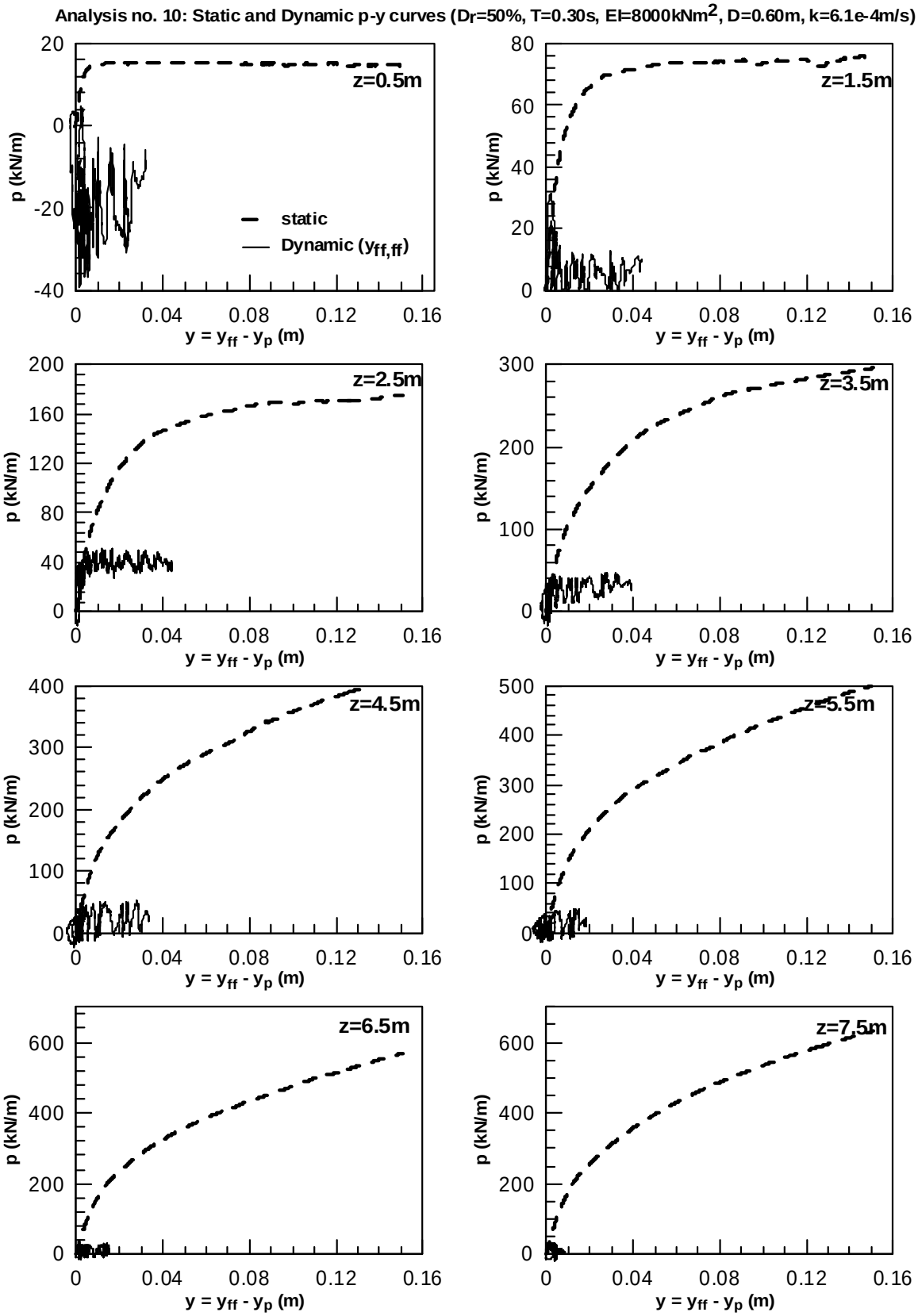
Analysis no. 10: Static and Dynamic p-y curves (Dr=50%, T=0.30s, EI=8000kNm2, D=0.60m, k=6.1e-4m/s)
z=0.5m
z=1.5m
z=2.5m
z=3.5m
z=4.5m
z=5.5m
z=6.5m
z=7.5m
static
Dynamic (yff,ff)
p (kN/m)
y = yff - yp (m)

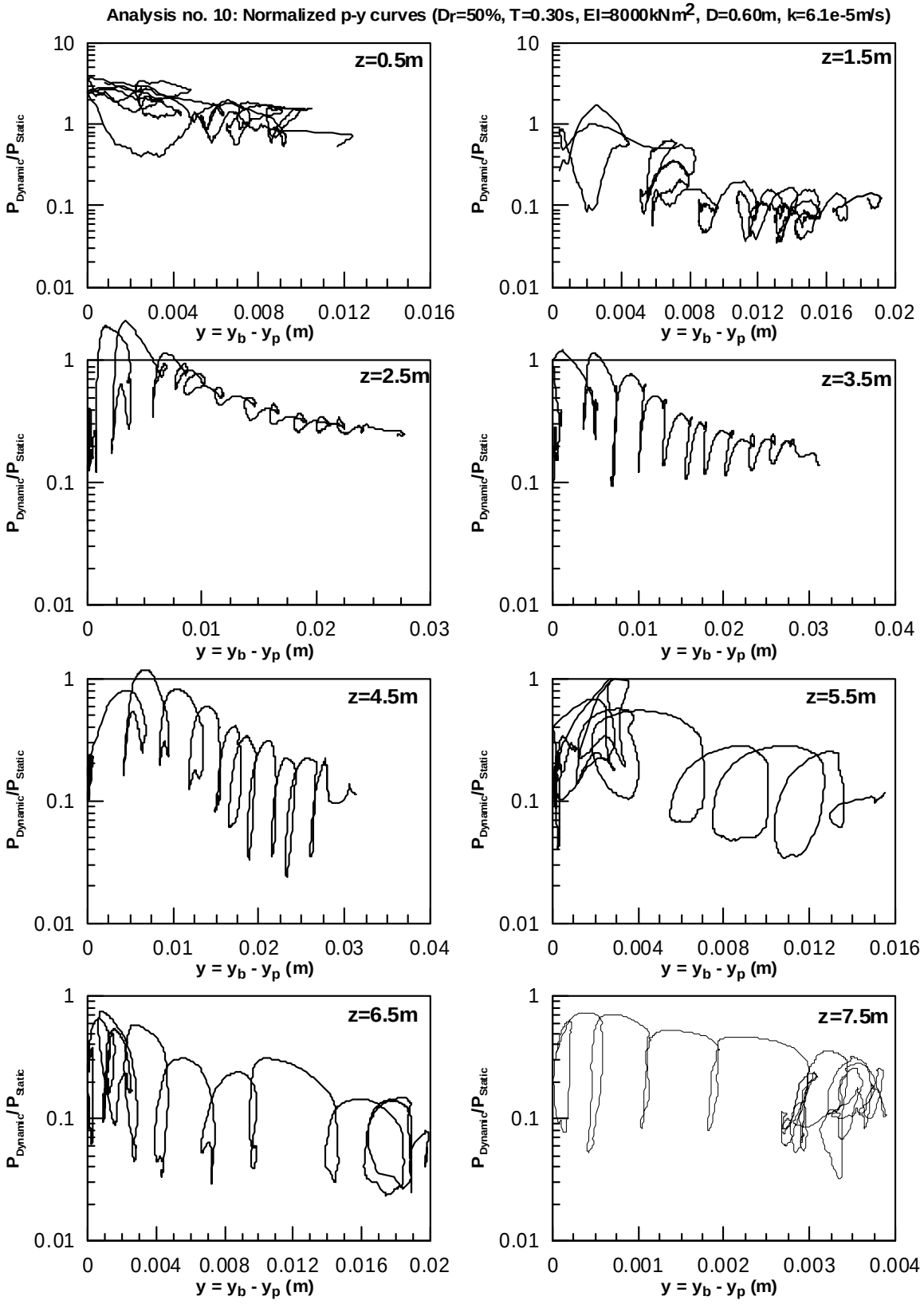
Analysis no. 10: Normalized p-y curves (Dr=50%, T=0.30s, EI=8000kNm2, D=0.60m, k=6.1e-5m/s)
z=0.5m
z=1.5m
z=2.5m
z=3.5m
z=4.5m
z=5.5m
z=6.5m
z=7.5m
P Dynamic/P Static
y = yb - yp (m)

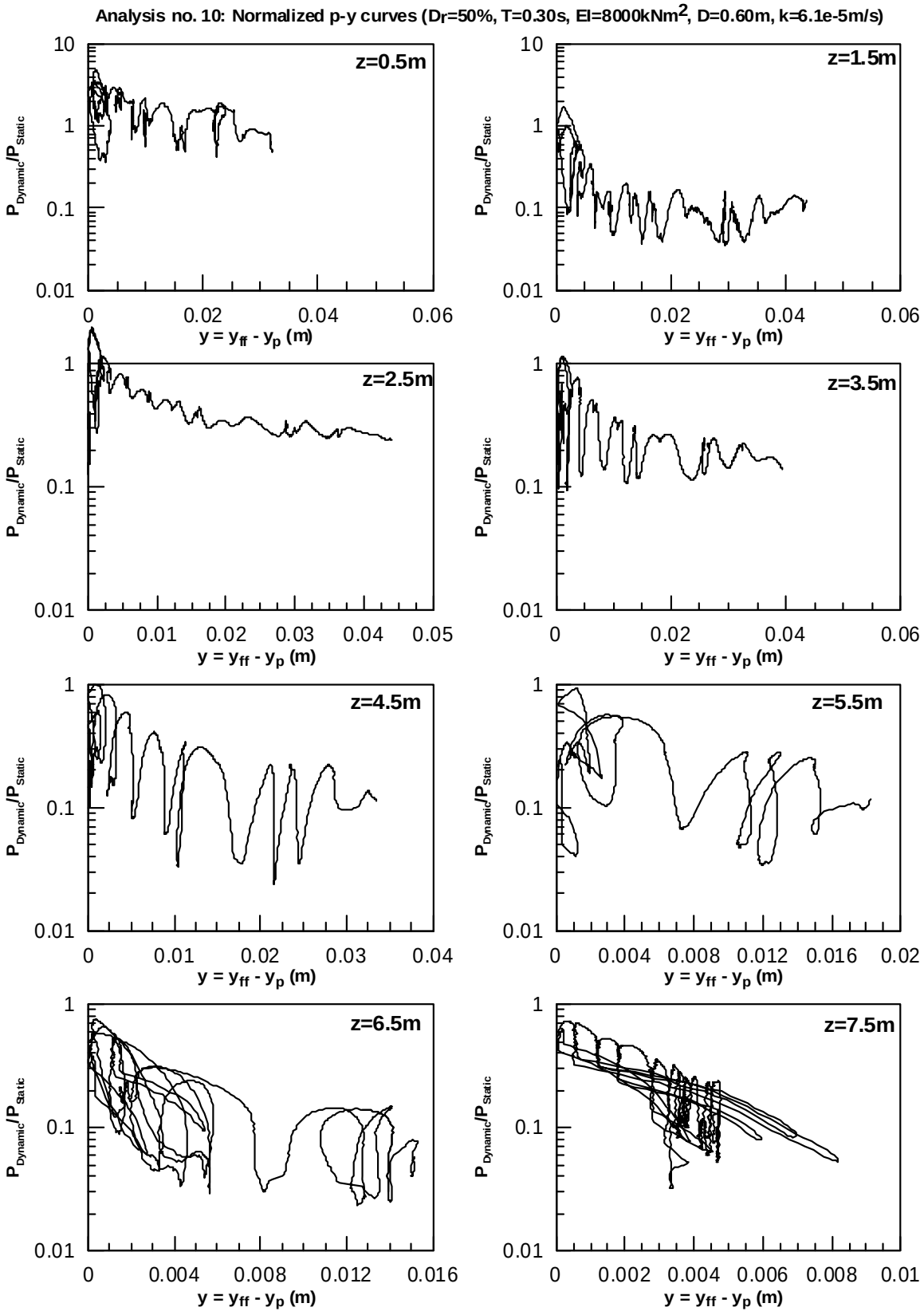
Analysis no. 10: Normalized p-y curves (Dr=50%, T=0.30s, EI=8000kNm2, D=0.60m, k=6.1e-5m/s)
z=0.5m
z=1.5m
z=2.5m
z=3.5m
z=4.5m
z=5.5m
z=6.5m
z=7.5m
P Dynamic/P Static
y = yff - yp (m)

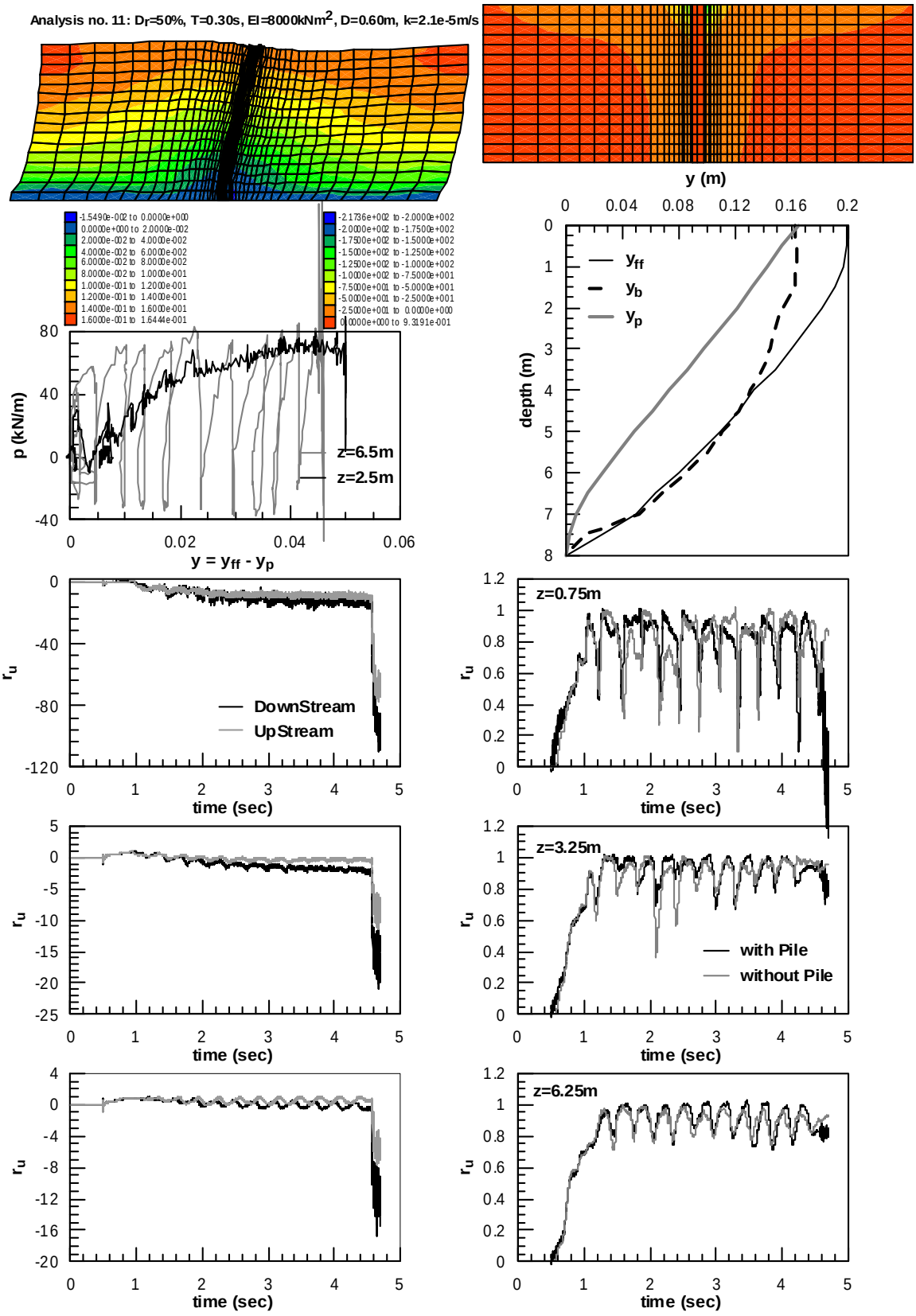
Analysis no. 11: Dr=50%, T=0.30s, EI=8000kNm2, D=0.60m, k=2.1e-5m/s
y (m)
depth (m)
yff
yb
yp
p (kN/m)
z=6.5m
z=2.5m
y = yff - yp
ru
DownStream
UpStream
time (sec)
z=0.75m
z=3.25m
with Pile
without Pile
z=6.25m

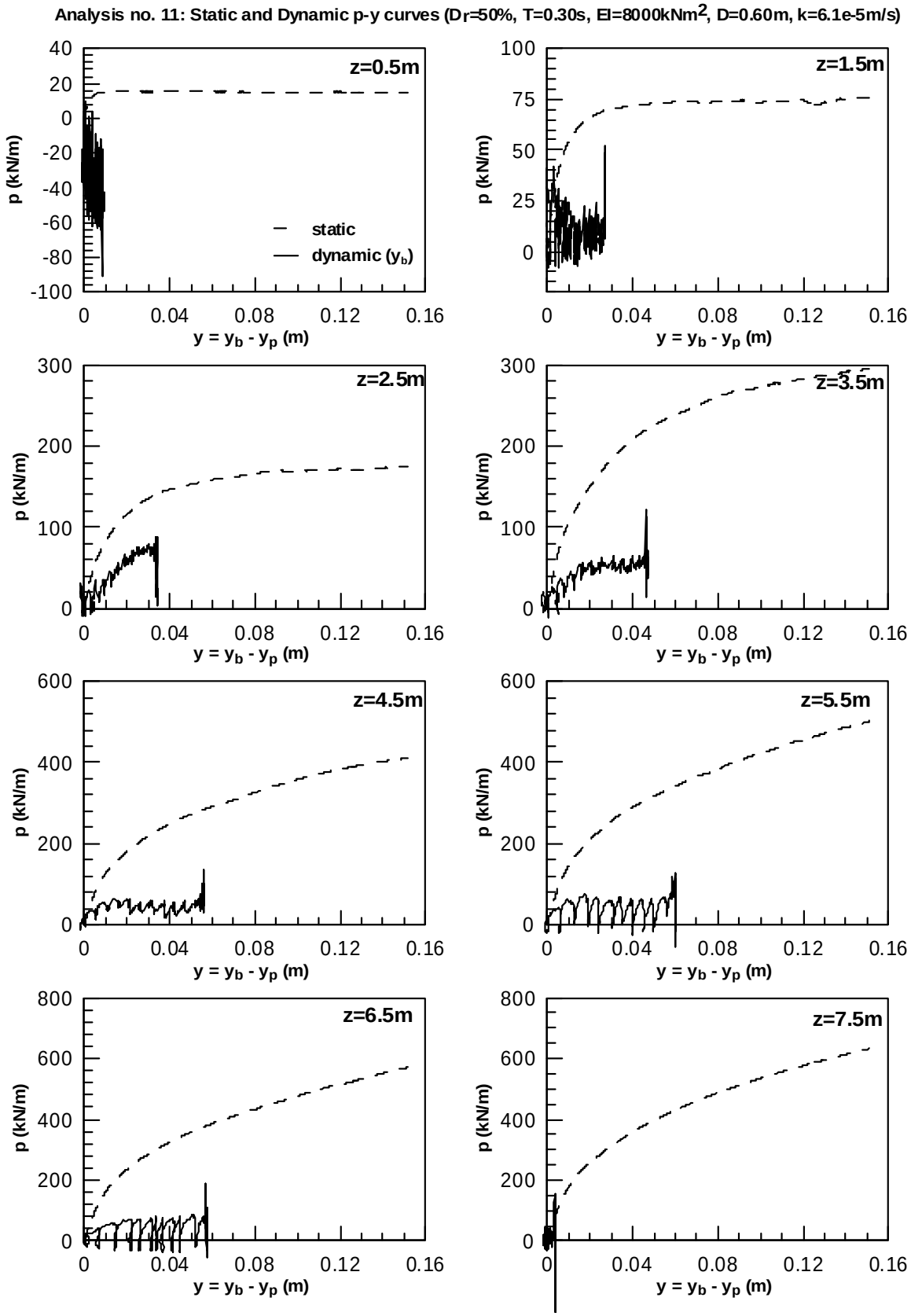
Analysis no. 11: Static and Dynamic p-y curves (Dr=50%, T=0.30s, EI=8000kNm2, D=0.60m, k=6.1e-5m/s)
z=0.5m
z=1.5m
z=2.5m
z=3.5m
z=4.5m
z=5.5m
z=6.5m
z=7.5m
static
dynamic (yb)
p (kN/m)
y = yb - yp (m)

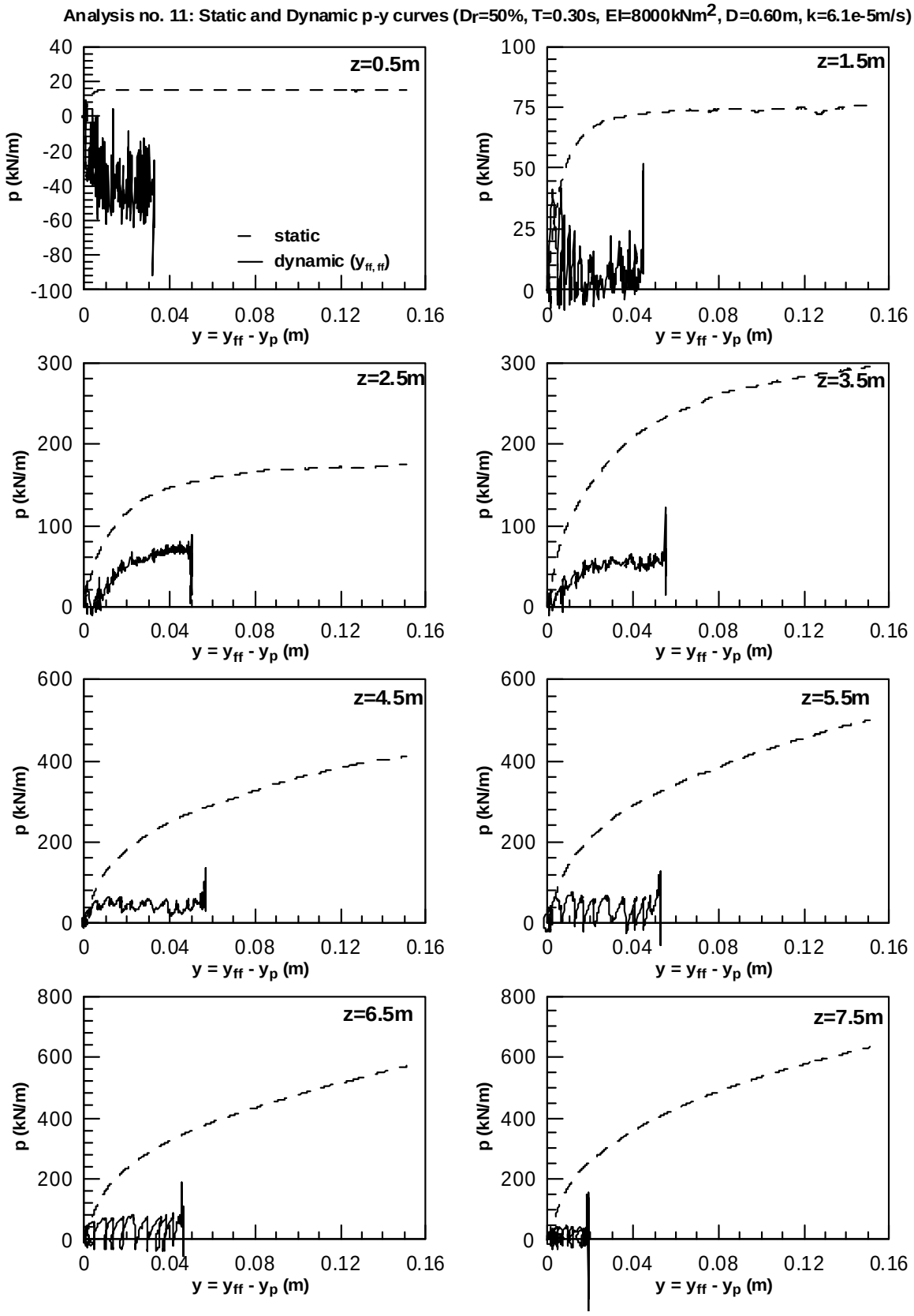
Analysis no. 11: Static and Dynamic p-y curves (Dr=50%, T=0.30s, EI=8000kNm2, D=0.60m, k=6.1e-5m/s)
z=0.5m
z=1.5m
z=2.5m
z=3.5m
z=4.5m
z=5.5m
z=6.5m
z=7.5m
p (kN/m)
y = yff - yp (m)
static
dynamic (yff, ff)

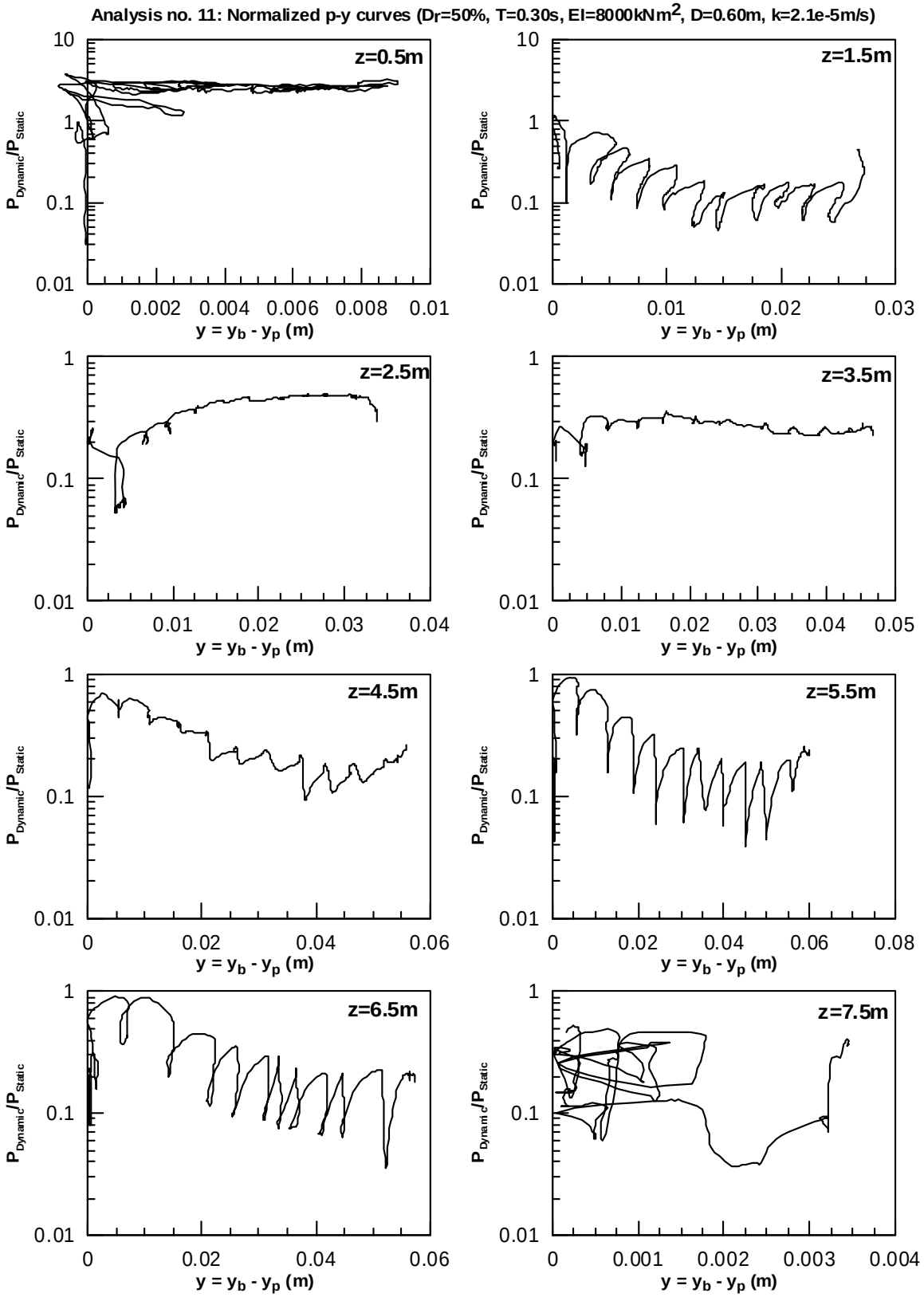
Analysis no. 11: Normalized p-y curves (Dr=50%, T=0.30s, EI=8000kNm2, D=0.60m, k=2.1e-5m/s)
z=0.5m
z=1.5m
z=2.5m
z=3.5m
z=4.5m
z=5.5m
z=6.5m
z=7.5m
P Dynamic/P Static
y = yb - yp (m)

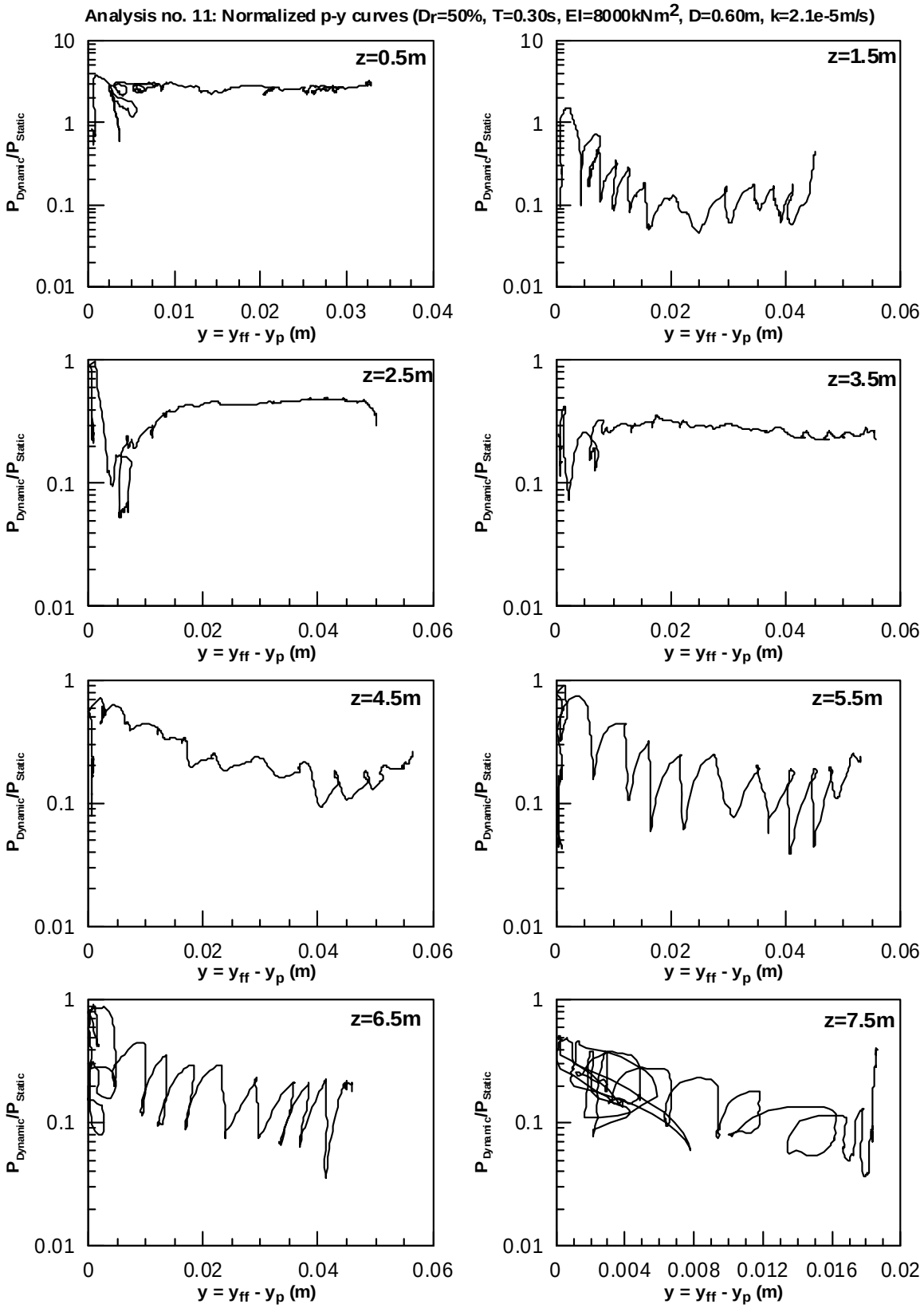
Analysis no. 11: Normalized p-y curves (Dr=50%, T=0.30s, EI=8000kNm2, D=0.60m, k=2.1e-5m/s)
z=0.5m
z=1.5m
z=2.5m
z=3.5m
z=4.5m
z=5.5m
z=6.5m
z=7.5m
P_Dynamic/P_Static
y = y_ff - y_p (m)

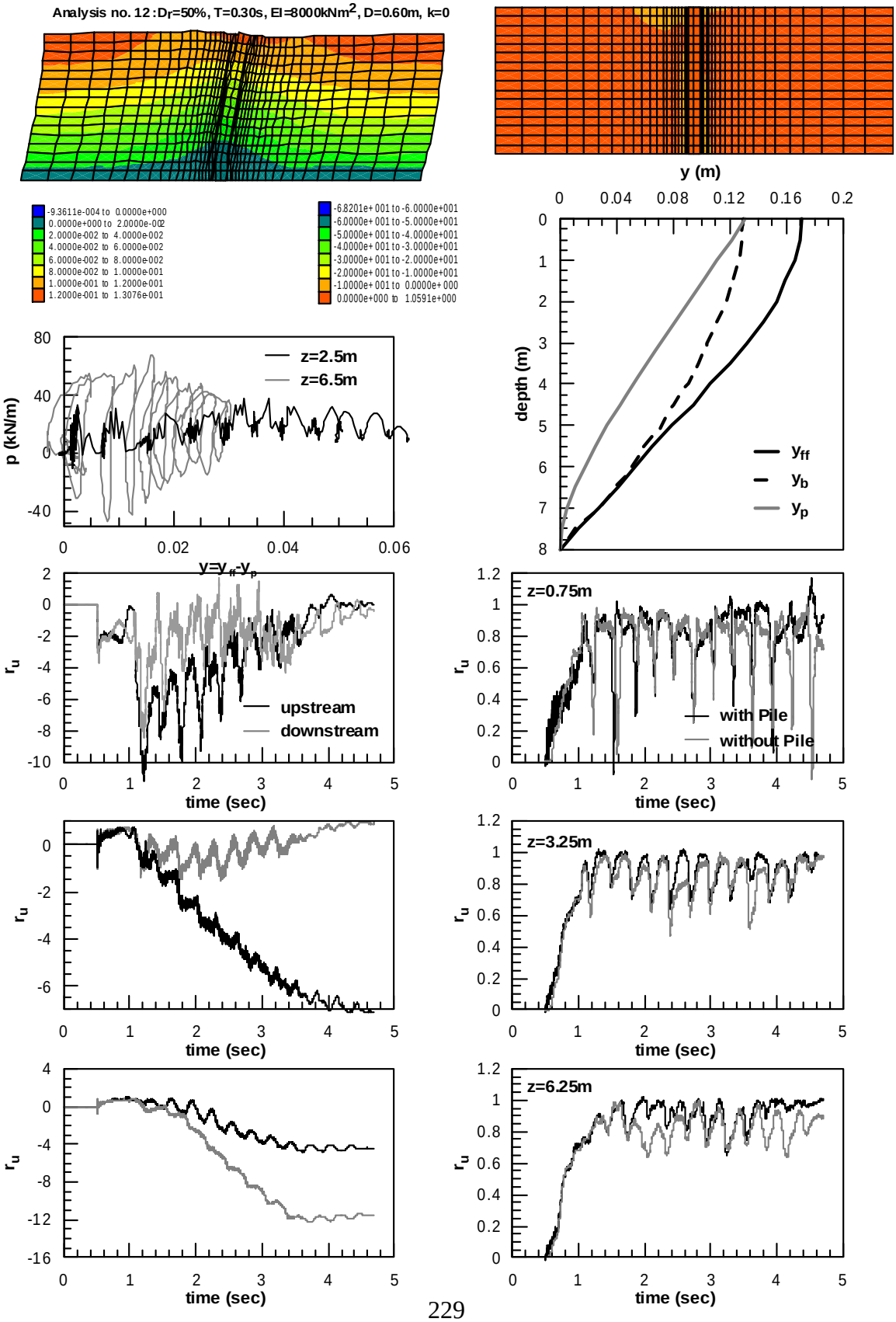
Analysis no. 12 : Dr=50%, T=0.30s, EI=8000kNm2, D=0.60m, k=0
-9.3611e-004 to 0.0000e+000
0.0000e+000 to 2.0000e-002
2.0000e-002 to 4.0000e-002
4.0000e-002 to 6.0000e-002
6.0000e-002 to 8.0000e-002
8.0000e-002 to 1.0000e-001
1.0000e-001 to 1.2000e-001
1.2000e-001 to 1.3076e-001
-6.8201e+001 to -6.0000e+001
-6.0000e+001 to -5.0000e+001
-5.0000e+001 to -4.0000e+001
-4.0000e+001 to -3.0000e+001
-3.0000e+001 to -2.0000e+001
-2.0000e+001 to -1.0000e+001
-1.0000e+001 to 0.0000e+000
0.0000e+000 to 1.0591e+000
y (m)
depth (m)
yff
yb
yp
p (kN/m)
z=2.5m
z=6.5m
y=yff-yp
ru
upstream
downstream
time (sec)
z=0.75m
with Pile
without Pile
z=3.25m
z=6.25m

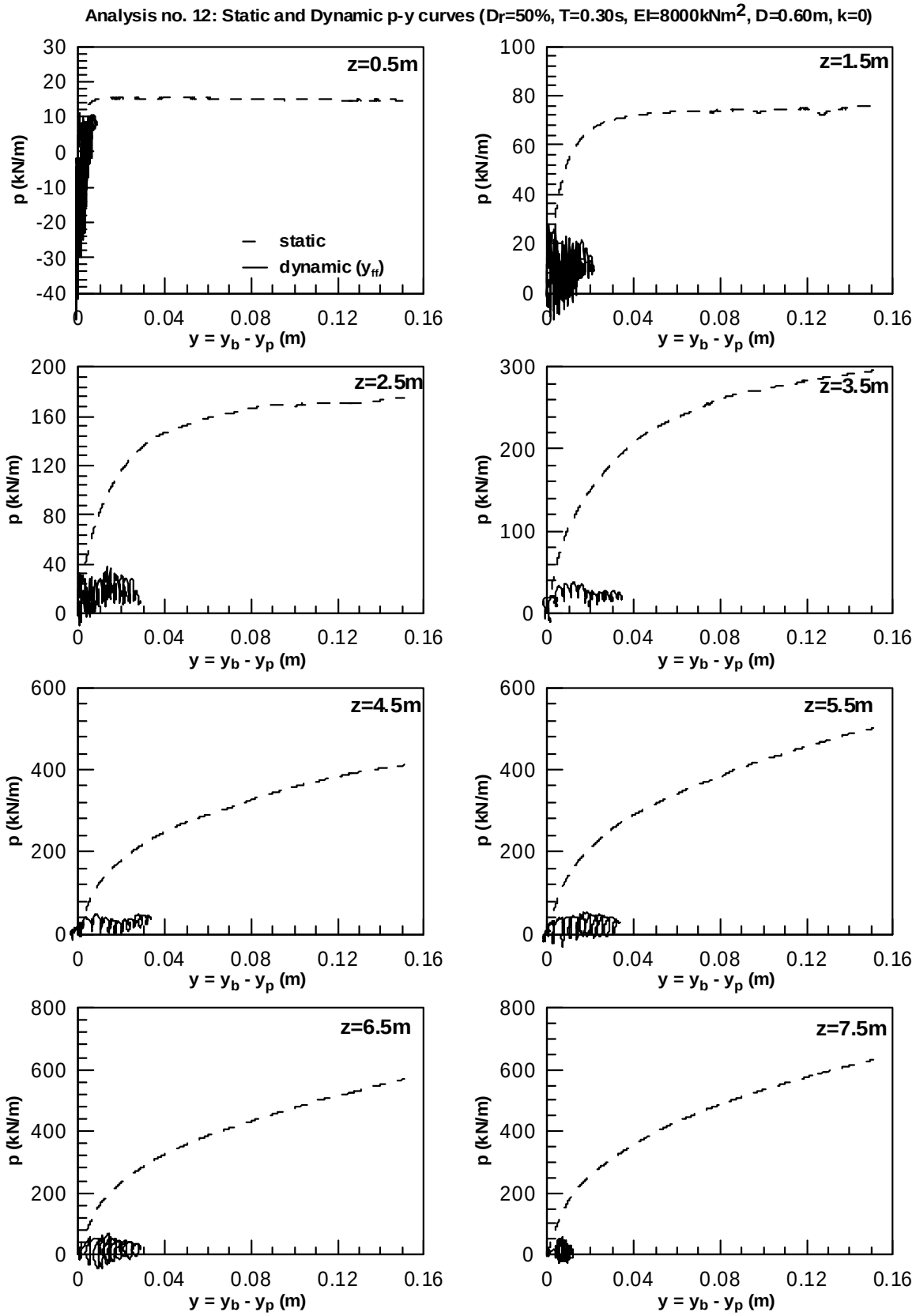
Analysis no. 12: Static and Dynamic p-y curves (Dr=50%, T=0.30s, EI=8000kNm2, D=0.60m, k=0)
z=0.5m
z=1.5m
z=2.5m
z=3.5m
z=4.5m
z=5.5m
z=6.5m
z=7.5m
static
dynamic (yff)
p (kN/m)
y = yb - yp (m)

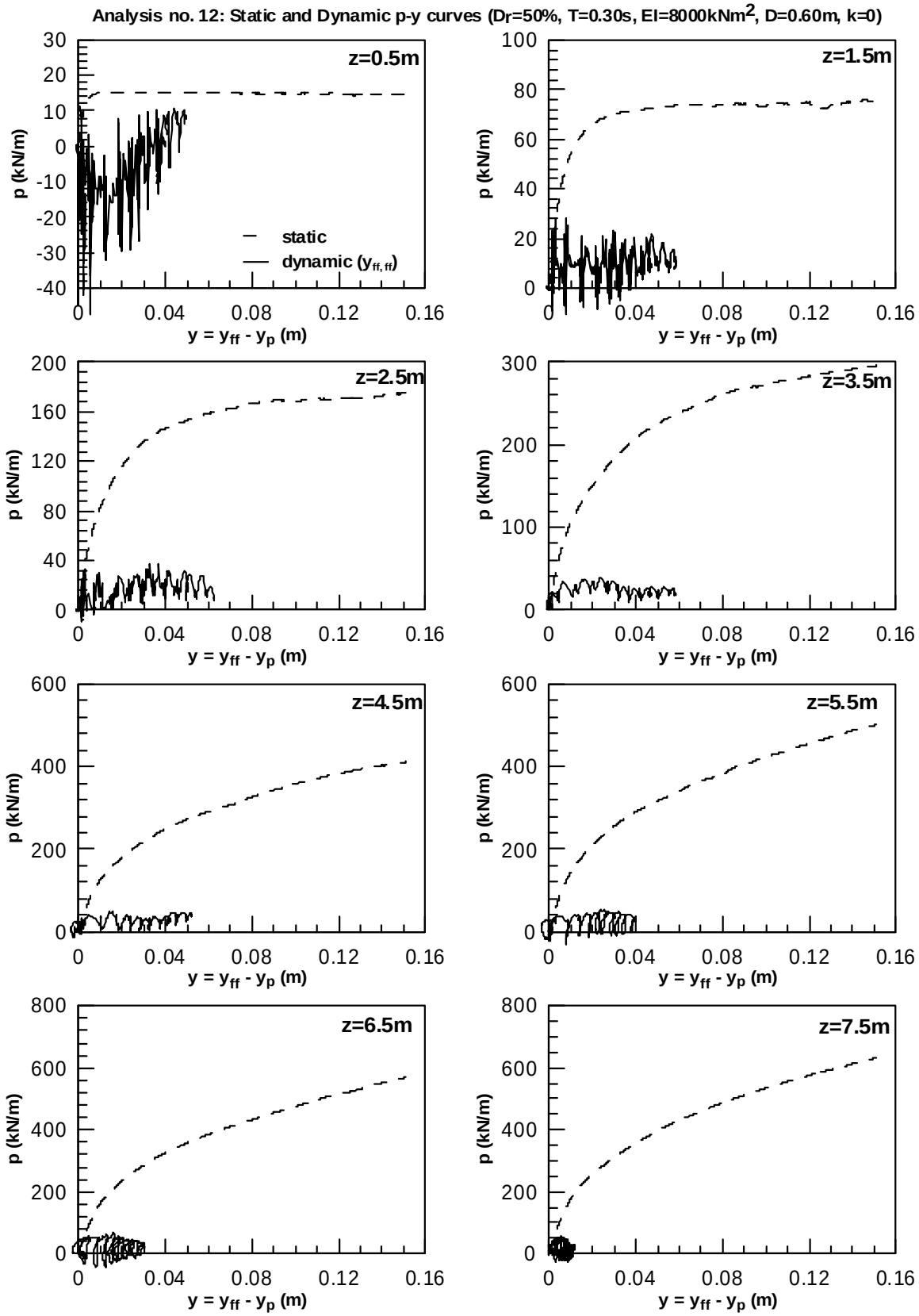
Analysis no. 12: Static and Dynamic p-y curves (Dr=50%, T=0.30s, EI=8000kNm2, D=0.60m, k=0)
z=0.5m
z=1.5m
z=2.5m
z=3.5m
z=4.5m
z=5.5m
z=6.5m
z=7.5m
static
dynamic (yff,ff)
p (kN/m)
y = yff - yp (m)

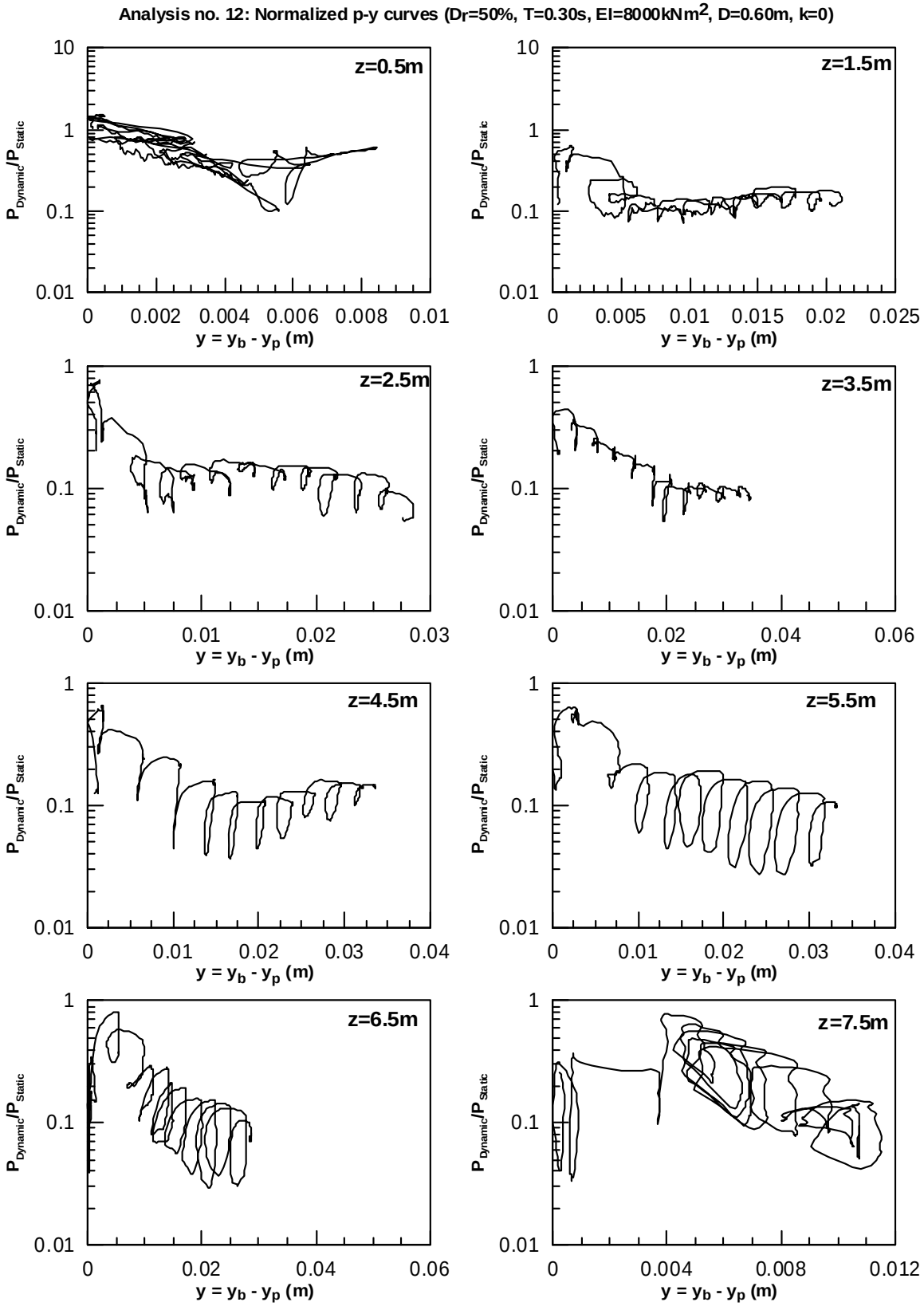
Analysis no. 12: Normalized p-y curves (Dr=50%, T=0.30s, EI=8000kNm2, D=0.60m, k=0)
z=0.5m
z=1.5m
z=2.5m
z=3.5m
z=4.5m
z=5.5m
z=6.5m
z=7.5m
P Dynamic/P Static
y = yb - yp (m)

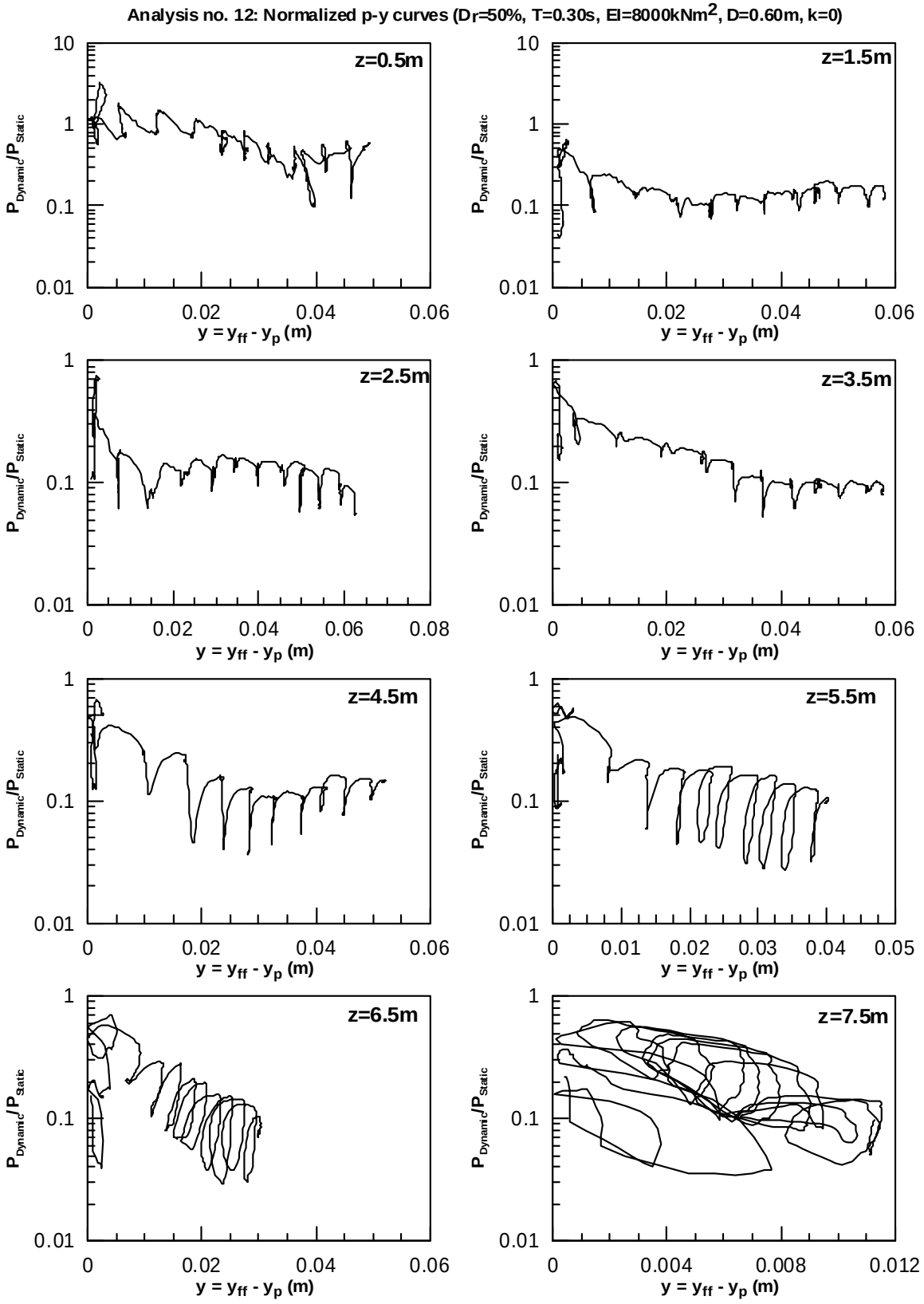
Analysis no. 12: Normalized p-y curves (Dr=50%, T=0.30s, EI=8000kNm2, D=0.60m, k=0)
z=0.5m
z=1.5m
z=2.5m
z=3.5m
z=4.5m
z=5.5m
z=6.5m
z=7.5m
P Dynamic/P Static
y = yff - yp (m)

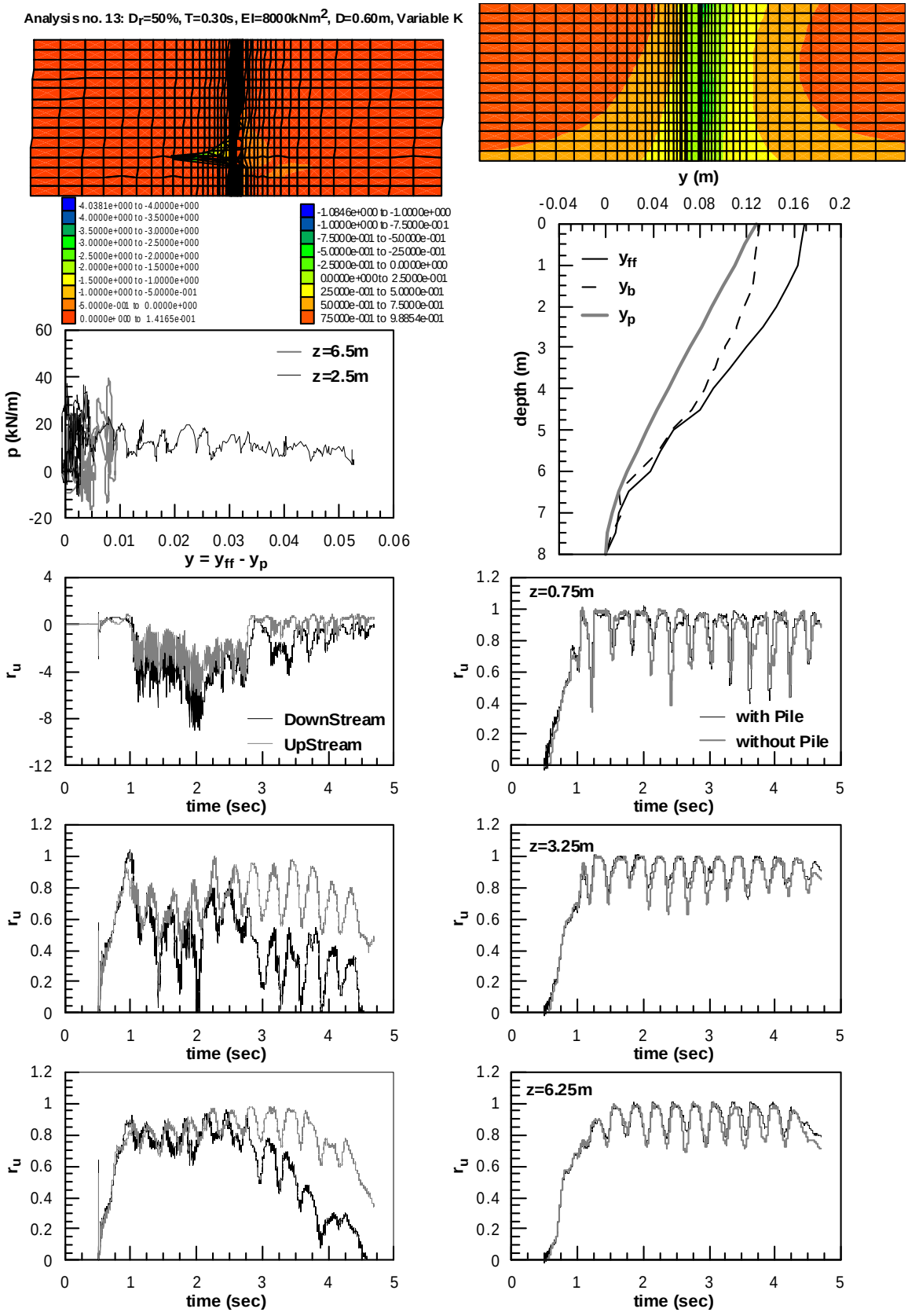
Analysis no. 13: D_r=50%, T=0.30s, EI=8000kNm^2, D=0.60m, Variable K
-4.0381e+000 to -4.0000e+000
-4.0000e+000 to -3.5000e+000
-3.5000e+000 to -3.0000e+000
-3.0000e+000 to -2.5000e+000
-2.5000e+000 to -2.0000e+000
-2.0000e+000 to -1.5000e+000
-1.5000e+000 to -1.0000e+000
-1.0000e+000 to -5.0000e-001
-5.0000e-001 to 0.0000e+000
0.0000e+000 to 1.4165e-001
-1.0846e+000 to -1.0000e+000
-1.0000e+000 to -7.5000e-001
-7.5000e-001 to -5.0000e-001
-5.0000e-001 to -2.5000e-001
-2.5000e-001 to 0.0000e+000
0.0000e+000 to 2.5000e-001
2.5000e-001 to 5.0000e-001
5.0000e-001 to 7.5000e-001
7.5000e-001 to 9.8854e-001
y (m)
p (kN/m)
z=6.5m
z=2.5m
y = y_{ff} - y_p
depth (m)
y_{ff}
y_b
y_p
r_u
DownStream
UpStream
z=0.75m
with Pile
without Pile
z=3.25m
z=6.25m
time (sec)

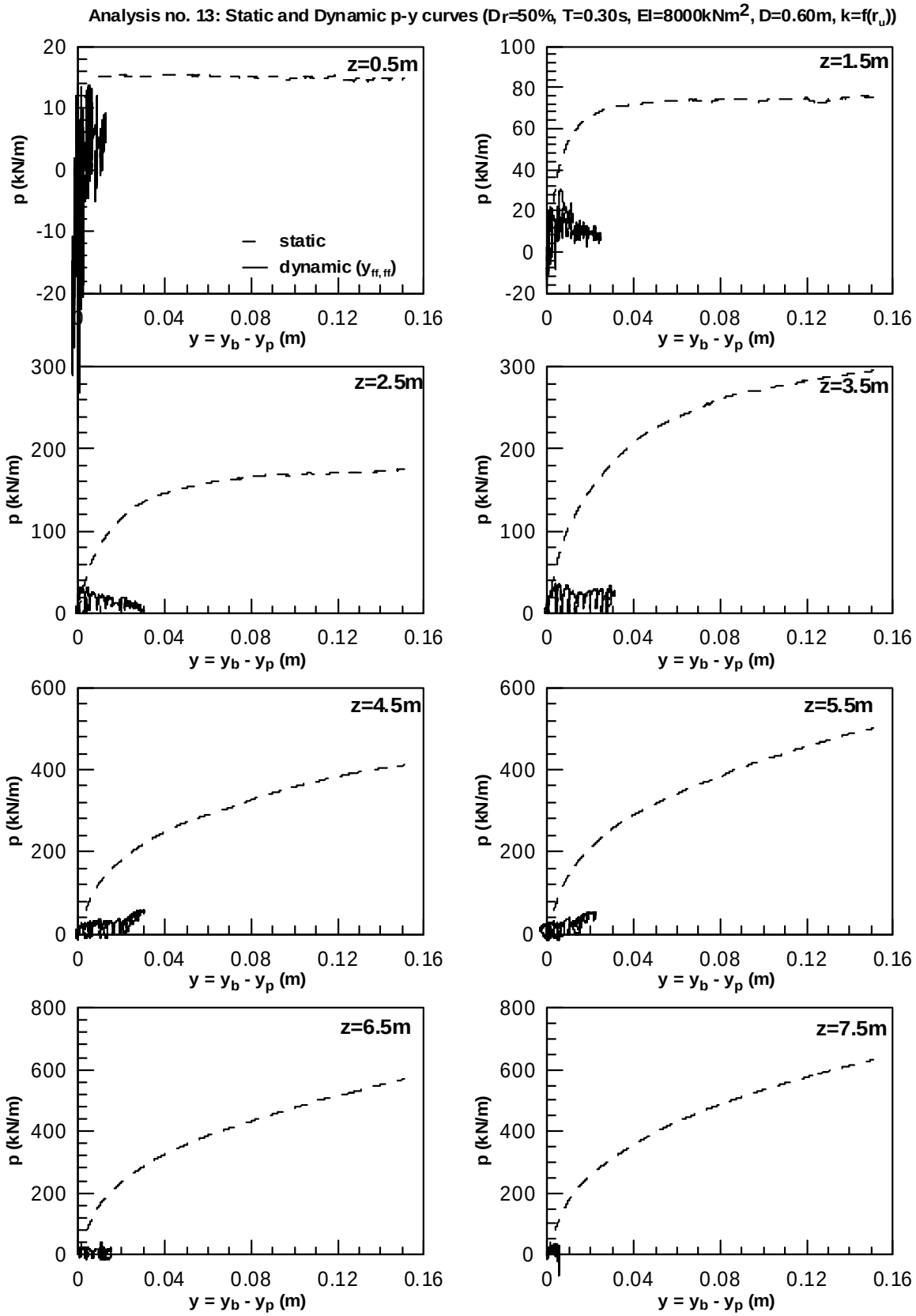
Analysis no. 13: Static and Dynamic p-y curves (Dr=50%, T=0.30s, EI=8000kNm2, D=0.60m, k=f(ru))
z=0.5m
z=1.5m
z=2.5m
z=3.5m
z=4.5m
z=5.5m
z=6.5m
z=7.5m
static
dynamic (yff, ff)
p (kN/m)
y = yb - yp (m)

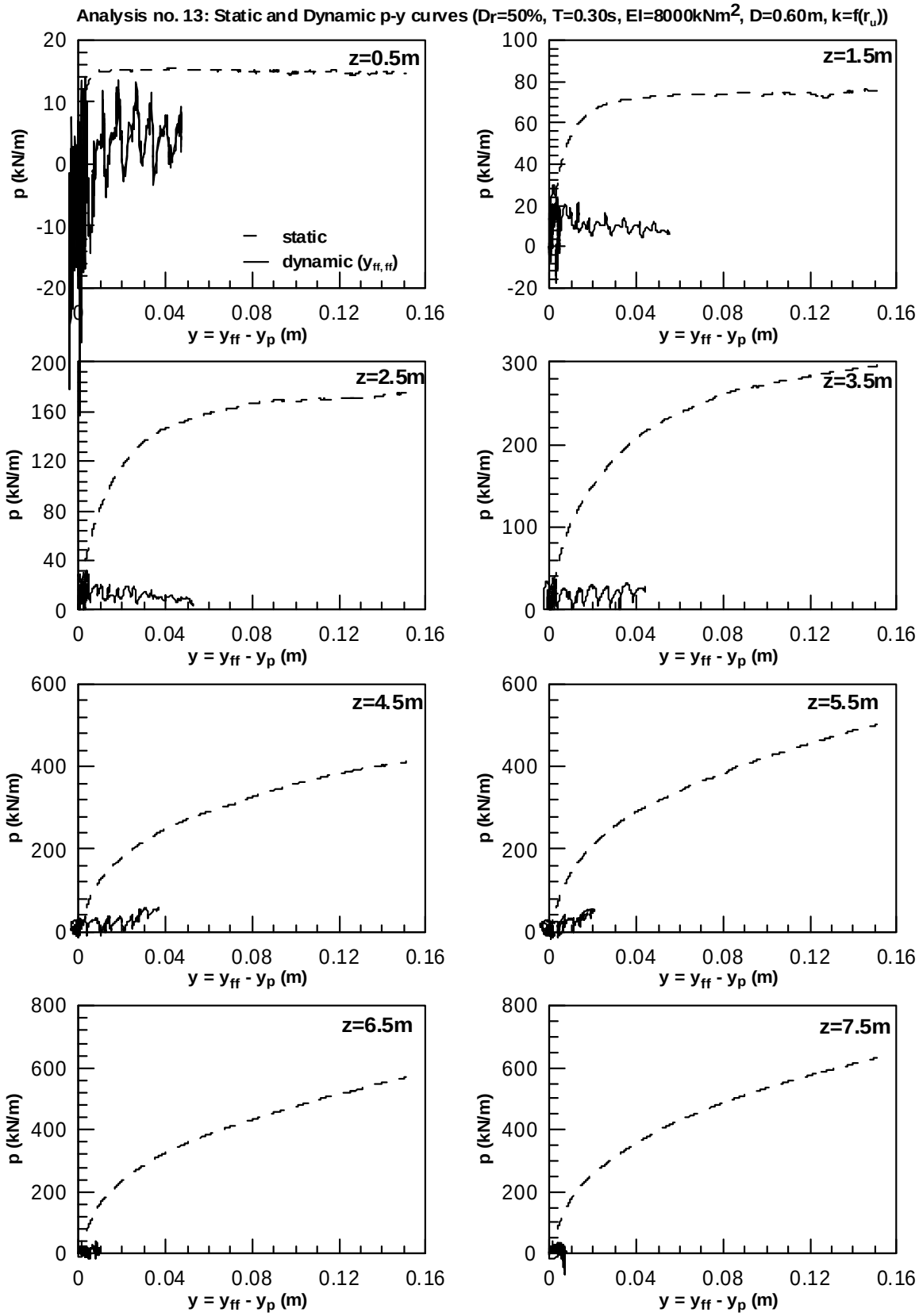
Analysis no. 13: Static and Dynamic p-y curves (Dr=50%, T=0.30s, EI=8000kNm2, D=0.60m, k=f(ru))
z=0.5m
z=1.5m
z=2.5m
z=3.5m
z=4.5m
z=5.5m
z=6.5m
z=7.5m
static
dynamic (yff,ff)
p (kN/m)
y = yff - yp (m)

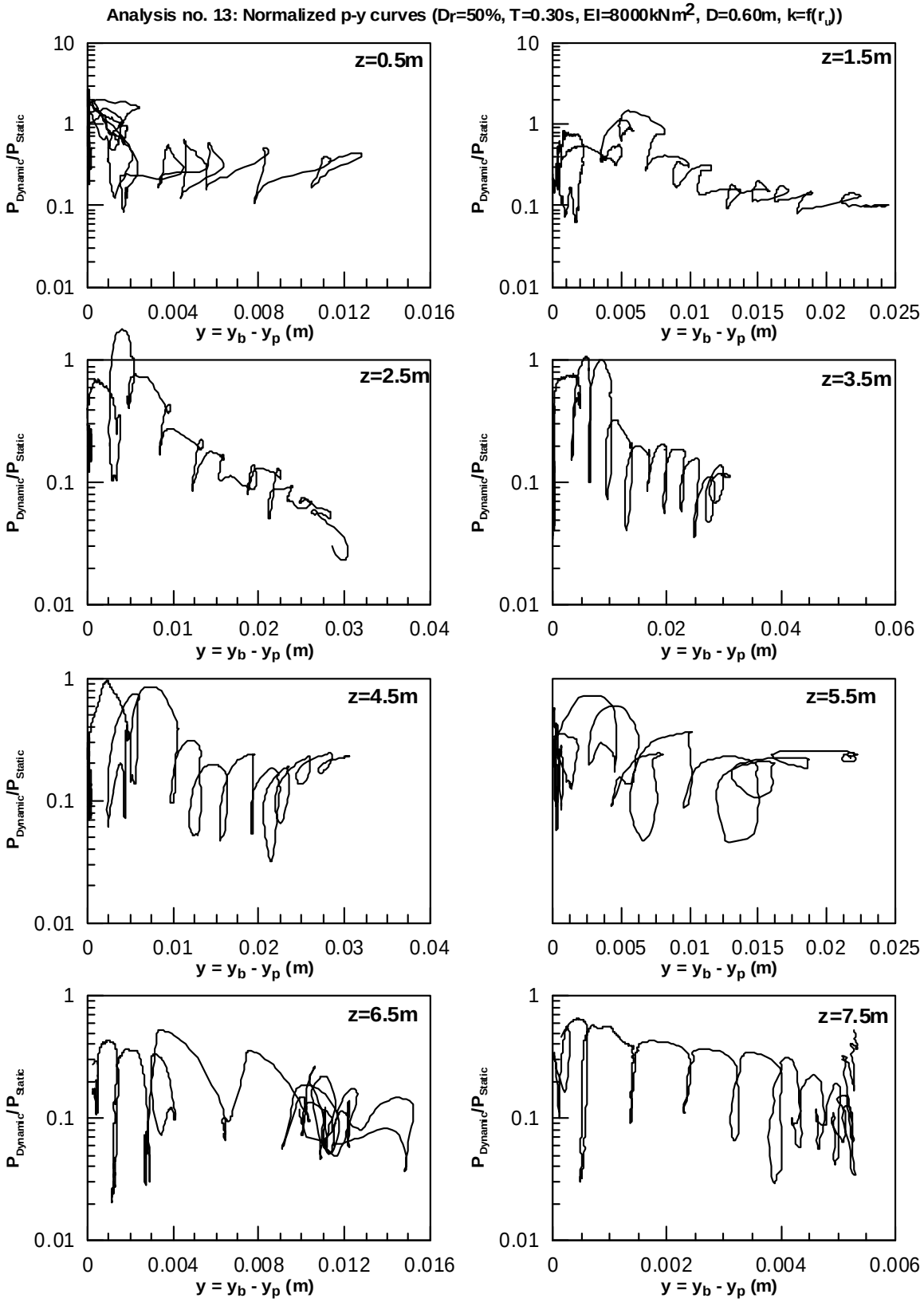
Analysis no. 13: Normalized p-y curves (Dr=50%, T=0.30s, EI=8000kNm2, D=0.60m, k=f(ru))
z=0.5m
z=1.5m
z=2.5m
z=3.5m
z=4.5m
z=5.5m
z=6.5m
z=7.5m
P Dynamic/P Static
y = yb - yp (m)

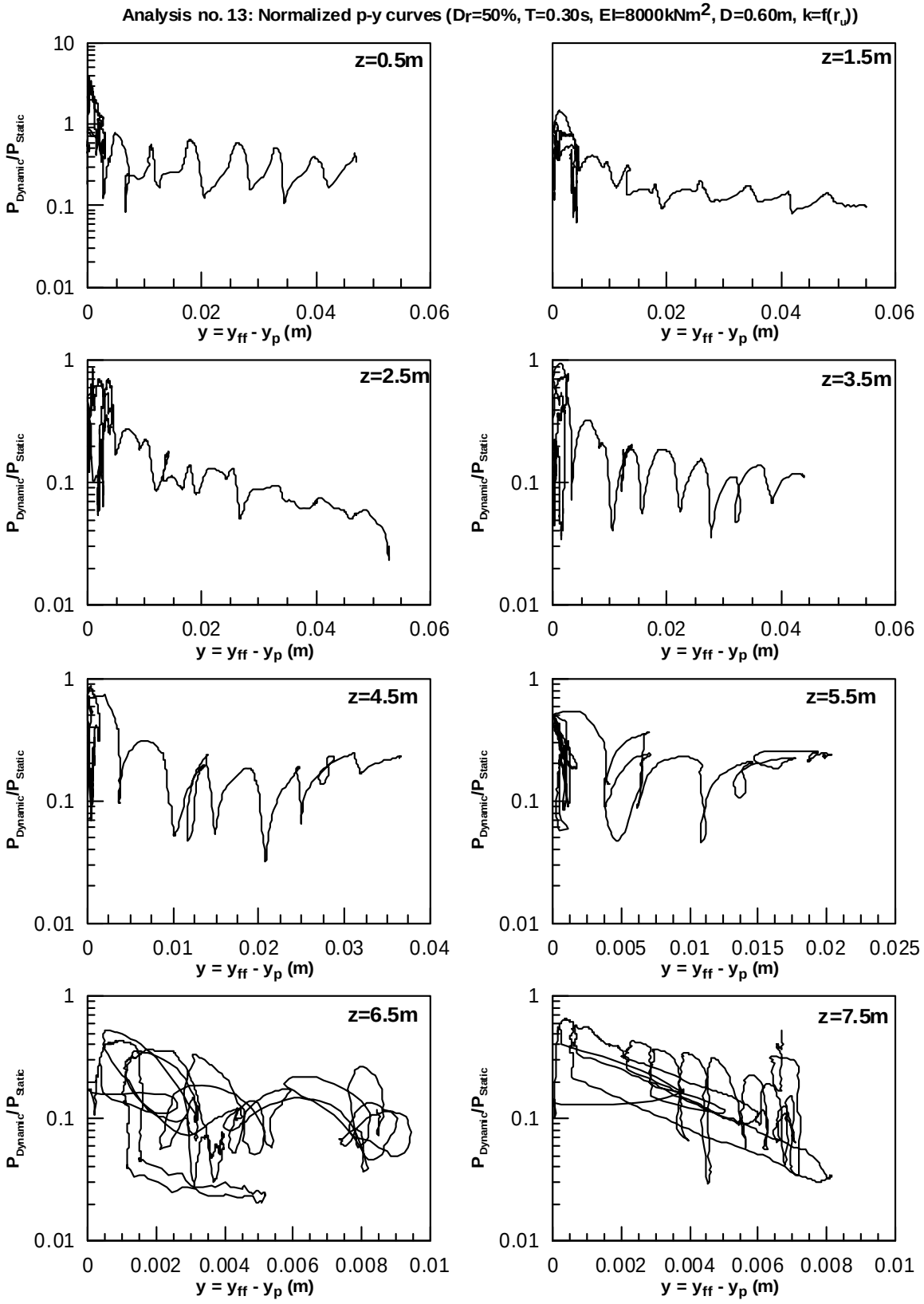
Analysis no. 13: Normalized p-y curves (Dr=50%, T=0.30s, EI=8000kNm2, D=0.60m, k=f(ru))
z=0.5m
z=1.5m
z=2.5m
z=3.5m
z=4.5m
z=5.5m
z=6.5m
z=7.5m
P Dynamic/P Static
y = yff - yp (m)

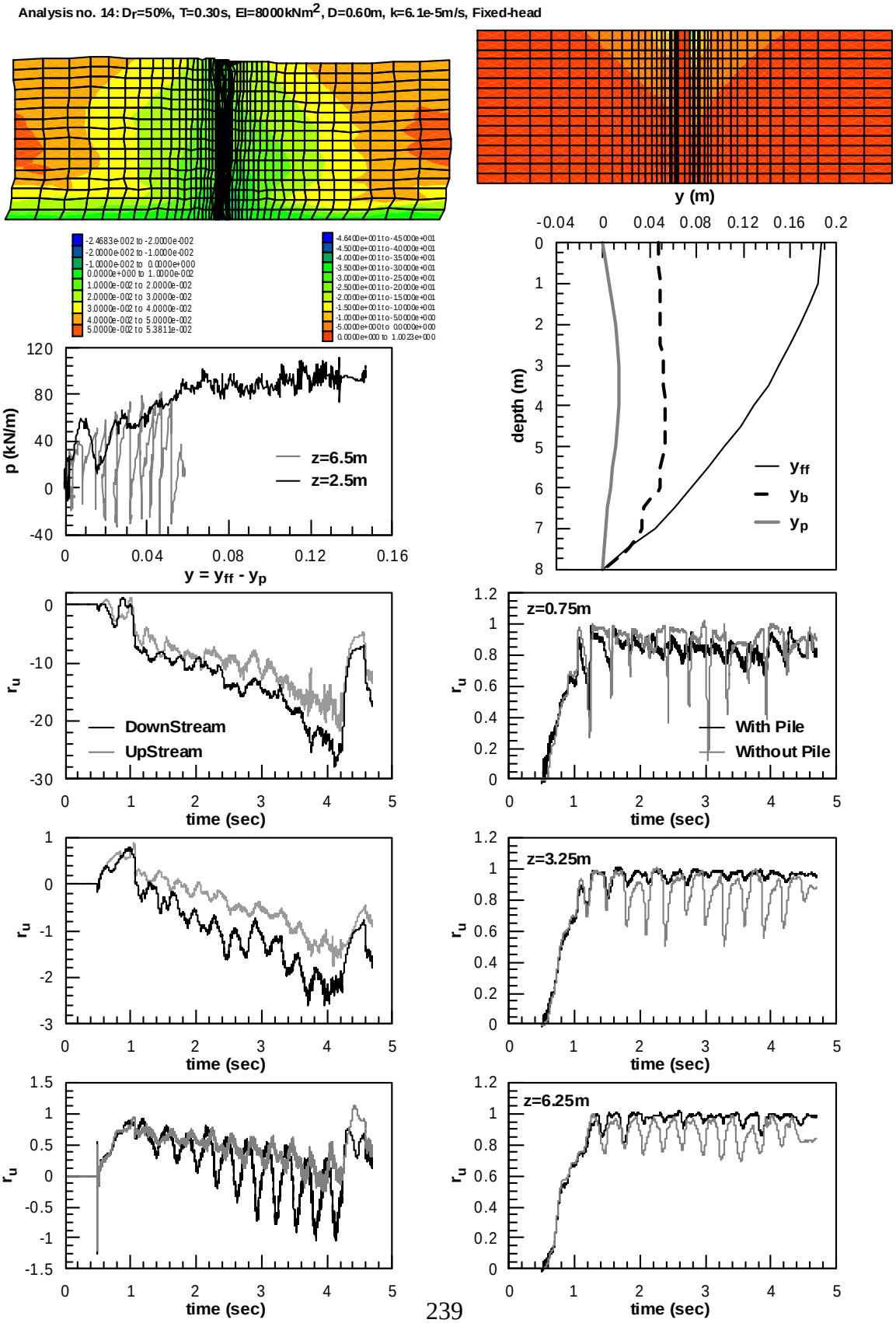
Analysis no. 14: Dr=50%, T=0.30s, EI=8000kNm2, D=0.60m, k=6.1e-5m/s, Fixed-head
-2.4683e-002 to -2.0000e-002
-2.0000e-002 to -1.0000e-002
-1.0000e-002 to 0.0000e+000
0.0000e+000 to 1.0000e-002
1.0000e-002 to 2.0000e-002
2.0000e-002 to 3.0000e-002
3.0000e-002 to 4.0000e-002
4.0000e-002 to 5.0000e-002
5.0000e-002 to 5.3811e-002
-4.6400e+001 to -4.5000e+001
-4.5000e+001 to -4.0000e+001
-4.0000e+001 to -3.5000e+001
-3.5000e+001 to -3.0000e+001
-3.0000e+001 to -2.5000e+001
-2.5000e+001 to -2.0000e+001
-2.0000e+001 to -1.5000e+001
-1.5000e+001 to -1.0000e+001
-1.0000e+001 to -5.0000e+000
-5.0000e+000 to 0.0000e+000
0.0000e+000 to 1.0023e+000
y (m)
-0.04 0 0.04 0.08 0.12 0.16 0.2
depth (m)
yff
yb
yp
p (kN/m)
z=6.5m
z=2.5m
y = yff - yp
ru
DownStream
UpStream
z=0.75m
With Pile
Without Pile
time (sec)
z=3.25m
z=6.25m

Analysis no. 14: Static and Dynamic p-y curves (D_r=50%, T=0.30s, EI=8000kNm^2, D=0.60m, k=6.1e-5m/s, Fixed-head)

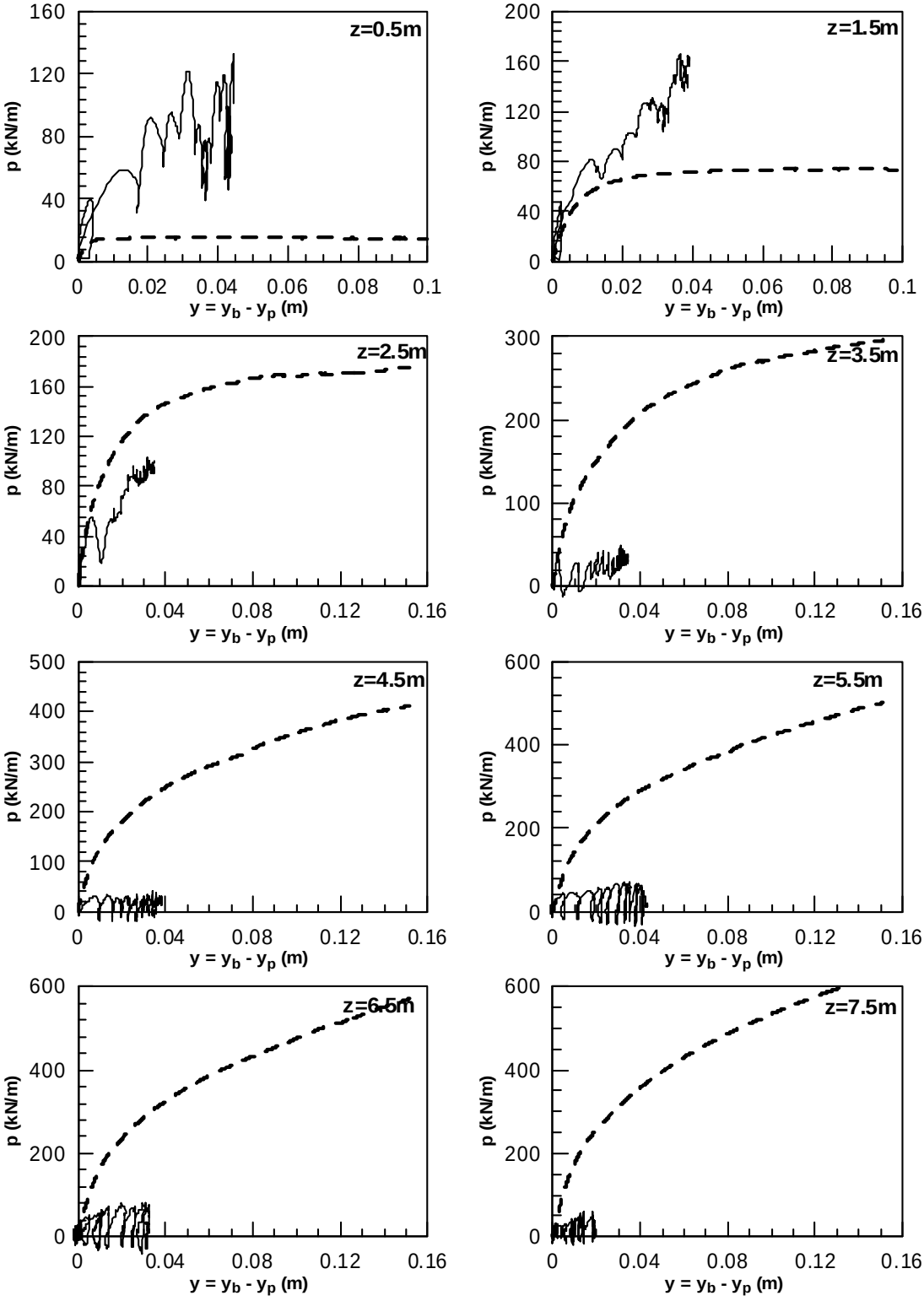

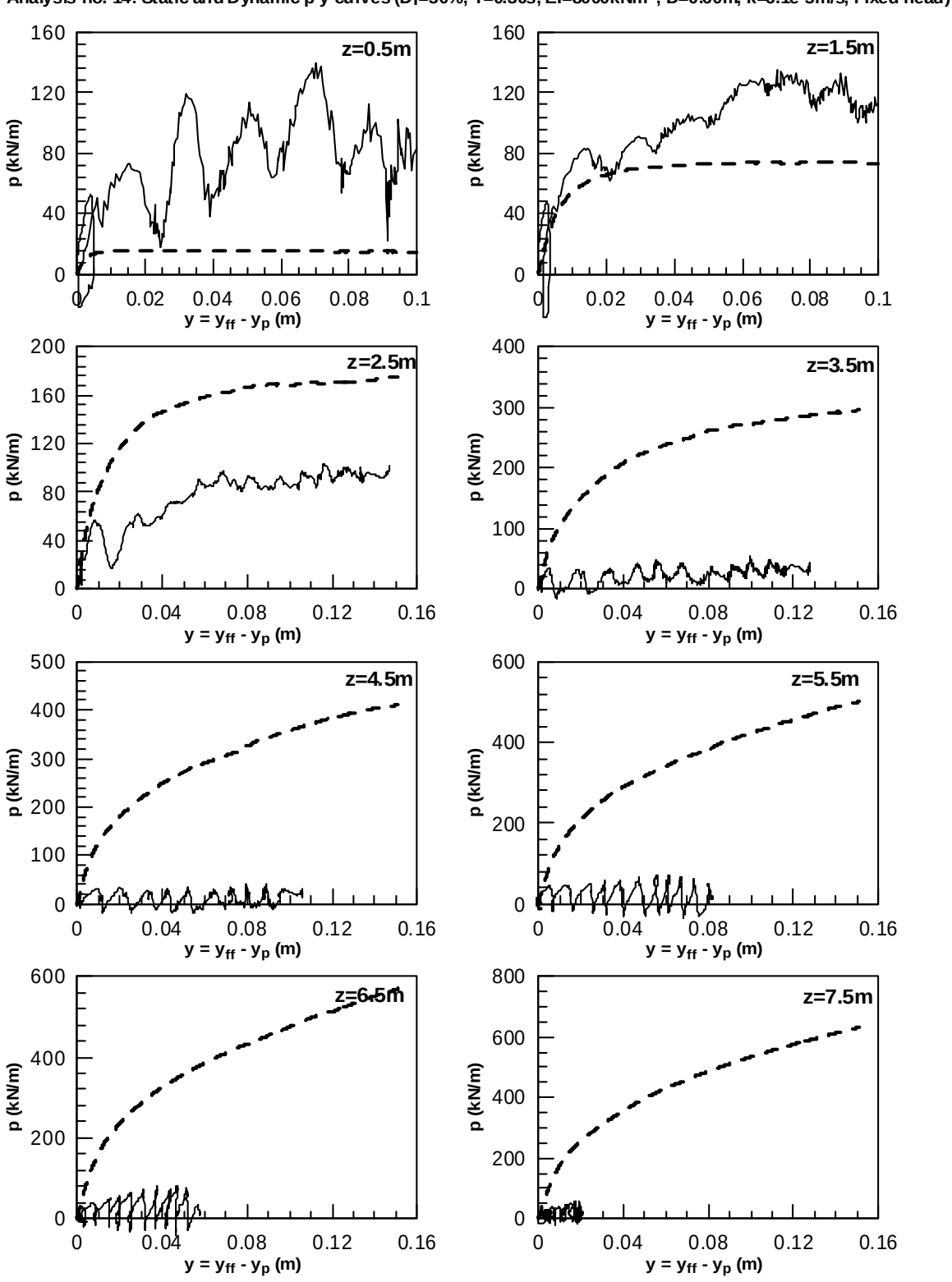
Analysis no. 14: Static and Dynamic p-y curves (Dr=50%, T=0.30s, EI=8000kNm2, D=0.60m, k=6.1e-5m/s, Fixed-head)
z=0.5m
z=1.5m
z=2.5m
z=3.5m
z=4.5m
z=5.5m
z=6.5m
z=7.5m
p (kN/m)
y = yff - yp (m)

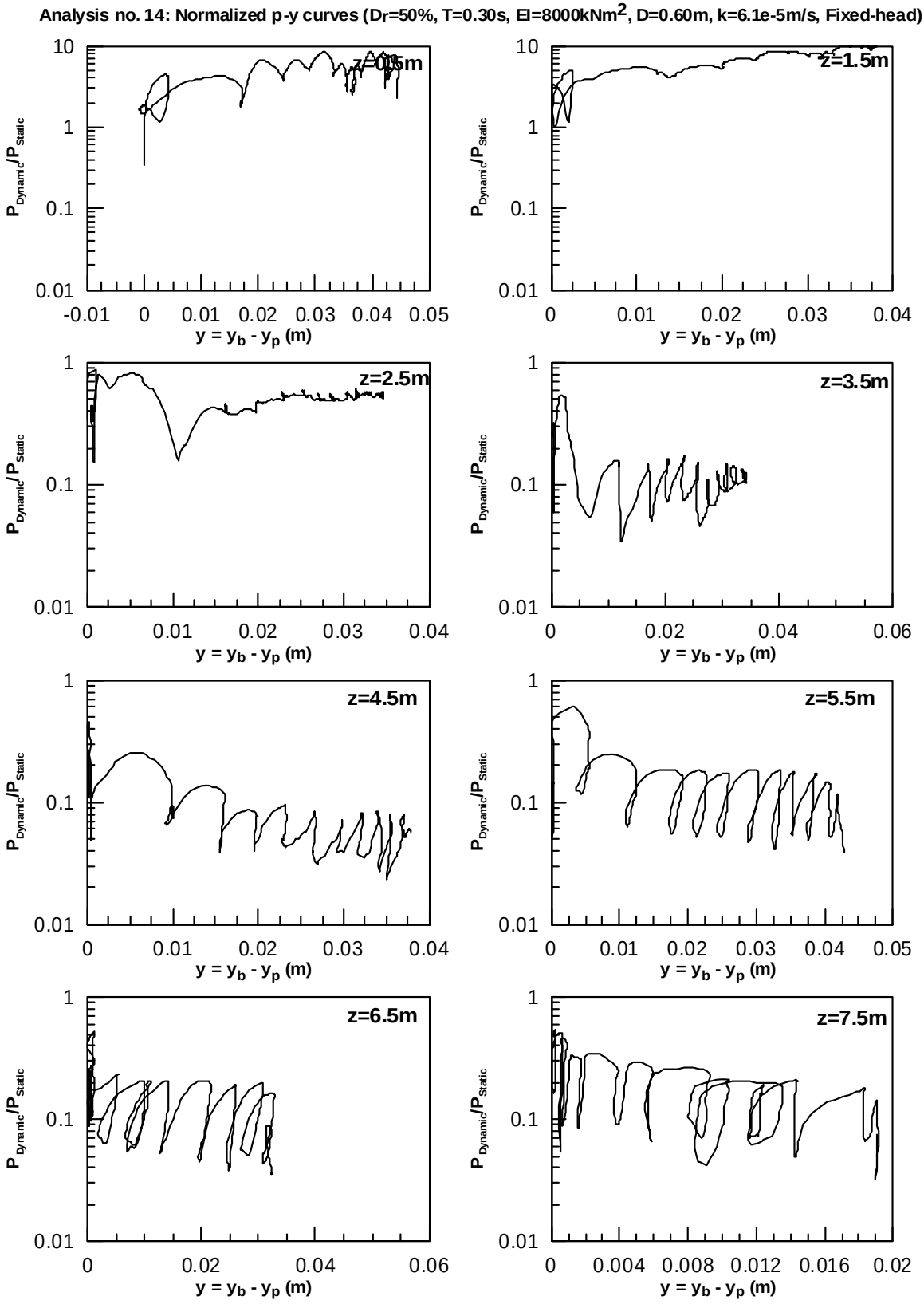
Analysis no. 14: Normalized p-y curves (Dr=50%, T=0.30s, EI=8000kNm2, D=0.60m, k=6.1e-5m/s, Fixed-head)
z=0.5m
z=1.5m
z=2.5m
z=3.5m
z=4.5m
z=5.5m
z=6.5m
z=7.5m
P_Dynamic/P_Static
y = y_b - y_p (m)

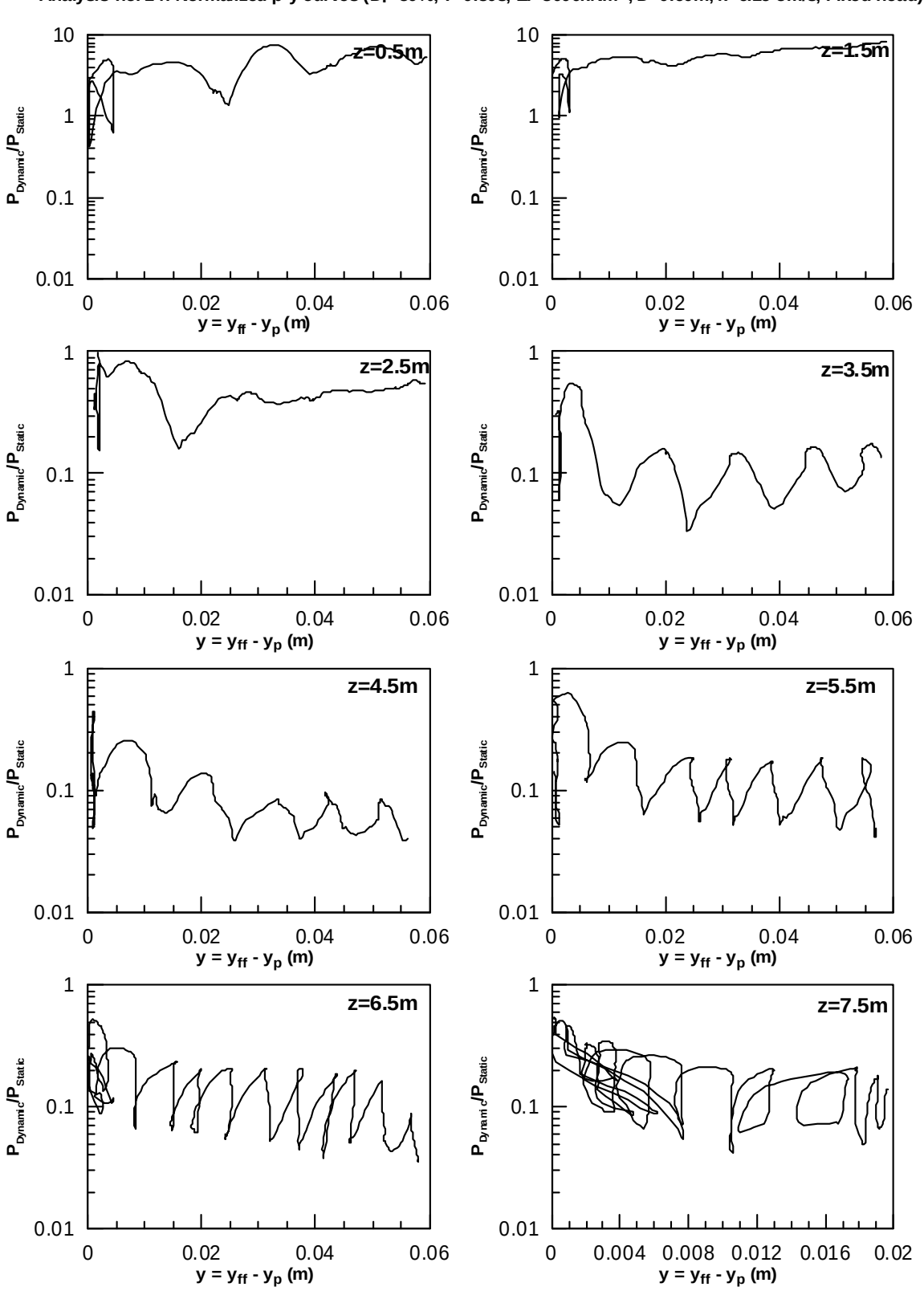
Analysis no. 14: Normalized p-y curves (Dr=50%, T=0.30s, EI=8000kNm2, D=0.60m, k=6.1e-5m/s, Fixed-head)
z=0.5m
z=1.5m
z=2.5m
z=3.5m
z=4.5m
z=5.5m
z=6.5m
z=7.5m
P_Dynamic/P_Static
y = y_ff - y_p (m)

References

Abdoun, T., Dobry, R., O'Rourke, T. D., and Goh, S. H., (2003), "Pile response to lateral spreads: Centrifuge modeling.", Journal of Geotechnical and Geoenvironmental Engineering.

Abdoun, T. (1997) "Centrifuge modeling of seismically induced lateral spreading of multilayer sand deposit and its effects on pile foundations." Ph.D. thesis, Rensselaer Polytechnic Institute, Troy, N.Y.

AIJ (2001), "Recommendations for design of building foundations", Architectural Institute of Japan.

Andrianopoulos, K.I., (2006), "Numerical modeling of static and dynamic behavior of elastoplastic soils", Doctorate Thesis, Department of Geotechnical Engineering, School of Civil Engineering, National Technical University of Athens (in Greek).

Andrianopoulos, K.I., Papadimitriou, A.G. and Bouckovalas, G.D., (2005), "Bounding surface models of sands:Pitfalls of mapping rules for cyclic loading. Proceedings", 11th International Conference on Computer Methods and Advances in Geomechanics, Torino, June, Vol. 1: 241-248.

Andrianopoulos K., Papadimitriou A., Bouckovalas G. (2010), "Bounding Surface Plasticity Model for the Seismic Liquefaction Analysis of Geostructures", Soil Dynamics and Earthquake Engineering, doi: 10.1016/j.soildyn.2010.04.001.

American Petroleum Institute, API, (1993), Recommended practice for planning, design, and constructing fixed offshore platforms, API RP 2A–WSD, 20th Ed., API, Washington, D.C.

Arulmoli, K., Muraleetharan, K.K., Hossain, M.M. and Fruth, L.S., (1992), "VELACS: verification of liquefaction analyses by centrifuge studies"; Laboratory Testing Program – Soil Data Report, Research Report, The Earth Technology Corporation.

Ashford, S. A., and Rollins, K. M., (2002), "TILT: The Treasure Island liquefaction test: Final report." Rep. No. SSRP-2001/17, Dept. of Structural Engineering, Univ. of California, San Diego.

Aydan O., Atak O.V., Ulusay R., Hamada H, and Bardet P.J. (2005), "Ground deformations and lateral spreading around the shore of Sapanca lake induced by the 1999 Kocaeli earthquake", Proceedings of Geotechnical Earthquake Engineering Satellite Conference Osaka, Japan, 10. September.

Bartlett SF and Youd TL (1992), "Empirical Analysis of Horizontal Ground Displacement Generated by Liquefaction-induced Lateral Spreads," Tech. Rep. NCEER-92-0021, National Center for Earthquake Engineering Research, Buffalo, N.Y., Hamada M. and O'Rourke TD(eds.), August 17.

Baziar, M. H., and A. Ghorbani, A., "Evaluation of lateral spreading using artificial neural networks". Soil Dynamics and Earthquake Engineering, 25 (2005), pp. 1–9.

Bhushan, K., Haley, S. C., Fong, P. T., (1979), "Lateral Load Tests on Drilled Piers in Stiff Clays", ASCE Journal of the Geotechnical Engineering Division, vol. 105, No.GT8, Proc. Paper 14789, pp. 969-985.

Boulanger, R. W., Kutter, B. L., Brandenberg, S. J., Singh, P., and Chang, D., (2003), "Pile foundations in liquefied and laterally spreading ground during earthquakes: Centrifuge experiments and analyses." Rep. No. UCD/CGM-03/01, Center for Geotechnical Modeling, University of California, Davis, Calif.

Bowles, S., (2004). "Microeconomics: Behavior, Institutions, and Evolution". Princeton University Press, Princeton,

Brandenberg, S.J. (2005), "Behavior of pile foundations in liquefied and laterally spreading ground", PhD dissertation, Dept. of Civil and Environmental Engineering., University of California, Davis, CA.

Brandenberg, S., Boulanger, R., Kutter, L., Chang, D. (2005): "Behavior of Pile Foundations in Laterally Spreading Ground during Centrifuge Tests", Journal of Geotechnical and Geoenvironmental Engineering.

Brandenberg, S. J., Boulanger, R. W., Kutter, B. L., and Chang, D., (2006), "Monotonic and cyclic beam on nonlinear Winkler foundation analyses of pile foundations in laterally spreading ground." Proc., 8th U.S. Conf. on Earthquake Engineering, Paper No. 8NCEE-001480, San Francisco.

Brandenberg, S. J., Boulanger, R. W., Kutter, B. L., Chang, D, (2007), "Static Pushover Analyses of Pile Groups in Liquefied and Laterally Spreading Ground in Centrifuge Tests", Journal of Geotechnical and Geoenvironmental Engineering

Bransby MF. (1996). "The difference between load transfer relationships for laterally loaded pile groups: Active p-y or passive p-delta", J of Geotech Eng, ASCE, Vol. 122, No. 12, pp. 1015-1033.

Broms, B. (1964a). "Lateral Resistance of Piles in Cohesive Soils," J. Soil Mechanics and Foundation Div., ASCE, 90(3), 27-63.

Byrne, D. E., L. R. Sykes, and D. M. Davis (1992), "Great thrust earthquakes and aseismic slip along the plate boundary of the Makran subduction zone", Journal of Geophysical Research 97,449 -478

Cubrinovski, M., Kokusho, T. and Ishihara, K., (2005a), "Interpretation from large-scale shake table tests on piles undergoing lateral spreading in liquefied soils", Soil Dynamics and Earthquake Engineering. in press.

Cubrinovski, M., and Ishihara, K., (2005b), "Assessment of pile group response to lateral spreading by single pile Analysis". ASCE Geotechnical special publication No. 145. 242-254.

Cubrinovski, M., Ishihara, K. & Poulos, H., (2006a), "Pseudo-static analysis of piles subjected to lateral spreading", Proc. New Zealand Workshop on Geotechnical Earthquake Engineering, 20-21 November. Christchurch, New Zealand.

Cubrinovski, M., Kokusho, T. & Ishihara, K., (2006b), "Interpretation from large-scale shake table tests on piles undergoing lateral spreading in liquefied soils". Soil Dynamics and Earthquake Engineering, Vol 26 (2-4): 275-286.

Dash, S R, Bhattacharya, S, Blakeborough, A & Hyodo, M., (2008), "'P-Y curve to model lateral response of pile foundations in liquefied soils", 14th World Conference on Earthquake Engineering, Beijing, (pp. -).

DNV-RP-C202 Recommended practice: Buckling strength of shells. Det Norske Veritas. Norway, 2002.

Dobry, R., Taboada, V., Liu, L., (1995), "Centrifuge modeling of liquefaction effects during earthquakes", Proc,. 1st Intl. Conf. on Earthq. Geotech. Engrg., K. Ishihara, ed., Tokyo, Japan, 3:1291-1324.

Dobry, R., Abdoun, T., O' Rourke T.D., Goh S.H. (2003), "Single piles in lateral spreads: Field Bending Moment Evaluation", ASCE Journal of Geotechnical and Geoenvironmental Engineering, Vol. 129, No. 10, October, pp. 879–889

Dungca J. R., J. Kuwano, A. Takahashi, T. Saruwatari, J. Izawa, H. Suzuki, and K. Tokimatsu (2006). "Shake table tests on the lateral response of a pile buried in liquefied sand", Soil Dynamics and Earthquake Eng., 26, 287-295.

Elgamal, A., Yang, Z., Parra, E., and Ragheb, A., (2003), "Modeling of Cyclic Mobility in Saturated Cohesionless Soils", International Journal of Plasticity, 19(6), 883-905.

Fan, C. C., Long, J. H., (2005), "Assessment of existing methods for predicting soil response of laterally loaded piles in sand", Computers and Geotechnics, 32

Finn, W. D. L. (1990), "Analysis of post-liquefaction deformation in soil structures", Proc., H. Bolton Seed Memorial Symposium, Vol 2, BiTech Pub., Richmond, British Columbia, May, pp. 291-311

Finn, W. D. L. (1991), "Assessment of liquefaction potential and post-liquefaction behavior of earth structures: development 1981-1991", Proc., 2nd International Conference on Recent Advances in Geotechnical Earthquake Engineering and Soil Dynamics, Missouri, March.

Finn, W. D. L., Ledbetter, R. H., and Wu, G., (1994). "Liquefaction in Silty Soils: Design and analysis." Ground Failures Under Seismic Conditions, Geotechnical Special Pub. No. 44, ASCE, S. Prakash and P. Dakoulas (eds.) October.

Georgiadis, M, Anagnostopoulos, C., Saflekou, S., (1992), "Cyclic lateral loading of piles in soft clay", Journal of Geotechnical Engineering, ASCE, Vol. 23, GT1, pp. 47-59.

Gibson, A. (1996). "Physical Scale Modeling of Geotechnical Structures at One-G," Ph.D. Dissertation, California Inst. of Tech., Pasadena.

Gonzalez, L., Abdoun, T., and Dobry, R., (2009), "Effect of Soil Permeability on Centrifuge Modeling of Pile Response to Lateral Spreading." ASCE Journal of Geotechnical and Geoenvironmental Engineering, Vol. 135, No. 1, pp. 62-73, January.

Gonzalez, L. (2005), "Centrifuge modeling of permeability and pinning reinforcement effects on pile response to lateral spreading" Ph.D. Thesis, Rensselaer Polytechnic Institute, Troy, NY, USA

Gu, W. H., Morgenstern, N. R., and Robertson, P. K. (1993), "Progressive failure of Lower San Fernando Dam", Journal of Geotechnical Engineering, ASCE, Vol. 119, No.2, February, pp. 333-349.

Hadush, S., Yashima, A., Uzuoka, R., (2000), "Importance of viscous fluid characteristics in liquefaction induced lateral spreading analysis", Computers and Geotechnics, 27 (2000), pp. 199–224.

Haigh, S. K., and Madabhushi, S. P. G., (2002). "Centrifuge modeling of lateral spreading past pile foundations." Proc., Int. Conf. on Physical Modelling in Geotechnics, St John's, Canada.

Hamada, M. and O'Rourke, T. (1992). "Case studies of liquefaction and lifeline performance during past earthquakes," Vol. 1, Japanese Case Studies Technical Rep NCEER-92-0001, M. Hamada and T. D. O'Rourke, eds., National Center for Earthquake Engineering Research, Buffalo, N.Y., February.

Hamada, M., Yasuda, S., Isoyama, R., and Emoto, K., (1986), "Study on liquefaction induced permanent ground displacements", Association for the Department of Earthquake Prediction in Japan, Tokyo, 87.

Hamada M. (1999), "Similitude law for liquefied-ground flow", Proceedings of the 7th U.S.-Japan Workshop on Earthquake Resistant design of lifeline facilities and countermeasures against soil liquefaction, pp. 191-205.

Han Z., Suleiman S., Bughrara, Y., (2007), "Cytology and pollen grain fertility in creeping bentgrass interspecific and intergeneric hybrids", Euphytica 156:1-2, 227-235 Online publication date: 21.May.2007.

Hetenyi, M. (1946) "Beams on elastic foundations," University of Michigan Press, Ann Arbor, Mich., United States.

Ishihara, K. and Cubrinovski, M., (2004), "Case studies of pile foundations undergoing lateral spreading in liquefied deposits, State of the art paper, Fifth Int. Conf. on Case Histories in Geotechnical Engineering, New York, CD-ROM.

Ishihara K. & Cubrinovski M. (1998), "Soil-pile interaction in liquefied deposits undergoing lateral spreading", XI Danube-European Conference, Croatia, May 1998

Japanese Geotechnical Society, JGS, (1998), "Special Issue No. 2 on Geotechnical Aspects of the January 17, 1995, Hyogoken-Nambu Earthquake." Soils Found., 2, 216.

Japan Road Association, JRA, (2002), " Specifications for highway bridges. Preliminary English Version, prepared by Public Works Research Institute _PWRI_ and Civil Engineering Research Laboratory _CRL_, Japan.

Japanese Geotechnical Society, JGS, (1996), "Special Issue on Geotechnical Aspects of the January 17, 1995, Hyogoken-Nambu Earthquake." Soils Found., 1, 359.

JHSE (1990): "Highway bridge design guide", Japanese Society of Highway Engineers, Tokyo, Japan.

Kim, B. T., Kim, N. K., Lee, W. J., Kim YS (2004), "Experimental Load-transfer Curves for Laterally Loaded Piles in Nak-dong River Sand," Journal of Geotechnical and Geoenvironmental Engineering, ASCE, 130(4): 416−425.

Kodner, R. L., Zelasko, J. S., (1963), "A hyperbolic stress-strain formulation for sands", Proc. 2nd Pan-American Conference on Soil Mechanics and Foundations Engineering, Brazil, I: pp. 289-324.

Kramer, S.L. (1996): "Geotechnical earthquake engineering", Prentice-Hall.

Kuwano, J., Ishihara, K., Haya, H., and Izu, F., (1991), "Analysis on permanent deformation of embankments caused by earthquaes." Soil and Foundations, JSSMFE, Vol. 31, No. 3, September.

Newmark, N. M. (1965). "Effects of earthquakes on dams and embankments.", Ge´otechnique, London, 15(2), 139–160.

O'Neill, M.W., Murchison, J.M., (1983), "An evaluation of p-y relationships in sands. A report to the American Petroleum Institute, PRAC 82-41-1, University of Texas, Huston.

Papadimitriou, A.G., Bouckovalas, G.D. (2002): "Plasticity model for sand under small and large cyclic strains: a multiaxial formulation", Soil Dynamics and Earthquake Engineering, 22 (3), pp. 191-204.

Papadimitriou, A.G., Bouckovalas, G.D. and Dafalias, Y.F., (2001), "Plasticity model for sand under small and large cyclic strains", Journal of Geotechnical and Geoenvironmental Engineering, ASCE, 127, no. 11, 973-983,

Rauch F. A. and Martin II R. J. (2000), "EPOLLS model for predicting average displacements on lateral spreads," Journal of Geotechnical and Geoenvironmental Engineering, Vol. 126, No. 4, April, pp 360-371.

Reese, L.C., Cox, W.R., and Koop, F.D., (1974), "Analysis of Laterally Loaded in Sand", Proceedings, Six Annual OTC, Vol 2. Paper No. 2080, Houston, Texas.

Reese, L.C. and Matlock, H., (1956), "Non-dimensional solutions for laterally-loaded piles with soil modulus assumed proportional to depth". Proceedings of the 8th Texas Conference on Soil Mechanics and Foundation Engineering, Austin, Texas, pp.1-41.

Reese, L. and Welch, R. (1975), "Lateral Loading of Deep Foundations in Stiff Clay," J. Geotech. Eng. Div., ASCE, 101 (GT7), 633-649.

Reese, L. (1977). "Laterally Loaded Piles: Program Documentation," J. Geotech. Eng., ASCE, 103(4), 287-305.

Rollins, K., Bowles, S., Brown, D., Ashford, S., (2007), "Lateral Load Testing of Large Drilled Shafts after Blast-Induced Liquefaction", 4th International Conference on Earthquake Geotechnical Engineering, Thessaloniki, Greece.

Sento N., Goto K., Namba S., Kobayashi K., Oh-oka H. & Tokimatsu K., (1999), "Case study for pile foundation damaged by soil liquefaction at inland site of artificial island", Second international conference on earthquake geotechnical engineering, 21-25th June 1999, Lisbon, Portugal

Terzaghi, K. (1955), "Evaluation of coefficients of subgrade reaction", Geotechnique, Vol. v, No. 4, pp. 297-326.

Tokida K., Matsumoto H., Azuma T. and Towhata I. (1993), "Simplified Procedure to Estimate Lateral GroundFlow by Soil Liquefaction", In: Cakmak A.S., Brebbia C.A.,Editors.Proceedings of the Fifth international Conference on Soil Dynamics and Earthquake Engineering, New York: Elsevier Applied Science, Vol. 6, pp. 381-396.

Tokimatsu, Kohji and Hiroko Suzuki (2004), "Pore water pressure response around pile and its effects on p-y behavior during soil liquefaction," Soils and Foundations, 44(6), 101-110.

Tokimatsu, K., Mizuno, H., and Kakurai, M. (1996). "Building damage associated with geotechnical problems." Special Issue of Soils and Foundations, Japanese Geotechnical Society, 219-234.

Tokimatsu K. (1999), "Performance of pile foundations in laterally spreading soils", Proc. 2nd Intl. Conf. Earthquake Geotechnical Engineering (P. Seco e Pinto, ed.), Lisbon, Portugal, June 21-25, Vol 3, pp. 957-964

Towhata, I., Tokida., Tamari, Y., Matsumoto, H., and Yamada, K. (1991), "Prediction of permanent lateral displacement of liquefied ground by means of variational principle", Proc., 3rd Japan- U.S. Workshop on earthquake resistant design of lifeline facilities and countermeasures for soil liquefaction, Tech. Rep. NCEER-91-001, T. D. O'Rourke and M. Hamada (eds.) February 1, pp. 237-251.

Towhata, I., Sasaki, Y., Tokida, K., Matsumoto, H., Tamari, Y., and Yamada, K. (1992), "Prediction of permanent displacement of liquefied ground by means of minimum energy principle" Soil and Foundations, JSSMEF, Vol. 32, No. 3, September, pp. 97-116.

Towhata I. & Toyota H. (1994), "Dynamic analysis of lateral flow of liquefied ground", Proc. 5th U.S.-Japan Workshop on Earthquake Resistant Design of Lifeline Facilities and Countermeasures Against Soil Liquefaction, Tech. Rep. NCEER-94-0026, T. D. O'Rourke and M. Hamada (eds), November 7, pp. 377-387

Towhata I. (2005) "Development of geotechnical earthquake engineering in Japan", Heritage lecture, 16th International Conference on Soil Mechanics and Geotechnical Engineering (16ICSMGE), Osaka, Japan, pp. 251-291.

Uzuoka R, Yashima A, Kawakami T, Konrad JM, (1998), "Fluid dynamics based prediction of liquefaction induced lateral spreading. Comput Geotech 22:243–282

Uzuoka, R., Sento, N., and Kazama, M., (2005), "Numerical analysis of rate-dependent reaction of pile in saturated or liquefied soil.", Proc., Seismic Performance and Simulation of Pile Foundations in Liquefied and Laterally Spreading Ground, Geotechnical Special Publication No. 145, ASCE, Reston, Va., 204–217.

Uzuoka, R., Kazama, M., Zhang, F., A. Yashima A. and Oka, F, (2005), " Prediction of Liquefaction Induced Earth Pressure on a GroupPile Foundation", International Symposium on Earthquake Engineering Commemorating Tenth Anniversary of the 1995 Kobe Earthquake (ISEE Kobe 2005), pp.B-191-202, 2005.1.

Valsamis, A., Bouckovalas, G., Chaloulos, Y., (2011), "Simplified Design of Single Piles under Liquefaction Induced Lateral Spreading", 5th International Conference on Earthquake Geotechnical Engineering, Santiago, Chile.

Valsamis A., Bouckovalas G. & Papadimitriou A, (2010), "Parametric investigation of lateral spreading of gently sloping liquefied ground", Soil Dynamics and Earthquake Engineering Volume 30, Issue 6, Pages 490-508

Valsamis (2008), "Numerical simulation of single pile response under liquefaction-induced lateral spreading", Doctorate Thesis, Department of Geotechnical Engineering, School of Civil Engineering, National Technical University of Athens.

Wilson, D. W., Boulanger, R. W., and Kutter, B. L. (2000). "Seismic lateral resistance of liquefying sand." J. of Geotechnical & Geoenvironmental Engrg., ASCE, Vol. 126, No.10, pp. 898-906.

Yasuda, S., and Berril, J. B. (2000). "Observations of the earthquake response of foundations in soil profiles containing saturated sands." Proc. GeoEng 2000 Conf., Melbourne, Australia, CD Rom

Yegian, M. K., Marciano, E. A., and Gharaman, V. G., (1991), "Earthquake-induced permanent deformation: probabilistic approach", J. Geotech. Eng. 117 (1), 35–50.

Youd L. T., Hansen M. C. and Bartlett F. S. (2002), "Revised multilinear regression equations for prediction of lateral spread displacement", Journal of Geotechnical and Geoenvironmental Engineering, Vol. 128, No. 12, December 1, pp 1007-1017.

Youd, T.L. and Perkins, D.M., (1987), "Mapping soil liquefaction severity index", Journal of Geotechnical Engineering, v. 113, no. 11, p. 1374-1392.

Zhang J. and Zhao X.J., (2005), "Empirical models for estimating liquefaction-induced lateral spread displacement," Soil Dynamics and Earthquake Engineering, Vol. 25, pp. 439-450.